Benchmark Composite Wing Design Including Joint Analysis and Optimization

Robert G. Albers

A dissertation

submitted in partial fulfillment of the

requirements for the degree of

Doctor of Philosophy

University of Washington

August, 2014

Reading Committee:

Mark E. Tuttle, Chair

Ramulu Mamidala

William B. Avery

Zelda B. Zabinsky

Program Authorized to Offer Degree:

Mechanical Engineering

University of Washington

Abstract

Benchmark Composite Wing Design Including Joint Analysis and Optimization

Robert G. Albers

Chairperson of Supervisory Committee:
Professor Mark E. Tuttle
Mechanical Engineering

A composite wing panel software package, named WING Joint OpTimization and Analysis (WINGJOTA) featuring bolted joint analysis, is created and presented in this research. Three areas of focus were the development of an analytic composite bolted joint analysis suitable for fast evaluation; a more realistic wing design than what has been considered in the open literature; and the application of two optimization algorithms for composite wing design. Optimization results from 14 wing load cases applied to a composite wing panel with joints are presented.

The composite bolted joint analysis consists of an elasticity solution that provides the stress state at a characteristic distance away from the bolt holes. The stresses at the characteristic distance are compared to a failure criterion on a ply-by-ply basis that not only determines first ply failure but also the failure mode. The loads in the multi-fastener joints used in this study were

determined by an iterative scheme that provides the bearing-bypass loads to the elasticity analysis.

A preliminary design of a composite subsonic transport wing was developed, based around a mid-size, twin-aisle aircraft. The benchmark design includes the leading and trailing edge structures and the center box inside the fuselage. Wing masses were included as point loads, and fuel loads were incorporated as distributed loads. The side-of-body boundary condition was modeled using high stiffness springs, and the aerodynamic loads were applied using an approximate point load scheme. The entire wing structure was modeled using the finite element code ANSYS to provide the internal loads needed as boundary conditions for the wing panel analyzed by WINGJOTA.

The software package WINGJOTA combines the composite bolted joint analysis, a composite plate finite element analysis, a wing aeroelastic cycle, and two optimization algorithms to form the basis of a computer code for analysis and optimization. Both the Improving Hit-and-Run (IHR) and the Multi-Particle Simulated Annealing (MPSA) algorithms were coded and used as the optimization routines in WINGJOTA. It was found that MPSA was able to find panel designs with lighter weights than IHR; however, the computation time was longer.

TABLE OF CONTENTS

LIST OF FIGURES

LIST OF TABLES

NOMENCLATURE

a	Hole radius (joints); Half ξ-axis length of element (FEM)
a_{ij}	Compliance matrix (analysis)
$a_{ij\ sk}$	Compliance terms, skin laminate (analysis)
$\bar{a}_{ij}$	Effective compliance matrix (joints)
A, **A**	Laminate extensional stiffness matrix (analysis); Real constant (joints)
A_b	Area of the bolt (joints)
$A_{i,j}$	Aerodynamic load distribution area (wing design)
$\overline{AE}_{xx}$	Effective axial modulus (wing design)
Abf	I-stringer bottom flange area
As	Smeared I-stringer area
Atf	I-stringer top flange area
Aw	I-stringer web area
Ask	Skin area
AEi	Effective axial rigidity of I-stringer
b	Half η-axis length of the element (FEM)
bbf	I-stringer bottom flange width
btf	I-stringer top flange width
B, **B**	Laminate coupling stiffness matrix (analysis); Real constant (joints)
C	Correlation coefficient (joints)
C_{ij}	Elastic coefficients (elasticity)
C_{bs}	Shear effect of correlation coefficient (joints)
C_{bb}	Bending effect of correlation coefficient (joints)
C_{bbr}	Bearing effect of correlation coefficient (joints)
C_{pbr}	Plate bearing effect of correlation coefficient (joints)
CP_j	Chord-wise pressure distribution number (wing design)
d	Hole diameter (joints)
d_k	Direction vector (stochastic methods)
d_0^t, d_0^b	Tension and bearing characteristic distances (joints)
d_{11}^{bf}	Longitudinal bending stiffness of the I-stringer bottom flange
d_{11}^{tf}	Longitudinal bending stiffness of the I-stringer top flange
d_{11}^{sk}	Longitudinal bending stiffness of the skin
D, **D**	n-dimensional unit sphere centered at the origin (SA); Laminate bending stiffness matrix (analysis); Washer diameter (joints)
e	Edge distance (joints); Bow at the panel midlength due to imperfection (analysis)
E	Young's modulus
E_0	Minimum energy of a system (SA)
E_1	Energy of a state just above a nongenerate local minimum of a system (SA)
E_b	Effective bearing modulus (joints)
E_l	Young's modulus of the lth bolt (joints)
$E_{x\ sk}$	Effective skin laminate axial modulus (analysis)

$E_{x\ panel}$	Effective stiffened panel axial modulus (analysis)
E_p	Plate modulus (joints)
E_s	Strap modulus (joints)
E_b	Bolt modulus (joints)
E_{pbr}	Plate bearing modulus (joints)
E_{sbr}	Strap bearing modulus (joints)
E_{bb}	Bolt bending modulus (joints)
E_{bbr}	Bolt bearing modulus (joints)
E_p	Plate modulus (joints)
$\overline{E}_{xx}^{ex}$	Effective axial modulus (wing design)
$\overline{E}_{xx}^{fl}$	Effective flexural modulus (wing design)
$\overline{EI}_{xx}$	Effective bending stiffness (wing design)
E_1	Young's modulus in the direction of the load axis (joints)
E_2	Young's modulus in the direction normal to the load axis (joints)
Ebf	Axial stiffness of the I-stringer bottom flange
Es	Axial stiffness of the smeared I-stringer
Esk	Axial stiffness of the skin
Etf	Axial stiffness of the I-stringer top flange
Ew	Axial stiffness of the I-stringer web
f	Objective function (function to be minimized); Generic function
f*	Global minimum (or maximum) of objective function
f_v	Bolt shear strength (joints)
$\overline{\Delta f}^{(+)}$	Average increase in the objective function over a predetermined number of moves (simulated annealing)
F, **F**	External loads vector
$F_{i,j}$	Aerodynamic load distribution point force (wing design)
F_S	Cumulative distribution function of the safety ratio (reliability)
$F_{\pm 45}$	Longitudinal tensile strength of ±45° plies
F_{max}	Initial objective function value
g	Arbitrary negative number (SA); Acceleration of gravity
$g_j(\mathbf{x})$	Inequality constraints
G	Shear modulus (analysis; joints)
G_b	Bolt shear modulus
G_l	Shear modulus of the lth bolt (joints)
h	Web height (joints); Plate thickness (FEM)
$h_k(\mathbf{x})$	Equality constraints
hw	I stringer web height
i	Index; $\sqrt{-1}$; Line number of the aerodynamic load node index (wing design)
I	Identity matrix
Im	Imaginary portion of a complex number
I_b	Moment of inertia of the bolt (joints)
I_{bf}	Moment of inertia of the I-stringer bottom flange
I_{tf}	Moment of inertia of the I-stringer top flange
I_{sk}	Moment of inertia of the skin

IEi	Effective flexural rigidity of the I-stringer and skin section
IEs	Effective flexural rigidity of the smeared I-stringer and skin section
j	Index; Local bolt axis direction index (joints); Chord number of the aerodynamic load node index (wing design)
J	Jacobian matrix (FEM)
k	Index
k_{gross}	Magnitude of the stress concentration in an anisotropic tensioned plate with a hole (joints)
K, **K**	System stiffness matrix (FEM)
K_p, K_s	Plate and strap constants (joints)
K_{tb}	Bearing stress concentration factor (joints)
K_{tc}	By-pass stress concentration factor (joints)
K_{te}	Elastic stress concentration factor (joints)
l	Lower limit of design variables (SA)
L	Pin load (joints); Panel length (analysis)
LP_i	Span-wise pressure distribution number (wing design)
m	Number of load cases
M, **M**	Specified number of successive iterations in which f does not change (SA); Moment resultants (analysis)
M^{max}	Maximum bending moment (analysis)
M	Move set (stochastic methods)
MS	Margin of safety
MTOGW	Maximum take-off gross weight (wing design)
n, **n**	Number of design variables; Local axis perpendicular to external boundary of joint (joints); Number of plies
n_e	Number of equality constraints
n_g	Number of inequality constraints
n_p	Number of problems to be evaluated (benchmarking)
n_s	Number of solvers (algorithms) to be evaluated (benchmarking)
nip	Number of integration points (FEM)
N, **N**	Stress resultants (axial, transverse, and shear) (analysis)
N_i	Number of bolts in ith row (joints)
N_i^{cr}	Critical buckling stress resultant (axial, hoop, or shear) (analysis)
N_i^{max}	Maximum allowable axial, transverse, and shear loads for first ply failure (analysis)
N_{xE}	Euler buckling load for a panel (analysis)
$N(\omega)$	Nonlinear term, equilibrium equations (FEM)
nbr	Number of bolt rows in the joint (joints)
p, **p**	Index; Member of the set of problems (benchmarking); Fastener pitch (joints)
P, **P**	Probability; Uniform lateral pressure (analysis); Set of problems (benchmarking)
PSF	Probabilistic Safety Factor (reliability)
P_t	Tensile load in the fastener (joints)
P_T	Target probability of failure (reliability)

P_{T_k}	Acceptance probability (SA)
q	Transverse loading (FEM)
Q, **Q**	Global laminate reduced stiffness matrix (analysis)
$\overline{Q}$	Local laminate reduced stiffness matrix
$\mathbf{Q}_j$	Virtual-load vector
r	Distance along radial direction (joints); Index; Number of bolts (joints)
r_c	Characteristic curve (joints)
$r_{p,s}$	Performance ratio of CPU time for problem p with solver s (benchmarking)
R, **R,** $\mathbb{R}$	Set of real numbers; Hole radius (joints); Strain ratios (joints)
R_{0t}, R_{0c}	Characteristic lengths for tension and compression (joints)
R_i	Load in individual bolt (joints)
R_l	Bolt radius (joints)
Re	Real number portion of a complex number
RAN	Random number
s, **s**	Member of the set of solvers (algorithms) (benchmarking); Roots of the characteristic equation (joints); I-stringer stringer pitch (analysis)
S	Design space or feasible region; Set of solvers (algorithms) (benchmarking); Shear strength (analysis, joints)
S^{actual}	Actual shear strength values from structural analysis (analysis)
S_C	Cross-ply laminate shear strength (joints)
t	Total joint laminate thickness (joints); Per ply thickness
$t_{p,s}$	CPU time required to solve problem p with solver s within ε (benchmarking); Thickness, plate and strap (joints)
$t_{sk,\ st}$	Skin and stiffener laminate thicknesses (analysis)
t_0	Thickness contribution of the 0º plies in a laminate (joints)
t_{45}	Thickness contribution of the ±45º plies in a laminate (joints)
t_{90}	Thickness contribution of the 90º plies in a laminate (joints)
tbf	I-stringer bottom flange thickness
ttf	I-stringer top flange thickness
tweb	I-stringer web thickness
tsk	I-stringer skin thickness
T	Temperature (control parameter) (SA); Applied torque (joints)
T_0	Starting temperature (SA)
u, **u**	Upper limit of design variables (SA)
u_i	Displacement vector components (FEM)
U_i	Material invariants (analysis)
U_{z1}, U_{z5}	Vertical displacement of the wing leading and trailing edges (wing design)
V	Geometric factors (analysis)
V_f	Fiber volume fraction of a laminate
w, **w**	Candidate points (optimization); Joint width at the net section (joints)
w_i	Weighting coefficients (FEM)
w(t)	Standard Brownian motion (SA)
W/S	Wing loading (wing design)
x, **x**	Distance along x-axis (joints); Vector of design variables with components x_i, i = 1, …, n; Local (bolt) x-axis (joints); Fiber angle

$\mathbf{x}^*$	Local minimum variable vector (stochastic methods)
$\hat{x}$	Incumbent (best) solution (stochastic methods)
x_c	Global x-axis coordinate of the center of the element (FEM)
X, **X**	Iteration points (stochastic methods); Global axis; Critical axial stress (analysis, joints)
X^{actual}	Actual axial strength values from structural analysis (analysis)
X_l	Local (and global) (bolt) x-axis center point (joints)
X_1, X_5	Chord-wise coordinate of the wing leading and trailing edges (wing design)
X_T, X_C	Longitudinal tensile and compression strength (analysis)
y, **y**	Local (bolt) y-axis (joints)
y_c	Global y-axis coordinate of the center of the element (FEM)
Y	Candidate points (stochastic methods); Global axis; Critical transverse stress (analysis, joints)
Y^{actual}	Actual transverse strength values from structural analysis (analysis)
Y_T, Y_C	Transverse tensile and compression strengths (analysis)
z_1, z_2	Points in the complex plane (joints)
zb	Centroid of the I-stringer cross-section
α	Cooling schedule constant (SA);
α_{root}	Angle-of-attack at the wing root (wing design)
α_{root_ref}	Reference angle-of-attack at the wing root (wing design)
β	Cooling schedule parameter; acceptance probability function (SA); Local laminate axis index (joints)
β_j	Angle of rotation of chord j relative to the root chord (wing design)
γ	Shear strain (analysis); Plate and strap constant for non-constant correlation coefficient bearing-bypass load calculation (joints)
Γ^e	Element perimeter or boundary (FEM)
δ	Distance parameter (SA); First arbitrary variation in the state variables satisfying the boundary conditions (analysis); Constant
Δ	Hole deflection (joints)
ε	Radius of hypersphere (IHR); Stopping tolerance (error) on bolted joint load analysis (joints); Strain
ε_b	Effective bearing strain (joints)
$\boldsymbol{\varepsilon^0}$	Midplane strains (axial, transverse, and shear; analysis)
ε_{max}	Maximum allowable strain (joints)
ζ_1, ζ_2	Conformal hole points in the complex plane (joints)
η	Natural coordinate of the ith node of an element (FEM)
θ	Fiber angle in laminates; Angle between the global and principal material coordinate systems (joints)
θ_f	Failure angle (joints)
κ, $\boldsymbol{\kappa}$	Stress failure criterion (joints); Midplane curvatures (axial, transverse, and shear; analysis)
λ, $\boldsymbol{\lambda}$	Constant
λ_k	Step size (IHR; SA)
μ	Coefficient of friction between fastener and hole (joints); Constant

ν	Index; Poisson's ratio (analysis)
ν_{12}	Principle Poisson's ratio (analysis; joints)
ξ	Natural coordinate of the ith node of an element (FEM)
π	Prescribed target distribution (SA)
ρ	Composite material density
ρ_b	Fastener material density
ρ_s	Probability of solver having a particular performance ratio (benchmarking)
σ	Stress; Standard deviation (stochastic methods)
σ_b	Bearing strength (joints)
σ_{b0}	0º constrained bearing strength (joints)
σ_C	0º longitudinal compression strength (joints)
σ_z	Transverse compressive stress (joints)
σ_N	Laminate notched strength (joints)
σ_{TC}	0º constrained transverse compression strength (joints)
σ_{b45}	±45º constrained bearing strength (joints)
σ^0	Laminate unnotched strength (joints)
$\bar{\sigma}$	Allowable stress (approximation); Effective stress (joints)
σ_1^{45}	Failure stress of 45° off-axis specimen in uniaxial test (joints)
τ	Shear stress; Performance ratio factor (benchmarking)
τ_N	Laminate notched shear strength (joints)
φ	Holomorphic function (joints); Percentage of ±45º and 90º plies contained in a laminate (joints)
φ_0	Holomorphic function for hole conformal mapping (joints)
ϕ, $\boldsymbol{\phi}$	Angle between global and local hole coordinate systems (joints); Holomorphic function (joints)
ϕ_0	Holomorphic function for hole conformal mapping (joints)
ϕ_i	Hermite interpolation functions (FEM)
χ	Constant
χ_0	Acceptance ratio (SA)
ψ_i	Lagrange interpolation functions (FEM)
ω	Rigid body rotation arbitrary constant (joints)
Ω^e	Element domain (area of element) (FEM)
∂D	Topological boundary of an n-dimensional unit sphere D (SA)
$[]^T$	Matrix transpose
$\mathcal{O}$	Order of
$( )_x$, $( )_y$	Quantity with respect to the global x- or y-axis (transverse and axial directions) (analysis; joints)
$( )_1$, $( )_2$	Quantity with respect to the lamina principal material directions (fiber and transverse directions) (joints)
$( )^0$ or $( )_0$	Initial values of a vector (IHR; SA)
$( )^\infty$	Remote or far field (joints)

ACKNOWLEDGEMENTS

I would like to express my deep appreciation and gratitude to my advisor, Professor Mark E. Tuttle, for his very dedicated guidance and mentorship he has provided to me through the years. His passion for teaching is apparent and benefited me greatly. His ability to challenge me in intellectual discussions on composite structures has certainly led to a greater understanding on my part. I look forward to continuing to work together professionally as friends and colleagues.

I would also like to thank Dr. William B. Avery who has been a friend and mentor to me since I met him some 15 years ago. The genesis of this dissertation came from discussions with him. I will continue to learn from him as long as I can.

I appreciate the extra work done by two of my committee members, Prof. Zelda B. Zabinsky and Prof. Ramulu Mamidala, in preparation of my dissertation. Thanks to Prof. Zabinksy for her teaching skills and guidance on the optimization portions of this research, which was a new subject for me. Prof. Mamidala has provided inspiration to me for a long time, and then was able to support this committee during this last quarter.

Thank you to the other members of the committee: Prof. Brian D. Flinn, who was also able to support me on short notice and provided excellent suggestions during the final defense; Prof. Steve Gribble, Computer Science, for some help with some (new to me) aspects of C++; and Prof. Ann Mescher, who served on my general exam committee.

Dr. Paul Labossiere, now at the University of Manitoba, and Prof. Keith Holsapple provided both understanding and insight into finite element analysis; I thank them both.

My graduate school learning began at the University of Illinois at Urbana-Champaign. I want to express my thanks to Prof. Scott R. White, who was my advisor for my MS. I know that my passion for advanced composite structures was inspired by a talk he gave our student section of the AIAA when I was still an undergraduate. Thank you to Prof. Nancy R. Sottos who sparked my interest in teaching at the college level.

I want to express my love and gratitude to my father, Robert “Doc”, for his encouragement, support, and lessons on car repair and “how stuff works”. No one pushed me harder than my stepmother, Marcia, who made me carry my math book home from school every day; I know she’s still pushing.

My mother, Susan, deserves thanks for her unwavering, absolute belief in me. Thank you to my stepfather, Greg, for his support and discussions on politics and history.

Finally, I have to thank my wife, Suzanne, for carrying far more than her fair share during the final leg of this degree.

DEDICATION

To my wife Suzanne for her constant love and support

To my daughter Kaylee and my son Jack for their inspiration

Chapter 1

INTRODUCTION

New commercial transport aircraft such as the Boeing 787 and the Airbus A350XWB have generated increased interest in structural composites for these aerospace applications. Walt Gillette, former Boeing Vice President of Engineering, Manufacturing and Partner Alignment has said that "everyone will see benefits of this technology [composite structures] -- Boeing and our partners, our customers and the flying public. By integrating this [fuselage] into a single composite structure, we reduced the number of parts in this section significantly and reduced the weight by almost 20 percent. That will mean lower costs for the airlines while for passengers it enables us to have bigger windows, lower cabin altitude pressurization, and higher cabin humidity." [1]. Boeing estimates a 19:1 part count reduction where composites replace aluminum, reducing the cost of the aircraft [2]. The Boeing 787 uses Torayca T800S/3900 epoxy prepreg to produce the empennage, unpressurized aft fuselage skins and stringers, the center fuselage, the mid-fuselage and aft wheel well bulkhead, the forward fuselage, floor beams, and cargo, access, and passenger doors. It is also used for the wings: the center wing box, fixed trailing edge, and the main wing box (skins, stiffeners, and spars). Other composite materials are used for the large window frames, highly loaded gussets, pressure pans, clips, brackets, engine nacelles, movable trailing edge control surface components, wing leading edge structures, rear pressure bulkhead, and main landing gear braces. Fifty percent of the 787's structural weight is composed of composite materials [3-4]. Aerospace companies continue to push new structural composite applications to improve both aircraft performance and cost in addition to decreasing the environmental impact of greenhouse gas emissions [5-12]. New design standards are being developed for aircraft primary structures manufactured from advanced composite materials.

The revolution in the use of advanced composite materials for transport aircraft primary structure calls for improved methods for design and analysis. During the preliminary design stage of aerospace vehicles the configuration is defined and the materials chosen. The next task is to determine the structural sizes that will provide an optimal structure while satisfying the many constraints imposed by multiple engineering disciplines on the structure [13]. It is well known that preliminary design decisions have a significant impact on overall system capability and total cost [14]. At the same time, the most complete and accurate detailed analysis codes are too computationally expensive for iterative applications [15].

Structural optimization (via mathematical programming and optimality criteria) of composite aircraft wings, both military and commercial, has been performed since the late 1960's. The structural optimization problem is to select optimal values of the design variables such that the specified objective function is minimized and a set of specified constraints are satisfied [16]. There have been many applications and associated algorithms developed to size a structural wing box for minimum weight [17-21]. Research on structural optimization of transport aircraft

composite fuselages has also been performed by the University of Washington Optimal Design of Composite Structures Group during the 1990's for the development of COSTADE [22-25].

Despite much research into optimization of composite structures, there has not been much work in the area of composite joint optimization for minimum weight. A common methodology for designing a composite structure is to size the joints first, and then size the remaining structure. This is done because ply-drop rules and other manufacturing constraints cause the joint to become the design driver in many instances. Local detailed joints that could be considered include spar caps to skin, ribs to spars, ribs to skins, etc.

Previous efforts in composite wing structural optimization focused on various aspects of wing design. Generally the research was concerned with a single aspect of the design, such as structures with a goal of natural frequency optimization. Other research was about the lay-out of the wing (topology) and made use of structural homogenization methods. Aeroelasticity, including flutter, was sometimes also used as part of the optimization. Still other work was related to manufacturing constraints and costs. Combinations of these aspects were combined in different ways as well, with the goal of producing a feasible wing design. However, very often these preliminary wing plan forms were either too simple or proprietary to the group performing the optimization to be really useful in the research community. Many academic optimizations were performed on square wings in which the components were connected by nodes only; no joint behavior was considered.

This thesis explored three areas of composite wing design. First, a composite bolted joint analysis was developed that could be computationally evaluated quickly. Chang et al. [26] developed an approach to the failure prediction of bolted composite joints. The method is well suited for parametric studies and design optimization as it is a two-dimensional approach. However, it relies on a finite element formulation to determine the stresses around the holes in the joint. This would likely be too computationally expensive for this optimization algorithm. In this study an analysis based on the work of Savin [27] is used to develop the stresses around the holes in the joint. The failure criterion of Yamada and Sun [28] is then applied at the characteristic distance [29] away from the hole edge. This serves as a constraint in the optimization problem.

Second, a benchmark composite subsonic transport wing design was created, based around a mid-size, twin-aisle aircraft. The benchmark design includes the leading and trailing edge structures and the center box inside the fuselage. Masses of the power plant, landing gear, control surfaces, fixed surfaces, and the wing tip were included. Fuel loads were determined and incorporated as distributed loads. The side-of-body boundary condition was modeled using high stiffness springs, and the aerodynamic loads were applied using an approximate point load scheme. The entire wing structure was modeled using the finite element code ANSYS to provide the internal loads needed as boundary conditions for the wing panel analyzed in this study.

Third, a software package named Wing Joint OpTimization and Analysis (WINGJOTA) combines the composite bolted joint analysis, a composite plate finite element analysis, a wing aeroelastic cycle, and two optimization algorithms to form the basis of a computer code. Both the Improving Hit-and-Run (IHR) and the Multi-Particle Simulated Annealing (MPSA)

algorithms were coded and used as the optimization routines in WINGJOTA. The IHR algorithm has been applied to the optimal design of a composite stiffened panel in the past [30-33]. These analyses were always around the particularities of a transport aircraft fuselage structure (thinner structures, blade and hat stiffeners, curved shells, etc.). Here I-cross-section stringers are used with a new stiffness smearing procedure along with the bolted joint analysis. The MPSA algorithm has not been used for composite structural optimization and is applied here [34]. The main feature of MPSA is the ability to simultaneously optimize over a large number of particles. Also, because of the nature of aerodynamics, the optimization algorithm is combined with the aeroelastic cycle [35] of aerodynamic loads, structural stiffness, and the updated structural design. Optimal designs from 14 load cases applied to a single wing sub-panel are presented.

The rest of the dissertation is organized as follows. Chapter 2 presents a review of the literature for structural optimization, stochastic optimization, composite structural analysis, including bolted joints, and wing analysis and design development. The composite bolted joint analysis and the other structural constraints used in this work are discussed in Chapter 3. Chapter 4 describes the benchmark composite wing design. Extensive finite element modeling in ANSYS was performed, at the element, sub-component, and full wing scales. All of the initial bolted joints in the wing are also described in this chapter. The WINGJOTA software package is described in detail in Chapter 5. Chapter 6 presents the results of the composite wing panel optimization for 14 load cases. A summary and suggestions for possible future work are presented in Chapter 7.

Chapter 2

LITERATURE REVIEW

2.1 Structural Optimization

Until the 1960's the vast majority of engineering research was focused on developing analysis capability (loading leads to stress, displacement, natural frequencies, etc.). However, there was some design synthesis development in the form of fully stressed and simultaneous failure modes from the late-19th century through the 1950's. The limitation of these methods became known with the arrival of the modern, digital computer (commercially in 1951 [36]). Optimization approaches can be divided into two categories, those that are generally applicable and those that are specific to structural optimization. Specific methods, such as fully stressed design, and mathematical programming methods of specialized form, such as dynamic programming and optimal control theory, have been shown to have limited use. Mathematical programming and optimality criteria approaches are extensively used in structural optimization [37]. Establishing a set of necessary and sufficient conditions for an optimum, and then constructing an algorithm that systematically leads to a solution that satisfies such conditions usually solve the optimization problem. The uncertainty about the nature of the absolute optimum and the computational efficiency of different procedures applied to different applications has fostered the development of numerous optimization algorithms and methods [38].

The structural design approach or philosophy must be determined *a priori* for a given optimization problem. The design should be classed as deterministic or probabilistic, the types of failure modes (any structural behavior characteristic subject to limitations) to be controlled identified, and differentiation between the service (limit) loads and overload (ultimate) loads [39]. If any of the quantities involved in the structural design are to be treated as random variables then it is a probabilistic problem. If all the quantities are treated as deterministic, then it is so classified. Types of failure modes include buckling, yielding, maximum strain, delamination, etc. A loading condition is one of several distinct sets of mechanical and thermal loads that approximately represent the effect on the structure of the environment to which it is exposed [36]. It may be that the limit and ultimate loading conditions have different failure modes. A design approach can be determined from these considerations [16].

Design variables are those quantities defining a structural system that are varied by the design modification procedure. Those quantities describing a structural system that are fixed at the outset of an optimization process are called preassigned parameters [36]. These quantities together describe the structural system under consideration. There are five basic types of design variables in structural optimization: the type of structure, topology or general arrangement, materials utilized, the geometry or configuration of the structure, and the physical dimensions of the structural elements [40]. Further, there are two classes of design problems: system design

and performance are specified by a finite number of design variables (finite domain), and systems that are described by functions on some given space domain (infinite domain) [41]. It is also important to distinguish between continuous and discrete design variables.

In a design space, the coordinates of a point define a structure by specifying all geometrical dimensions and material constants. A properly posed optimization problem is always restricted to a design subspace, i.e., commercial transport wing structure and polymeric matrix composite materials [42]. A feasible design is one that meets all the requirements imposed on it. These requirements or restrictions that must be satisfied are called constraints [16]. Side or technological constraints impose geometric requirements for design variables. Behavior constraints impose failure mode requirements. The set of points that satisfies all of the side and behavior constraints in the design space is called the feasible region [36].

The selection of the objective function can be one of the most important activities in the structural optimization process. The objective function (also the called the cost, criterion, or merit function) is the function of design variables that provides a basis for choice between alternative acceptable designs [36] and whose minimum or maximum value is sought in an optimization procedure. If the function is relatively "flat" it is insensitive to variations in the design variables and optimization process, and therefore will not be useful to an optimization algorithm to improve the design except locally to the optimum. To avoid this issue a multicriterion objective function can be formulated. In the method of objective weighting each individual criterion is multiplied by a constant reflecting its relative importance [43]. Alternatively, the most important criterion is selected as the only objective function and limits are imposed on the other criterion [16].

The structural optimization problem is to minimize a specified objective function by selecting optimal values of the design variables such that a set of specified constraints are satisfied [16]. The standard mathematical formulation is given as

$$\text{Minimize } f(\mathbf{x}) \tag{2.1a}$$
$$\text{Such that } g_j(\mathbf{x}) \geq 0,\ j = 1, \ldots, n_g \tag{2.1b}$$
$$h_k(\mathbf{x}) = 0,\ k = 1, \ldots, n_e \tag{2.1c}$$

where f denotes the objective function (function to be minimized); $\mathbf{x}$ is the vector of design variables with components x_i (i = 1, …, n, the number of design variables); $h_k(\mathbf{x})$ are the equality constraints, and $g_j(\mathbf{x})$ are the inequality constraints [37]. An inequality constraint is said to be active or binding at a feasible point when it is an equality, and inactive if it is not [44]. This problem is solved mainly by the use of iteration procedures in which each step is designed to provide a better solution. These iteration procedures are methods of mathematical programming [42].

For optimization problems with only inequality constraints the nested approach is generally used. Here the structural analysis is nested inside the optimization procedure, and is repeated for a sequence of trial designs. The simultaneous analysis and design (SAND) or integrated formulation can be used in cases where it is impractical to eliminate equality constraints [45], [46]. As the name implies, the analysis and design procedures are integrated and performed at

the same time; repeated nonlinear analyses are not required where the SAND formulation is used. However, this approach is generally not used in problems involving elastic analysis models [16].

2.1.1 Historical Development of Structural Optimization – Early Work

Classical methods for minimum weight layout of highly idealized frameworks (Geometrical Optimization) were initially developed by Maxwell [47] and later by Michell [48]. Aircraft structural components were optimized mathematically for weight beginning during World War II. The simultaneous failure mode design optimization method was used, where the component is sized such that several of the failure modes become critical at the same time [49-51]. Mathematical programming techniques developed in the operations research community were applied to problems in civil engineering during the 1950's [52-54] and led to the development of structural synthesis [55].

During the 1960's progress was made along two main lines: component-type problems of fundamental and recurring nature, and first-generation, system-level structural synthesis programs based on mathematical programming. Component-type problems were characterized by a small number of design variables, a variety of complex failure modes and loadings, and, in some instances, objective functions other than weight [36]. In 1965 Fox proposed a method of generating constraint surface normals using approximations to the stiffness matrix [56]. Haug et al. provide a mathematical theory of structural design sensitivity analysis [57]. The differences between fully-stressed design and structural synthesis was made apparent by Razani [58], who provides an optimality test for a fully-stressed design and, to further refine the design, a means of using an optimal search on free variables to produce the optimal design. Fully stressed design methods are based on stress ratio-type recursive redesign rules for modifying member sizes at each iteration so as to make the maximum stress in each member equal to the allowable stress while assuming no force redistribution. However, a fully stressed design does not necessarily reflect a minimum weight design.

By the end of the decade it was apparent that mathematical programming could not be efficiently applied to realistic structures due to limitations on computing power. As a result, the optimality criteria approach was developed by Prager et al. [59-60] (analytical forms) and Venkayya [61] (numerical forms), among others. This approach establishes the criteria that defines an optimum point (optimality condition) and then develops a recursive algorithm that meets that criterion [62].

The structural optimization field was therefore divided into two groups; one focused on implementation of redesign procedures based on fully-stressed design concepts and discretized optimality criteria, and the other attempted to improve the computational efficiency of the mathematical programming approach. Design oriented structural analysis methods were developed based on finite element structural systems. These can be placed in three main categories, 1) sensitivity analysis, i.e., methods for obtaining rates of change of response quantities with respect to design variables, 2) techniques for repetitive reanalysis using Taylor series expansion, reduced basis, iteration, or combinations of these [63], and 3) rapid iterative

reanalysis using a linear approximation to the generalized stiffness and inertia matrices for a finite element analysis using the direct stiffness approach [64]. A renewed interest in mathematical programming was seen with the introduction of formal approximation concepts [65] in the mid- to late-1970's.

It was not until the late 1970's that duality theorems for nonlinear programming were used to show equivalency of the optimality criteria and mathematical programming approaches to optimization. This was based on earlier work in nonlinear programming [66-67]. Fleury [68-69] showed that both the optimality criteria and mathematical programming approaches to structural optimization are based on solving a sequence of explicit problems. The main difference between these approaches lies in the way the gradients of the constraints are defined; the optimality criteria method generally takes into account a small number of critical constraints (active constraints), in which case the virtual load procedure is the most efficient way of obtaining gradients. Most mathematical programming methods use the gradients of all the stress and displacement constraints, and the pseudo load technique is employed. Another difference is in the solution algorithms used. Optimality criteria methods rely on the dual methods of convex programming, where the unknowns are the Lagrangian multipliers associated with the constraints. Primal methods, such as projection and feasible direction methods, are generally used in mathematical programming.

Schmit and Fleury [70] demonstrated the use of dual methods and approximation concepts to develop an improved structural synthesis method. In this approach most of the computational effort is put towards finding the maximum of the dual function, subject only to simple non-negativity constraints on the dual variables. The algorithm finds the maximum by operating in a sequence of gradually increasing dimensional dual subspaces such that the problem never exceeds the number of critical constraints by more than one. This reduces the number of stages needed to converge the overall iterative design process and resolves two of the main difficulties with optimality criteria methods.

Capable structural optimization software tools were developed during the 1970's by industry, academia, and the United States government. These included CONMIN (CONstrained function MINimization) [71], ASOP (Automated Structural Optimization Program) [72-74], VIPASA (Vibration and Instability of Plate Assemblies including Shear and Anisotropy) [75-79]; and STAGS (STructural Analysis of General Shells) [80] in the aerospace field.

The basic program structure of structural analysis is as follows [62]:

1. Finite element analysis of the initial proposed design.
2. Evaluation of all the constraint functions and ranking of them according to criticality. Only the actual and potential critical constraints are retained during the current design cycle.
3. Calculation of the gradients (sensitivities) of the current retained set of constraints.
4. Construction and solution of the approximate optimization problem using the gradients.
5. Evaluate the quality of the proposed new design by updating the data and reanalyzing. Terminate the loop if the solution has converged to an acceptable optimum point. Otherwise, repeat from step two.

This structural optimization approach is shown in Figure 2.1, and it consists of an outer loop (design cycle) and an inner loop (optimization iteration). Each design cycle includes analysis, constraint deletion, sensitivity calculations, and an optimization iteration. The inner loop consists of an approximate analysis and a run through the optimizer to solve the approximate problem. There are two keys to efficient structural optimization: the creation of high quality, appropriate approximations that reduce the number of design cycles necessary for convergence, and the ability to rapidly analyze the approximate functions to reduce the cost of the optimization iteration [62].

2.1.2 Historical Development of Structural Optimization – 1979-1992

During the 1980's research focused on making the approach outlined above more efficient. Existing optimization methods were refined during this period, leading to a second generation of approximation methods. The overall efficiency and reliability of the optimization process is dependent upon the concept of using intermediate variables and responses to create a high quality approximation. Using intermediate variables that are more complex functions of the original design variables reduces the number of variables. Similarly, using intermediate responses rather than the original responses during sensitivity calculations cuts down on calculation time. Second generation approximation methods are often more efficient and reliable than previous methods [62].

Methods of local optimization continued to be developed. The Interior Method, extending Karmarkar's Method, was an improvement on the Simplex Method and allowed for the solution of large linear programming problems [37]. However, the emphasis during this time began to shift from local to global optimization. There are two basic approaches: deterministic and probabilistic or stochastic. An example of a deterministic global optimization algorithm is the use of Interval Optimization, which uses interval-valued functions called inclusion functions. Although first introduced by Moore in 1966 [81], it did not become practical until this time period (proof of convergence and further adaptations [82-83]).

Probabilistic algorithms search for the global optimum through the generation of random points in the design space. Random searches are easily coded and are often robust, i.e., they may not be sensitive to the irregularities of the objective function. These types of algorithms are recommended for problems with computationally inexpensive objective functions, although they can be applied to problems with expensive functions [84]. Pure Random Search was introduced in 1958 ([85]), and the algorithms improved throughout the 1970's and 1980's. Sequential Random Search was developed to improve the effectiveness of a search routine by using successive accumulation [86]. Computational results of these methods are generally better than those of the deterministic methods [87].

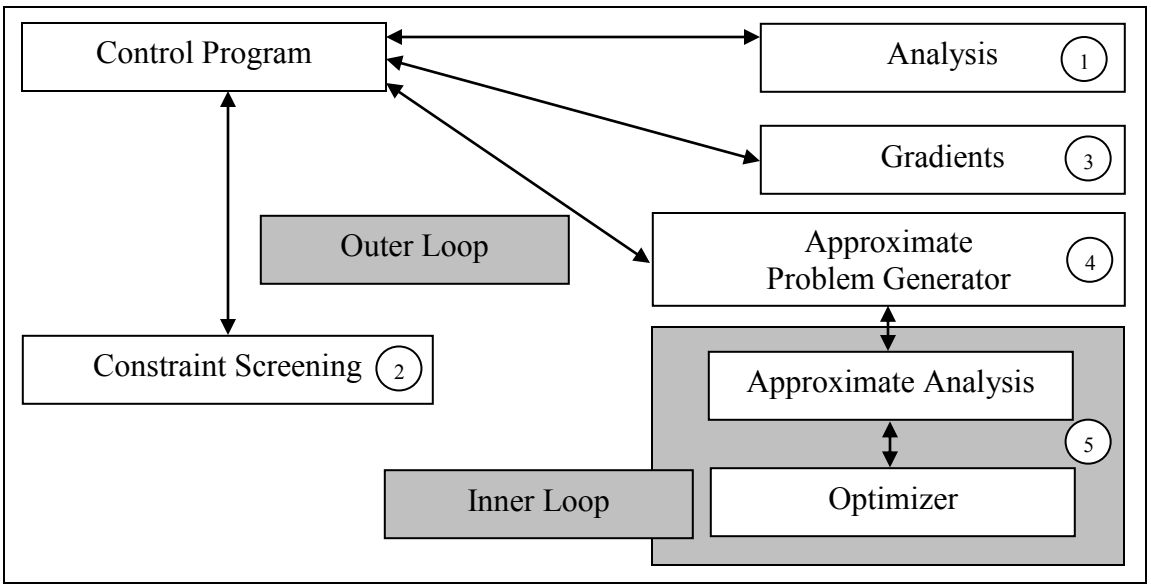

Figure 2.1: Typical Modern Structural Optimization Approach (after [62])

Simulated Annealing (SA) is a global, probabilistic optimization technique that utilizes an analogy first described by Metropolis et al. in 1953 [88] to describe the physical annealing process. Pincus [89] used this analogy for an algorithm to solve continuous global optimization problems with discretization. However, it was not until the 1980's that SA was applied to combinatorial optimization applications, for example, the design of complex, integrated circuits to minimize interference among their connecting wires [90], and the traveling salesman problem [91-92]. The theory of SA, including proofs of asymptotic convergence, was explored by van Laarhoven and Aarts [93] and Dekkers and Aarts [94]. Collins et al. [95] published an annotated bibliography in 1988 that referenced in particular the types of cooling schedule used. The basic idea is to find a neighborhood and sample; accept some increasing values to move into another neighborhood; reduce the "temperature" according to a cooling schedule; and move towards the global optimum.

Evolutionary Computation (EC) is a family of global, probabilistic optimization techniques that rely on Darwin's theory of evolution [96] and biology for their basis [97]. Genetic Algorithms (GA), Evolution Strategies, Evolutionary Programming, Differential Evolution, and Cultural Algorithms [98] are examples of EC paradigms. Based on work first performed in the 1950's and 1960's, GA's were described in a classical sense by Holland in 1975. The Fundamental Theorem of GA or the Schema Theorem (GA's focus on promising regions at exponentially increasing rates) and the Principle of Minimal Alphabets (implying it is better to select the smallest alphabet, which is binary) are discussed [99]. During the 1980's their use grew greatly, being applied to optimization problems like wire routing, scheduling, adaptive control, game playing, cognitive modeling, the transportation and traveling salesman problems, and optimal control [100]. However, issues with the Fundamental Theorem, cardinality, and the No Free Lunch theorem for the classical GA were discovered and addressed in late 1980's and early 1990's. Additional capabilities were added to classical GA as well, including handling of

discrete problems and constraints [101] and the exploitation of the inherent parallel nature of GA [102].

During the 1980's private industry and the United States government, often jointly, developed many structural optimization tools. For the aerospace industry these include PASCO (Panel Analysis and Sizing Code) [103-104]; POSTOP (Postbuckled Open-Stiffened Optimum Panels) [105-106]; ADS (Automated Design Synthesis) [107]; DOT (Design Optimization Tools) [108]; PANDA2 [109-114]; and ASTROS (Automated Structural Optimization System) [13].

2.1.3 Historical Development of Structural Optimization – 1992-present

Global optimization for constrained problems became an area of active research two decades ago. Most of the deterministic, mathematical programming optimization methods up to this time were efficient at finding the optimal point of a unimodal objective function. Multimodal functions, as are often found in structural optimization, were more difficult to optimize. Also, no general criterion like the zero gradient criterion for local minimum exist for the global minimum [84]. One way to find a global minimum is to randomly restart the optimization at multiple initial points; however, as the number of design variables increases this approach becomes increasingly computationally expensive. This problem gave rise to stochastic or probabilistic optimization algorithms that were, by design, global in nature [37].

The theory associated with the computational complexity of algorithms is called complexity theory, and was originated by Hartmanis and Stearns in 1965 [115]. At issue is the efficiency of a given algorithm to solve a given problem, e.g., the ability to solve a nonlinear optimization problem in polynomial time versus exponential time. Nemirovsky and Yudin [116] studied complexity in relation to convex problems. Vavasis [117-118] has found that running time grows exponentially with the degree of nonconvexity. Another facet of global optimization was shown by Stephens and Baritompa [119], and that is that "global optimization requires global information". For both deterministic and stochastic algorithms a guarantee of finding the global optimum value does not exist. Algorithms must be designed for specific real-world problems and utilize nonlocal information, such as the Lipschitz constant of the function on a domain subset.

Stochastic algorithms continued to be developed and expanded to more areas of research. Improving Hit-and-Run (IHR) was formulated by Zabinsky et al. [120] and shown to be adaptable to mixed continuous and discrete variable problems, such as for composite structures [121]. The algorithm can be compared to SA by formulating it with a constant temperature of zero. Similarly, SA was formulated for use in constrained and mixed domain global optimization problems. Ingber [122] provided a summation of the applications and variations on the basic SA algorithm in 1993. Applications include the traveling salesman problem [123], circuit design [90], neural networks [124], biology [125], geophysics [126], financial systems [127], and military tracking problems [128]. Romeijn and Smith published two major papers in 1994 that described a new algorithm called Hide-and-Seek that is based on SA but uses an adaptive cooling schedule [129-130]. This new algorithm, as well as hit-and-run [131] and IHR, was used to produce a reflection generator to reduce the occurrence of "jamming" in global

optimization algorithms by Romeijn et al. [132]. This resulted in improved performance for the mixed global optimization of composite structures.

Additional research into GA also continued. Ingber and Rosen [133] compared GA to Very Fast Simulated Reannealing (VFSR) [134], an improved SA technique. It should be expected that there are systems for which one of GA or SA will be better suited than the other; however, they found strong evidence that VFSR can be expected to be much more efficient than GA. Fox [135] provided an integrated algorithm called probabilistic tabu search [136-138] with attraction and spatial memory that combines SA, GA, and tabu search. This accelerates the original SA algorithm by the use of intelligent moves by taking advantage of temporal and spatial memory. Koehler [139] began to question the fundamental theories behind GA (the Fundamental Theorem of GA and the Principle of Minimal Alphabets [99]) in light of new No Free Lunch theorems [140-141]. A new, sound theoretical framework for GA called the Simple Genetic Algorithm was formulated, primarily by Vose [142]. An overview of EC for multimodal function optimization was given by Roy and Parmee [143], where the strengths and weaknesses of various EC techniques. They tout Adaptive Restricted Tournament Selection as being useful as it does not require prior knowledge of the problem.

Growing out of EC and research into both aggregate motion (flocking behavior) and particle systems for computer graphics, Particle Swarm Optimization (PSO) was described in 1995 by Kennedy and Eberhart [144-145] as a method for optimization of continuous nonlinear functions. It is also related to EC. The basic algorithm was modified (improved convergence and diversity of the swarm) and applied to structural optimization in later years. Reynolds [146] and Heppner and Grenander [147] both provide computer simulations of the movement of flocks of birds. Further, the particles in the algorithm act more akin to a swarm than a flock, displaying five basic principles of swarm intelligence (proximity and quality principles, diverse response, and the principles of stability and adaptability) [148]. Particle systems, as described by Reeves [149], are composed of mass-less and volume-less "points" that have velocities and accelerations. These are the characteristics that make PSO unique.

Two papers presented at the 9th AIAA/ISSMO Symposium on Multidisciplinary Analysis and Optimization Conference introduced PSO into structural optimization applications for aerospace vehicles. Schutte and Groenwold [150] used it for the design of truss structures and therefore introduced stress and displacement constraints during the initial stages of the swarm searches. Venter and Sobieszczanski-Sobieski [151-152] took PSO a step further by applying it to the multidisciplinary optimization of a transport aircraft wing. Joints were not considered; however, they did perform a bi-level optimization where aerodynamic optimization is performed at the system level and the structural optimization is considered as a sub-problem. Their results were encouraging.

The American Institute of Aeronautics and Astronautics (AIAA) Technical Committee on Multidisciplinary Design Optimization (MDO) published a white paper in 1991 that developed the need for MDO for aerospace vehicles, reviewed current state-of-the-art, and pointed the way forward for producing "a systematic and mathematically-based" technology referred to as MDO [153]. MDO can be described as "a methodology for the design of systems in which interaction between several disciplines is considered and there are design variables that directly affect more

than one of the disciplines" [152]. Sobieszczanski-Sobieski and Haftka wrote a comprehensive review article in 1997 specifically on aerospace MDO, covering mathematical components, and simultaneous aerodynamic and structural, and structural and control optimization [154]. The development of advanced aerospace systems through distributed design discipline teams was the subject of a 2001 paper by Morris [155]. A related methodology is Multi-Objective Optimization (MOO), where instead of a single objective function and multiple constraints a collection of objective functions are systematically and simultaneously optimized. This is also known as vector optimization and was reviewed by Marler and Arora [156].

Another area of active research in the last decade is that of semi-infinite programming (SIP) and semidefinite programming (SDP). SIP deals with optimization problems where either the decision variables or the constraints are finite, but not both. Therefore, it occupies an intermediate position between mathematical programming and fully general optimization or infinite programming. Applications included operations research, optimal control, economics, game theory, and air pollution control (free boundary value problems) [157]. More recently Geletu and Hoffmann [158] solved generalized SIP's by the integral global optimization method, continuing ten years of work on SIP's with one semi-infinite constraint where the index set depends on the variable to be minimized. Research in SDP was revived along with an interest in convex analysis during the 1990's. SDP can be viewed as an extension and generalization of linear programming, the difference being that SDP is considered over a nonpolyhedral convex (positive semidefinite) cone [159]. Ben-Tal and Nemirovski [160] applied SDP to the structural optimization problems of truss and shape design.

Metamodeling techniques, such as response surface methodology [161-162], kriging [163-164], polynomial regression [165-167], multivariate regression splines, and radial basis functions continued to be built upon and expanded for structural optimization [168]. These approaches attempt to reduce the computational requirements of a large multidisciplinary optimization problem by "modelling the model". They have been used extensively for aerospace vehicle structural optimization [169, 154].

Structural optimization software development during this time was again driven by the United States government with researchers drawn from private industry and academia. VICONOPT (VIpasa with CONstraints and OPTimization) was put forward as a development of VIPASA and VICON by Williams et al. [170] and Bulter and Williams [171]. Designed as a composite optimization routine for buckling and vibration of plates [172-174], it was used by Fischer et al. for the multilevel optimization of a composite aircraft wing [175].

The National Aeronautics and Space Administration (NASA)/Boeing Advanced Technology Composite Aircraft Structures (ATCAS) program spawned another major software code, the Cost Optimization Software for Transport Aircraft Design Evaluation (COSTADE) tool. It is a multidisciplinary structural analysis and optimization tool that includes cost, weight, design, stress, and manufacturing modules, and was developed by Boeing in conjunction with University of Washington (UW), Sikorsky, Northrop, the Massachusetts Institute of Technology, and

Dow/United Technologies [176-179]. The contribution of the UW is apparent in papers such as Mabson et al. [22], Kim and Tuttle [23], and Neogi et al. [24].

It was also during this time that the major finite element analysis software companies began to explore optimization. MSC.Software Corp. (Santa Ana, CA) developed Solution 200 (SOL 200) from several previous solution packages to introduce design sensitivity and optimization to the MSC.Nastran finite element code [180]. Improvements were made to include simplified composite laminate modeling techniques, improved integration with other codes, and the development of external response criteria for SOL 200 called DRESP3 [181]. Client-server technology has been incorporated into the MSC.Nastran Toolkit to provide a way for custom, user-written applications to communicate with MSC.Nastran through application programming interfaces (API). The new, generalized framework is shown in Figure 2.2. In contrast, ANSYS could not perform an aeroelastic optimization [15].

Vanderplaats Research and Development, Inc. (Colorado Springs, CO) coded a software suite of modules that is primarily a design optimization tool with some finite element analysis capability [182]. It combines the most advanced methods for structural optimization for design of structures, according to company literature. A series of papers were published in 2002 that demonstrated its usefulness for composite structural optimization [183-185]. Collier Research Corp. (Hampton, VA) utilized funds from the U.S. Air Force and NASA to develop a program for automating airframe structural analyses using closed-form, empirically based, analytic solutions [186-198]. Improvements in the analysis methods utilized by the program continued [199-203], while recently a finite element analysis capability was added [204-205].

General purpose and popular optimization software packages such as VisualDOC [35, 206], iSIGHT 207-208], OPTIMUS [209], and ModelCenter [210] were compared for performance and ease of use by Hong et al. [211]. They had various strengths and weaknesses, but they all lacked the ability to control multiple design modules simultaneously.

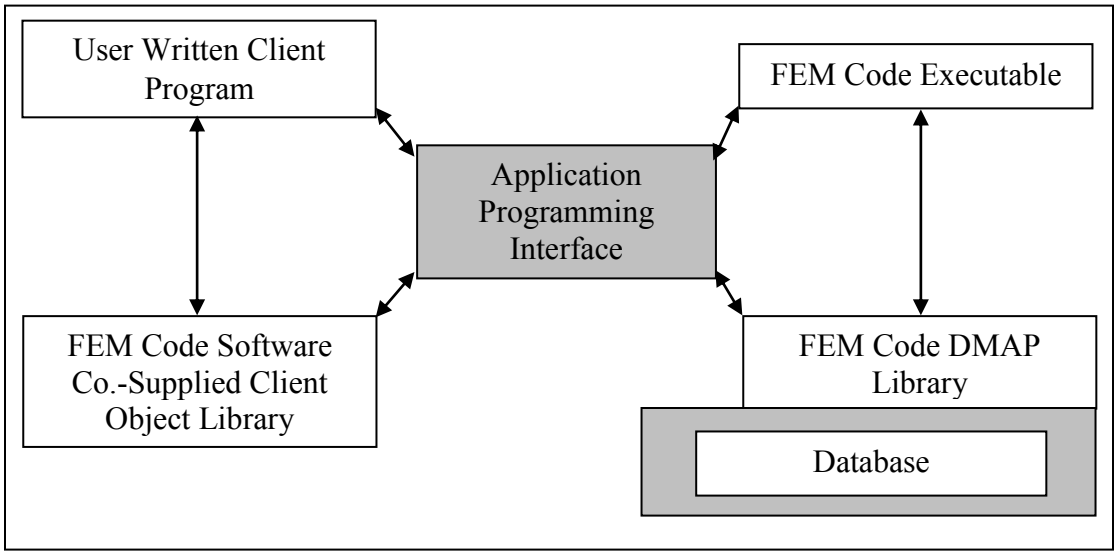

Figure 2.2: Improved Integration Scheme for FEM Code/User Codes (after [181])

One of the newer approaches to structural optimization is Reliability-Based Design Optimization (RBDO) or Robust Design Optimization (RDO). A review of these methods prior to 1997 can be found in Su and Renaud [212]. RBDO was applied to aeroelastic structures by Allen and Maute [213]. One of their comments is that deterministic methods produce less accurate results concerning a probabilistic system than a probabilistic analysis would as uncertainty information is not taken into account. Vittal and Hajela [214] explored approaches to incorporating reliability in MDO frameworks. Noise in the probability of failure or safety index can make it difficult to converge on the global optimum. This problem led to the use of the Probabilistic Sufficiency (or Safety) Factor (PSF), described by Qu and Haftka [215]. In 2004 the RBDO of isogrid stiffened panels subjected to system reliability constraints was performed [216]. Material properties and geometric manufacturing tolerances were random variables. The PSF is used to convert reliability-based global optimization to sequential deterministic global optimization. This was done via both PANDA2 and the DIvide RECTangles (DIRECT) algorithm [217-219]. The PSF's are evaluated by Monte Carlo simulation, using response surface approximations to reduce the computational cost:

$$PSF = F_S^{-1}(P_T) \tag{2.2}$$

where F_S is the cumulative distribution function of the safety ratio (i.e., strength over stress) and P_T is the target probability of failure. This approach addresses the desire for three-dimensional plots of weight (performance), reliability (safety), and manufacturing considerations (cost) that would further enable aircraft designers [220], particularly if the capability to optimize composite laminates is included [221].

Today, at least in the aerospace industry, research continues in structural optimization with new emphasis in large systems and parallelization of algorithms for computer simulations of vehicle systems. Simpson et al. provided an excellent review of "Design and Analysis of Computer Experiments in Multidisciplinary Design Optimization [222]. A forward swept, regional airliner composite wing was optimized recently by Bach et al. [223] using computational fluid dynamics (CFD) for calculating aerodynamic loads. Internal structural loads were found using a finite element model that was updated at each optimization iteration. Both I- and blade-stringer stiffened panels were explored for minimum weight. Martins and his co-workers [224-225] have been working on optimization of transport aircraft wings using a gradient-based aeroelastic design optimization framework that can be both high-fidelity (CFD and FEM) and incorporate a high number of constraints, including flutter. The aerostructural analysis is mathematically coupled for aerodynamic shape and internal structure optimization, with objective functions such as takeoff gross weight and minimum fuel burn. However, there are no consideration of bolted joints in the analysis.

Many of the same research areas mentioned in this section continue; for example, the Proceedings of the 54th AIAA/ASME/ASCE/AHS/ASC Structures, Structural Dynamics, and Materials Conference, Boston, MA, April 8-11, 2013, contains over 100 papers relevant to this thesis topic. The Proceedings of the 15th AIAA/ISSMO Multidisciplinary Analysis and Optimization Conference, Atlanta, Georgia, June 16-20, 2014, contains at least another 110 papers.

2.2 Stochastic Global Optimization Methods

Pure Adaptive Search (PAS) and Adaptive Search (AS) are idealized stochastic global optimization algorithms that provide theoretical limits on the complexity of practical stochastic search algorithms. PAS is a random search algorithm that generates new iterates according to a probability distribution (typically uniform) in the improving region, at each iteration. It assumes that it is possible to generate points in the feasible region according to the Boltzmann distribution. Introduced by Patel et al. [226] and expanded upon by Zabinsky and Smith [227] it exhibits linear time computational complexity in dimension for the class of global optimization problems whose objective function possesses a finite Lipschitz constant and whose feasibility region is convex. Later, Romeijn and Smith [129] found that AS is a generalization of the PAS algorithm, and further that SA can be seen as an approximate implementation of AS. The number of iterations is bounded by the number for PAS within same accuracy. Zabinsky [228] provides an extensive discussion of stochastic global optimization methods, including convergence behaviors and examples.

Three algorithms are discussed here: Improving Hit-and-Run (IHR), Multi-Particle Simulated Annealing (MPSA), and the Multiresolution Estimated Gradient Architecture (MEGA). IHR and MPSA are used for the analysis in this dissertation.

2.2.1 Improving Hit-and-Run (IHR)

The Hit-and-Run algorithm generates a sequence of points that asymptotically approach uniform distribution and is used to approximate the ideal performance of PAS and AS. It was introduced in 1984 by Smith [131]. A practical sequential, random, global optimization algorithm came from combining Hit-and-Run and PAS, called Improving Hit-and-Run (IHR); it uses Hit-and-Run to generate an improving point in the level set at each iteration of PAS. It can be considered a limiting form of SA; SA algorithms will accept non-improving points with some probability, whereas IHR will reject these points [120]. In several studies IHR has been shown to be approximately polynomial ($\mathcal{O}\ n^{5/2}$) in dimension for some positive definite quadratic functions with multiple local optima, as is the case for composite structures optimization [229, 25]. For more complex functions further investigations were needed; Markov chain models were used to analyze IHR and predict the expected number of iterations needed to find the global optimal for the algorithm [32]. Other authors have also done work with Hit-and-Run algorithms [230-231].

IHR was modified in the early 1990's to be capable of handling mixed discrete and continuous variables for composite design. Two approaches were developed, the Continuous Step and the Discrete Step methods. The Continuous Step method [227] looks at the objective function as a continuous step function, where the design variables are continuous but the function can only take discrete values. The next iteration point is determined by generating a random direction from the current point and search along that direction. The optimization strategy was initially to search the entire design space, with subsequent searches involving subsets of the space (fiber angles, stringer, geometry variables, etc.). This technique reduces the size of box constraints to a user-defined volume (a reduced box), which is always centered on the current point (not allowed outside the original box), using circular and reflective mapping rules. The Discrete Step method

[232] is a variation of this, where the objective function is a discrete step function of the discrete design variables. Instead of generating a direction from the current point, the current point is rounded to the closest discrete value, and the line search is performed from that new, rounded point. Up to a 20% improvement was found in the mechanical performance optimized with this method.

A summary of the Improving Hit-and-Run (IHR) algorithm is given as [31]:

Step 0: Initialize an iteration counter k = 0 and a starting point $x_0 \in S$.

Step 1: Generate a candidate point $x_k \in S$.

Step 1a: Generate a direction vector d_k using a direction generator.

Step 1b: Generate a step size λ_k using a point selection method. λ_k must satisfy

$$\{\lambda_k \in R \mid x_k + \lambda_k d_k \in S\}$$

Step 2: Update the new point if it improves the objective function, i.e., set

$$x_{k+1} = \begin{cases} x_k + \lambda_k d_k, & f(x_k + \lambda_k d_k) < f(x_k) \\ x_k, & \text{otherwise} \end{cases}$$

Step 3: If the convergence or stopping criterion is met, stop. Otherwise, increment k and go to Step 1.

Other variables include d_k, which is the direction sought that improves f(**x**), and λ_k, which is the step size. ε is used to denote a small number to define the radius of a hypersphere.

There are three basic direction generators:

1. Coordinate Direction (CD): this method varies one design variable at a time, and the points are uniformly distributed over the coordinate directions and differ from the current point by ε.
2. Hyperspherical Direction (HD): varies all the design variables at once, and the points are uniformly distributed on a hypersphere of radius ε, centered on the current point [233].
3. Cyclic Coordinate Direction (cCD): varies one design variable at a time, and the points are uniformly distributed over the coordinate directions chosen in a cyclic manner and differ from current point by ε [31].

A feasible line segment is defined as that portion of a line that is inside the search bounds. There are three point selection methods:

1. Selection from locations uniformly distributed along the entire feasible line segment.
2. Selection from locations uniformly distributed along the improving direction portion of a feasible line segment.
3. Same as method two, but decreases the search bounds to the last trial point after each attempt.

A line joining the current point with a trial direction point defines a trial direction. Once a direction is selected, f(**x**) is evaluated at an associated trial point. If the trial direction is an improving direction, then a one-dimensional line search is performed in d_k to find x_{k+1} (improving point). The current improving direction search is terminated if no improving point is found after a maximum number of searches along the feasible line segment. The trial point then

becomes the next current point. Heglund [234] found that it was more efficient to allow the algorithm to sample once per direction generated by the Markov kernel if the candidate point was infeasible. If that were the case, the algorithm then generates a new direction from the original point and samples a new candidate point. The algorithm stopping criteria is either a user specified maximum number of iterations or the condition that no improving direction is found in the maximum number of direction tries [233]. A known possibility with Markov chain Monte Carlo methods is if there is a small Metropolis ratio between the design points X and the points that are easily accessible from X by the Markov kernel it is possible to get stuck at a point $X \in S/S^*$, where S is the sub-set of real numbers the algorithm is operating within and S* is the global optima. Whether this happens or not depends on the cooling schedule, the Markov kernel being used, and the structure of the objective function [34].

Kristinsdottir used both CD and HD direction generators [32]. The results showed that the HD generator performed slightly better than the CD. However, the major result was that increases in dimension of the function increased the number of new points linearly. This is consistent with the hypothesis that IHR can be used for large dimension composite design problems without excessive computational penalty. The HD direction generator was used in this work (see Chapter 5).

Graesser et al. [233] provided one of the first formulations for global composite structural optimization using IHR. The design variables were the laminate ply orientations, the number of plies, and the geometry of the stringers in the stiffened panel. The constraints were the fiber angles and the axial, transverse, and shear critical strains. Figure 2.3 is a flowchart of the algorithm. The objective function was given as

$$f(x) = \frac{1}{m}\sum_{j=1}^{m}\left[\sum_{k=1}^{n}\left[\left(\delta \exp\frac{\left|\varepsilon_1^k\right|_j - \varepsilon_1^{cr}}{\varepsilon_1^{cr}}\right)^2 + \left(\delta \exp\frac{\left|\varepsilon_2^k\right|_j - \varepsilon_2^{cr}}{\varepsilon_2^{cr}}\right)^2 + \left(\delta \exp\frac{\left|\gamma_{12}^k\right|_j - \gamma_{12}^{cr}}{\gamma_{12}^{cr}}\right)^2\right]\right] \tag{2.3}$$

where

$$\delta = \begin{Bmatrix} 1, \varepsilon_i^{cr} - \left|\varepsilon_i^k\right|_j > 0 \\ nm, \varepsilon_i^{cr} - \left|\varepsilon_i^k\right|_j < 0 \end{Bmatrix} \tag{2.4}$$

and ε_1^k, ε_2^k, and γ_{12}^k are the axial, transverse, and shear strains, and the superscript cr denotes the critical value. This objective function features an exponential transformation function and a magnification factor that cause the value of the function to be very high in the neighborhood of the three normalized ply strains. It is also discontinuous, and will jump in value if a ply strain value exceeds its allowable critical strain. Multiple load conditions applied to a single laminate result in a summation of the objective functions of the individual load conditions [233].

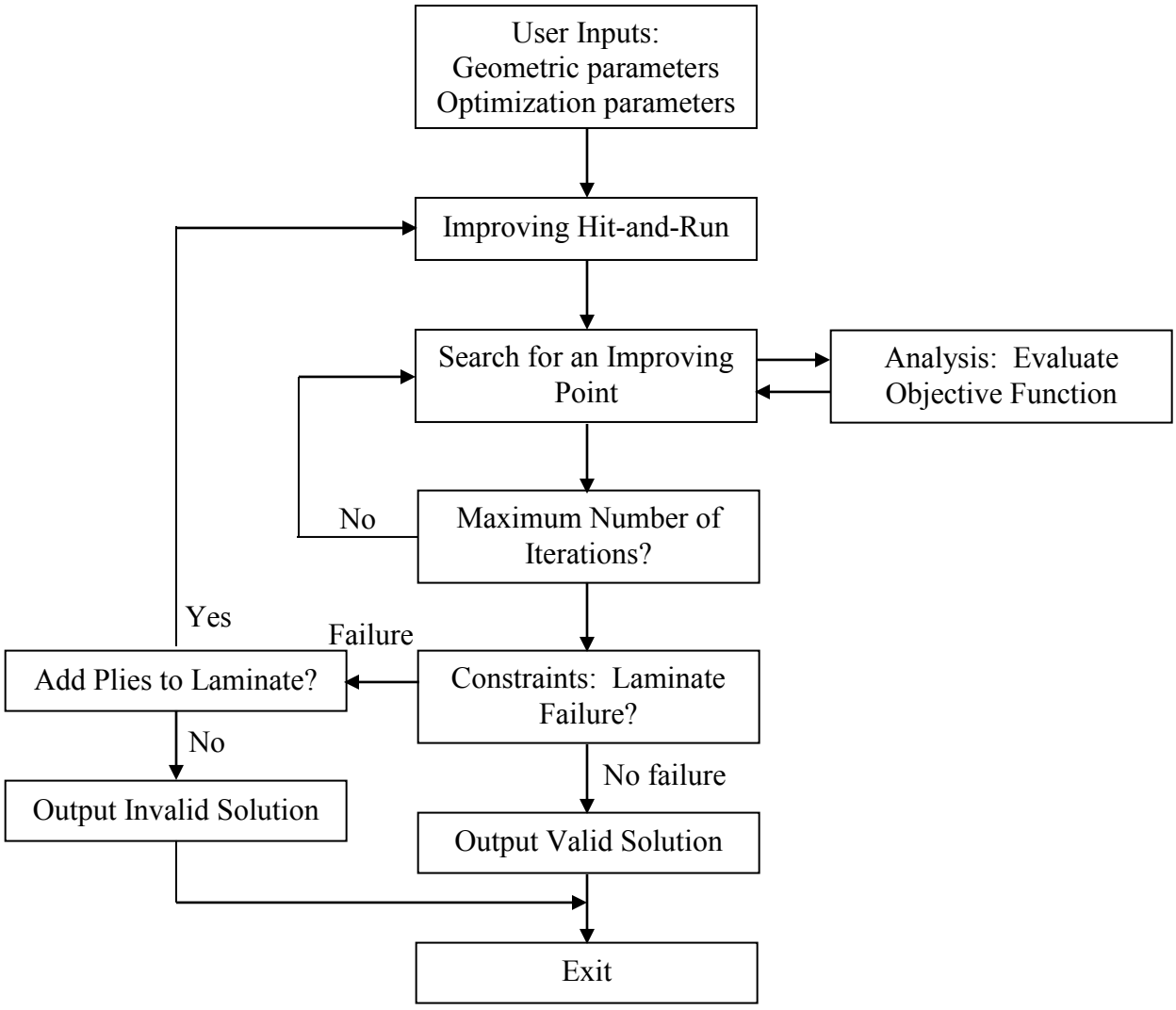

Figure 2.3: Optimization Algorithm Flowchart, Graesser et al. [233]

2.2.2 Multi-Particle Simulated Annealing (MPSA)

The MPSA algorithm developed by Molvalioglu et al. [34] was motived by an interacting Metropolis algorithm presented by del Moral [235], which in turn was developed based on the original ideas of Feynman [236] and Kac [237]. The algorithm begins by sampling independent points (particles) in the feasible region. Every iteration samples candidate points from the current set using a Markov kernel (in this case, the Hit-and-Run generator [131]). The next set of points is determined by randomly selecting from this intermediate set according to their Metropolis ratio, i.e., the particles are moved randomly according to their Metropolis ratio.

A summary of the Multi-Particle Simulated Annealing (MPSA) Algorithm is given as [34]:

Step 0: *Initialization.* Set k = 0. Sample N points y_1^i, i = 1 ,…, N on Ω according to the initial probability η_1. Set the temperature parameter γ_0 to a positive value.

For τ = 1, 2, …

Step 1: *N-Particle Exploration.* Move the particles to intermediate locations $\hat{y}_1^i \in \Omega$ with the probability $E\left(y_\tau^i, d\hat{y}_\tau^i\right)$, i = 1, …, N which is defined by the Markov (exploration) kernel E.

Step 2: *N-Particle Selection.* Check the stopping criteria. If the criteria is not met, move the particles i = 1, …, N to the intermediate locations $\hat{y}_{\tau 1}^j$ of particles j = 1, …, N and set $\hat{y}_{\tau+1}^i \leftarrow \hat{y}_\tau^j$ with probability

$$s_j(\gamma_\tau) = \left(\frac{G_{\gamma_\tau}\left(\hat{y}_\tau^j\right)}{Z_{\gamma_\tau}} \right) \tag{2.5}$$

where $G_{\gamma_\tau}(y) = \exp\left(\frac{-f(y)}{\gamma_\tau}\right)$ and $Z_{\gamma_\tau} = \sum_{k=1}^{N} G_{\gamma_\tau}\left(\hat{y}_\tau^j\right)$. Update the objective function and the temperature parameter $\gamma_\tau = (1+k)^{-0.99}$. Increment k and return to Step 1. If the criteria is met, stop.

A stochastic global optimization algorithm called the Interacting-Particle Algorithm (IPA) is a later version of MPSA and is a development of SA and GA. In these algorithms the sample points are controlled by a set of parameters that are determined *a priori*; in the case of SA through the use of the temperature parameter, and in the case of GA through cross-over, mutation, and selection rates. In reference [238] the sampling is controlled by a meta-controller that takes in observed feasible points and objective function values and provides feedback on the parameters the algorithm is using for choosing the next points. The IPA may be an algorithm explored more in future work in this area of composite structural optimization.

2.2.3 Multiresolution Estimated Gradient Architecture (MEGA)

In 2006 Hazen and Gupta created a new global optimization algorithm named MEGA that focuses on the search strategies of gradient descent, memory, and multiresolutional search [239-240]. Multiple new operating points are determined and evaluated in each iteration. The algorithm is initialized by randomly choosing a set of starting points uniformly over the search space. The number of initial points and parallel searches scales quadratically and linearly, respectively, with the dimensionality of the problem. These points are then clustered into neighborhoods at every iteration, providing local memory for the gradient estimation for the gradient decent steps that follow. Previously evaluated points are maintained in a database that provides information for the next estimated gradient. There may be some practical issues with implementing discrete functions, particularly if the initial operating points are not sufficiently distributed [240]. The algorithm has been applied to the problem of locating multiple

transmitters within a geographic area [241] and compared to the Fully-Informed Particle Swarm algorithm for the purpose of exploring different gradient information to direct searches [242].

The MEGA could be applied to composite structural optimization; this may be a topic of future research.

2.2.4 Optimization Algorithm Performance

Comparing different optimization algorithms can be difficult, especially for stochastic, global algorithms. Algorithms can be compared in multiple ways, including the speed of the algorithm (rate of convergence to a good solution); the quality of the solution; the ease of use and quality of the description; numerical stability; and CPU (central processing unit) time. Dolan and Moré [243] proposed a method called performance profiles. The bulk of the work pertained to linear programming problems, but recommendations on nonlinear, global optimization are made.

The most common comparison is made with the average number of function evaluations to get within some small epsilon of the global optimum. This is only valid for test problems where the optimum value and optimum design values are known. Another common measure is the best value of the objective function obtained after some n number of evaluations. However, this can be sensitive to the number chosen. Sometimes a rank ordering of algorithm performance is provided, but may not include the size of improvement between the algorithms. In research papers individual algorithm performance is often reported as success when getting within epsilon in maximum CPU time or number of iterations. Failures are often not reported in the main results of the paper.

Performance profiles are an attempt to provide a more informative description of an algorithm's utility for solving a set of optimization problems. The performance metric is a cumulative distribution function; this helps to filter out the results of a few, difficult problems for a given algorithm. Consider a given number of problems to be evaluated, n_p, and a given number of solvers (algorithms) to be evaluated, n_s. Further, p is a member problem of the set of problems P, and s is a member solver of the set of solvers S. Let CPU time represent raw data from optimization trials, i.e., $t_{p,s}$ is the CPU time required to solve problem p with solver s within some epsilon. The performance ratio is then defined as

$$r_{p,s} = \frac{t_{p,s}}{\min\left\{t_{p,s} : s \in S\right\}} \tag{2.6}$$

if successful. Let $r_{p,s} = r_m$ if not successful. This provides a normalization of performance. The probability that solver s has a performance ratio within a factor τ, a member of the set of all real numbers, of the best possible ratio

$$\rho_s(\tau) = \frac{1}{n_p}\left|p \in P : r_{p,s} \le \tau\right| \tag{2.7}$$

In Appendix D the IHR and MPSA algorithms are compared for a known test problem.

2.3 Composite Structural Optimization

Composite structural optimization began to be considered in the late 1960's. Foye studied minimum weight optimization of laminates using a random search method in 1968 [244]. The program could handle ten biaxial load cases and a minimum shear stiffness requirement for a laminate of up to 30 plies. The maximum number of randomly searched ply stacks was 500. Woods and Sams [245] suggested that geometric optimization, or configuration parameter method, could be used for composite problems due to the use of truss elements and the restriction to axial forces only. Here a parameter is created from the geometry and loading of the problem. This configuration parameter is minimized instead of the original objective function, providing simplification. Waddoups proposed a systematic "try them all" approach and later structural synthesis for minimum weight optimization of laminates [246-247]. Schmit and Farshi [248] introduced a method for the design of symmetric laminates subject to multiple in-plane loading conditions and strength and stiffness constraints using the method of inscribed hyperspheres. This method finds an optimum of a nonlinear, multidimensional objective function subject to nonlinear inequality constraints [249]. The thickness of each ply is treated as a continuous design variable to avoid the difficulties associated with discrete integer design variables. Orientation angles are also treated as design variables although the weight objective function is independent of these variables; this can be a source of difficulty for optimization.

McCullers [250] stated that the design of a composite laminate "requires the determination of the number of plies and the orientation of each ply for the material(s) selected, which increases the magnitude and complexity of the design problem. Therefore, although optimization techniques are very useful in metal design problems, they are almost essential for the efficient design of composite structures." The additional degrees of freedom (discrete variables, changing relative percentages of different angle plies in a laminate) involved make structural optimization with composite materials inherently more difficult than with a generally isotropic material. The nature of the functions involved make composite structural optimization a global problem with the associated design space containing many local minima [37, 251]. For composite laminate optimization, there are too many variables to use grid, pure random, or multi-start search algorithms, as they are exponential in dimension [25].

There are many papers and books in the literature on composite structural optimization. Various global optimization algorithms have been used; IHR and SA approaches have already been mentioned. GA were also used extensively [252-254]. In addition Haftka and Gürdal have published a book chapter and whole book that cover composite laminate optimization [37, 255].

2.3.1 Composite Design Problem Formulation

There are several approaches or objectives to composite structural optimization. Performance (strength and stiffness, buckling load, strain, and natural frequency), weight, and cost can all be optimized for individually or in a multidisciplinary analysis. One way to measure performance

is margin of safety (MS), where the definition of the MS depends on the analysis criteria used and that a negative MS represents a failed structure. Strain and buckling are load dependent analysis criteria, and the MS is defined as

$$MS = \frac{F^{allow}}{F^{\max}} - 1 \tag{2.8}$$

where F is the measure of the analysis criteria, F^{allow} is the allowable value defined by the user, and F^{max} is the maximum value seen by the structure. Load independent analysis criteria, such as strength and stiffness, are defined with

$$\mathrm{MS} = \frac{\mathrm{F}^{\mathrm{actual}}}{\mathrm{F}^{\mathrm{req}}} - 1 \tag{2.9}$$

where F^{actual} is obtained from structural analysis and F^{req} is the required criteria value.

Typically, an optimization problem would then have an objective function of the form [232]

$$\text{Performance: } \max f(\mathbf{x}) = \min f'(\mathrm{MS}_{\text{load dependent}}, \mathrm{MS}_{\text{load independent}}) \tag{2.10}$$

2.3.2 Composite Mechanical Property Analyses

Classical Lamination Theory (CLT) [256] is most often expressed as

$$\begin{Bmatrix} \boldsymbol{\varepsilon}^{\mathbf{0}} \\ \boldsymbol{\kappa} \end{Bmatrix} = \begin{bmatrix} \mathbf{A} & \mathbf{B} \\ \mathbf{B} & \mathbf{D} \end{bmatrix}^{-1} \begin{Bmatrix} \mathbf{N} \\ \mathbf{M} \end{Bmatrix} \tag{2.11}$$

where $\boldsymbol{\varepsilon}^{\mathbf{0}}$ are the midplane strains and $\boldsymbol{\kappa}$ are the midplane curvatures (axial, transverse, and shear); **A**, **B**, and **D** are the laminate extensional, coupling, and bending stiffness matrices, respectively; and **N** and **M** are the stress and moment resultants. CLT makes use of the Kirchhoff-Love hypothesis [257] for thin plate behavior (all strains are in-plane and within the elastic range) [258].

There are multiple ways to model strength failure. One of the simplest is called the first ply failure criteria, and was demonstrated for composite optimization use by Neogi et al. [232]:

$$\begin{Bmatrix} \mathrm{X}^{\mathrm{actual}} \\ \mathrm{Y}^{\mathrm{actual}} \\ \mathrm{S}^{\mathrm{actual}} \end{Bmatrix}_{\mathrm{sk,st}} = \frac{1}{\mathrm{t}_{\mathrm{sk,st}}} \begin{Bmatrix} \mathrm{N}_{\mathrm{x}}^{\max} \\ \mathrm{N}_{\mathrm{y}}^{\max} \\ \mathrm{N}_{\mathrm{xy}}^{\max} \end{Bmatrix}_{\mathrm{sk,st}} \tag{2.12}$$

where (X^{actual}, Y^{actual}, and S^{actual}) are the actual strength values from structural analysis, (N_x^{max}, N_y^{max}, and N_{xy}^{max}) are the maximum allowable loads for first ply failure, and $t_{sk,\ st}$ are the skin and stiffener laminate thicknesses, respectively.

Stiffened composite panels possess three basic failure modes: stiffness, strength, and buckling failures. Common analysis models used to analyze these failures include smeared or homogenized analysis, analytical modeling, finite strip analysis methods, and ultimately 2D and 3D finite element analysis. However, these latter two methods are not ideal for optimization as choosing the appropriate mesh is difficult or expensive computationally, and numerical noise is introduced through the discretization process interferes with gradient-based optimization algorithms [259].

The stiffened panel smearing technique used by Neogi et al. [232] is based on the compliance matrix of the skin to generate the matrix for the panel. The axial terms are modified to account for the presence of the stiffeners along the x axis:

$$[a]_{panel} = \begin{bmatrix} a_{11sk}\left(\frac{E_{xsk}}{E_{xpanel}}\right) & a_{12sk}\left(\frac{E_{xsk}}{E_{xpanel}}\right) & a_{16sk}\left(\frac{E_{xsk}}{E_{xpanel}}\right) \\ a_{12sk}\left(\frac{E_{xsk}}{E_{xpanel}}\right) & a_{22sk} & a_{26sk} \\ a_{16sk}\left(\frac{E_{xsk}}{E_{xpanel}}\right) & a_{26sk} & a_{66sk} \end{bmatrix} \tag{2.13}$$

where $a_{ij\ sk}$ are the compliance terms for the skin laminate, $E_{x\ sk}$ is the effective skin laminate axial modulus, and $E_{x\ panel}$ is the effective panel axial modulus. The model is acceptable for obtaining load paths, stiffness constraints, and general buckling load estimates; however, it cannot be used for stress calculations or to capture local and stiffener buckling failures [259].

For specific applications analytical models like that of Stroud and Agranoff [260] can approximate the response of stiffened panels in combination with smeared models. Internal loads and stress resultants can be calculated, as well as some local buckling effects. Stiffened panels can also be modeled as an assembly of plates or shells in a method known as finite strip analysis [261]. For each component the field equations are solved and boundary conditions at the interfaces are matched between adjacent members. This is a more general method, as interactions between the skins and stiffeners and variations in geometry or periodicity in the structure can be captured [259]. This method was implemented in PASCO [104], VICONOPT [170, 173], and COSTADE [23].

Two- and three-dimensional finite element analyses using shell elements can also be used to predict stiffness and stability of panels. However, high computational cost is incurred when trying to accurately model stresses at the boundary conditions and at skin / stiffener interfaces. Software such as STAGS [80] incorporates specialized features for stiffened panel analysis that standard finite element modeling codes do not, such as the ability to incorporate initial

imperfections and use of non-linear analyses for post-buckling behavior prediction [259]. In 1984 Stroud [262] compared buckling loads for composite stiffened panels using PASCO, EAL, and STAGS computer programs and found that, for long wavelength buckling modes, the effect of anisotropy is minimal for most practical cases. Leissa [263] provides a survey of buckling analyses of composite plates and shells.

Buckling failure of laminate skins can be modeled in multiple ways; for an MS formulation, a buckling allowable can be calculated for the most critical loading condition (axial, hoop, or shear) [232],

$$N^{cr} = K \max\left\{|N_x|, |N_y|, |N_{xy}|\right\} \tag{2.14}$$

where the factor K is determined using a load interaction equation [176]

$$K = \frac{-\left(\frac{N_x}{N_x^{cr}} + \frac{N_y}{N_y^{cr}}\right) \pm \sqrt{\left(\frac{N_x}{N_x^{cr}} + \frac{N_y}{N_y^{cr}}\right)^2 + 4\left(\frac{N_{xy}}{N_{xy}^{cr}}\right)^2}}{2\left(\frac{N_{xy}}{N_{xy}^{cr}}\right)^2} \tag{2.15}$$

More recently Lockheed-Martin Aeronautics has developed several structural strength criteria analysis algorithms. A procedure called TM1 [181] optimizes flat and curved composite panels subject to axial loading. Strength constraints are based on allowable lamina fiber strains, while the buckling constraints are calculated using equations for the buckling of a simply-supported, rectangular, orthotropic plate [264]. The procedure produces panel thickness and ratio of 0º/90º/±45º plies to provide minimum panel weight without violating the calculated strength and buckling constraints.

The PRESS procedure [181] calculates the bending moments, in-plane loads, strains, and maximum deflection of a flat, composite, rectangular plate loaded with a uniform pressure distribution. Local strain effects at the panel edges (boundary conditions) and at the panel center (maximum deflection) are computed [265]. Again, panel thickness and ratio of 0º/90º/±45º plies are output from the routine. MSC.NASTRAN has incorporated a simplified approach to composite laminate modeling. It is can be assumed that, in a preliminary design stage, the effect of stacking sequence on the laminate stiffness is small (MEM option). This is especially true for aircraft wing structures, where membrane (axial) effects typically dominate the wing skin responses. If some effect of the change in stiffness is to be included the SMEAR option can be used to assume uniform distribution of plies in the laminate. However, this option ignores the axial-bending coupling effects that may be present. The BEND option is also available to provide a way to account for dominating bending effects [181].

Lamination parameters have been utilized as a way to reduce the number of design variables necessary for a structural optimization algorithm. Recently, Wu et al. [266] formulated an explicit, closed-form set of expressions that define the feasible region of two in-plane and two

out-of-plane lamination parameters that enable the optimization of variable angle tow (VAT) composite plates. They used GA to optimize a composite plate for buckling.

Postbuckling analysis could also be a constraint for this type of composite wing structural optimization. There is a body of work by Lagace et al. [267-269] and Adali et al. [270-272] on this topic.

2.3.3 Composite Manufacturing Constraints

Traditional composite manufacturing constraints can include minimum gage, property linking, ply percentage upper and lower bounds, and a maximum property drop-off rate (ply drop rate). The property drop-off rate (or ply drop rate) between neighboring elements can be computed by

$$\text{Rate} = (\text{prop}_0 - \text{prop}_1)/\text{distance} \tag{2.16}$$

where prop_0 is the element property of interest of the parent and prop_1 is that for the adjacent element. The distance is computed along element surfaces between the elements' centroids [181]. Other ideas about manufacturing constraints will be found in Wang and Costin [273], Kristinsdottir [274], Bare et al. [275], and Niu [276].

2.3.4 Composite Optimization with the Particle Swarm Optimization Algorithm

In addition to the multidisciplinary optimization of a transport aircraft wing using aluminum [151-152] and an approach to find an optimum aircraft configuration [277], there are several papers that deal with composite structural optimization directly. In 2004 Tayal and Wang [278] explored using PSO with mixed variables. Kathiravan and Ganguli [279] used PSO to optimize the strength of a composite box beam, as did Suresh et al. [280]. A vector evaluated particle swarm optimization (VEPSO) algorithm was used to optimize generic composite structures using various failure criteria as constraints [281].

2.4 Composite Wing Structural Optimization

Military and commercial aircraft design optimization methods and software tools have developed rapidly from the late 1960's [282]. Driving this trend has been the need for both reduced time-to-service and reduced lifecycle costs, particularly for wing designs that utilize composite materials. However, due to the proprietary nature of the aerospace industry, there are few benchmark models available for study by researchers in the design and optimization field. An exception is the military Intermediate Complexity Wing (ICW), which was developed in the 1970's to provide a platform from which to compare different approaches to optimization [283-288, 181]. Some of the approaches taken during this time were Wing Design Optimization With Aeroelastic Constraints (WIDOWAC) [289], the aeroelastic Tailoring and Structural Optimization (TSO) procedure, also known as the Wing Aeroelastic Synthesis Procedure [250], and the Flutter And STrength Optimization Program (FASTOP) [290, 285-286].

During the 1980's optimization algorithm development, topology optimization, and composite panel structural analysis were areas of active research. However, it was not until the 1990's and 2000's that composite wing structural optimization was once again studied in a comprehensive way. Optimization with aeroelasticity (Striz) [291-292] aeroservoelasticity (Livne) [293-295], and response surface methodologies (Haftka) [296-299] were applied to the wing optimization problem.

2.4.1 Shape Optimization / Topology

Wing planform shape design can play an important role in structural optimization. When considering the interaction between aerodynamic and structural characteristics of an evolving wing design make shape optimization essential. However, it is more complex and difficult than sizing structural optimization alone due to difficulties associated with accuracy in the finite difference calculation of sensitivity derivatives, the need to control mesh deformation, parameterization of structural shape, and repeated generation of stiffness and mass matrices [21].

Giles [20] improved and generalized the TSO to make the Equivalent LAminated Plate Solution (ELAPS) a powerful tool for optimization. Multiple trapezoidal plates were used to represent more general wing planforms, and static deflections, stresses, and vibration frequencies and modes were calculated. In 1989 this methodology was extended to unsymmetric airfoils and the inclusion of temperature distributions [300]. Results for these methods show close agreement with full finite element solutions. ELAPS was further improved by the introduction of automatic differentiation [301].

Analytic expressions for stiffness and mass matrix elements were formulated by Livne [21], negating the need to perform numerical integration. From these formulas analytic expressions for the derivatives of displacements, stresses, and natural frequencies with respect to shape design variables were developed. The shape sensitivities for stress and displacement are dependent on the motion of the grid points as the planform shape varies because these points are used for stress and displacement evaluations [57], and this is taken into account. It was shown that the analytic derivatives were more accurate than the finite difference derivatives. The sizing design variables in this study were the spar and rib cap areas and the composite layer thicknesses.

Other major methods include the homogenization design method [302] and shape parameterization [303].

2.4.2 Aeroelasticity

It is recognized that "aeroelasticity is a primary design parameter affecting structural optimization, vehicle stability, control effectiveness, and overall performance" [304]. Static aeroelasticity concerns changes in aerodynamic loads due to changes in angle of attack caused by a flexible structure and is therefore driven by the structural stiffness of a wing. Section 4.2

discusses the aerodynamic loads analysis used in this dissertation. Natural frequencies of vibration are not dynamic in that they are inherent to the structure, regardless of the aerodynamic forces present. Flutter, on the other hand, is a dynamic aeroelastic instability. A system experiencing steady state oscillations without damping is critical in flutter. There is a transfer of energy from the air to the structure, and the amplitude of the oscillations increases with time, resulting in a divergent instability [305].

Optimizing both structural and flutter requirements for wing design is necessary. Flutter requirements may add reinforcement and stiffness to certain areas of the wing; weight changes may be required in the structure as a result [306]. Figure 2.4 illustrates the aeroelastic problem complexity. Collar [307] provides a historical development of aeroelasticity, and Garrick [308] provides one for flutter theory.

The aeroelastic cycle will be part of this work as described in Chapter 5. However, as only a wing panel will be optimized, flutter and natural frequency analyses were not performed.

2.5 Composite Bolted Joints

Mechanically fastened joints for composite structures have been studied since the materials were first introduced in the mid-1960's. It was discovered that composite joints behaved differently than metal joints due to the brittle nature of the new materials. A more detailed analysis to quantify the stress concentrations is necessary to predict joint static strength as there is no local yielding as in metals. Despite this existing analysis techniques for determining multi-fastener joint load apportionment (bearing – bypass) in metals are sufficient. Bearing-bypass refers to the load taken by a particular fastener (bearing) versus the load that passes by and is reacted elsewhere in the joint (bypass). Early research has concentrated on developing two-dimensional analyses to predict stresses and strength at a single fastener within the joint [309].

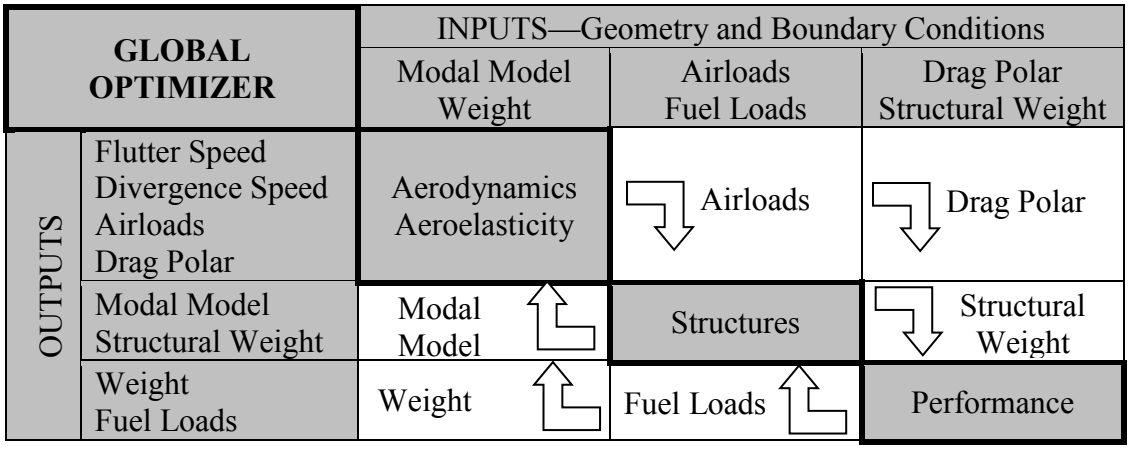

Figure 2.4: Aeroelastic Problem with All Couplings (after [15])

There are two basic types of joints: lightly loaded, single-row fastener designs, and highly loaded, multi-row fastener designs. A multi-fastener design pattern distributes load accumulated on aerodynamic surface into another structure efficiently [309]. The first implementation of highly loaded composite joints was on the Rockwell B-1 Lancer horizontal stabilizer [310].

Optimal weight structures are dependent on its joints and not its basic structure in the acreage. The design of composite joints is particularly important since the weight advantages of the material over metals may be eroded at the joint due to composite's relatively poor performance in bearing [311]. A well-designed joint reduces structural weight while increasing structural efficiency and payload. To achieve efficient designs the failure modes and loads must be accurately predicted for any multi-fastener geometry or material lay-up [312]. Optimum joints are designed to obtain near equal loading of each fastener of equal diameter [309] and have potential shear or tensile failures occur simultaneously and at a mean stress as close as possible to the bearing failure stress. Maximum joint strength occurs when the joint geometry is sufficient to suppress the tensile and shear modes so that failure occurs in bearing [313].

Recently Shroff and Kassapoglou [314] performed an analysis on a composite fuselage structure that focuses on a bolted joint connection and its effect on the surrounding structure. The first step was a global finite element analysis on the structure to obtain internal loads; a local FEM was then applied to the joint. This is similar to the present study. A "try them all" approach was used for optimization for weight, but there is recognition that the joint drives the basic structure and is critical for composite structural weight optimization.

2.5.1 Joint Structural Analysis

Joint structural analysis is generally performed using finite element analysis (FEA) methods, but because of the complexity of composite joints several further analyses are usually performed. These include the computation of individual loads and orientation at each fastener and a stress analysis of load transfer for each critical fastener using fastener loads from previous analyses. Two basic approaches have evolved in the aircraft industry. The first type performs the analysis in two steps: 1) calculation of individual bolt flexibilities, and 2) finite element analysis with the fastener flexibilities as input. The second type includes the computation of the joint flexibility as a special FEA in the overall FEA of the joint [309].

The lack of analytic solutions for composite joint problems is a function of the relative complexity of the design space. Variables can include [315]:

- Laminate stacking sequence
- Geometric parameters (width, edge distance, fastener pitch and diameter, and thickness)
- Fastener fit and magnitude of friction force between the hole and fastener
- Contact arc between the hole and fastener (non-linear effects)
- Fastener flexibility and clamp-up force (3D effects)
- Bearing deflection and hygrothermal effects (non-linear)
- Failure criterion applied

Therefore there are many "rules of thumb" that are applied to composite joint design, including that there should never be more than $3/8^{th}$ of the fibers in any one of the basic laminate directions (0º, ±45º, and 90º), nor should there ever be less than $1/8^{th}$. These aspects of composite joint design led Hart-Smith to note, "…those who have yet to discard their laminate optimization computer programs still occasionally design structures which violate this principle and, on test, show a distinct unwillingness to accept the load transfer at their joints that had been expected of them" [316].

The major structural limitation for composite joints is that they are inherently anisotropic, being particularly weak in through-thickness, or z-axis, strength [309]. Generalized two-dimensional anisotropic elasticity theory can be used to represent the stress concentrations near holes in composite materials. There are two different formalisms in this theory: Lekhnitskii assumes equilibrium and enforces compatibility (strain) [317], whereas Stroh assumes compatibility (strain) and enforces equilibrium [318-319]. Isotropic elasticity theories were extended to anisotropic materials by both Lekhnitskii [320] and Savin [321-322], using the first of the two formalisms mentioned above. In addition to the two-dimensional nature of the analysis uniform loads are also assumed. Solutions are generated for structures with general hole geometries in infinite anisotropic plates using analytic functions of complex variables, generally following Muskhelishvili [323]. The application of Savin's solutions to the holes for bolted joints in this work is discussed in Section 4.3.

2.5.1.1 Load Sharing in a Joint

Load sharing is dependent on the number, diameter, and material of the bolts and the stiffness of the joining members. The first and last bolt in a joint with a single row of fasteners will be more highly loaded if the members are of equal stiffness. However, fastener and joint flexibilities cause fastener deflection in shear and bending, joint motion due to localized bearing distortions, and fastener rigid body rotation in single shear joints that effect load sharing. For composite laminates the joint flexibility should take into account the material orientation, ply fractions, and stacking sequence of the laminates being joined [309].

The load distribution in multi-fastener joints has been an issue in aeronautical engineering since its inception. Performance demands made the issue more critical with the advent of World War II; in 1946 Tate and Rosenfeld published a technical note for the National Advisory Committee for Aeronautics (NACA) on the determination of bearing-bypass loads in bolted joints [324]. The joint stress is given by

$$\sigma = \sum_{i=1}^{r} \frac{R_i}{wt_n} = K_{te}\sigma_T + K_{tb}\sigma_b \tag{2.17}$$

where bolt loads R are given by

$$R_i = \frac{\left[R_{i+1} - \lambda \sum_{r=1}^{i-1} R_r + \mu \right]}{(1+\lambda)}, i - 1,2,...n-1 \tag{2.18}$$

$$\lambda = \frac{2K_p + K_s}{C}, \text{ and } \mu = \frac{2K_p P}{C} \tag{2.19}$$

$$R_{i+1} = \frac{C_i}{C_{i+1}} R_i + N_i \frac{\left(2K_p + K_s\right)}{C_{i+1}} R_i - \frac{2K_p}{C_{i+1}} P + \frac{\left(2K_p + K_s\right)}{C_{i+1}} \sum_{r=1}^{i-1} R_r \tag{2.20}$$

K_p is the plate constant $\left(\frac{p}{wt_p E_p}\right)$, and K_s is the strap constant $\left(\frac{p}{wt_s E_s}\right)$. This same load sharing analysis was used recently by Bhachu et al. [325] for a study of hole tolerance while optimizing for quality, manufacturing, and performance cost for an aluminum joint.

Hart-Smith [326] calls C the correlation coefficient; it is a function of material properties and geometry:

$$C = \frac{K_{tc} - 1}{K_{te} - 1} = C_{bs} + C_{bb} + C_{bbr} + C_{pbr} \tag{2.21}$$

where K_{tb} is the bearing stress concentration factor [29] given by

$$K_{tb} = \frac{K_{tc}}{\left(\frac{w}{d}\right) - 1} \tag{2.22}$$

K_{tc} is the by-pass stress concentration factor, and K_{te} is the elastic stress concentration factor, given by

$$K_{te} = 2 + \left(1 - \frac{d}{w}\right)^3 \tag{2.23}$$

Further, C_{bs} is the shear effect; C_{bb} is the bending effect; C_{bbr} is the bearing effect; and C_{pbr} is the plate bearing effect, given by the following equations:

$$C_{bs} = \frac{2t_s + t_p}{3G_b A_b} \tag{2.24}$$

$$C_{bb} = \frac{8t_s^3 + 16t_s^2 t_p + 8t_s t_p^2 + t_p^3}{192E_{bb} I_b} \tag{2.25}$$

$$C_{bbr} = \frac{2t_s + t_p}{t_s t_p E_{bbr}} \tag{2.26}$$

$$C_{pbr} = \frac{1}{t_s E_{sbr}} + \frac{2}{t_p E_{pbr}} \tag{2.27}$$

where A_b is the area of the bolt $\left(\frac{\pi d^4}{4}\right)$ and I_b is the bolt moment of inertia $\left(\frac{\pi d^4}{64}\right)$.

Chapter 3 discusses bolt flexibility and load sharing further.

2.5.1.2 Analysis of Failure in Bolted Joints

There are multiple failure modes for composite joints (see Figure 2.5). Net section (tension or cleavage) failure can occur in the composite. Shear-out failure may occur depending on hole spacing, edge distances, or lay-up before bearing failure is reached. Bearing failure is caused by matrix failure immediately ahead of the fastener. In addition, failure may occur by fastener failure or pull-out. Generally delamination may be present but is not the primary cause of failure [309].

Cleavage failures only occur with 0º/±θº laminates with a low proportion of ±θº fibers. The failure initiates in a single shear mode, followed by failure of the net section on one side of the laminate. For example, a 67% 0° / 33% ±45 ° CFRP laminate will display this type of failure. Since these types of laminates are not useful for high strength, multiple fastener joint applications cleavage failures will not be considered in this study. Similarly, pull-out failures will not be considered, as they are associated with countersunk rivets and single shear joints. Peeling stresses, induced by out-of-plane bending, cause failure by pulling the joint apart [313].

Collings experimentally investigated the strength of mechanically fastened composite joints. Tensile failure of a composite joint with both axial and bias fibers is given by

$$\sigma_N = \frac{P}{(w - nd) * t} \tag{2.28}$$

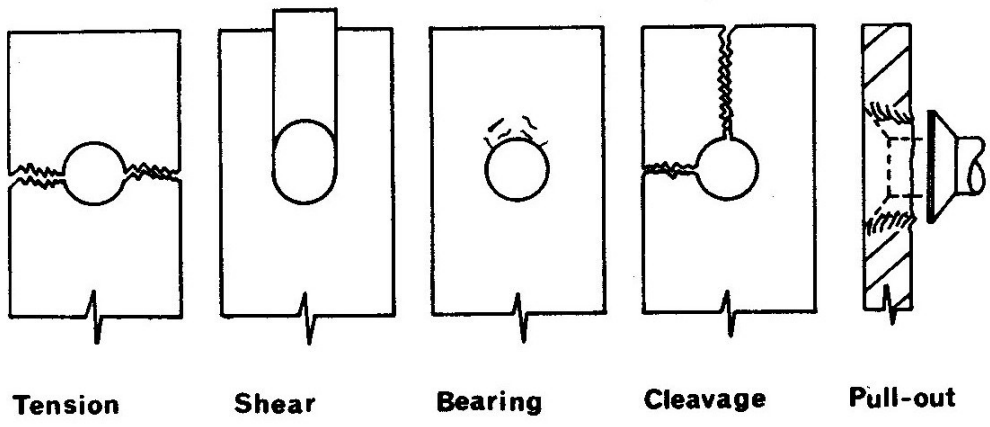

Figure 2.5: Modes of Failure for Mechanical Joints in Fiber Reinforced Polymer Composites [313]

where σ_N is the laminate notched tensile strength, P is the failing load of the laminate, w is the joint width at the net section, n is the number of holes of diameter d occurring at that section, and t is the joint thickness [327]. The failure stress shown is typical for thin, graphite/epoxy laminates with at least 10% of the fibers in the load direction. It has been shown that first fiber failure occurs around 85% of net strength [313].

As with tensile strength, the shear strength of a joint is largely determined by the laminate stacking sequence. The shear strength of a joint is given by

$$\tau_N = \frac{P}{2et} \tag{2.29}$$

where τ_N is the laminate notched shear strength and e is the edge distance (distance between the hole center and the free edge, parallel to the load). Again, the failure stress shown is typical. The strength is best measured using loaded-hole shear tests [327].

Bearing failure is caused by compressive stresses around the loaded half of the circumference of a hole loaded by a fastener. The mechanism of failure occurs in shear, through both the fibers and the matrix, initiating at the hole edge where the maximum stress is developed [328]. Collings [327] showed that the compressive strength of the load-direction (0º) fibers was the important factor in bearing strength. Stacking sequence is a factor; non-homogeneous lay-ups reduced the bearing strength by 16% in this study. Bearing strength is usually expressed as an average stress acting uniformly over the cross-sectional area of the hole,

$$\sigma_b = \frac{P}{ndt} \tag{2.30}$$

Other aspects of composite bolted joint strength analyses include assumptions about failure types vs. design [329]; comparisons with experimental data [330, 327-328, 331, 313]; loading around bolt holes [332-333]; combined bearing-bypass loading [334]; bolt modeling [335]; fracture mechanics [336-338]; failure of thick laminates [312]; and hole elongations and fastener deflections [339].

2.5.1.3 Failure Criteria

The design of mechanically fastened composite joints must of course assure against all possible joint failure modes. Conventional practice is to design the joint to fail in net section and bearing [309].

The Whitney-Nuismer characteristic distance approach to composite joint failure modes was developed for isotropic plates with circular holes and extended to anisotropic plates. It was assumed that the characteristic distance is a material property independent of laminate geometry and stress distribution. It represents the distance over which the material must be critically stressed to find a sufficient flaw size to initiate failure. For a circular hole in an isotropic, infinite

plate with an origin at the center of the hole with an applied uniform tensile stress along the y-axis at infinity, the normal stress along the x-axis is given by

$$\frac{\sigma_y}{\bar{\sigma}} = 1 + \frac{1}{2}\left[\frac{R}{x}\right]^2 + \frac{3}{2}\left[\frac{R}{x}\right]^4 \tag{2.31}$$

where σ_y is the normal stress along the x-axis, $\bar{\sigma}$ is the far field stress, R is the radius of the hole, and x is the distance along the x-axis [340]. The stress failure criterion is then

$$\frac{\sigma_N}{\sigma^0} = \frac{2}{\left(2 + \xi^2 + 3\xi^4\right)} \tag{2.32}$$

where σ_N is the laminate notched strength, σ_0 is the laminate unnotched strength, and

$$\xi = \frac{R}{R + d_0} \tag{2.33}$$

where d_0 is the characteristic distance. For quasi-isotropic fiberglass laminates it was found that a value of 0.04 for d_0 is a good approximation [29].

Lekhnitskii [317] provides an accurate stress solution in the vicinity of a hole in an infinite, anisotropic plate,

$$k_{gross} = 1 + \sqrt{2\left(\sqrt{\frac{E_1}{E_2}} - \nu_{12}\right) + \frac{E_1}{G}} \tag{2.34}$$

which is necessary to apply the Whitney-Nuismer method for predicting composite joint failure. Here k_{gross} is magnitude of the stress concentration, E_1 is the Young's modulus in the direction of the load axis, E_2 is the Young's modulus in the direction normal to the load axis, G is the in-plane shear modulus, and ν_{12} is the principle Poisson's ratio. This solution can be extended to an assumed pressure distribution for a loaded bolt, and can be combined with boundary integral methods to include the effects of edges and multiple holes.

Cohen et al. extended the average stress criterion to include the in-plane tangential, radial, and shear stress components that are significant in joint failure [312]. As a point stress criterion the equation is

$$\left[\left(\frac{\sigma_{tt}(r,\phi)}{\sigma_{tt}^0(\phi)}\right)^2 + \left(\frac{\sigma_{rr}(r,\phi)}{\sigma_{rr}^0(\phi)}\right)^2 + \left(\frac{\tau_{rt}(r,\phi)}{\tau_{rt}^0(\phi)}\right)^2\right] = \kappa^2 \tag{2.35}$$

where

$$\phi = 0^{o} \rightarrow 90^{o} \text{ and} \tag{2.36a}$$

$$\kappa^2 = \begin{cases} \geq 1, \text{failure} \\ < 1, \text{pass} \end{cases} \tag{2.36b}$$

The hole circumferential location is ϕ; σ_{tt}^0, σ_{rr}^0, and τ_{rt}^0 are the unnotched laminate tensile, radial, and shear strengths, respectively. As an average stress criterion the equation is (after Whitney-Nuismer):

$$\left\{ \frac{1}{d_0(\phi)} \int_R^{R+d_0(\phi)} \left[\left(\frac{\sigma_{tt}(r,\phi)}{\sigma_{tt}^0(\phi)} \right)^2 + \left(\frac{\sigma_{rr}(r,\phi)}{\sigma_{rr}^0(\phi)} \right)^2 + \left(\frac{\tau_{rt}(r,\phi)}{\tau_{rt}^0(\phi)} \right)^2 \right] dr \right\}_{\phi=0^\circ \rightarrow 90^\circ} = \kappa^2 \tag{2.37}$$

Generally the dominant stress is the tangential tensile component, and the above equation reduces to

$$\left\{ \frac{1}{d_0(\phi)} \int_R^{R+d_0(\phi)} \sigma_{tt}(r,\phi) dr \right\}_{\phi=0^\circ \rightarrow 90^\circ} = \sigma_{tt}^0(\phi) \tag{2.38}$$

The stress distribution $\sigma_{tt}(r, \phi)$ is calculated by a finite element analysis and is fit to an n^{th} order polynomial using a least-squares technique. A regression method to determine the coefficients for the polynomial, and after a change of variables,

$$\frac{R}{d_0} \sum_{i=1}^{n} \frac{b_i}{i} \left(\xi^i - 1 \right) = \sigma_{tt}^0 \tag{2.39}$$

where b_i are the coefficients of the polynomial [312].

To predict failure locations in thick laminates a maximum strain criterion was used. The following quantities were plotted as a function of ϕ:

$$R_1^+ = \frac{\varepsilon_{11}^+}{\varepsilon_{11}^T} \quad R_1^- = \frac{\varepsilon_{11}^-}{\varepsilon_{11}^C} \quad R_{12} = \frac{\gamma_{12}}{\gamma_{12}^U} \quad R_2^+ = \frac{\varepsilon_{22}^+}{\varepsilon_{22}^T} \quad R_2^- = \frac{\varepsilon_{22}^-}{\varepsilon_{22}^C} \tag{2.40}$$

where ε_{11}, ε_{22}, and γ_{12} are the fiber longitudinal, transverse, and shear strain components, respectively. The superscripts + and – indicate tensile and compressive strains and T, C, and U indicate ultimate tensile, compressive, and ultimate strains, respectively. These strain ratios are normalized by the largest value for each laminate type. The results show the locations around the hole of the largest strains and the likely failure locations [312].

Kradinov et al. [341-343] have developed an approach to the failure prediction of bolted composite joints. The method is well suited for parametric studies and design optimization as it

is robust with respect to joint geometry. Finite laminate planform dimensions, uniform and variable laminate thickness and lay-up; bolt interaction, torque, flexibility, hole clearance and interference; and platen dimensions and material properties are all part of the analysis. However, it uses the Lekhnitskii formulation [317] instead of the Stroh formulation [318-319] to formulate the anisotropic elasticity problem. Using the Stroh approach and notes by Savin [321], Chern and Tuttle [344-345] found that for certain anisotropic plates the Lekhnitskii formulation does not hold for displacements; free body rotations are not taken into account. Therefore, the Kradinov analysis does not hold true for all combinations of laminate stacking sequences for displacements.

Chapter 3 will detail the specific composite bolted joint analysis used in this study.

2.5.1.4 Joint Analysis Software

Many different composite joint analysis software codes have been developed since the 1980's. These include BJSFM [346], BREPAIR [347], BOLT [348], SAMCJ [349], and SAMCEFF-BOLT [350]. Lockheed-Martin Aeronautics has developed a procedure for the analysis of composite bolted joints called IBOLT [181, 351]. Analysis can be performed for a rectangular plate of known thickness and geometry with a hole in its center subjected to biaxial tension, off-axis bearing, and shear loads [337]. Temperature and moisture effects are included during the calculation of stiffness, strength, and strain. IBOLT computes the fastener criteria margins and predicts the required element thickness increment for the combined effect of in-plane load and lateral pressure loads.

2.5.2 Joint Design Considerations

There are many aspects to mechanically fastened composite joints, including the effects of geometry, lay-up and stacking sequence, fastener selection, hygrothermal, and various impacts to fatigue performance. Thoppul et al. [352] provide a review of the mechanics of composite bolted joints, including relevant experimental aspects. Many of these design considerations are introduced here.

2.5.2.1 Geometry

The width of the joint is important to its tensile strength. Joint width (or fastener pitch) is chosen so that a tension failure occurs at a mean stress as close as possible to the bearing strength of the material. The width effect can be expressed in terms of the bearing strength that can be sustained by the joint at failure [313]. Similarly, the edge distance (distance from the center of the hole to the edge of the laminate parallel to the loading direction) of the joint is important to its shear strength. For most laminates shear stress decreases with increasing edge distance. Collings found that for a 50%/50% 0º/±45º graphite/epoxy laminate the peak bearing stress can be obtained at an edge distance over hole diameter ratio of approximately five [313].

Collings [327] found that hole size, for reasonable ranges, has little influence on net tensile strength or shear strength of a graphite/epoxy joint. Further, hole size had little effect on the

bearing strength of the joint, provided sufficient lateral constraint from the clamping of the fastener. However, bolt pitch or spacing does have an effect on the tensile strength of the joint [330].

Fastener interaction has been studied and shown to be a small effect when basic joint design criteria are met, including fastener spacing to permit installation. There is little loss of efficiency when the number of holes is increased, and multi-row fastener joint behavior can be predicted from single-row fastener designs [327]. For joint efficiency a single-row of fasteners with a close pitch is preferred over a multi-row geometry when possible, i.e., when there is no possibility of bearing failure [313]. Large fastener pitch joints must be checked for potential inter-fastener buckling in the laminate [330].

2.5.2.2 Lay-up and Stacking Sequence

The relative number of a particular fiber orientation and its position within a laminate effect the structural capability of the joint. Laminates with at least 10% of the fibers aligned in the direction of the load are considered to be at near-optimum strength and are capable of taking high stresses. Tensile failure rarely occurs in laminates with greater than 50% axial (0º) fibers due to in-plane shear [313]. "Rules of thumb" that are applied to composite joint design include that there should never be more than $3/8^{th}$ of the fibers in any one of the basic laminate directions (0º, ±45º, and 90º), nor should there ever be less than $1/8^{th}$ [316]. In 0º/±45º graphite/epoxy laminates maximum shear strength joints can be obtained from using 25-50% ±45º plies [313]. In 0º/±45º graphite/epoxy laminates maximum bearing strength joints can be obtained from using approximately 75% ±45º plies. There is little effect of joint thickness if the fasteners are properly tightened [328].

2.5.2.3 Fastener Selection

Fasteners for composite joints must be designed specifically to allow full development of joint strength by taking into account the unique material properties of composites. They must not be susceptible to corrosion (including galvanic corrosion), and therefore are generally made from titanium and a few corrosion resistant stainless steels. The bearing area of the fastener tail and head must be relatively large to avoid "pull-through" failures. Fasteners must be able to be installed without causing damage to the surrounding laminate, leading to two-piece and blind fastener designs [309].

To address these issues MIL-HDBK-17 recommends tension head, 100º countersunk titanium fasteners for double shear joints. The full bearing capability of the joint cannot be achieved without using fasteners with high fixity, or good clamp-up. Fixity is a function of fastener stiffness, fit, installation forces, torque applied, and rotational resistance of the fastener head and collar. Relatively high tolerance holes should also be used, although not interference fit ones [309]. Collings [327] and Garbo and Ogonowski [353] both found that optimal fastener clamping strength for graphite/epoxy joints to be 22 MN/m^2, or a torque applied to the bolt of 3.4N-M.

2.5.2.4 Hygrothermal Effects

Kim and Whitney [354] studied the effects of temperature and moisture on the pin bearing strength of graphite/epoxy composite laminates. They found that temperature has a greater effect on bearing strength than moisture. A combination of hot and wet conditions lowered the strength a further 10% beyond that of the temperature alone. The greatest strength reduction seen was 40%. Other workers have studies these effects as well [355-357].

2.5.3 Fatigue

Fatigue performance of composite joints is generally superior to metal joints when properly designed. The major damage mechanism in fatigue is bearing failure in the form of hole elongation with net section failure for the static residual test. Factors in fatigue performance include material system, geometry, attachment details, loading mode, and environmental conditions. Clamp-up forces have a significant effect on delaying laminate failure by suppressing delamination failure modes and changing the fastener head restraint [309]. However, long-term relaxation due to the viscoelastic nature of the matrix, especially in hot and wet conditions, often negates this effect from consideration during strength evaluations [358].

Composite joint fatigue is also influenced by the loading mode [359-360]; joint geometry [360, 309]; attachment and fastening details [359-362]; laminate lay-up [359]; environmental conditions [359]; laminate thickness [360, 309]; and residual stress state [309].

2.6 Finite Element Analysis and Global Structural Optimization

Today finite element analysis (FEA) is the standard method for large scale analysis of continua; it has been used for not only structural analysis, but for heat transfer, fluid flow, lubrication, electric and magnetic fields, etc. [363]. It is a method of discretization, and developed from ideas from both mathematics (weighted residuals [364] and variational methods [365]) and engineering (direct continuum elements [366-367] and piecewise continuous trial functions [368-369]). Zienkiewicz [370-371] provides a brief history of the development of the method in relation to computational mechanics in general.

Neogi [31] studied the effects of load redistribution during structural optimization. The internal loads of a structure can be calculated through closed-form solutions or through a finite element analysis. The frequency of load reanalysis was explored, ranging from never to every optimization iteration. The hypothesis was that as the structure's physical characteristics (thicknesses, geometries, and stiffnesses) change during optimization the internal loads will move towards areas of high stiffness. At the next iteration the internal load distribution will therefore be different, prompting the question of feasibility if the initial loads are used throughout a structural optimization exercise.

To explore these effects of load redistribution Neogi utilized a simple 3-bar truss structure with a closed-form solution. The optimization problem was to minimize a weight-based objective function, using the independent cross-sectional areas of the trusses as design variables, with maximum stress constraints on each truss member. He found that the rate of convergence was lower if load updates were not included, i.e., load redistribution improves optimization convergence. Further, it was found that intermittent load updates during optimization resulted in either an infeasible or sub-optimal design. Therefore, in this study, finite element analysis will be used for both generating the proper initial load distribution and to update those load distributions during optimization following every iteration.

2.7 Summary of Literature Review

This thesis addresses a structural optimization problem that touches on multiple areas of study. This review was an attempt to introduce the reader to the many aspects of composite wing structural optimization, including bolted joints and aeroelasticity. The overarching topic of structural optimization is discussed, first as to how the general problem is formulated, followed with an overview of its historical development. Much of the development of methods and algorithms follows the development of computing power. Next, stochastic global optimization methods are described in Section 2.2, including the two algorithms used in this work, IHR and MPSA.

Composite structural optimization is discussed in Section 2.3. Continuous fiber materials have been the subject of much structural optimization work due to the anisotropic nature of the materials and resulting structures. Much of the research has been centered on aerospace. Design practice, mechanical property analyses, and manufacturing constraints are briefly described. The structural optimization of a composite wing is then described in several aspects. These include historical development, shape optimization and topology, aeroelasticity and flutter, and natural frequency determination.

Composite bolted joints are discussed next. There are many aspects of a composite bolted joint and many are described. The structural analysis technique used here is reviewed. Load sharing, failure and failure criteria, and some analysis software are detailed. The multitude of design considerations for a joint are reported, including geometry, stacking sequence, fastener selection, and hygrothermal effects. Joint fatigue is considered through the influences of loading mode, geometry, attachment details, stacking sequence, hygrothermal effects, thickness, and residual strength.

Due to the relationship between global structural optimization and reanalysis a finite element analysis will be used to update internal load distributions during optimization following every iteration. The finite element model is described in Appendix A.

In Chapter 3 the composite bolted joint analysis developed for this study is discussed.

Chapter 3

COMPOSITE BOLTED JOINT ANALYSIS

The composite bolted joint analysis was developed from work done by Chang et al. [371] that included a finite element analysis for the joint stresses. The finite element analysis was replaced by an elasticity solution by Savin [27] that provides the stress state at a characteristic distance away from the bolt holes. The stresses at the characteristic distance are compared to a failure criterion on a ply-by-ply basis that not only determines first ply failure but also the failure mode. The loads in the multi-fastener joints used in this study were determined by an iterative scheme that provides the bearing-bypass loads to the elasticity analysis. Failure criteria for the skin panel, rib flanges, and spar flange used in this study are also described.

3.1 Joint Flexibility and Design

Determination of the bolt load distribution in a joint is highly dependent on fastener flexibility, i.e., the behavior of the fasteners as elastic beams. Tate and Rosenfeld [324] derived a linear elastic theory for the loads carried by individual bolts in a joint, and in doing so created a "bolt constant", or "correlation coefficient" C that relates the various contributions from beam mechanisms to joint flexibility. This approach to bolted joint design was introduced in Chapter 2. The constant C for two different joint designs are discussed: single- and double-shear joints.

Nelson, Bunin, and Hart-Smith provide the equations for the single-shear joint correlation coefficient [372]. Hart-Smith modified the NACA 1051 equation to account for the bolt rotation that occurs in the single-shear joint. The equations were introduced in Chapter 2 but are repeated here for clarity:

$$C = C_{bs} + C_{bb} + C_{bbr} + C_{pbr} \tag{2.21}$$

where C_{bs} is the shear effect; C_{bb} is the bending effect; C_{bbr} is the bearing effect; and C_{pbr} is the plate bearing effect, given by the following equations:

$$C_{bs} = \frac{2t_s + t_p}{3G_b A_b} \tag{2.24}$$

$$C_{bb} = \frac{8t_s^3 + 16t_s^2 t_p + 8t_s t_p^2 + t_p^3}{192E_{bb} I_b} \tag{2.25}$$

$$C_{bbr} = \frac{2t_s + t_p}{t_s t_p E_{bbr}} \tag{2.26}$$

$$C_{pbr} = \frac{1}{t_s E_{sbr}} + \frac{2}{t_p E_{pbr}} \tag{2.27}$$

Here t_p and t_s are the thicknesses of the plate and strap, respectively, A_b is the area of the bolt $\left(\frac{\pi d^4}{4}\right)$, and I_b is the bolt moment of inertia $\left(\frac{\pi d^4}{64}\right)$. These equations are used for the single-shear joints in the wing design (rib-to-spar, rib-to-skin, and spar-to-skin). In these single-shear cases the plates and straps are composite laminates. A double-shear joint with two fastener rows is shown in Figure 3.1 with relevant geometry labels.

In the case of the double-shear joint it was found that the NACA 1051 equations for the correlation coefficient did not represent experimental test results accurately [373]. The bolt shear, bending, and bearing deformation terms were reduced as the deformations were too large compared to the strap bearing deformation. Lee [374] modified the equations appropriately to match test observations, resulting in

$$C_{bs} = \frac{t_s - t_p}{5G_b A_b} \tag{3.1}$$

$$C_{bb} = \frac{L_{eff}^3}{12E_{bb}I_b} \tag{3.2}$$

$$C_{bbr} = \frac{3t_s + t_p}{3t_s t_p E_{bbr}} \tag{3.3}$$

$$C_{pbr} = \frac{1.1}{t_s\sqrt{E_{s1}E_{s2}}} + \frac{1.1}{t_p\sqrt{E_{p1}E_{p2}}} \tag{3.4}$$

where E_{s1} and E_{s2} are the axial and transverse Young's moduli of the strap, E_{p1} and E_{p2} are the axial and transverse Young's moduli of the plate, and L_{eff} is given as

$$L_{eff} = \frac{t_s}{3} + \frac{t_p}{5} \tag{3.5}$$

These equations are used in this study for the double-shear joints in the wing design (side-of-body (SOB) skin/stringer, SOB skin/spar, and SOB rib). These joints vary in strap and plate definitions; in some cases, an average of laminate stiffnesses was taken to account for their unique design.

For joint design automation within the optimization program there are design considerations and checks based on composite bolted joint experience and research. The first check in the design is the hole diameter to laminate thickness ratio [313]:

$$\frac{d}{tn} \geq \frac{1}{3} \tag{3.6}$$

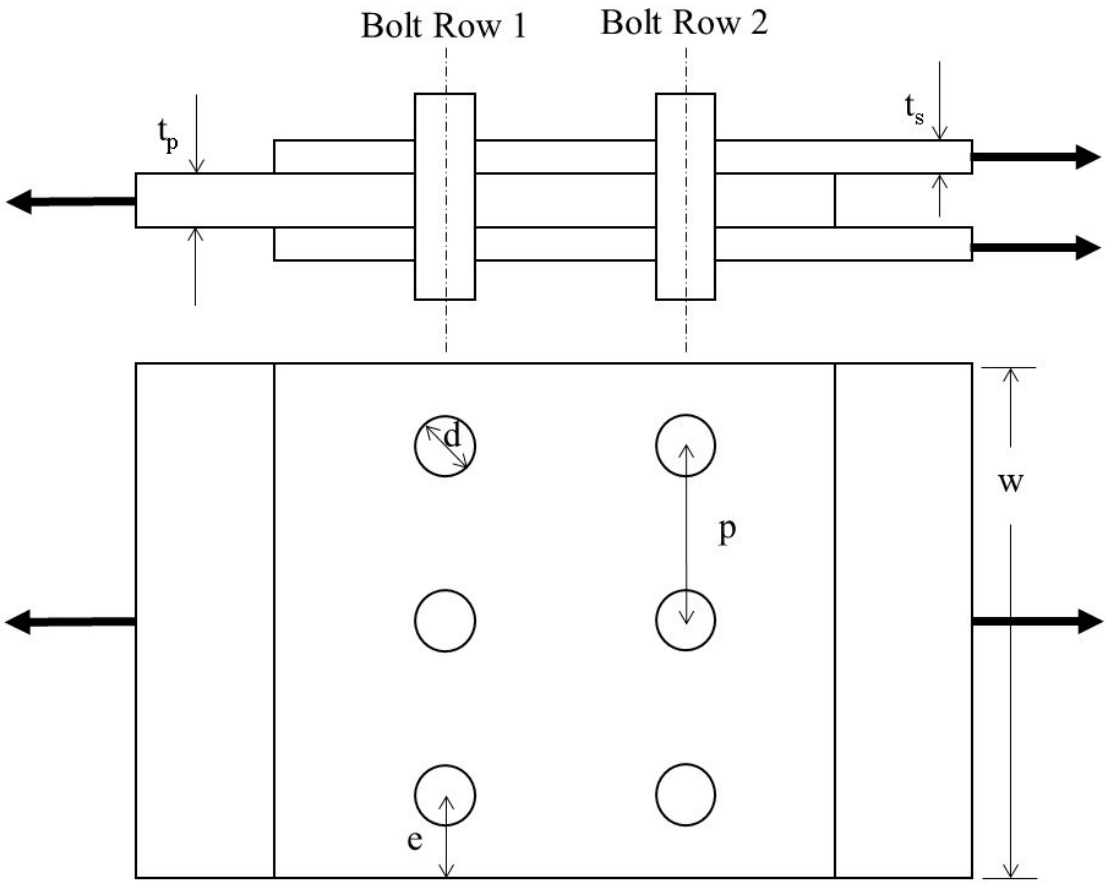

Figure 3.1: Double-shear Joint

This is expressed in the program as a way of choosing a fastener diameter from a list of discrete sizes provided; the joint thickness is compared through a series of inequalities to the discrete bolt sizes. As the optimizer chooses different numbers of plies in a joint laminate the program can resize the bolt appropriately. Bolt diameters that are too small for the joint tend to fail early; bolts that are too large are inefficient and can cause premature net section failures.

The second design consideration is for edge margin, i.e., the distance from the edge of the hole to the edge of the laminate [313]:

$$\frac{e}{d} \geq 3 \tag{3.7}$$

This provides the program a way of determining the length of the fastener rows by subtracting off the required edge margin from the total joint length. The third design consideration, fastener pitch, can be used to determine the number of bolts in a row where the edge margin is greater than one [375-376]:

$$K_{te} = 2 + \left(1 - \frac{d}{w}\right)^3 \tag{2.23}$$

$$p = d * K_{te} \tag{3.8}$$

where p is the fastener pitch. The number of bolts in a given row, N, can then be determined simply as

$$N = \frac{(w - 2e)}{p} \tag{3.9}$$

With these calculations the bolt diameters, edge margin, fastener pitch, and the number of bolts in a row are known. Together these expressions allow the determination of the bearing-bypass load in the composite bolted joint.

3.2 Bolted Joint Bearing-Bypass Analysis

A multi-fastener joint is a statically-indeterminate structural system, and individual bolts do not generally carry equal loads in the elastic range. With a series of assumptions around material and structure linearity, a relationship between the loads R_i of any two successive bolts can be obtained:

$$R_{i+1} = \frac{C_i}{C_{i+1}} R_i + N_i \frac{(2K_p + K_s)}{C_{i+1}} R_i - \frac{2K_p}{C_{i+1}} P + \frac{(2K_p + K_s)}{C_{i+1}} \sum_{r=1}^{i-1} R_r \tag{2.20}$$

where K_p is the plate constant and K_s is the strap constant. A critical assumption is that the bolts in any transverse row are loaded equally and are identical [377]. To solve this model of loads a simplification is performed. For single-shear joints,

$$R_i = \frac{\left[R_{i+1} - \lambda \sum_{r=1}^{i-1} R_r + \mu \right]}{(1+\lambda)}, i - 1,2,...n-1 \tag{2.18}$$

$$\lambda = \frac{2K_p + K_s}{C}, \text{ and } \mu = \frac{2K_p P}{C} \tag{2.19}$$

For double-shear joints, where the bolts in one row may not be the same as another, a non-constant correlation coefficient is assumed:

$$R_i = \left(\frac{C_{i+1}}{C_i + \gamma} \right) R_{i+1} + \left(\frac{2K_p}{C_i + \gamma} \right) P - \frac{\gamma \sum_{r=1}^{i-1} R_r}{C_i + \gamma}, i - 1,2,..n-1 \tag{3.10}$$

$$\gamma = 2K_p + K_s \tag{3.11}$$

These equations are solved using a form of Gauss-Seidel iteration [378-379]. First, an initial

estimate of the load in each bolt row is set:

$$R_{i0} = \frac{P}{nbr} \tag{3.12}$$

where nbr is the number of bolt rows in the joint. Equation (2.20) or (3.10), whichever is appropriate to the joint being analyzed, is used to generate new estimates for the bolt loads R_i. The last bolt load is given by

$$R_n = P - \sum_{r=1}^{n-1} R_r \tag{3.13}$$

The iteration continues until, for all bolts, the change from one iteration to the next is less than a constant, ε (here, ε is 1.0×10^{-6} [377]) or the number of iterations reaches 1,000. The bypass load for that bolt row is the difference between the applied load and the bolt row load.

Three calculations were performed to exercise the algorithm. First, an example analysis from Tate and Rosenfeld [324] was used to illustrate the bolt load sharing in a metallic, five-row joint. The example joint design variables are shown in Table 3.1. Second, the correlation coefficient C was halved for all the bolt rows; it can be seen in Figure 3.2 that the ratios of the loads in the bolts changes as expected. The first and last bolt rows become more highly loaded with more bolt flexibility. Third, to look at non-constant correlation coefficients that are present in some of the joints in this study, only C1 (the first bolt row) was halved. Again, Figure 3.2 shows the expected result that first bolt takes a large portion of the joint load.

For the next part of the analysis the net section stresses and the bypass stresses are calculated for each joint and bolt row. The stresses around the circumference of the bolt holes can now be determined.

3.3 Stress Analysis of an Anisotropic Composite Plate with a Hole

As discussed in Section 2.5.1, a two-dimensional elasticity theory for infinite, anisotropic plates with holes was put forward by Savin [27]. For such a plate with in-plane loading only (no bending) and assuming no thermal or moisture effects the stress resultants can be written (following [380])

$$\begin{Bmatrix} \varepsilon_{xx}^0 \\ \varepsilon_{yy}^0 \\ \gamma_{xy}^0 \end{Bmatrix} = \begin{bmatrix} a_{11} & a_{12} & a_{16} \\ a_{12} & a_{22} & a_{26} \\ a_{16} & a_{26} & a_{66} \end{bmatrix} \begin{Bmatrix} N_{xx} \\ N_{yy} \\ N_{xy} \end{Bmatrix} \tag{3.14}$$

Table 3.1: Tate and Rosenfeld Numerical Example for Bolt Load Calculation

Inputs:	Symbol	Value
Number of bolt rows	nbr	5
Bolt Diameter (m)	d	0.00635
Bolt Stiffness (GPa)	E_b	200
Plate Thickness (m)	t_p	0.0079375
Strap thickness (m)	t_s	0.0047625
Fastener Pitch (m)	p	0.0254
Plate Width (m)	w	0.0508
Plate & Strap Stiffness (GPa)	E_p, E_s	72.4
Load (N)	P	4.45
Strap Constant (m/N)	$K_s = \left(\frac{p}{wt_s E_s}\right)$	1.45E-06
Plate Constant (m/N)	$K_p = \left(\frac{p}{wt_p E_p}\right)$	8.68E-07
Correlation Coefficient (Bolt Constant)	C	1.3065E-05
	$\lambda = \frac{2K_p + K_s}{C}$	0.244165
	$\mu = \frac{2K_p P}{C}$	0.133181
Number of Iterations		63

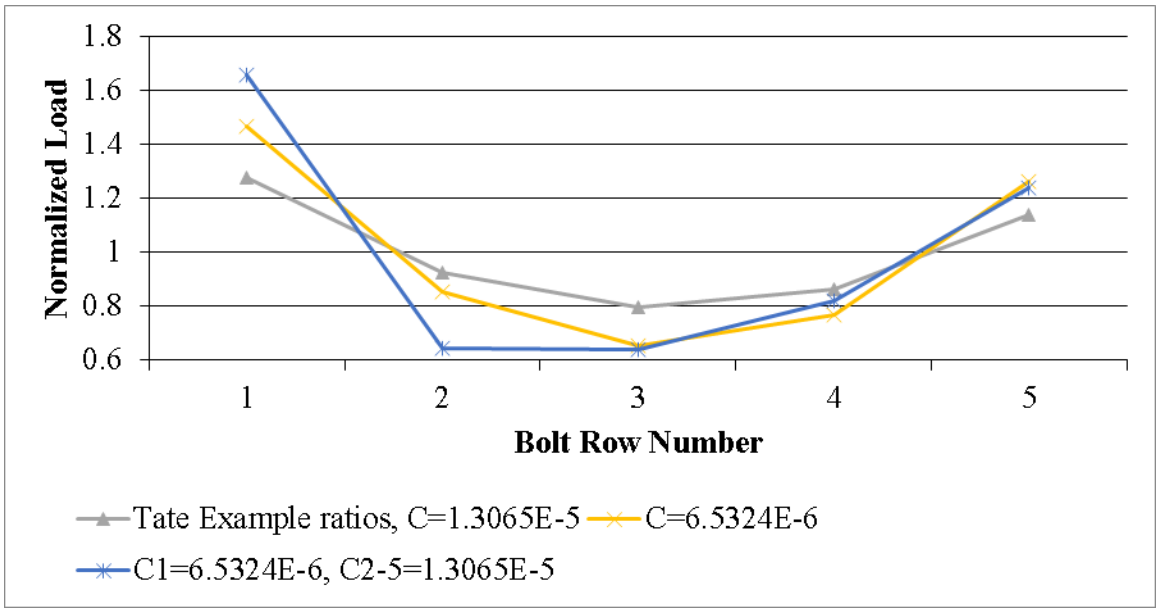

Figure 3.2: Normalized Joint Load vs. Bolt Row Number for Tate Example, C = 1.3065E-5; C = 6.5324E-6; and C1 = 6.5324E-6, C2-5 = 1.3065E-5

where ε^0 are the midplane strains, [a] is the compliance matrix, and N are the stress resultants. In the Savin formulation the effective stresses are required rather than the stress resultants. The strain is constant through the thickness of the laminate as there is no bending; the superscript 0's are therefore dropped from the strain variables. We now have

$$\begin{Bmatrix} \varepsilon_{xx} \\ \varepsilon_{yy} \\ \gamma_{xy} \end{Bmatrix} = \begin{bmatrix} \bar{a}_{11} & \bar{a}_{12} & \bar{a}_{16} \\ \bar{a}_{12} & \bar{a}_{22} & \bar{a}_{26} \\ \bar{a}_{16} & \bar{a}_{26} & \bar{a}_{66} \end{bmatrix} \begin{Bmatrix} \bar{\sigma}_{xx} \\ \bar{\sigma}_{yy} \\ \bar{\sigma}_{xy} \end{Bmatrix} \tag{3.15}$$

where

$$\begin{aligned} \bar{a}_{ij} &= t a_{ij} \\ \bar{\sigma}_{ij} &= \frac{N_{ij}}{t} \end{aligned} \tag{3.16}$$

are the effective compliance matrix terms and effective stresses, respectively.

Muskhelishvili [323] proposed a "characteristic equation", a fourth-order polynomial, to represent any anisotropic panel:

$$\bar{a}_{11} s^4 - 2\bar{a}_{16} s^3 + \left(2\bar{a}_{12} + \bar{a}_{66}\right) s^2 - 2\bar{a}_{26} + \bar{a}_{22} = 0 \tag{3.17}$$

This is based on the biharmonic equation for generally orthotropic materials. Considering potential energy, it can be shown that the characteristic equation has no real roots, i.e., they are all complex or imaginary:

$$\begin{aligned} s_{1,3} &= \alpha_1 \pm i\beta_1 \\ s_{2,4} &= \alpha_2 \pm i\beta_2 \end{aligned} \tag{3.18}$$

where α and β are real constants and β are greater than zero and i is the square root of -1. Two distinct roots, those with positive imaginary parts, are sufficient for a general solution of the problem; these are called the principal roots:

$$\begin{aligned} s_1 &= \alpha_1 + i\beta_1 \\ s_2 &= \alpha_2 + i\beta_2 \end{aligned} \tag{3.19}$$

From equation (3.17) it can be seen that the roots of the characteristic equation $s_{1,2}$ are dependent on the elements of the effective compliance matrix and therefore on the material properties and stacking sequence of the laminate only.

At this point it is important to point out that, for general laminates, the roots of the characteristic equation must be found using numerical solution of the complex polynomial. The standard way of performing this calculation is the Jenkins-Traub three-stage complex algorithm [381-382].

This algorithm is available in Fortran and in C++; however, the analysis completed during this study does not include the Jenkins-Traub algorithm due to time and funding constraints. Instead, the focus is on specially orthotropic laminates, i.e., those with a_{16} and a_{26} equal to zero. Practically this means the laminate in this analysis must be both symmetric and balanced. This is reasonable for several reasons: 1) specially orthotropic laminates are generally used in industry; 2) the bending coupling of the thick laminates necessary for the wing will be relatively small; 3) consideration of circular holes only; and 4) only in-plane loading in the laminates is considered.

By limiting consideration to specially orthotropic laminates, the characteristic equation becomes

$$\bar{a}_{11}s^4 + \left(2\bar{a}_{12} + \bar{a}_{66}\right)s^2 + \bar{a}_{22} = 0 \tag{3.20}$$

Noting that

$$\begin{aligned} a_{11} &= \frac{1}{E_{xx}} \\ a_{12} &= -\frac{\nu_{xy}}{E_{xx}} \\ a_{22} &= \frac{1}{E_{yy}} \\ a_{66} &= \frac{1}{G_{xy}} \end{aligned} \tag{3.21}$$

for the laminate, the characteristic equation can be written in an alternate form [383, 344]:

$$s^4 + 2\chi s^2 + \lambda^2 = 0 \tag{3.22}$$

where

$$\begin{aligned} \chi &= \left(\frac{E_{xx}}{2G_{xy}} - \nu_{xy} \right) \\ \lambda &= \sqrt{\frac{E_{xx}}{E_{yy}}} \end{aligned} \tag{3.23}$$

There are three possible relationships between χ and λ; for all three cases α_1 is $-\alpha_2$ (which may be equal to zero). The three cases are as follows:

Case I: $\chi < \lambda$

$$\begin{aligned} s_1 &= -\sqrt{-\chi - i\sqrt{\left(\lambda^2 - \chi^2\right)}} = \alpha + i\beta \\ s_2 &= \sqrt{-\chi - i\sqrt{\left(\lambda^2 - \chi^2\right)}} = -\alpha + i\beta \end{aligned} \tag{3.24}$$

Case II: $\chi > \lambda$

$$s_1 = \sqrt{\chi - i\sqrt{\left(\chi^2 - \lambda^2\right)}} = i\beta_1 \tag{3.25}$$

$$s_2 = \sqrt{\chi + i\sqrt{\left(\chi^2 - \lambda^2\right)}} = i\beta_2$$

Case III: $\chi = \lambda$ $$s_1 = s_2 = \sqrt{\chi} = i\beta = i \tag{3.26}$$

Note that Case III corresponds to isotropic or quasi-isotropic materials.

Savin [27] utilized holomorphic functions to find the stresses around a hole in an infinite, anisotropic plate of the form

$$\begin{aligned} \phi(z) &= A\ln z_1 + \left(B^* + iC^*\right)z_1 + \phi_0 \\ \varphi(z) &= B\ln z_2 + \left(B'^* + iC'^*\right)z_2 + \varphi_0 \end{aligned} \tag{3.27}$$

Here A, B, B*, C*, B'*, and C'* are real constants; for a case with no traction force acting on the hole boundary, A and B are zero. The remaining constants are concerned with the stresses at infinity. These will not be discussed further since those stresses are known and displacements of the system are not part of the analysis (see Chern and Tuttle, [345]). Instead the focus is on the remaining holomorphic functions $\varphi_0(z_1)$ and $\psi_0(z_2)$. To solve for these a conformal mapping is used to transfer points around the hole in the real, (x, y) plane into a unit circle in two complex, (z_1, z_2) plane:

$$\begin{aligned} z_1 &= x + s_1 y = x + \alpha_1 y + i\beta_1 y = \frac{a\left(1 + is_1\right)}{2}\zeta_1 + \frac{a\left(1 - is_1\right)}{2\zeta_1} \\ z_2 &= x + s_2 y = x + \alpha_2 y + i\beta_2 y = \frac{a\left(1 + is_2\right)}{2}\zeta_2 + \frac{a\left(1 - is_2\right)}{2\zeta_2} \end{aligned} \tag{3.28}$$

for the circular bolt holes discussed here; a is the hole radius, and (x, y) are centered on the hole. After inversion, the functions become

$$\begin{aligned} \zeta_1 &= \frac{z_1 \pm \sqrt{z_1^2 - a^2\left(1 + s_1^2\right)}}{a\left(1 + is_1\right)} \\ \zeta_2 &= \frac{z_2 \pm \sqrt{z_2^2 - a^2\left(1 + s_2^2\right)}}{a\left(1 + is_2\right)} \end{aligned} \tag{3.29}$$

The algebraic sign for the square roots in equations (3.29) must be chosen such that ζ_1 and ζ_2 are inside the unit circle, i.e., $\left|\zeta_1\right| \le 1$ and $\left|\zeta_2\right| \le 1$ at the current (x, y) position. Whatever sign is used here must be recorded and used again for calculations of the derivatives of the holomorphic functions to be discussed.

Utilizing the remote, far field stresses the holomorphic functions proposed in Savin [27] can be written as

$$\phi_0(z_1) = \frac{-i\left[a\overline{\sigma}_{xx}^{\infty} + ias_2\overline{\sigma}_{yy}^{\infty} + a(s_2+i)\overline{\tau}_{xy}^{\infty}\right]}{2(s_1-s_2)}\zeta_1$$
$$\varphi_0(z_2) = \frac{i\left[a\overline{\sigma}_{xx}^{\infty} + ias_1\overline{\sigma}_{yy}^{\infty} + a(s_1+i)\overline{\tau}_{xy}^{\infty}\right]}{2(s_1-s_2)}\zeta_2 \tag{3.30}$$

where the remote stresses are given as

$$\overline{\sigma}_{ij}^{\infty} = \frac{N_{ij}^{\infty}}{t} \tag{3.31}$$

Note here that the denominators in equations (3.30) can equal zero if the principal roots of the characteristic equation are equal, i.e., for an isotropic or quasi-isotropic material. This represents an indeterminate solution. Since quasi-isotropic laminates are so common in industry and could easily be part of some optimal solution for the wing design a method to obtain an approximate solution for quasi-isotropic laminates was proposed by Tung [384]. Specifically, in the case of repeated roots, the first principal root is increased by 1%, while the second principal root is decreased by 1%. This small spread in the values of s_1 and s_2 prevents the numerical issues associated with repeated roots.

To obtain the effective stresses around the hole the derivative of the holomorphic functions $\varphi_0(z_1)$ and $\psi_0(z_2)$ must be derived; this can be done as a holomorphic function by definition is complex differentiable in a neighborhood of every point in its domain. These derivatives are given as

$$\phi_0'(z_1) = \frac{d\phi_0}{dz_1} = \frac{-i\left[a\overline{\sigma}_{xx}^{\infty} + ias_2\overline{\sigma}_{yy}^{\infty} + a(s_2+i)\overline{\tau}_{xy}^{\infty}\right]}{2(s_1-s_2)}\left\{\frac{1}{a(1+is_1)}\left[1 \pm \frac{z_1}{\sqrt{z_1^2 - a^2(1+s_1^2)}}\right]\right\}$$
$$\varphi_0'(z_2) = \frac{d\varphi_0}{dz_2} = \frac{i\left[a\overline{\sigma}_{xx}^{\infty} + ias_1\overline{\sigma}_{yy}^{\infty} + a(s_1+i)\overline{\tau}_{xy}^{\infty}\right]}{2(s_1-s_2)}\left\{\frac{1}{a(1+is_2)}\left[1 \pm \frac{z_2}{\sqrt{z_2^2 - a^2(1+s_2^2)}}\right]\right\} \tag{3.32}$$

Recall that the algebraic sign in the brackets in equations (3.32) must be the same as was required to satisfy the conditions on equations (3.29).

From the derivation of the characteristic equation, the in-plane stresses at any point in the plate around the hole can now be found in terms of the holomorphic function derivatives:

$$\overline{\sigma_{xx}} = \overline{\sigma_{xx}^{\infty}} + 2\,\mathrm{Re}\left[s_1^2\phi_0'(z_1) + s_2^2\varphi_0'(z_2)\right]$$
$$\overline{\sigma_{yy}} = \overline{\sigma_{yy}^{\infty}} + 2\,\mathrm{Re}\left[\phi_0'(z_1) + \varphi_0'(z_2)\right] \tag{3.33}$$
$$\overline{\tau_{xy}} = \overline{\tau_{xy}^{\infty}} - 2\,\mathrm{Re}\left[s_1\phi_0'(z_1) + s_2\varphi_0'(z_2)\right]$$

To obtain the circumferential stress around the hole, the angle between the x-axis and the tangential c-axis must be calculated from the slope (see Figure 3.3)

$$\Phi = \tan^{-1}\left(\frac{\partial y}{\partial x}\right) = \tan^{-1}\left(\mp \frac{ax}{a^2\sqrt{1-(x/a)^2}}\right) \tag{3.34}$$

and the stress transformation equations must be used:

$$\begin{Bmatrix} \overline{\sigma}'_{xx} \\ \overline{\sigma}'_{yy} \\ \overline{\tau}'_{xy} \end{Bmatrix} = \begin{bmatrix} \cos^2(\theta) & \sin^2(\theta) & 2\cos(\theta)\sin(\theta) \\ \sin^2(\theta) & \cos^2(\theta) & -2\cos(\theta)\sin(\theta) \\ -\cos(\theta)\sin(\theta) & \cos(\theta)\sin(\theta) & \cos^2(\theta)-\sin^2(\theta) \end{bmatrix} \begin{Bmatrix} \overline{\sigma}_{xx} \\ \overline{\sigma}_{yy} \\ \overline{\tau}_{xy} \end{Bmatrix} \tag{3.35}$$

The circumferential stress $\overline{\sigma_{cc}}$ is then given as

$$\overline{\sigma}_{cc} = \overline{\sigma}_{xx}\cos^2\Phi + \overline{\sigma}_{yy}\sin^2\Phi + 2\overline{\tau}_{xy}\cos\Phi\sin\Phi \tag{3.36}$$

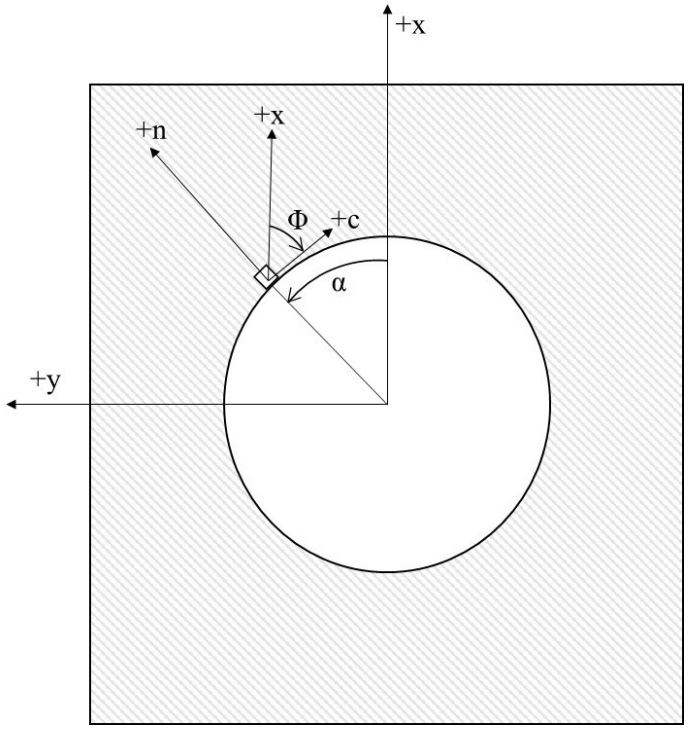

Figure 3.3: A Stress Element at an Edge of a Circular Hole Showing the Angular Position α, the Normal and Circumferential Axes n and c, and the Angle Between the x- and c-Axes Φ (after [380])

As a check of the analysis a composite bolted joint tested by Nelson et al. [372] was run through the in-plane stress analysis procedure. However, the laminate tested, labeled JT12CF, is not specially orthotropic. It is a 96-ply laminate, similar in layup to that found in Table 4.18, except there are no plain weave plies. The material properties were used to calculate the effective compliance matrix terms as before; Table 3.2 shows these and the resulting principal roots of the characteristic equation. Because the WINGJOTA cannot accommodate the laminate, Mathematica was used to determine the principal roots s_1 and s_2. These were then manually inserted into the program to run the rest of the analysis. To compare this tested laminate and a similar, specially orthotropic one, WINGJOTA was also run with the $\bar{a}_{16}$ and $\bar{a}_{26}$ terms set to zero and the resulting principal roots used for the analysis. As can be seen from Figure 3.4, at the hole edge the circumferential stresses are different. However, as the next section will explore, when the stresses are calculated away from the hole edge at what is called the characteristic distance, the differences for these thick laminates becomes much less pronounced.

Now that the stresses around the circumference of the bolt holes can be determined, a failure criterion is applied that will show both failure strength and mode.

Table 3.2: Effective Compliances and Principal Roots of Example Thick, Graphite-Epoxy Laminate [372]

		JT12CF	Specially Orthotropic
Effective compliance terms (m^2/N)	$\bar{a}_{11}$	1.59260E-11	1.59260E-11
	$\bar{a}_{12}$	-6.95002E-12	-6.95002E-12
	$\bar{a}_{16}$	-3.096440E-13	0.0
	$\bar{a}_{22}$	2.78613E-11	2.78613E-11
	$\bar{a}_{26}$	-6.67139E-13	0.0
	$\bar{a}_{66}$	5.30512E-11	5.30512E-11
Principal Roots	s_1	0.20168+i(0.94757)	0.21773+i(1.12926)
	s_2	-0.20168+i(0.94757)	-0.21773+i(1.12926)

3.4 Failure Strength and Failure Mode Analysis

Camanho noted in his Ph.D. thesis in 1999 [385] that there was "no definitive method to predict joint strength" in the literature, a statement that is still true today. For this work a method of determining if failure in a composite joint has occurred was sought that would be compatible with the rapid reanalysis and optimization algorithm. Therefore, it was desired to have a method that was analytic and relatively simple. The ability to predict the failure mode of the joint was also necessary to avoid tension and shear failures. Several methods were explored, including those of Xiong [339] and Kradinov et al. [341-343]; however, these were difficult to implement and may not have the computation simplicity necessary for this algorithm.

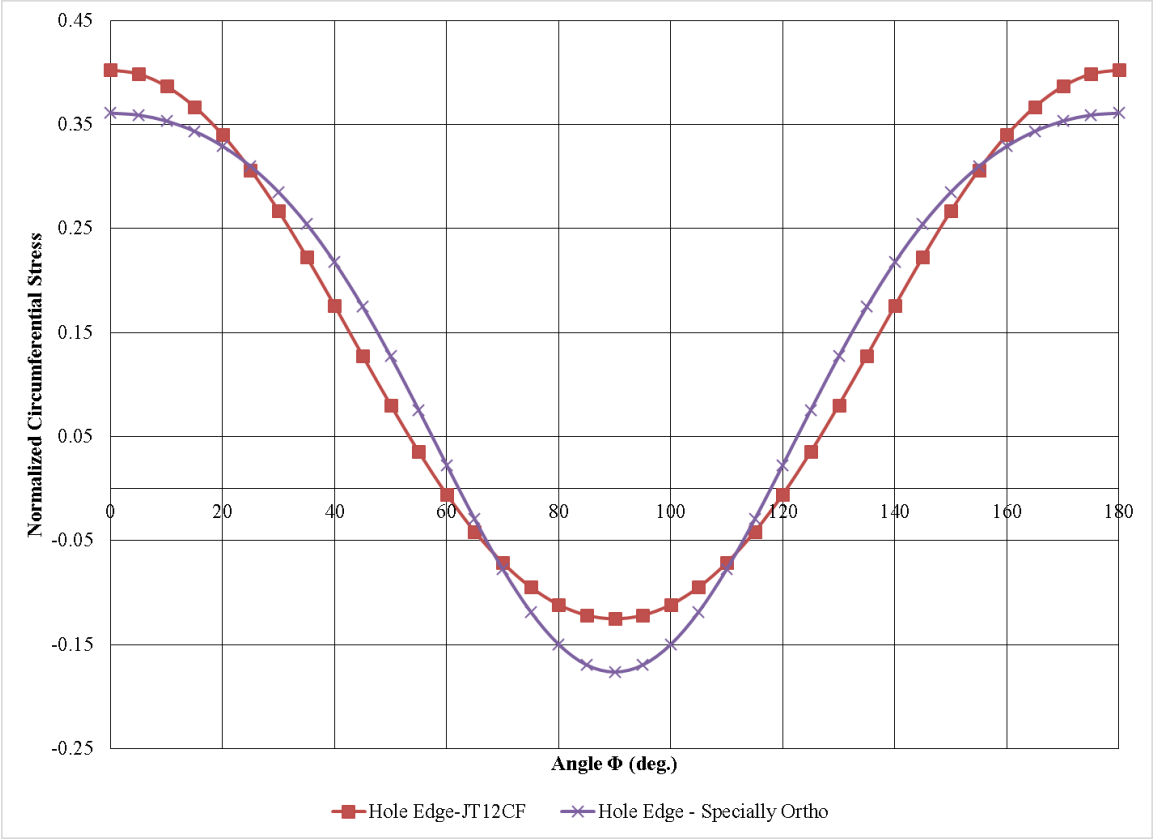

Figure 3.4: Normalized Circumferential Stress vs. Angle Φ Around a Circular Hole, JT12CF Laminate

3.4.1 Joint Failure Strength

A method proposed by Chang et al. in 1982 was chosen for implementation, with an important substitution [371]. There are two steps to the method: 1) determine the stress distribution in the laminate of the joint by the use of a finite element methods, and 2) determine the failure load and mode utilizing Yamada's failure criterion [28]. The finite element analysis used in the paper is two-dimensional and although fairly simple and compared favorably to experimental data, it would be computationally expensive to implement for each of the six types of joints in this wing design multiple times. Therefore, the stresses in the joint laminates are determined using the analyses presented in the previous sections of this chapter, i.e., the Savin solution and the Tate and Rosenfeld load distribution algorithm.

The failure hypothesis proposed in Chang et al. [371] is that failure occurs when any ply fails on a characteristic curve according to a chosen failure criterion. The characteristic curve, first proposed by Whitney and Nuismer [29, 386], is specified by characteristic lengths R_{0t} and R_{0c} for tension and compression, respectively. These parameters are only dependent on material properties and can be determined experimentally. However, Garbo and Ogonowski [353] found that the values of the characteristic lengths are approximately the same for carbon-epoxy

composites. The following values are used during the present study. Note that these values are user specified, so as experimental data becomes available for the composite of interest they can be specified:

$$R_{0t} = 0.02 \text{ in} = 0.000508 \text{ m}$$
$$R_{0c} = 0.025 \text{ in} = 0.000635 \text{ m}$$

It is interesting to note that Camanho and Lambert [387] provided a method for composite joint failure analysis similar to what is performed here. One aspect of that work was the derivation of a numerical method to determine the characteristic lengths. The assumptions, however, include that the laminate is quasi-isotropic; therefore, numerical determination of the characteristic lengths was not utilized.

The characteristic curve (Figure 3.5) is described as

$$r_c(\theta) = R + R_{0t} + (R_{0c} - R_{0t}) \cos(\theta) \tag{3.37}$$

The failure criterion chosen by Chang et al. and utilized here is the one developed by Yamada and Sun in 1978 [28]. It is based on two assumptions: 1) the entire laminate is cracked along the fiber interfaces at the final stage of failure, i.e., only the axial and shear moduli are considered effective, and 2) the cross-ply laminate shear strength is appropriate as it takes into account the lamination effect. This causes the apparent shear strength of the laminate to be higher than a lamina. Failure occurs when, for any ply, $e \geq 1$:

$$\left(\frac{\sigma_{xx}}{XT}\right)^2 + \left(\frac{\tau_{xy}}{Sc}\right)^2 = e^2 \begin{cases} e < 1, & no \quad failure \\ e \geq 1, & failure \end{cases} \tag{3.38}$$

Here XT is the longitudinal tensile strength and Sc is the shear strength of a symmetric, cross-ply laminate that has the same number of plies of the laminate under consideration.

After the characteristic curve is found for each bolt the Savin solution procedure is used to determine the stresses at those points on the characteristic curve around the holes. The equivalent loads at those points are found. The Classical Lamination Theory (CLT) is then used to generate mid-ply strains, local and global strains, and local and global stresses in the laminate. The Yamada criterion is applied, ply-by-ply, to determine ply failure. The angle at which the failure occurs is known because the failure is determined at the characteristic curve, which extends completely around the holes. This provides an estimate of the failure mode, as follows:

$$\begin{aligned} 15° < \theta_f < 15° &\rightarrow \text{bearing mode} \\ 30° < \theta_f < 60° &\rightarrow \text{shearout mode} \\ 75° < \theta_f < 90° &\rightarrow \text{tension mode} \end{aligned} \tag{3.39}$$

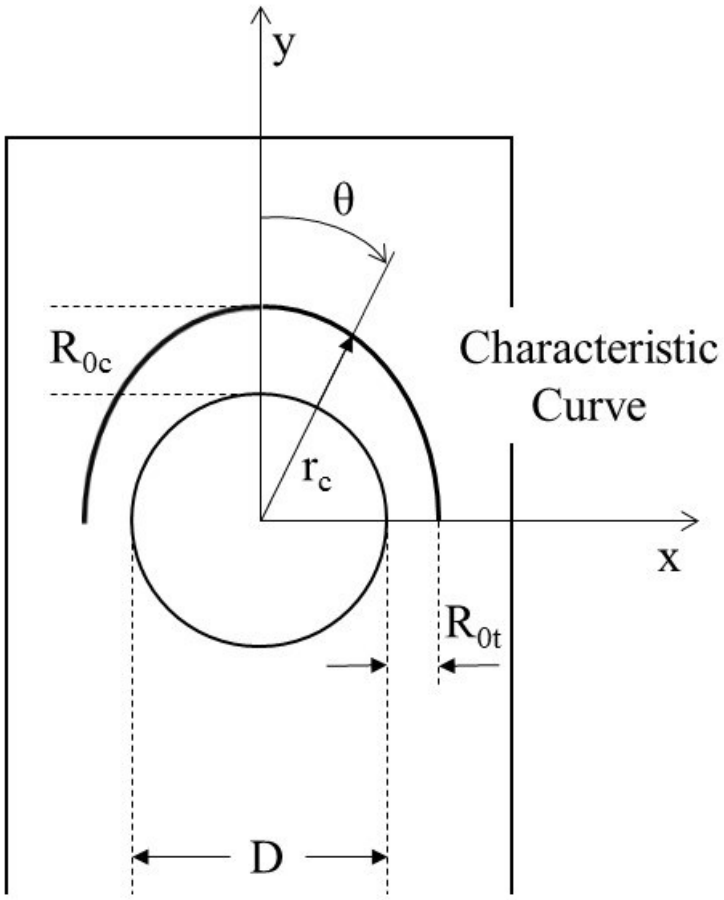

Figure 3.5: Description of the Characteristic Curve (after [371])

where θ_f is the failure angle. These angles apply to each of the four quadrants of the characteristic curve. Bearing mode failures are generally seen as the desirable failure mode in composite joint design. Shear and tension failures are cause to signal WINGJOTA to stop analyzing for the Yamada failure criterion ply-by-ply; this was done to allow the study of how the failure mode is effected by the laminate stacking sequence and thickness. However, all three failure modes are considered a first-ply failure and cause the program to generate a new composite laminate for the joint being analyzed.

One effect that taking the failure criterion at the characteristic curve is that the peak stresses are reduced and the difference between a general and specially orthogonal laminate tend to be negligible. Considering the JT12CF example composite joint previously analyzed (see Figure 3.4) the same normalized circumferential stresses were calculated at the characteristic curve for the accurate, general laminate, and the specially orthotropic analog. As can be seen in Figure 3.6, any differences are nullified by moving away from the hole edge.

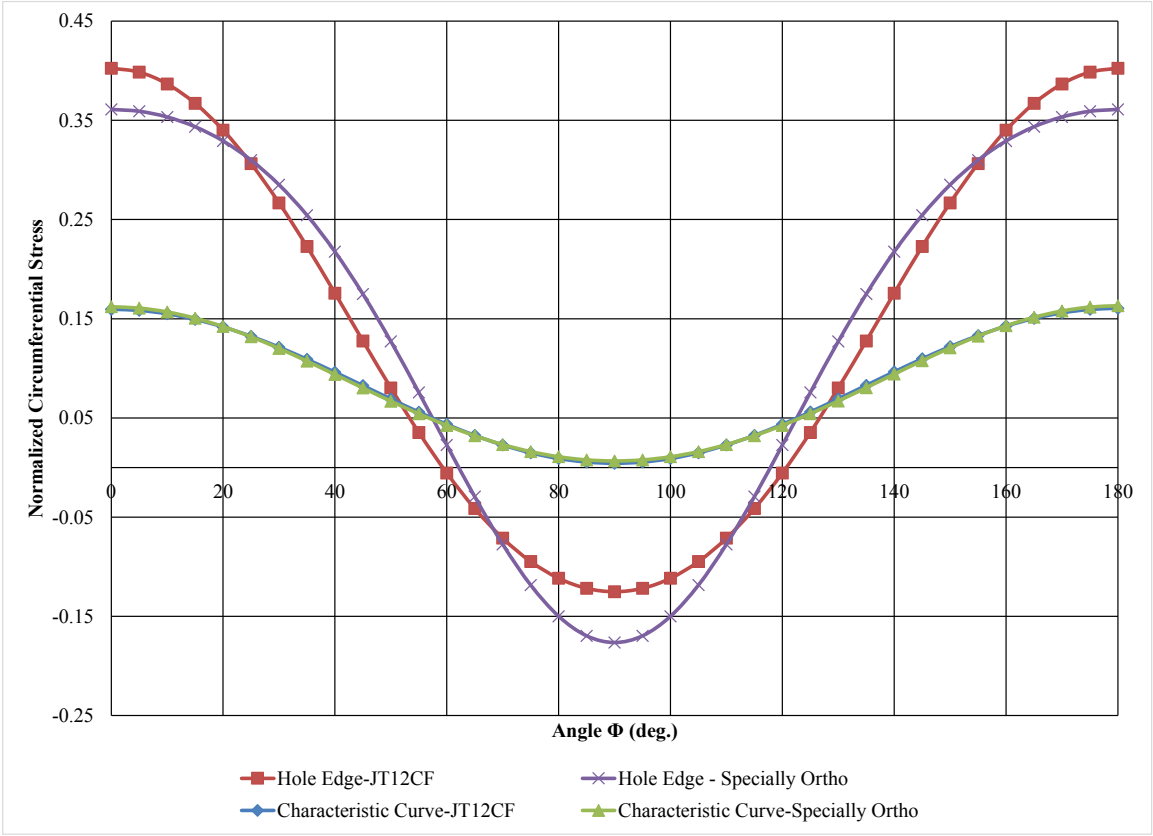

Figure 3.6: Normalized Circumferential Stress vs. Angle Φ Around a Circular Hole and at the Characteristic Curve, JT12CF Laminate

3.4.2 Other Failure Criteria

There were two other failure criteria considered in this work: the maximum strain and a modified Tsai-Wu failure criteria. The maximum strain criterion is simply a set ε_{max} for the joint laminate. Nelson et al. [372] set this as

$$\varepsilon_{max} = 0.005 \tag{3.40}$$

This failure check is applied to the laminates in the joint using the bypass loads generated. The other failure criterion is a modified form of one proposed by Tsai and Wu [388] in 1971 based on a quadratic interaction:

$$F_{ij}\sigma_i\sigma_j + F_i\sigma_i = 1 \tag{3.41}$$

where F_{ij} and F_i are strength parameters. For the case of two-dimensional stress (i, j = 1, 2, 6) and accounting for the lack of coupling between shear and normal components [389],

$$F_{11}\sigma_1^2 + 2F_{12}\sigma_1\sigma_2 + F_{22}\sigma_2^2 + F_{66}\sigma_6^2 + F_1\sigma_1 + F_2\sigma_2 = 1 \tag{3.42}$$

Based on uniaxial tests, five of the six strength parameters can be found in terms of experimental strength results for a given composite:

$$\begin{aligned} F_{11} &= \frac{1}{X_T X_C} \\ F_{22} &= \frac{1}{Y_T Y_C} \\ F_{66} &= \frac{1}{S^2} \\ F_1 &= \frac{1}{X_T} - \frac{1}{X_c} \\ F_2 &= \frac{1}{Y_T} - \frac{1}{Y_c} \end{aligned} \tag{3.43}$$

where X_T and X_C are the longitudinal strength in tension and compression, respectively; Y_T and Y_C are the transverse strength in tension and compression, respectively; and S is the shear strength. The sixth strength parameter, F_{12}, can be obtained from a biaxial test, which is difficult to perform experimentally. Therefore, in 1981 Ogonowski used a modified Tsai-Wu criterion for compostie joint analysis. This criterion was equation (3.42) with equations (3.43) substituted in; F_{12} set to zero [346]. This is what was utilized in this work. Since that time, Tuttle [380] has proposed performing a uniaxial test with a 45° off-axis specimen. The resulting failure stress, σ_1^{45}, can be substituted into equation (4.42). Solving for F_{12} results in

$$F_{12} = \frac{1}{2\left(\sigma_1^{45}\right)^2}\sigma_1^2\left[4 - \sigma_1^{45}\left\{2\left(F_1 + F_2\right) + \sigma_1^{45}\left(F_{11} + F_{22} + F_{66}\right)\right\}\right] \tag{3.44}$$

The last check on composite bolted joint performance is for bolt failure. For the double-shear joints in the wing design there is data on failure load for the various bolts directly from the vendor (see Table 4.17) For the single-shear joints the following equation was used:

$$f_v = R_i \frac{4}{\pi(2a)^2} \tag{3.45}$$

where f_v is the shear strength of the bolts and R_i is the load in each individual bolt.

For the I-stringer stiffened panel, the bending strains were calculated using a composite beam theory model [390]. Axial strain caused by bending in any skin panel and stiffener are defined by

$$\left(\varepsilon_x^{skin}\right)_{bending} = \frac{M_x c_{skin}}{(EI)_{panel}} \tag{3.46}$$

$$\left(\varepsilon_x^{stringer}\right)_{bending} = \frac{M_x c_{stringer}}{(EI)_{panel}} \tag{3.47}$$

where M_x is the axial bending moment, c_{skin} and $c_{stringer}$ are the distances from the neutral axial to the indiviual plies in the skin, bottom flange, and top flange laminates, and $(EI)_{panel}$ is the effective bending stiffness of the panel. These bending strains are added to the local strains induced by the in-plane loads to give a total local strain in the panel:

$$\begin{Bmatrix} \varepsilon_x^i \\ \varepsilon_y^i \\ \gamma_{xy}^i \end{Bmatrix}_{skin} = \begin{Bmatrix} \varepsilon_x \\ \varepsilon_y \\ \gamma_{xy} \end{Bmatrix}_{panel} + \begin{Bmatrix} \varepsilon_x^i \\ 0 \\ 0 \end{Bmatrix}_{bending} \quad \text{for i = 1, 2, …, nl} \tag{3.48}$$

$$\begin{Bmatrix} \varepsilon_x^j \\ \varepsilon_y^j \\ \gamma_{xy}^j \end{Bmatrix}_{stringer} = \begin{Bmatrix} \varepsilon_x \\ \varepsilon_y \\ \gamma_{xy} \end{Bmatrix}_{panel} + \begin{Bmatrix} \varepsilon_x^j \\ 0 \\ 0 \end{Bmatrix}_{bending} \quad \text{for j = 1, 2, …, nlbf or nltf} \tag{3.49}$$

where nl is the number of plies in the skin laminate and nlbf and nltf are the number of plies in the bottom flange and top flange laminates, respectively. Once these local strains are calculated the global strains are found through coordinate transformation as per the usual CLT methods [25]. These strains and resulting stresses were evaluated for the panel with the Maximum Strain and modified Tsai-Wu criterion as discussed above.

A full analysis of the initial laminate in a side-of-body joint configuration follows in the next section.

3.5 Example Joint Analysis

An example composite bolted joint that was tested by Bunin [391] was chosen to exercise the analysis program. This joint, labeled JT12CF, was previously analyzed in the previous Sections 3.3 and 3.4. In this section the full failure analysis will be performed by WINGJOTA. The laminate is a 96-ply "hard" layup sequence (37.5% 0°, 50% 45°, and 12.5% 90° plies) similar to Table 4.18. The test coupon was made from Toray T-300 carbon fibers and Ciba-Geigy 914 epoxy resin; based on data availability, T800HB-/-3900-2 carbon/epoxy unidirectional laminate was used here. Table 4.16 lists the material properties used. Material strength properties had to be estimated based on several sources. Hart-Smith [392] provides some ways of estimating strength properties; for instance, he found that the transverse lamina strengths of uni-directional tapes Y_T, Y_C, and $F_{\pm 45}$ are a tenth of X_T or X_C, whichever is greater ($F_{\pm 45}$ is the longitudinal tensile strength of ±45° plies). Further, it was suggested that the shear strength S is half that of Y_T. The value of Sc from Chang et al. [26] for T-300/SP286 carbon epoxy was used here. Table 3.3 shows the strength properties used for the materials in the wing design. The strength properties of the example joint element (T330/914) are not known.

Table 3.3: Assumed Material Strength Properties

T800HB / 3900-2 Tape	MPa	T700S / 3900-2 Fabric	MPa
X_T	1765	X_T	721.3
X_C	1255	X_C	728.0
$Y_T = Y_C$	176.5	$Y_T = Y_C$	714.5
S	88.3	S	88.8
S_c	124.1	S_c	124.1

Other design aspects of the example joint JT12CF include:

- Bolt diameter D = 0.01905 m
- Two rows, three bolts each, 12 total bolts
- Plate thickness = 0.02535 m
- Plate width = 0.2286 m

This example joint was analyzed by WINGJOTA using the method described in this chapter. A load of 333.6 kN was chosen to exercise the program. Stress resultants (Figure 3.7), mid-plane strains (Figure 3.8), global strains (Figures 3.9-3.12), and global stresses (Figures 3.13-3.16) are shown for plies 1, 2, 4, and 5.

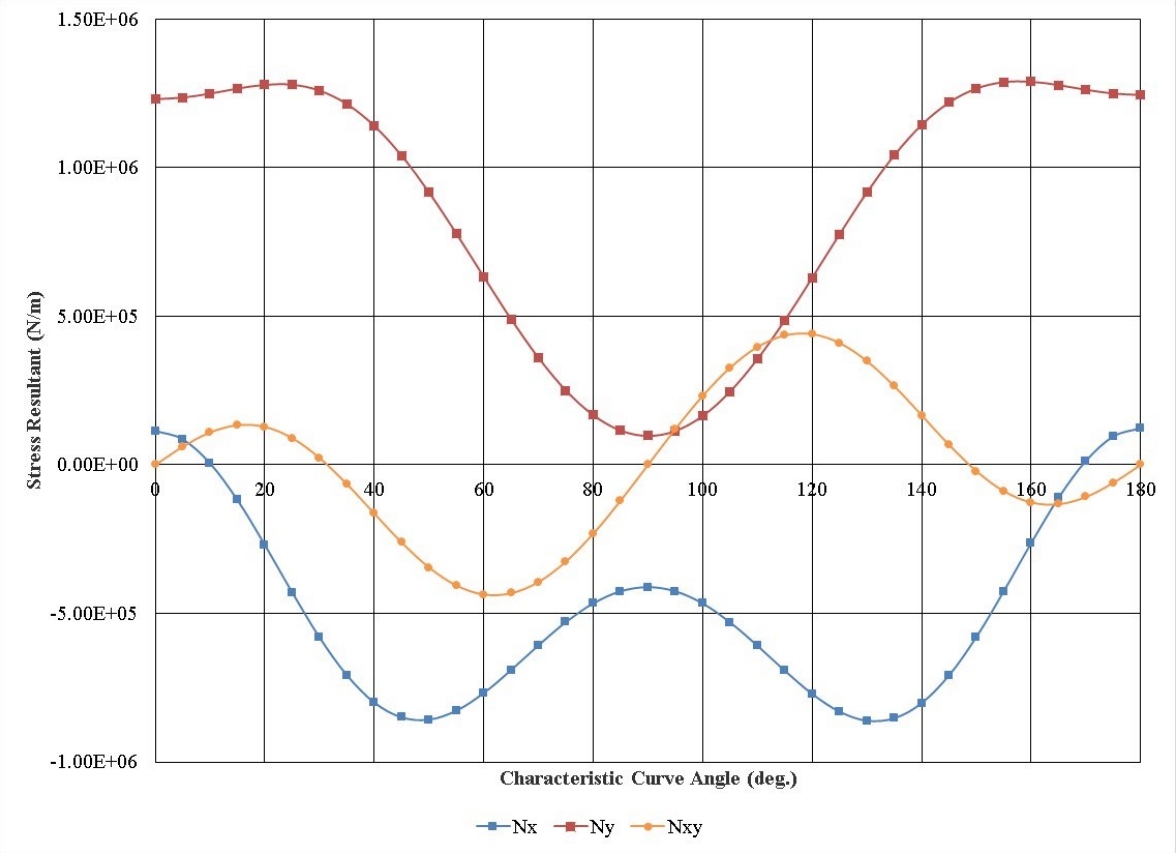

Figure 3.7: Stress Resultants around the Characteristic Curve, JT12CF Laminate, Py = 333.6 kN

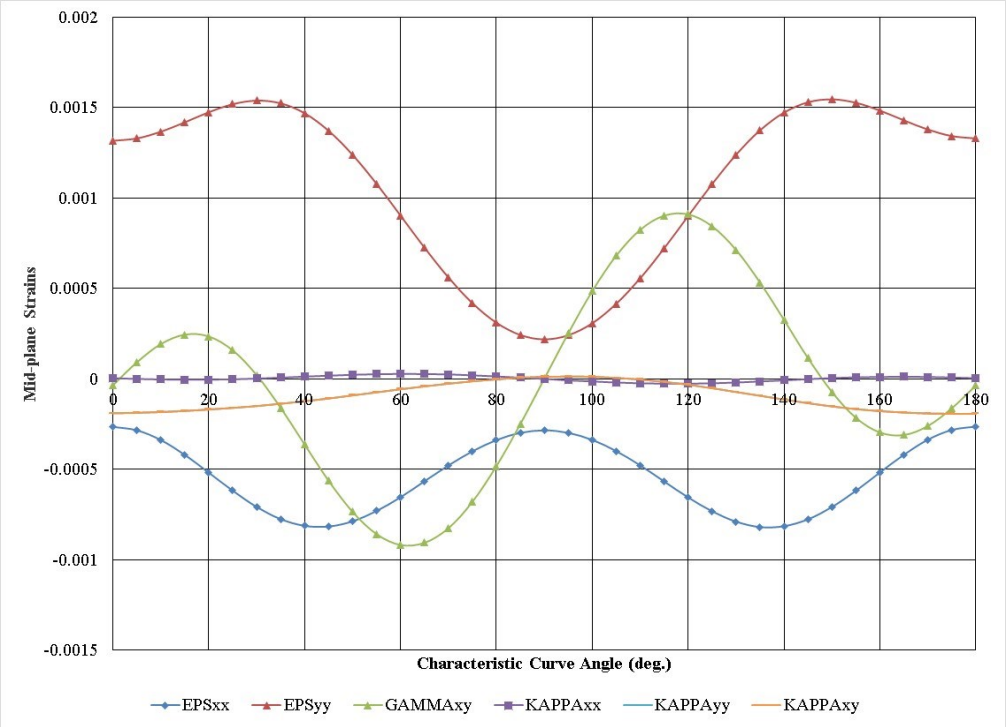

Figure 3.8: Mid-plane Strains around the Characteristic Curve, JT12CF Laminate, Py = 333.6 kN

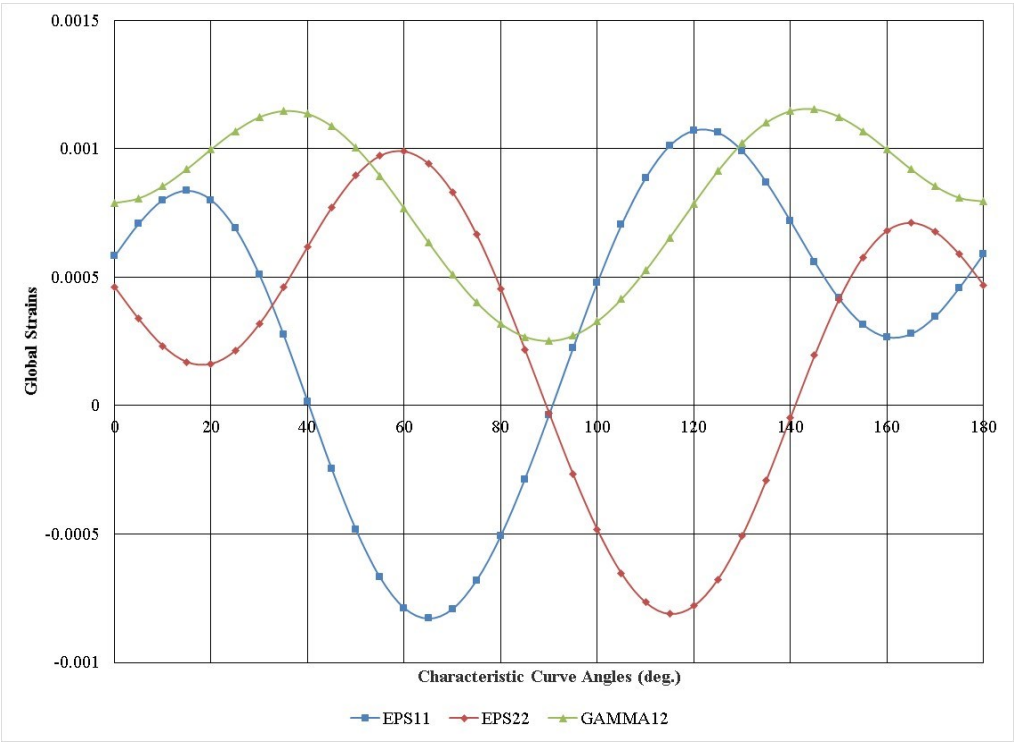

Figure 3.9: Global Strains around the Characteristic Curve, Ply 1 (45°), JT12CF Laminate, Py = 333.6 kN

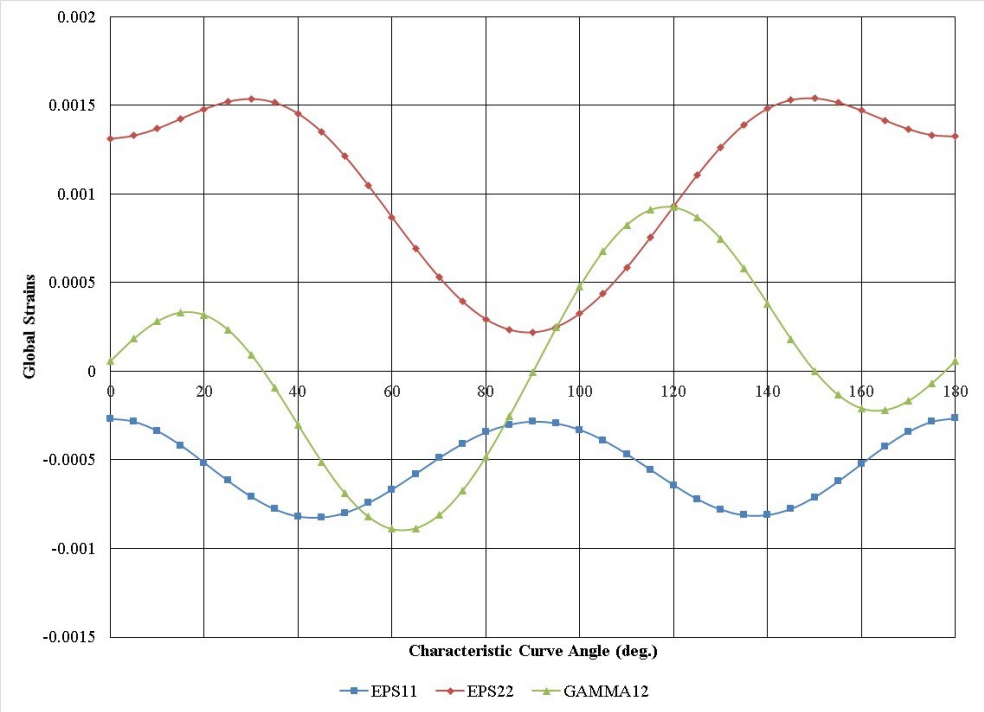

Figure 3.10: Global Strains around the Characteristic Curve, Ply 2 (0°), JT12CF Laminate, Py = 333.6 kN

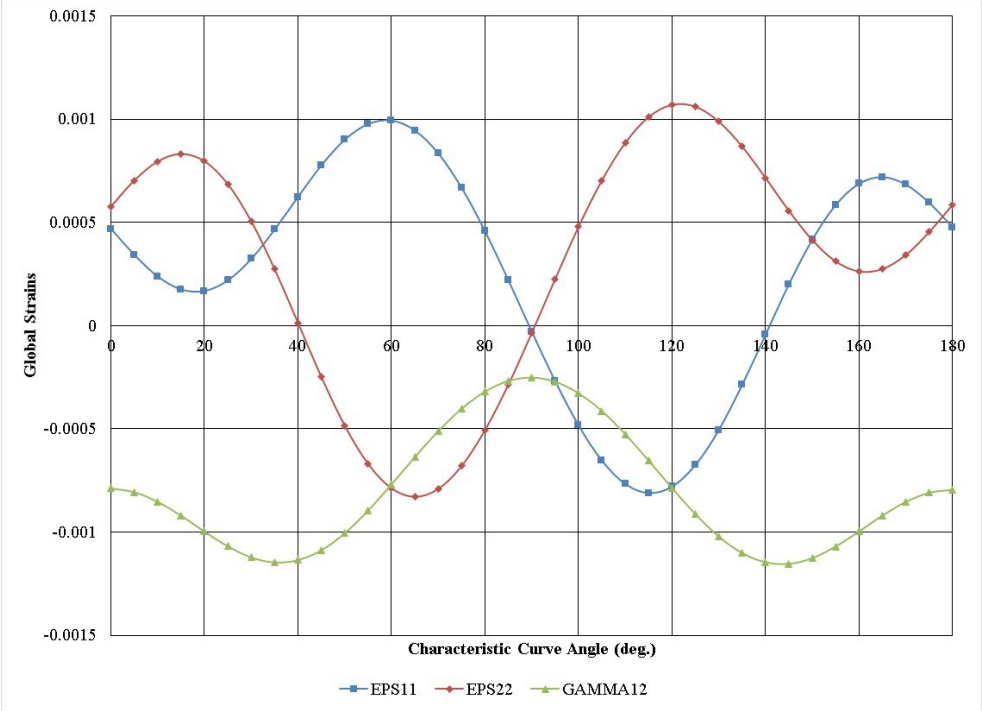

Figure 3.11: Global Strains around the Characteristic Curve, Ply 4 (-45°), JT12CF Laminate, Py = 333.6 kN

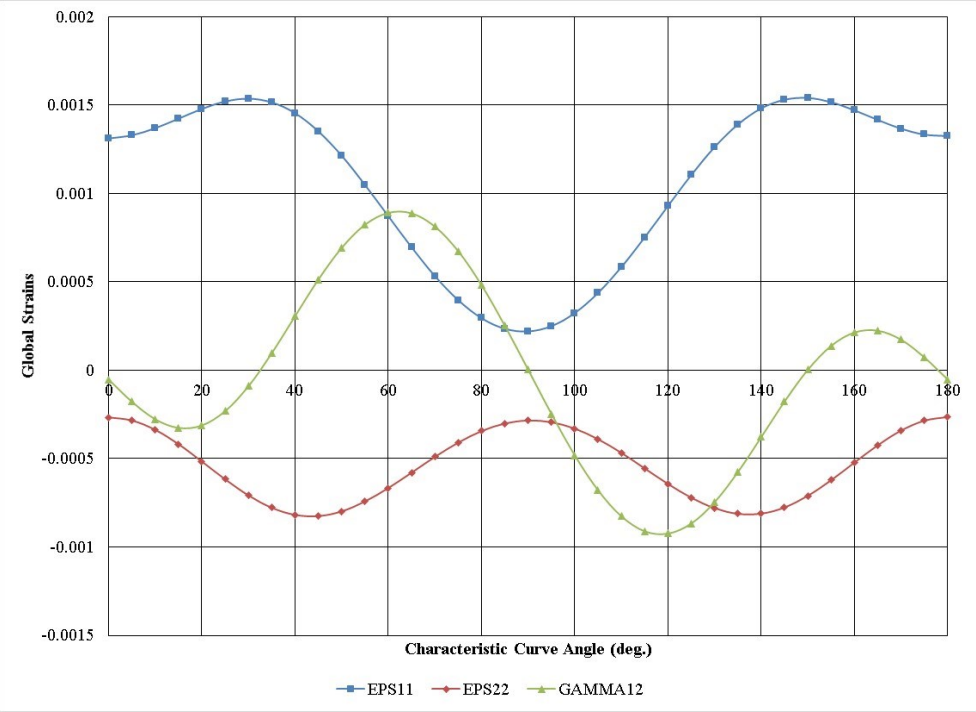

Figure 3.12: Global Strains around the Characteristic Curve, Ply 5 (90°), JT12CF Laminate, Py = 333.6 kN

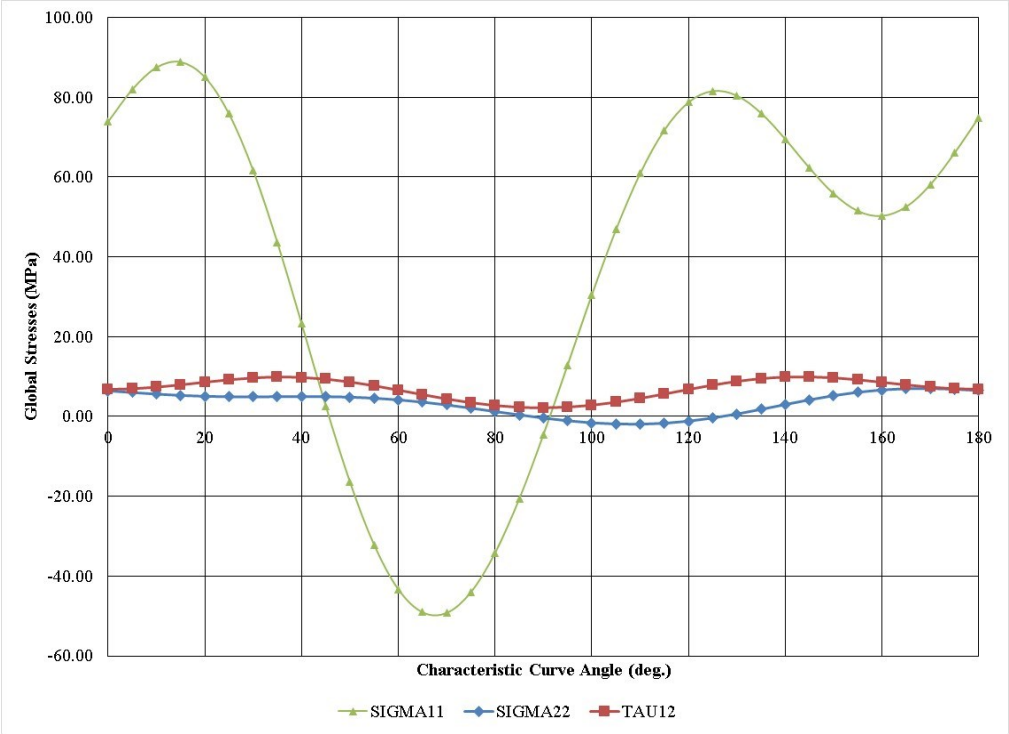

Figure 3.13: Global Streses around the Characteristic Curve, Ply 1 (45°), JT12CF Laminate, Py = 333.6 kN

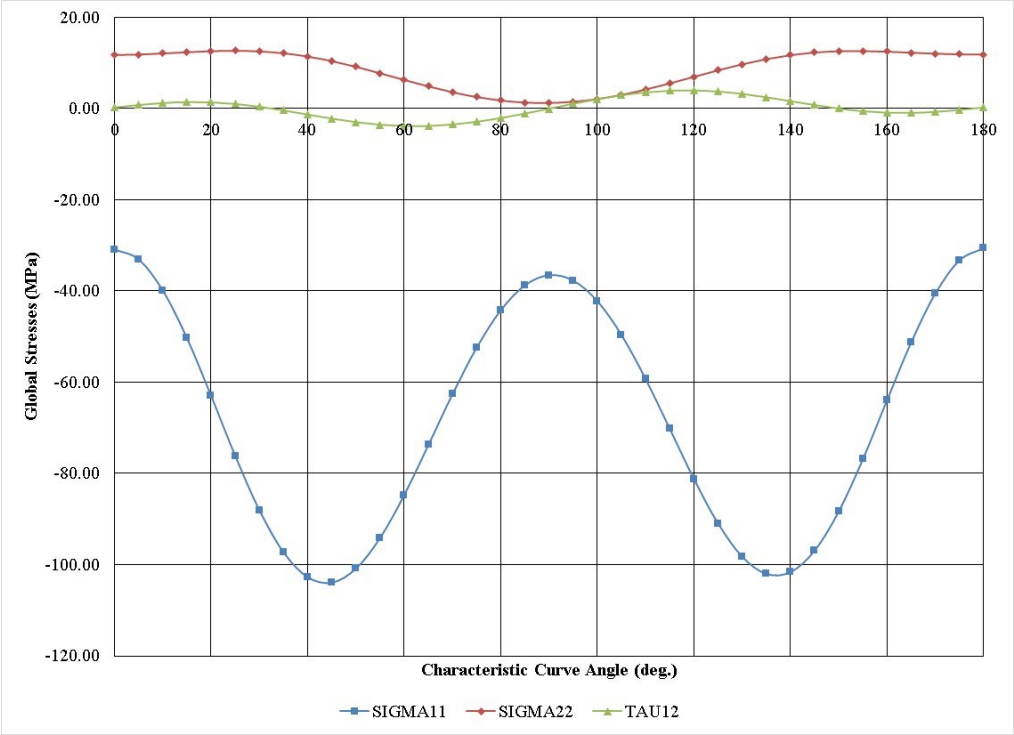

Figure 3.14: Global Streses around the Characteristic Curve, Ply 2 (0°), JT12CF Laminate, Py = 333.6 kN

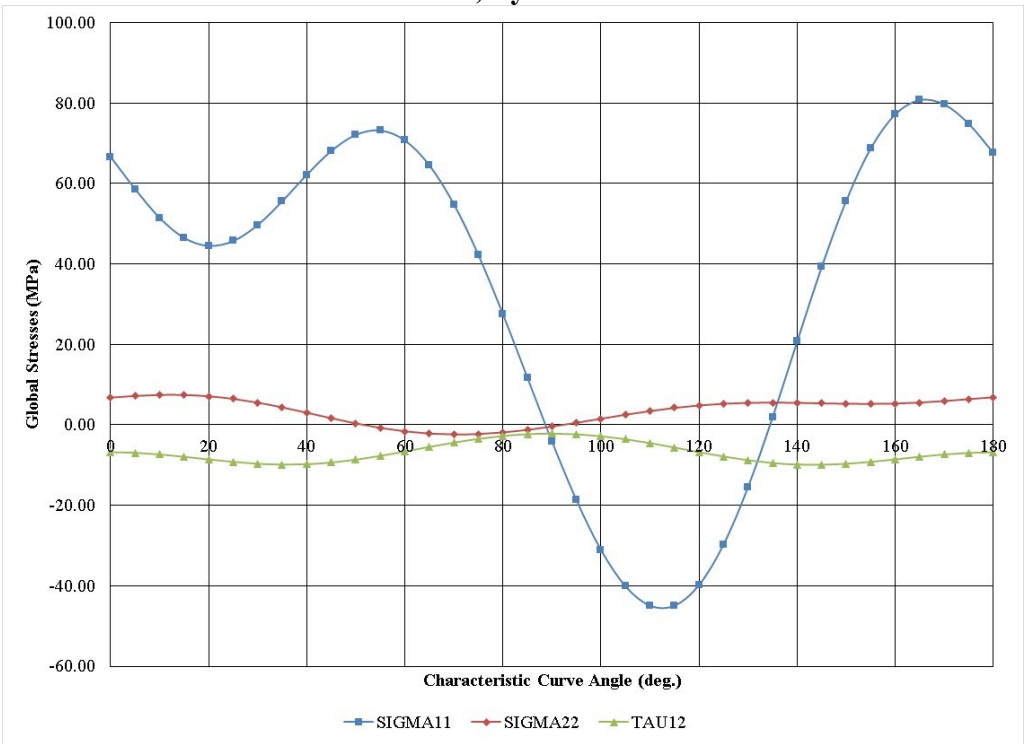

Figure 3.15: Global Streses around the Characteristic Curve, Ply 4 (-45°), JT12CF Laminate, Py = 333.6 kN

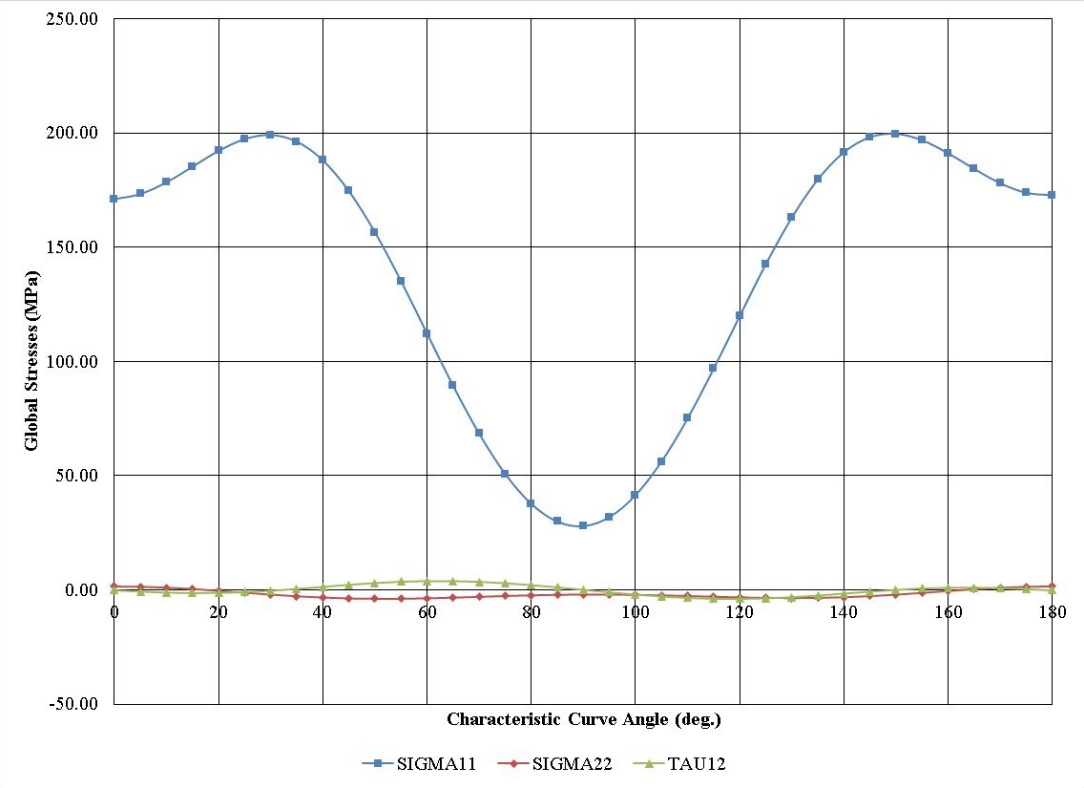

Figure 3.16: Global Streses around the Characteristic Curve, Ply 5 (90°), JT12CF Laminate, Py = 333.6 kN

The next part of the exercise was to determine the failure strength of the joint via WINGJOTA. Nelson et al. [372] reported an ultimate, catastrophic failure load of 1.57 kN. That load was analyzed and it was found, via the Yamada criterion and the angle of failure along the characteristic curve, that the joint failed in tension. The applied loads were reduced, showing progressively changing failure mode from tension to shear. The first ply failure load for this joint was found to be approximately 1.13 kN. This first-ply failure load is approximately 30% less than the reported ultimate failure load. However, as shown in Figure 3.17, the program correctly assigns bearing and bypass loads to the joint. Given the difficulties obtaining correct material properties, including the splice plate material, this is acceptable for this portion of the optimization algorithm.

There is some recognition in the research field that two-dimensional analysis of composite bolted joints for strength is a difficult proposition. Camanho [385] shows that methods based on boundary stresses and failure theories, i.e., when there is no localized damage analysis, underestimate joint strength. This is because bearing failure is governed by three-dimensional effects; 2D failure criteria applied to a hole boundary do not account for the 3D stresses are present that contribute to damage. Experimental results around stacking sequence and lateral constraints on joint strength are unable to be fully described by 2D models. One of his conclusions is that one must use 3D models to accurately predict composite joint strength. Unfortunately, those methods are also generally computationally expensive and not suitable for a global optimization routine for composite design.

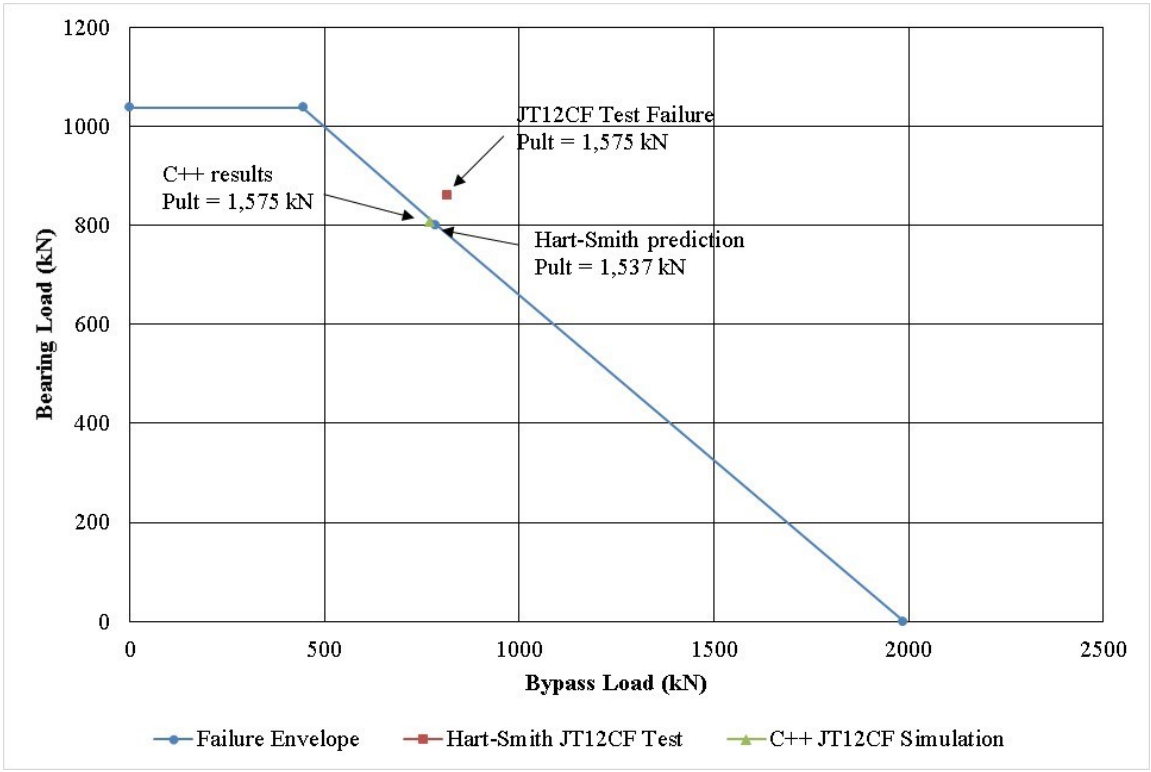

Figure 3.17: Bearing Loads vs. Bypass Load, Test Results vs. C++ Program, JT12CF Laminate, Py = 1,575 kN

3.6 Summary and Conclusions

A method of performing composite bolted joint analysis was described for both single- and double-shear joints. The analysis starts with some general design rules and joint flexibility calculations based on fastener and laminate material properties. A numerical method of determining the bearing-bypass ratios for the joint was incorporated into the analysis. An example joint problem was shown that the correct ratios are being generated by WINGJOTA. Next, an elasticity solution for stresses around a circular hole in an infinite, anisotropic plate was described. Again some examples were generated that show agreement with previous results. The elasticity solution is then utilized, with the Yamada failure criterion, to determine joint strength by taking the stresses present at the characteristic curve of the laminate. Finally, a previously tested composite joint was analyzed using the method described here. The ultimate strength of the joint tested and the first ply failure reported by the analysis differ by about 30%. The analysis method used in this work is sufficiently fast to provide a constraint condition for WINGJOTA.

Chapter 4

BENCHMARK COMPOSITE WING MODEL

A new benchmark wing model that includes sufficient detail to support flutter and divergence, aeroelastic tailoring, buckling and post buckling, vibration and natural frequency analyses is proposed. The idea behind this wing model is that the laminate design of the wing root joint is used for the entire wing structural box (upper and lower skin panels, ribs, and front and rear spars). The initial structural configuration is purposely over designed to provide a feasible starting point for subsequent structural optimization. The wing model is more detailed than exists in the literature, and has been made freely available to researchers through a website [393]. A more detailed wing design is necessary to allow more advanced analyses during optimization to avoid a situation where positive strength margins are not obtained during final design [202]. The benchmark wing model can be used for optimization algorithm comparisons. The full wing model developed during this study serves as the initial design for the wing panel optimized by WINGJOTA in Chapter 6. It is also used to solve for internal design loads that are used as boundary conditions for the wing panel finite element model contained in WINGJOTA. The finite element module is discussed in Section 4.5.

4.1 Composite Wing Model Preliminary Design

The preliminary design of this subsonic transport composite wing is focused on the main structural torque box, consisting of two spars, 40 ribs, and upper and lower stiffened skin panels, including the wing carry-through structure (center box) inside the fuselage. The wing model is representative of those used on medium-size twin-aisle commercial aircraft such as the Boeing 767. The wing box is of the two-spar type. The ribs are perpendicular to the front and rear spars, not the airstream. The engine is mounted on ribs 8, 9, and 10. It is assumed that there are no access holes in the lower skin panel, no lightening holes in spars or ribs, and the spars are one piece. Figure 4.1 shows the coordinates used to develop the wing planform.

Wing loading (maximum take-off weight (MTOW) / wing area (A)) ratio determines the loading for the initial wing design. Table 4.1 shows the basic wing information used to determine the wing loading of the wing model. A comparison is made to a model wing used by Nelson et al. [372] to study composite bolted joints. It can be seen that the wing loadings of these two model wings are nearly identical. Therefore, it was assumed that the running loads in the side-of-body joint would be similar in both cases (see Table 4.2). The side-of-body joint of the Nelson study was used as the baseline joint for the model wing used here (see Section 5.2.4).

A supercritical airfoil, the BACXXX, was chosen for study [394-395]. Normalized dimensions for this airfoil were provided from the University of Illinois at Urbana-Champaign Airfoil Coordinates Database (see Table 4.3 and Figure 4.2) [396]. The front spar is located at 19.5% of the airfoil, while the rear spar is at 67.4% at the wing root.

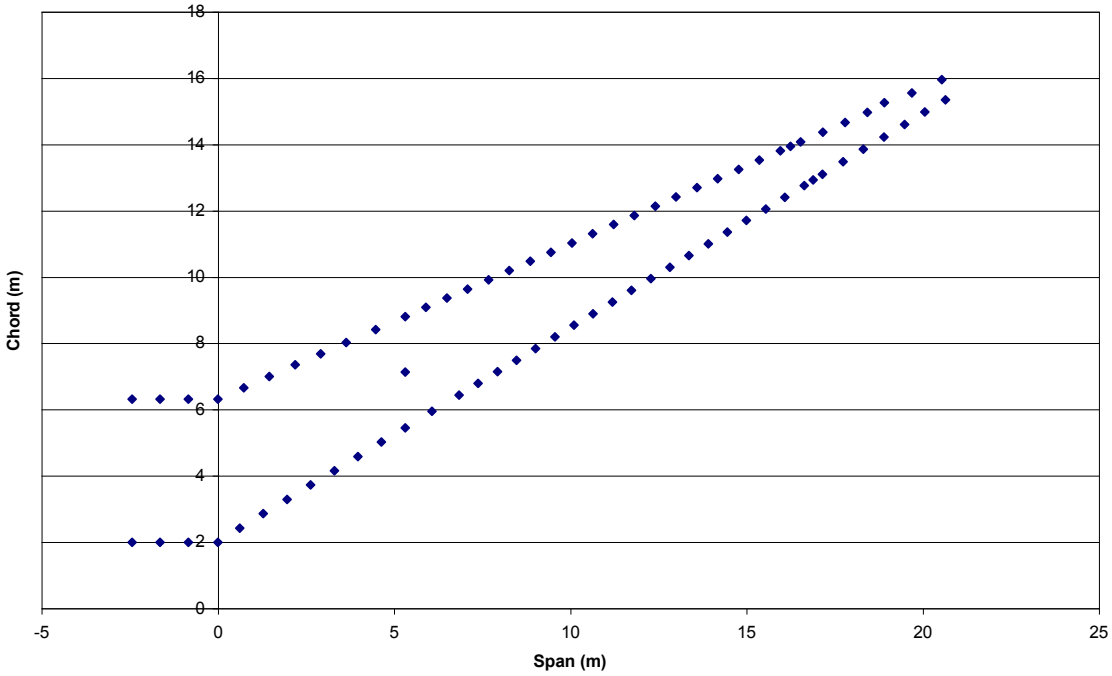

Figure 4.1: Wing Model Coordinates, Plan View

Table 4.1: Basic Data Utilized to Produce Wing Model

	Model D-3243-22 [372]	Model Wing, based on 767-300 [397]	Scale Factor
Maximum Takeoff Weight (kg)	96,842	135,670	1.40
Semi-Span s (m)	20	21.1	1.06
Wing Area A (m^2)	204.6	283.3**	1.38
Aspect Ratio AR = s^2/A	7.82*	6.29	0.80
Wing Chord at Root (m)	8.26	8.57**	1.04
Wing Chord at Tip (m)	1.57	2.29**	1.46
Taper Ratio	0.190	0.267	1.41
Thickness/Chord Ratio at Root		0.151	
Thickness/Chord Ratio at Tip		0.103	
Wing Loading (kg/m^2)	473.32	478.89	**1.01**
Maximum Fuel Capacity (l)	48,352	63,216	1.31
Fuel Weight (kg)	38,817	50,750	1.31
Nacelle & Engine Weight (kg)		5,347	
Engine Thrust (N)		223,500	
Control Surface Weight (kg)		587	
Landing Gear Weight (kg)		13,918	

* AR for Model D-3243-22 assumed to be similar to 757 [397]
** [398]

Table 4.2: Wing Model Load Intensities

	Model D-3243-22 (N/m) (Nelson 1983)	Model Wing (N/m)
Rib -3		
LE	7.18E+05	7.26E+05
2	1.14E+06	1.15E+06
3	2.49E+06	2.52E+06
4	3.84E+06	3.88E+06
5	4.85E+06	4.91E+06
TE	5.39E+06	5.46E+06
Rib 2.5		
LE	1.28E+06	1.29E+06
2	1.42E+06	1.44E+06
3	2.89E+06	2.92E+06
4	4.26E+06	4.31E+06
5	5.45E+06	5.51E+06
TE	6.29E+06	6.36E+06
Rib 8		
LE	5.48E+06	5.55E+06
2	5.78E+06	5.85E+06
3	5.36E+06	5.42E+06
4	3.64E+06	3.69E+06
TE	5.04E+06	5.10E+06
Rib 13.5 / 17		
LE	2.28E+06	2.30E+06
2	4.59E+06	4.64E+06
TE	4.83E+06	4.89E+06
Rib 22.5 / 31.5		
LE	5.60E+05	5.67E+05
TE	7.18E+05	7.26E+05

The front spar has a sweep of 33° while the trailing edge sweep is 25°. The thickness-to-chord ratio varies linearly from the wing root to the tip, 15.1% to 10.3%, and the quarter-chord sweep is 31.5° [399]. The wing root chord is 8.57 m (28 ft. 1 in.) and the wing tip chord is 2.29 m (4 ft. 10 in.), giving a taper ratio of 0.267. The semi-span is 21.1 m (44 ft. 8 in.), and the wing area is 283.3 m^2 (3049 $ft.^2$) [397]. The upper and lower wing skin panels are stiffened with I-stringers. The stringer spacing is 0.205 m (8 in.); there are 21 stringers in the center box, and these terminate along the leading edge. The wing thickness was modeled from an example transport wing thickness-to-span chart for the upper and lower wing surfaces found in Niu [400]. The model waterline-to-span chart is presented in Figure 4.3. SolidWorks was used to develop the solid model [401]. Figure 4.4 shows the general arrangement of the wing. Wing model preliminary design information can be found in Table 4.4; the calculations there are based on a method proposed by Torenbeek [402].

Table 4.3: Boeing BACXXX Supercritical Airfoil Coordinates

BOEING BACXXX AIRFOIL			
Upper		Lower	
X	Y	X	Y
0	0	0	0
0.0005	0.0037	0.0005	-0.0018
0.001	0.005	0.001	-0.0027
0.0025	0.0078	0.0025	-0.0043
0.005	0.0112	0.005	-0.0058
0.015	0.0207	0.015	-0.0098
0.02	0.0242	0.02	-0.0112
0.025	0.0271	0.025	-0.0125
0.0375	0.0334	0.0375	-0.0152
0.05	0.0384	0.05	-0.0175
0.075	0.0465	0.075	-0.0216
0.1	0.0521	0.1	-0.0254
0.125	0.0566	0.125	-0.0288
0.15	0.0599	0.15	-0.032
0.2	0.0643	0.2	-0.0375
0.25	0.0665	0.25	-0.0417
0.3	0.0674	0.3	-0.0445
0.35	0.0673	0.35	-0.0458
0.4	0.0667	0.4	-0.0457
0.45	0.0654	0.45	-0.0443
0.5	0.0636	0.5	-0.0417
0.55	0.0613	0.55	-0.0383
0.6	0.0585	0.6	-0.0344
0.65	0.0548	0.65	-0.0303
0.7	0.0503	0.7	-0.026
0.75	0.045	0.75	-0.0218
0.8	0.0384	0.8	-0.0174
0.85	0.0307	0.85	-0.0132
0.9	0.0218	0.9	-0.009
0.95	0.0116	0.95	-0.0047
1	0.0004	1	-0.0004

The leading and trailing edge structures, including control surfaces and systems, are not part of the structural model. Their masses, however, are represented as concentrated boundary forces on the structural box in the finite element model. The composite trailing edge fixed structure, inboard and outboard flaps, inboard aileron, aileron, speed brakes, and spoilers, and the leading edge fixed structure and slat masses were calculated from historical data and equations found in Torenbeek [402-403], Roskam [404], and Jenkinson et al. [397]. The loads are applied as nodal forces and moments at the appropriate rib stations according to the thickness taper ratio over the

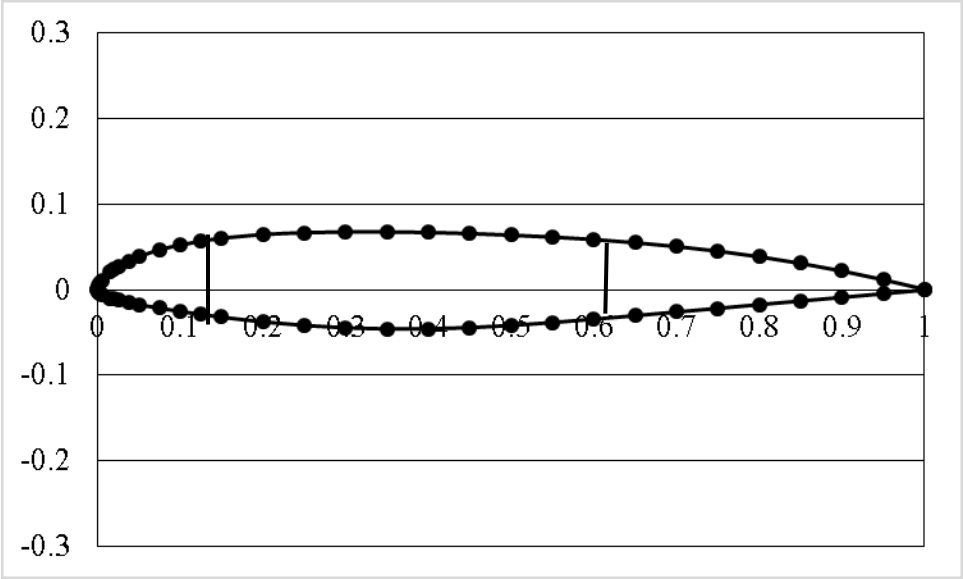

Figure 4.2: Normalized Coordinates for Supercritical Airfoil BACXXX [396]

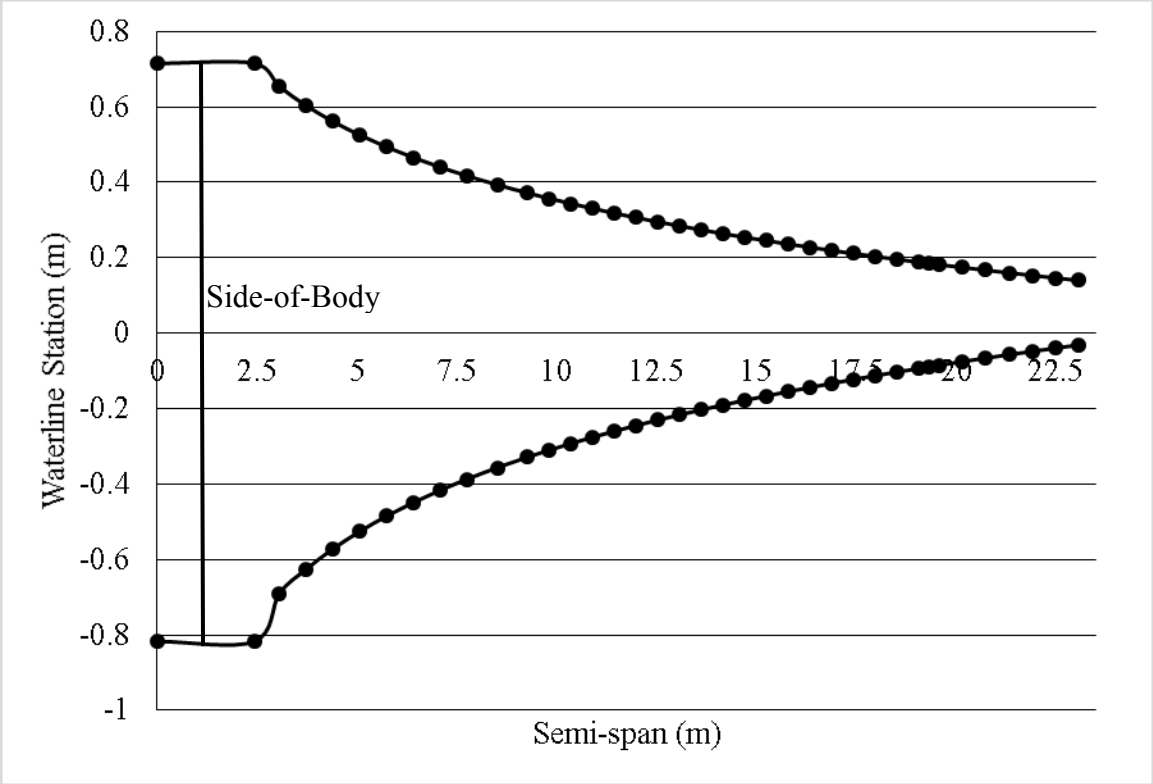

Figure 4.3: Waterline vs. Span for the Wing Model Upper and Lower Surfaces

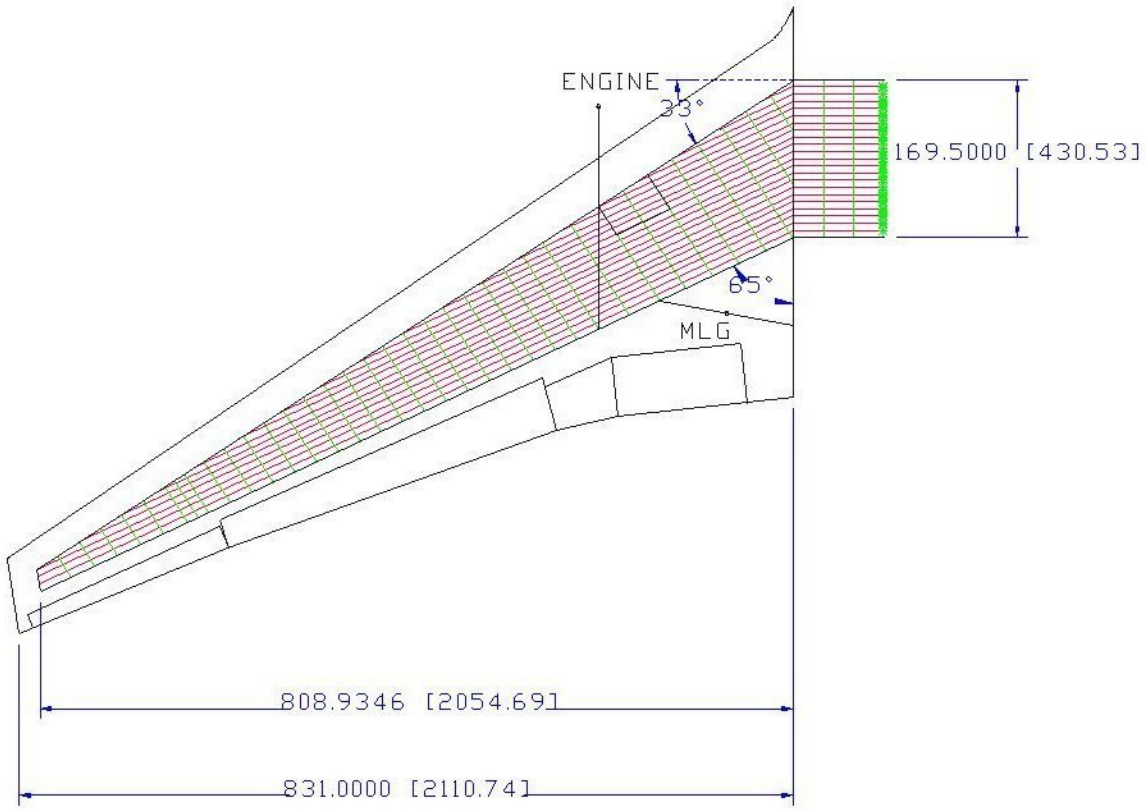

Figure 4.4: General Wing Model Geometry (dimensions are inches [cm])

span of the control surface. The masses of the engine, nacelle, and landing gear are also included as applied loads. The average weight of the two engines used on the 767 (Pratt and Whitney PW 4062 [405] and the General Electric CF6 [406]) was used (see Table 4.5). The nacelle weight was calculated and distributed over four points on the wing (engine center-of-gravity, leading edge of rib 12, mid-point of rib 13, trailing edge of rib 14) by ratios of 40%, 30%, 20%, and 10%, respectively. The main landing gear weight was calculated using Torenbeek's methods [403]. Secondary structure, engine, nacelle, and landing gear masses can be found in Table 4.6. Fuel loads were derived from the volumes enclosed in each rib bay and are applied as surface pressures inside each bay, with a linearly varying load on each rib and spar. Fuel density was assumed to be 802.8 kg/m^3 (50.1 lb/ft^3) [407]. These fuel loads do not take into account the dry bay typically located inboard of the engine nacelle [400].

The initial laminate design of the composite wing was taken from Nelson et al. [372] and is based on the wing root joint laminate requirements. The maximum take-off gross weight (MTOGW) is assumed to be 135,670 kg (300,000 lbs), which implies a nominal wing loading of 478.89 kg/m^2 (98 lbs/ft^2) [397]. The wing loading of the model considered herein is nearly identical to those assumed during the Nelson study, so the same initial laminate was chosen. It consists of 96 plies of T800HB-/-3900-2 carbon/epoxy unidirectional laminate and two outer plies of T700S-/-3900-2 carbon/epoxy plain weave laminate. Material properties for these composite materials were culled from several sources [408-409, 177]. Laminate stacking sequence rules given by Nelson et al. [372] were used to design the laminate.

Table 4.4: Aluminum Wing Model Weight Prediction

Design Weights	
Maximum Take-off Weight (MTOW) (kgf)	135,882
Maximum Landing Weight (MLW) (kgf)	118,159
Maximum Zero Fuel Weight (MZFW) (kgf)	109,494
Geometry	
Reference Area S (m^2)	283.3
Span b (m)	42.2
Mid-chord sweep angle $\Lambda_{1/2}$ (°)	26.0
Leading edge sweep angle Λ_{le} (°)	33.0
Quarter-chord sweep angle $\Lambda_{1/4}$ (°)	31.5
Root chord (y=0) c_r (m)	11.532
Tip chord (y=b/2) c_t (m)	2.198
Aspect ratio A	6.29
Taper ratio λ	0.191
Center section span b_{cs} (m)	4.861
Thickness/chord ratio - root t/c	0.133
Thickness/chord ratio - 40% span t/c (Rib 14)	0.0848
Thickness/chord ratio - 70% span t/c_{ref} (Rib 26)	0.0878
Thickness at root (y=0) t_r (m)	1.533
Thickness at y = b_{cs}/2 (SOB) t_{cs} (m)	1.533
Thickness at tip t_t (m)	0.171
Taper ratio of wing tank λbar	0.241
Span of fuel tank b_F (m)	37.796
Mean geometric chord cbar (m)	6.713
Mean profile thickness t_{ref} (m)	1.000
Fixed leading edge area S_{fle} (m^2)	51.0
Fixed trailing edge area S_{tfe} (m^2)	30.6

Design Conditions	
Design cruising speed V_C (m/s)	236.6
Design cruising Mach number M_C	0.8
Design dive speed V_D (m/s)	333.4
Design dive Mach number M_D	0.862
Design dive dynamic pressure q_D (N/m^2)	68,093
Design gust speed U_{de} (m/s)	15.3
Atmosphere	
Density ρ 20,000 ft. (kg/m^3)	0.6528
Acceleration of gravity g 20000 ft. (m/s^2)	9.807
Density ρ_{SL} 0 ft. (kg/m3)	1.225
Manoeuver Load Factor	
n_{ult}	3.75
Powerplant	
Nacelle & engine weight W_P (kgf)	5,355
% of MTOW	7.88
Number of engines Ne	2
Materials	
Specific weight, aluminum (N/m^3)	28.1
Shear modulus, aluminum (Pa)	2.81E+10
Constants	
Correction factor for rib weight k_r	0.5

Table 4.4: Aluminum Wing Model Weight Prediction (continued)

Geometry	
Leading edge slat area S_{slat} (m^2)	28.3
Trailing edge flap area S_{tef} (m^2)	36.9
Trailing edge spoiler area S_{lift} (m^2)	15.8
Aileron area S_a (m^2)	11.2
Structural wing box area (m^2)	142.9

Constants	
Non-optimum extra panel thickness δ_{NO} (m)	0.0005
Correction factor for stiffness weight penalty f(λ)	0.05
Correction factor for fixed leading edge/slat strengthening k_{fle}	1.4
Correction factor for fixed trailing edge/double slotted flaps Δ	45
Correction factor for trailing edge double slotted variable flaps k_{tef}	2

Calculation of Input Data

Structural span bs (m)	46.95	Root bending moment, gust load MBr (N-m)	9.40E+06
Cantilever ratio RC	16.33	Mass relief, fuel, bending and shear	-0.01355
Lateral position of center of pressure ηcp	0.497308	Estimated wing weight 12% MTOW (kgf)	16,306
Lift-curve slope CLα (1/rad)	5.940599	Mass relief, mass, bending and shear	-0.096
Mass parameter μ	37.74083	Mass relief, powerplant	-0.035
Gust relief factor Kg	0.771638	Relief factor r	0.85545
Lateral position of fuel ybar/bF/2	0.31886	Mean root stress level ρg/σbarr (1/m)	8.1E-05
Lateral position of fuel ybar (m)	6.03	Structural efficiency ηt	0.8
Lateral position of fuel ηf/Lateral position of cp ηcp	0.574257	Mean root stress / shear stress σbarr/τbar	2.4
Root bending moment, lift and fuel mass MBr (N-m)	2.59E+08		

Weight Calculations (kgf, except as noted)

Bending and shear material weight, 1st term, WBASIC	7,042	Fixed trailing edge structure weight Wtfe	673
Rib weight, 2nd term, WBASIC	752	Leading edge slat weight Wslat = Wlef	835
Primary wing box weight WBASIC	7,794	Trailing edge flap weight Wtef	1,620
Weight correction, sheet taper & joints ΔWNOsheet	475	Aileron weight (inboard & outboard) Wa	219
Weight correction, SOB joint ΔWNOsob	136	Spoiler average specific weight (N/m^2)	110
Weight correction, LG attachment ΔWNOlg	473	Spoiler weight Wlift	178
Weight correction, engine attachment ΔWNOeng	187	Aileron and spoiler weight Wa+s	397
Total non-optimum weight correction ΔWNO	1,271	Flap support extra rib weight	81
Weight correction, aeroelasticity ΔWST	2,037	Ailerons support extra rib weight	44

Table 4.4: Aluminum Wing Model Weight Prediction (continued)

Weight Calculations (kgf, except as noted)				
Primary Wing Structure Weight WPRIM	11,101		Support structure/extra rib weight Wmisc	125
Fixed leading edge structure weight Wfle	1,176		Secondary Wing Structure Weight WSEC	4,827
Wing Weight Ww	15,928			

Table 4.5: Engine Data [405-406]

Engine	Thrust (N)	Mass (kg)	Length (m)
Pratt & Whitney PW4062	275,790	4,273	3.9
General Electric CF6-80C2	282,462	4,386	4.3
Model Engine (Average)	279,126	4,330	4.1

Table 4.6: Secondary Structure, Power Plant, and Landing Gear Masses

Structure	Total Mass (kg)
Flaps	647
Fixed Trailing Edge	269
Ailerons	88
Spoilers	71
Slats	333
Fixed Leading Edge	470
Engine	4,330
Nacelle	1,018
Landing Gear	13,918

To incorporate the I-stringers into the finite element model a smeared property stiffener ply was added to the laminate design. The I-stringer design is based on matching the effective bending stiffness of the titanium doubler at the wing root joint, and all the stringers are assumed identical. Further, the top and bottom flanges were assumed to be the same width, and the laminate design is identical to the skin design. This results in an I-stringer that has the geometry and properties shown in Table 4.7. Using the methods developed by Tuttle [380], the effective axial and bending stiffnesses of the skin/I-stringer combination were found. This information is used to develop an equivalent stiffener ply, with equal axial stiffness, thickness, and density. The smeared ply was then added to the laminate definition for the SHELL99 elements in the finite element model. In this model they do not taper spanwise. Calculations for the smeared property stiffener ply are shown in Appendix B. Figure 4.5 shows the I-stringer configuration and its equivalent smeared stringer element dimensions.

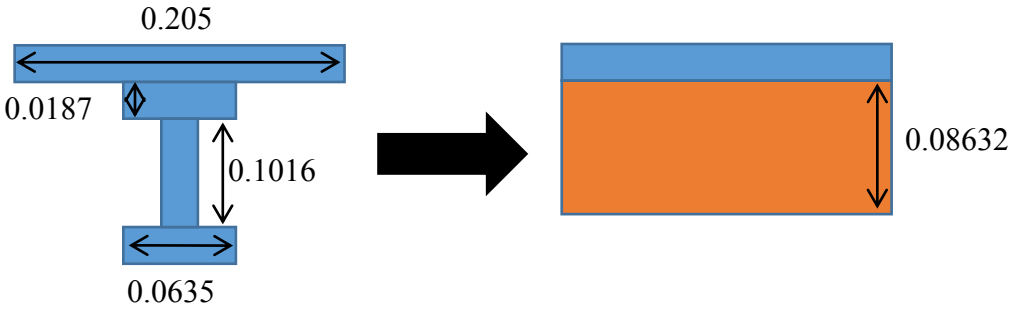

Figure 4.5: I-stringer and Equivalent Smeared Panel Geometries (dimensions in m)

Table 4.7: Panel I-stringer Design and Equivalent Property Ply

Width, top & bottom flange	0.0635 m
Thicknesses	0.0187 m
Web height	0.1016 m
Effective Axial Modulus $\overline{E}_{xx}^{ex}$	74.1 GPa
Effective Flexural Modulus $\overline{E}_{xx}^{fl}$	73.3 GPa
Effective Axial Stiffness $\overline{A}\overline{E}_{xx}$	3.16E+08 N
Effective Bending Stiffness $\overline{E}\overline{I}_{xx}$	7.62E+05 N-m^2
Equivalent Effective Axial Modulus $\overline{E}_{xx}^{ex}$	17.9 GPa
Equivalent Thickness	0.08632 m
Equivalent Density	374 kg/m^3

4.2 Torenbeek Aerodynamic Loads Analysis

The aeroelastic cycle, described as an algorithm by Gimmestad [410], is incorporated into WINGJOTA to capture the effect a bending wing has on the aerodynamic forces it generates. Aerodynamic pressure is applied to the structural box as nodal forces in the ANSYS finite element model. Torenbeek has suggested a simplified method of calculating these forces that are representative of a transport wing that has been used by others [35] for wing structural optimization. Using this method the wing area is divided into 32 areas and 45 point loads (nine chords and five span lines). The pressure distribution is converted into point loads applied on the lower skin panel nodes using

$$F_{i,j} = \frac{W/S \cdot LP_i \cdot CP_j \cdot A_{i,j}\left(\alpha_{root} + \beta_j\right)}{\alpha_{root\_ref}} \tag{4.1}$$

where i and j are the line and chord number of the node, W/S is the wing loading (here, 5425 N/m^2 [397]), LP_i is the span-wise pressure distribution number, CP_j is the chord-wise pressure distribution number, $A_{i,j}$ is the area associated with each node, α_{root} is the angle-of-attack at the root, α_{root_ref} is the reference angle-of-attack (here, 1.5°), and β_j is the angle of rotation of chord j relative to the root chord. LP_i and CP_j are shown in Figures. 4.6 and 4.7. Initially α_{root} equals α_{root_ref} and β_j is zero. β_j is defined as

$$\beta_j = \frac{\left(U_{z1,j} - U_{z5,j}\right)}{\left(X_{i,j} - X_{5,j}\right)} \tag{4.2}$$

where U_z is the vertical displacement at the leading edge (1) and trailing edge (5) for each chord j, and the denominator represents the chord length for chord j. After structural deformation, α_{root} changes according to

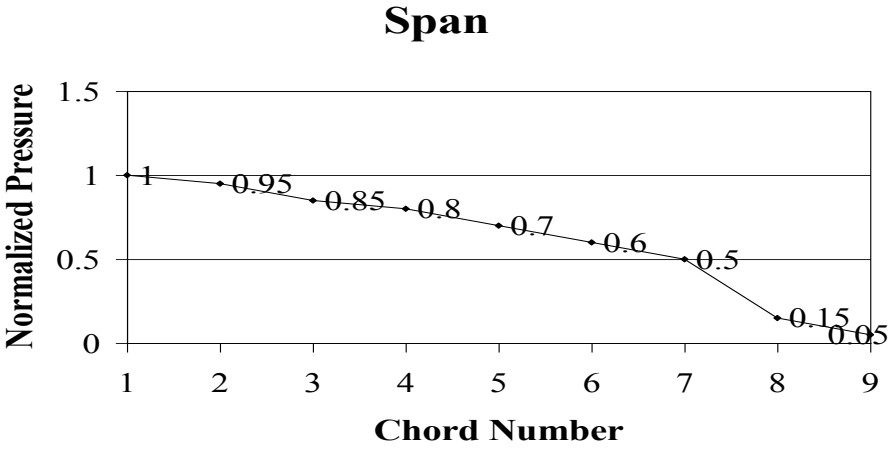

Figure 4.6: Span-wise Pressure Distribution LPi

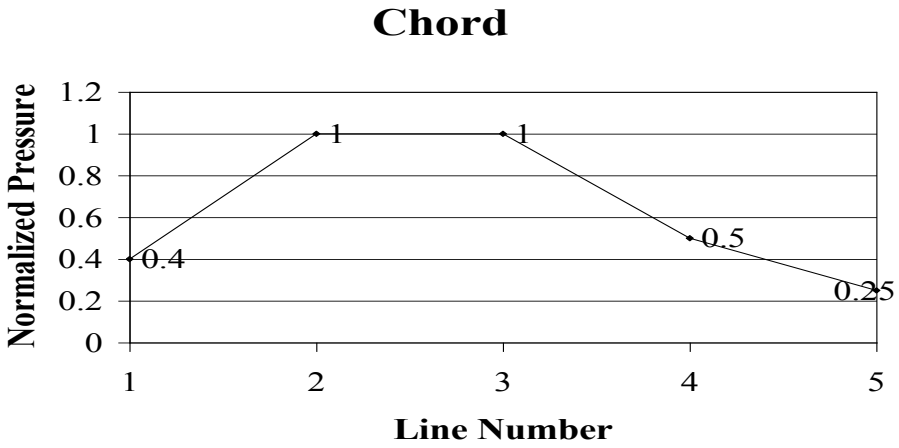

Figure 4.7: Chord-wise Pressure Distribution CPj

$$\alpha_{root} = \alpha_{root\_ref} - \frac{W/S\left[\sum_{j=1}^{9}\left(\sum_{i=1}^{5} LP_i \cdot A_{i,j}\right) CP_j \cdot \beta_j\right]}{0.5 \cdot MTGOW} \tag{4.3}$$

where MTOGW is the maximum take-off gross weight. The aeroelastic cycle is then used to find the converged aerodynamic nodal forces. Practical limits on the angle of attack are a positive maximum of approximately +35°; a practical minimum is -5°. An angle of +10° will cause the first drop in the coefficient of lift [411-412]. Figure 4.8 shows the aerodynamic load distribution grid and the resulting aerodynamic loading of the wing model.

Table 4.8 shows the aerodynamic forces applied to the structural model. Moments were applied at the leading and trailing edge rib lower nodes to simulate the aerodynamic loads on the secondary structures and surface pressures were applied to individual elements on the lower skin surface; this allows the loads to follow the deflection of the wing.

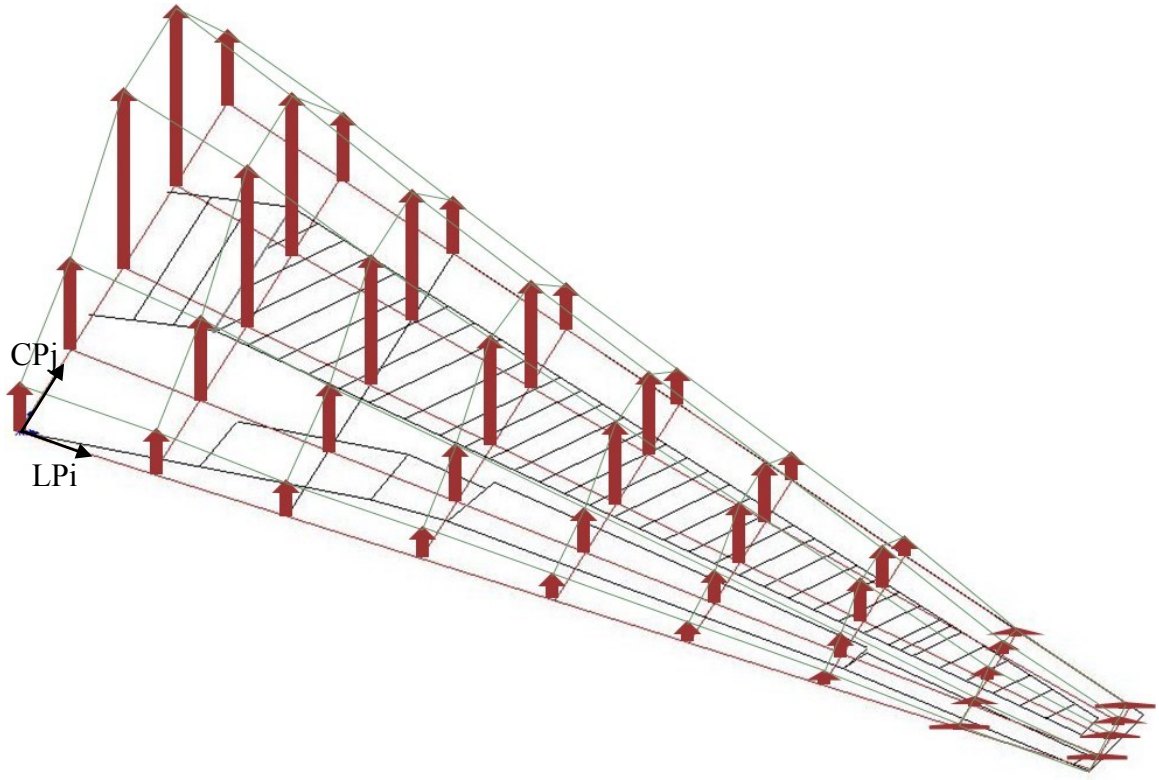

Figure 4.8: Torenbeek Aerodynamic Load Distribution Grid and Resulting Aerodynamic Loads Shown on Composite Wing Design.
Maximum value = 43,712 N

4.3 Wing Model Preliminary Finite Element Model and Results

The wing model finite element analysis was performed using ANSYS [413], a multiphysics finite element program. A stepping-stone approach was taken to producing this composite structural model with non-linear geometry. A simple composite plate with an applied pressure load was modeled using both the SYMM program [380] and two different element types in ANSYS (see Section 4.3.1). The results lead to various composite box beam models being created to explore element options and ANSYS capabilities to model a composite wing (see Section 4.3.2). Using that information a full wing model was developed (Section 4.3.3). Section 4.4 discusses the initial composite bolted joint designs that will used in this work.

Table 4.8: Applied Aerodynamic Moments and Pressures

Chord No. (Span)	Line No. (Chord)	Normalized Initial Nodal Forces (N)	Applied Moments (N-m)	Applied Surface Pressure (Pa)
1	1	17,480		
	2	43,707	6.15E+04	7.52E+05
	3	43,712	0.00E+00	3.32E+05
	4	21,845	-5.28E+04	4.24E+05
	5	10,917		
2	1	15,730	2.31E+04	3.97E+05
	2	39,329	0.00E+00	8.18E+05
	3	39,331	0.00E+00	5.83E+05
	4	19,637	-7.07E+04	5.11E+05
	5	9,805		
3	1	12,505	1.73E+04	1.41E+05
	2	31,263	0.00E+00	2.93E+05
	3	31,262	0.00E+00	2.86E+05
	4	15,574	-4.80E+04	2.91E+05
	5	7,759		
4	1	10,286	1.33E+04	1.25E+05
	2	25,671	0.00E+00	3.06E+05
	3	25,705	0.00E+00	3.08E+05
	4	12,793	-3.29E+04	2.60E+05
	5	6,348		
5	1	7,710	9.31E+03	8.36E+04
	2	19,237	0.00E+00	1.96E+05
	3	19,291	0.00E+00	2.03E+05
	4	9,565	-1.96E+04	2.75E+05
	5	4,720		
6	1	5,502	6.16E+03	6.62E+04
	2	13,757	0.00E+00	1.47E+05
	3	13,778	0.00E+00	1.45E+05
	4	6,779	-1.04E+04	1.07E+05
	5	3,330		
7	1	3,658	3.76E+03	4.10E+04
	2	9,145	0.00E+00	1.13E+05
	3	9,146	0.00E+00	1.07E+05
	4	4,465	-4.61E+03	1.00E+05
	5	2,178		
8	1	819		
	2	2,047	7.74E+02	3.53E+04
	3	2,048	0.00E+00	1.58E+04
	4	986	-4.19E+02	1.78E+04
	5	474		
9	1	226		
	2	566	NA	2.11E+03
	3	566	NA	9.30E+03
	4	269	NA	8.60E+03
	5	128		

4.3.1 Composite Plate Finite Element Modeling

A large, thick composite plate was modeled in ANSYS as a starting point and to verify that the finite element model was in agreement with analytic solutions. The plate was 3.41 m square and 60 plies thick, having a "hard" stacking sequence matching that of the initial side-of-body bolted joint design (see Section 4.4). A constant pressure of 1,000 Pa was applied over the whole surface. The analytic solution was provided by the SYMM program, which produces solutions for symmetric, generally-orthotropic laminate plates subjected to type S4 simple supports [380]. The same plate was analyzed in ANSYS using both SOLID46 and SHELL99 elements. From the results (Table 4.9) it can be seen that both element types provide solutions that are close to the theoretical one, with the SHELL99 elements providing a slightly better answer. Figures 4.9 and 4.10 show the ANSYS SHELL99 plate model geometry and boundary conditions and solution, respectively.

4.3.2 Composite Box Beam Finite Element Modeling

Prior to modeling the whole wing in ANSYS various composite box beams of the same root chord (3.41 m) and different length to width ratios (up to 20) were produced and analyzed. End ribs were included. SHELL99 elements were used exclusively; based on the results of the test laminate plate (previous section) and difficulty meshing the box beam with quadrilateral elements, SOLID46 elements were not used. These models were used to determine the correct method of assuring element fiber orientation. Two material systems and three beam flexural rigidities were used; an isotropic, titanium beam; and two composite laminate beams with a quasi-isotropic lay-up and a "hard" lay-up, each of 60 plies. The titanium box beams were modeled two ways: as an isotropic shell and as a layered shell (SHELL93) where all plies have the same properties. An upward, side, and combined load cases were run. The program BEAM was used to calculate the location of the centroid and the effective axial and flexural rigidities of the composite box beam [380] (see Table 4.10). In addition to the basic loading on a cantilevered beam, two other modeling aspects were tested. These were the use of spring elements (COMBIN14, [414]) at all nodes that would simulate a side-of-body rib as a new, additional boundary condition, and the use of linearly-varying pressure loading on the shell elements to simulate fuel volume inside the beam.

Table 4.9: Analytic vs. ANSYS Solutions for Composite Plate Test Laminate

	Deflection (m)	**Error (%)**
SYMM	0.067084	
SOLID46	0.064219	4.3
SHELL99	0.067392	0.5

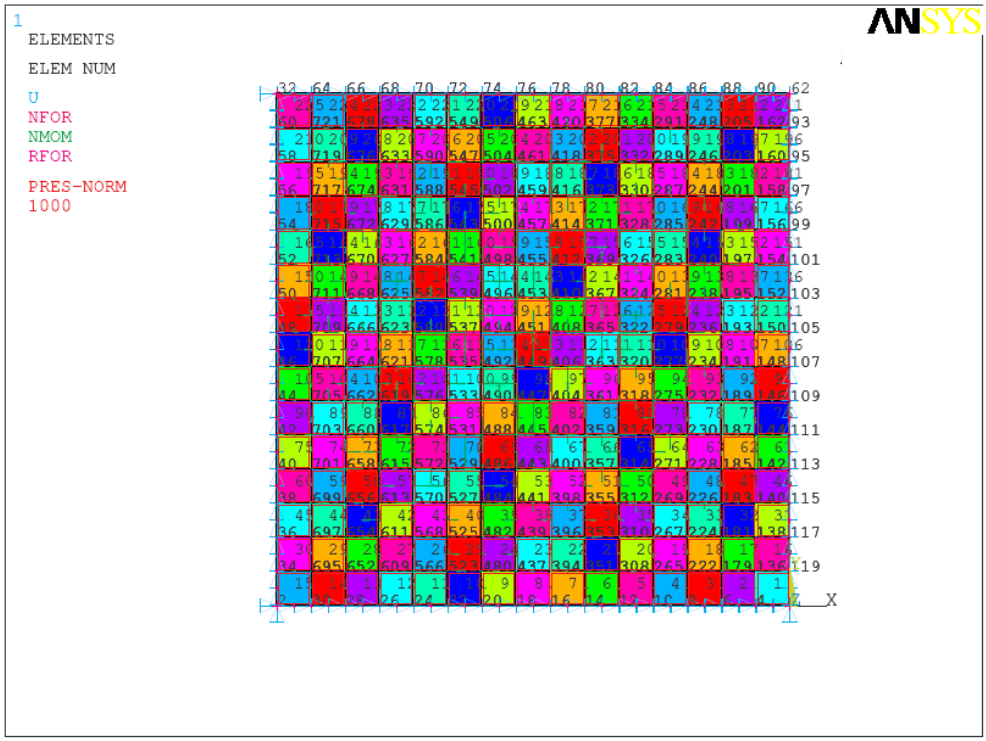

Figure 4.9: Geometry, Mesh, and Boundary Conditions of ANSYS SHELL99 Test Laminate

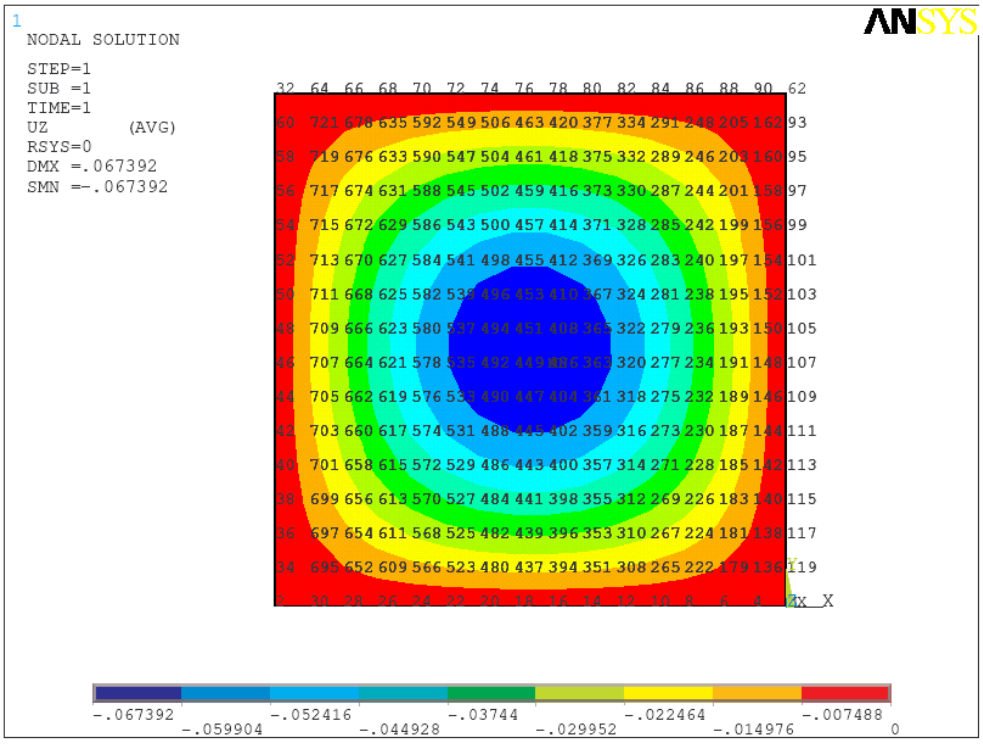

Figure 4.10: Deflection (m) Plot for ANSYS SHELL99 Test Laminate

Table 4.10: Flexural Stiffnesses of Various Materials for Box Beams

Flexural Stiffnesses (N-m^2)	Up Load	Side Load
Composite Quasi Laminate	1.62E+09	9.13E+09
Composite Hard Laminate	1.96E+09	1.10E+10
Titanium Solid Shell or SHELL93	3.10E+09	1.74E+10

The first study with box beams was for the effect of beam length to width ratio. The length of the box beams was varied from one up to 20 and included the ratio of the wing model (6.8). An upward load of 40,000 N, side load of 86,800 N, and a combination of these loads were applied to the box beams. Displacements were found using the BEAM program-generated flexural stiffnesses and an analytic solution and compared to the solutions ANSYS was providing. The results are shown in Table 4.11. A typical ANSYS box beam model is shown in Figure 4.11. Figure 4.12 shows the typical results of the four material models for the wing-based length to width ratio. Figures 4.13-4.15 illustrate the effect of shortening the length of the box beam on the results. The error increases dramatically for lower ratios; however, it can be seen that for the ratio associated with the wing the error is still within reason.

The use of springs in the modeling of the side-of-body joint was done by Livne et al. [415]. The stiffness of these root springs is very high (3.0647×10^7 N/m) compared with wing stiffness, practically cantilevering the wing. This was modeled in ANSYS on the box beams; the model is shown in Figure 4.16. A comparison was made between the effect of having springs located at the side-of-body and applying fixed conditions at the same location (20.79 m from the free end) (see Table 4.12 and Figure 4.17). This was done using the hard composite laminate. One can see that the side-of-body has a significant effect on the tip displacement of the beam.

The third study on the box beams involved that of how to model fuel in the wing box. The first thought was to use FLUID80 volume elements [414]. However, this proved to be difficult in the actual wing model. Surface pressures were then applied to the sides and bottom of the box beam to simulate fluid. The pressure applied to the bottom skin is constant, whereas it varies linearly on the walls. A comparison was made between the FLUID80 model, pressure applied only to the bottom skin, and applied to the bottom and sides of the beam (see Table 4.13 and Figures 4.18-4.21. A quasi laminate was used in this case. It can be seen that the results of the pressure loading fairly match that of the fluid element model.

Table 4.11: Length to Width Ratio Box Beam Study Results (Up and Side Loads)

Length:Width Ratio	Displacement UZ (m)	Displacement UY (m)	ANSYS Up (m)	ANSYS Side (m)	Error Up	Error Side
68.2/3.41 = 20						
Quasi	2.6057	1.0048	2.5444	1.0149	2.4%	-1.0%
Hard	2.1569	0.8317	2.0993	0.8254	2.7%	0.8%
Iso Ti	1.3654	0.5265	1.3374	0.5257	2.1%	0.2%
93 Ti	1.3654	0.5265	1.3374	0.5257	2.1%	0.2%
34.1/3.41 = 10						
Quasi	0.3257	0.1256	0.3332	0.1331	-2.3%	-6.0%
Hard	0.2696	0.1040	0.2652	0.1046	1.7%	-0.6%
Iso Ti	0.1707	0.0658	0.1685	0.0664	1.3%	-0.9%
93 Ti	0.1707	0.0658	0.1685	0.0664	1.3%	-0.9%
23.3/3.41 = 6.8						
Quasi	0.1039	0.0401	0.1074	0.0424	-3.4%	-5.9%
Hard	0.0860	0.0332	0.0861	0.0341	-0.1%	-2.7%
91 Hard	0.0860	0.0332	0.0863		-0.4%	
Iso Ti	0.0544	0.0210	0.0545	0.0215	-0.1%	-2.6%
93 Ti	0.0544	0.0210	0.0545	0.0215	-0.1%	-2.6%
17.05/3.41 = 5						
Quasi	0.0407	0.0157	0.0447	0.0178	-9.8%	-13.2%
Hard	0.0337	0.0130	0.0348	0.0138	-3.2%	-6.3%
Iso Ti	0.0213	0.0082	0.0219	0.0087	-2.6%	-5.5%
93 Ti	0.0213	0.0082	0.0219	0.0087	-2.6%	-5.5%
6.82/3.41 = 2						
Quasi	0.0026	0.0010	0.0038	0.0016	-44.6%	-58.9%
Hard	0.0022	0.0008	0.0031	0.0013	-45.7%	-54.4%
Iso Ti	0.0014	0.0005	0.0018	0.0008	-34.0%	-44.7%
93 Ti	0.0014	0.0005	0.0019	0.0008	-35.9%	-44.7%
3.41/3.41 = 1						
Quasi	0.0003	0.0001	0.0011	0.0005	-223.0%	-289.1%
Hard	0.0003	0.0001	0.0009	0.0004	-242.7%	-276.9%
Iso Ti	0.0002	0.0001	0.0005	0.0002	-192.2%	-231.3%
93 Ti	0.0002	0.0001	0.0005	0.0002	-192.2%	-231.3%

Table 4.11: Length to Width Ratio Box Beam Study Results (Combined Loading) (continued)

Length:Width Ratio	ANSYS Combo UX (m)	ANSYS Combo UY (m)	ANSYS Combo UZ (m)
68.2/3.41 = 20			
Quasi	-0.0697	-1.0151	2.5446
Hard	-0.0567	-0.8256	2.0993
Iso Ti	-0.0361	-0.5257	1.3374
93 Ti	-0.0361	-0.5257	1.3374
34.1/3.41 = 10			
Quasi	-0.0183	-0.1332	0.3332
Hard	-0.0142	-0.1046	0.2652
Iso Ti	-0.0091	-0.0664	0.1686
93 Ti	-0.0091	-0.0664	0.1686
23.3/3.41 = 6.8			
Quasi	0.0085	-0.0425	0.1075
Hard	-0.0068	-0.0341	0.0861
91 Hard	-0.0067	-0.0342	0.0863
Iso Ti	-0.0043	-0.0216	0.0545
93 Ti	-0.0043	-0.0216	0.0545
17.05/3.41 = 5			
Quasi	-0.0047	-0.0178	0.0447
Hard	-0.0036	-0.0139	0.0374
Iso Ti	-0.0023	-0.0087	0.0219
93 Ti	-0.0023	-0.0087	0.0219
6.82/3.41 = 2			
Quasi	-0.0008	-0.0016	0.0038
Hard	-0.0007	-0.0013	0.0031
Iso Ti	-0.0004	-0.0008	0.0019
93 Ti	-0.0004	-0.0008	0.0019
3.41/3.41 = 1			
Quasi	-0.0003	-0.0005	0.0011
Hard	-0.0002	-0.0004	0.0009
Iso Ti	-0.0001	-0.0002	0.0005
93 Ti	-0.0001	-0.0002	0.0005

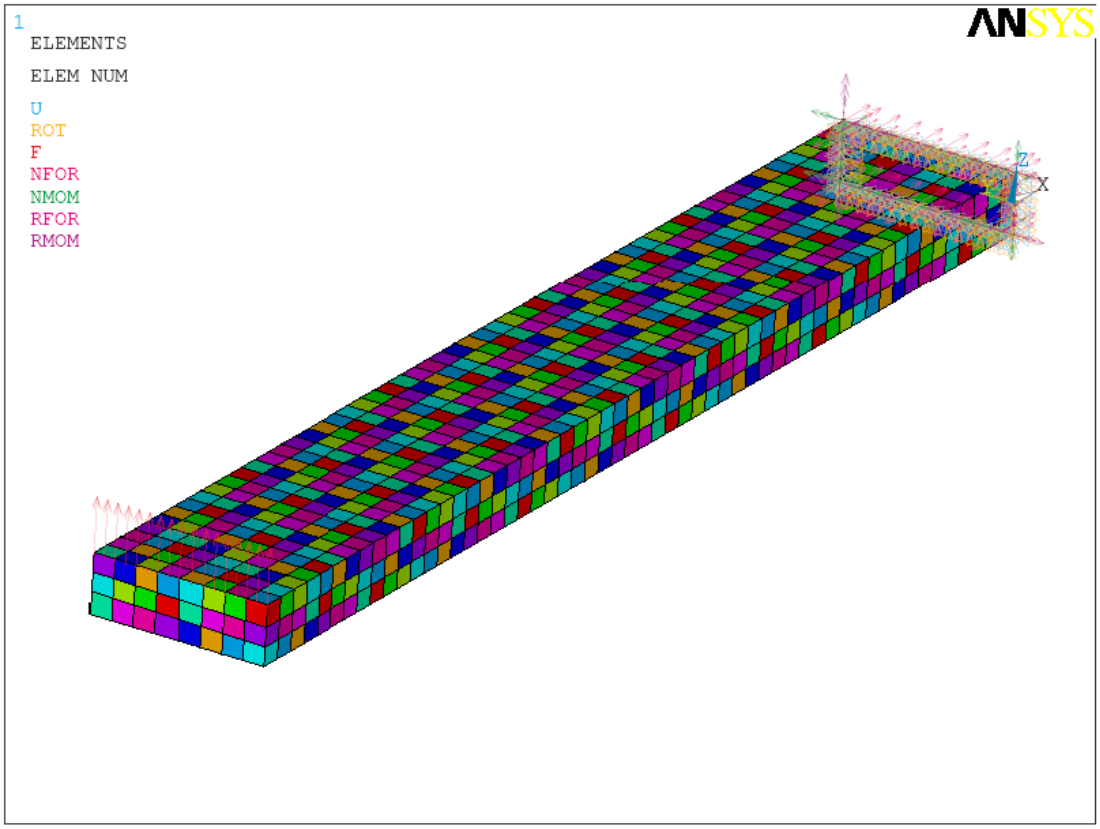

Figure 4.11: ANSYS Box Beam Model, Hard Composite, Up Loading

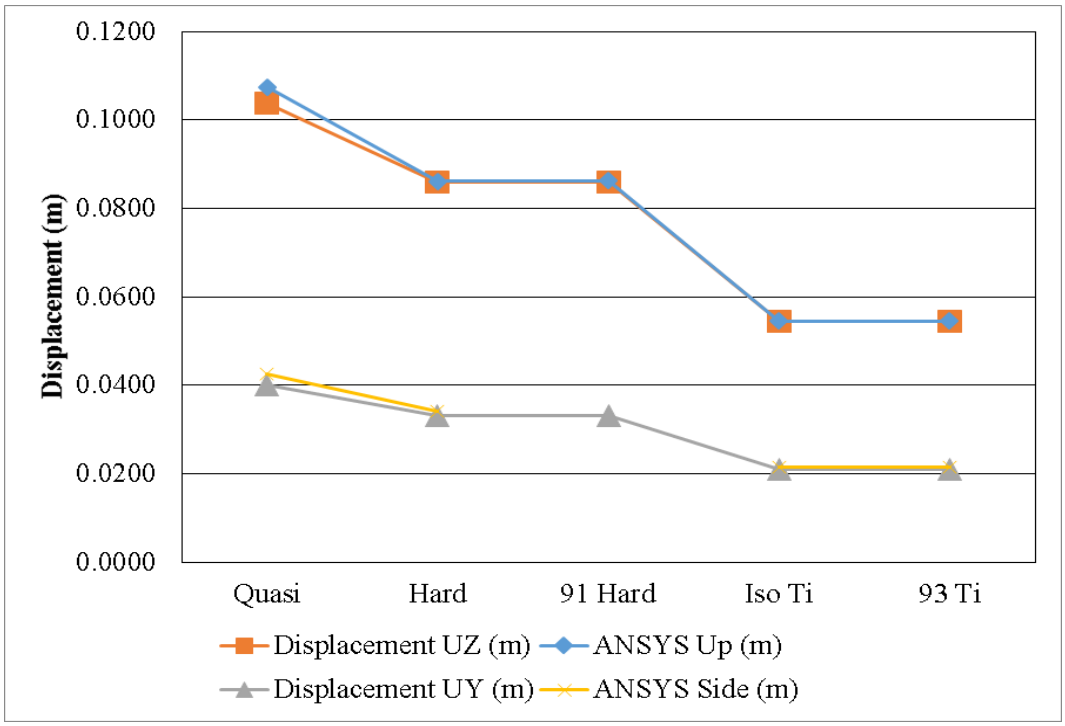

Figure 4.12: Box Beam Wing Ratio, Theory vs. ANSYS Displacements

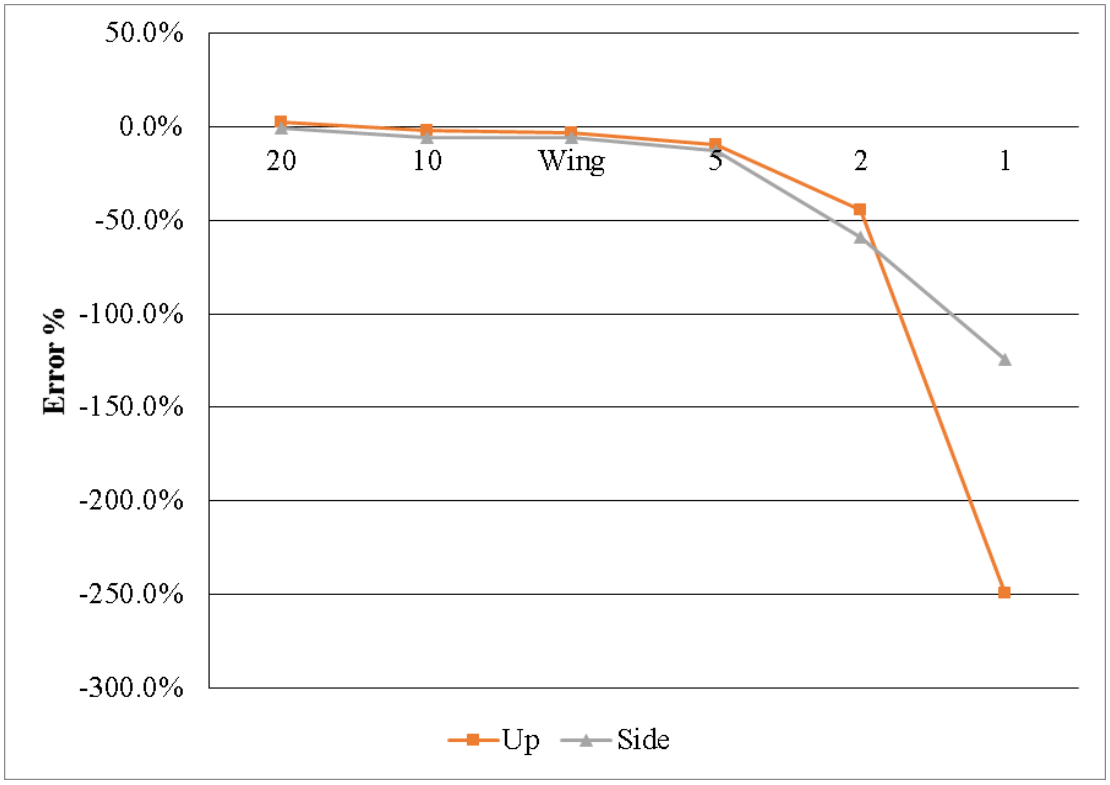

Figure 4.13: Quasi Composite Box Beam, Error Percentage vs. Length:Width Ratio

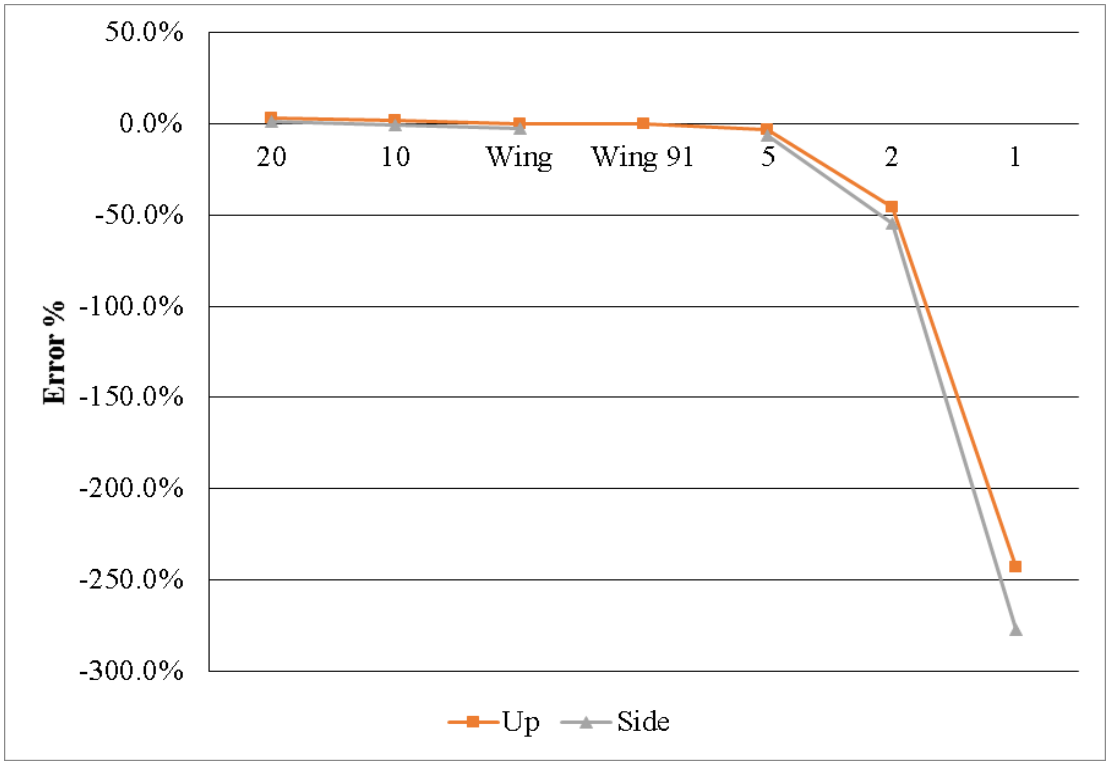

Figure 4.14: Hard Composite Box Beam, Error Percentage vs. Length:Width Ratio

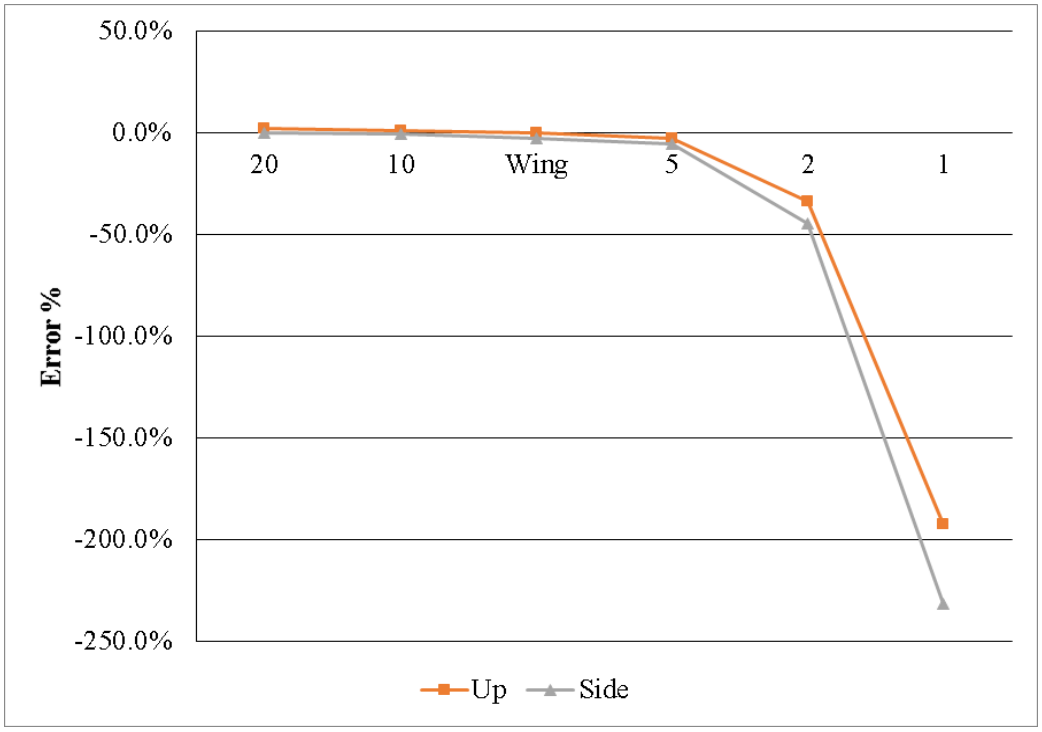

Figure 4.15: Titanium Box Beam, Error Percentage vs. Length:Width Ratio

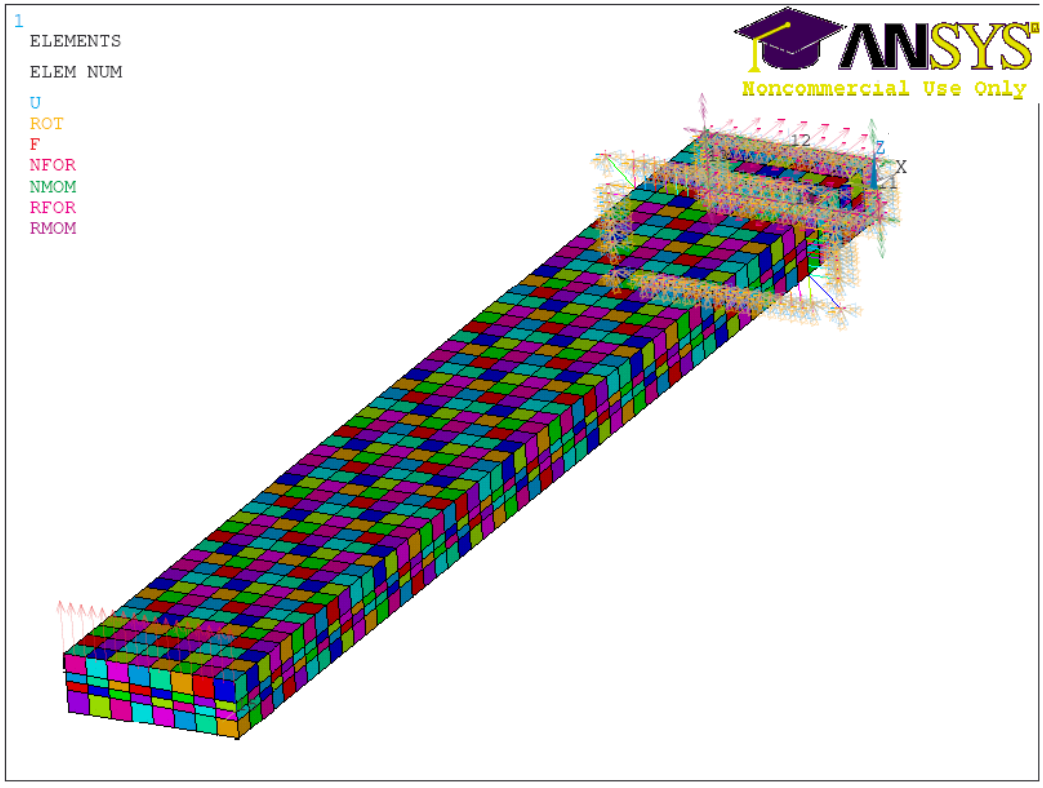

Figure 4.16: Hard Composite Box Beam with Spring Side-of-Body, Up Loading

Table 4.12: Effect of Side-of-Body Fixity on Box Beam Deflections

	Displacement UZ (m)	Displacement UY (m)	ANSYS Up (m)	ANSYS Side (m)	Error Up	Error Side
Fixed SOB	0.0611	0.0236	0.0617	0.0245	-1.0%	-3.8%
Spring SOB	0.0611	0.0236	0.0789	0.0326	-29.1%	-38.5%

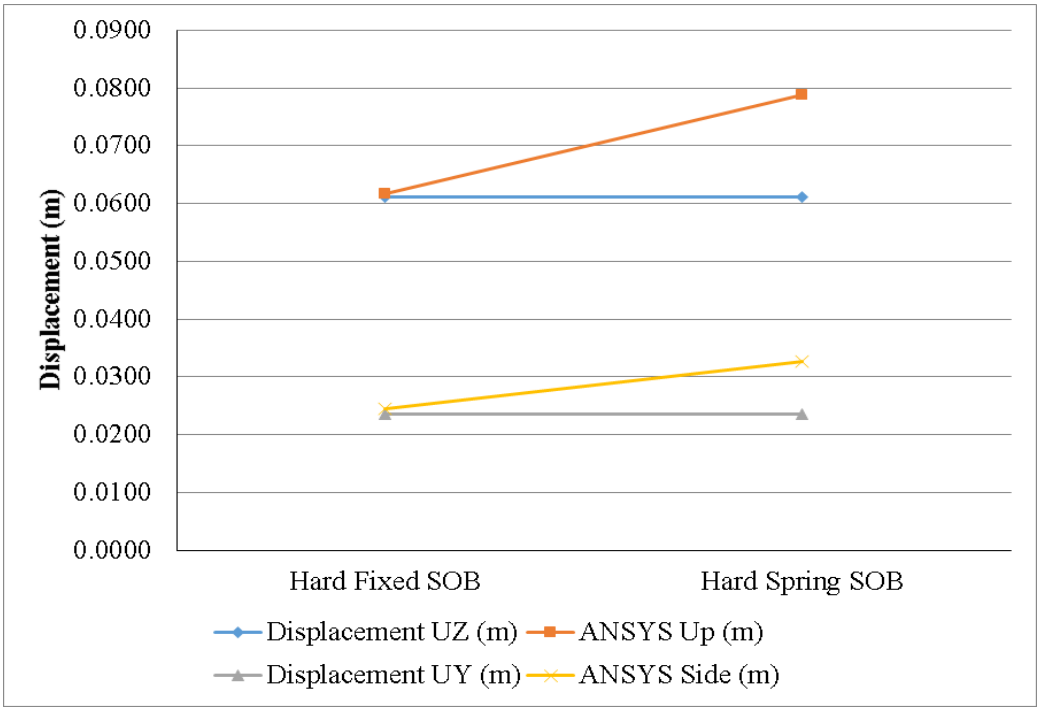

Figure 4.17: Hard Composite Box Beam, Spring SOB Modeling, Wing Ratio Theory vs. ANSYS Displacements

Table 4.13: Fuel Volume Modeling, Volume Elements vs. Surface Pressures

	ANSYS UX (m)	ANSYS UY(m)	ANSYS UZ (m)
Quasi Fuel Volume	0.0311	-0.0068	0.8294
Quasi Fuel Pressure	0.0279	-0.0061	0.7503
Quasi Fuel Pressure Sides	0.0279	-0.0046	0.7500

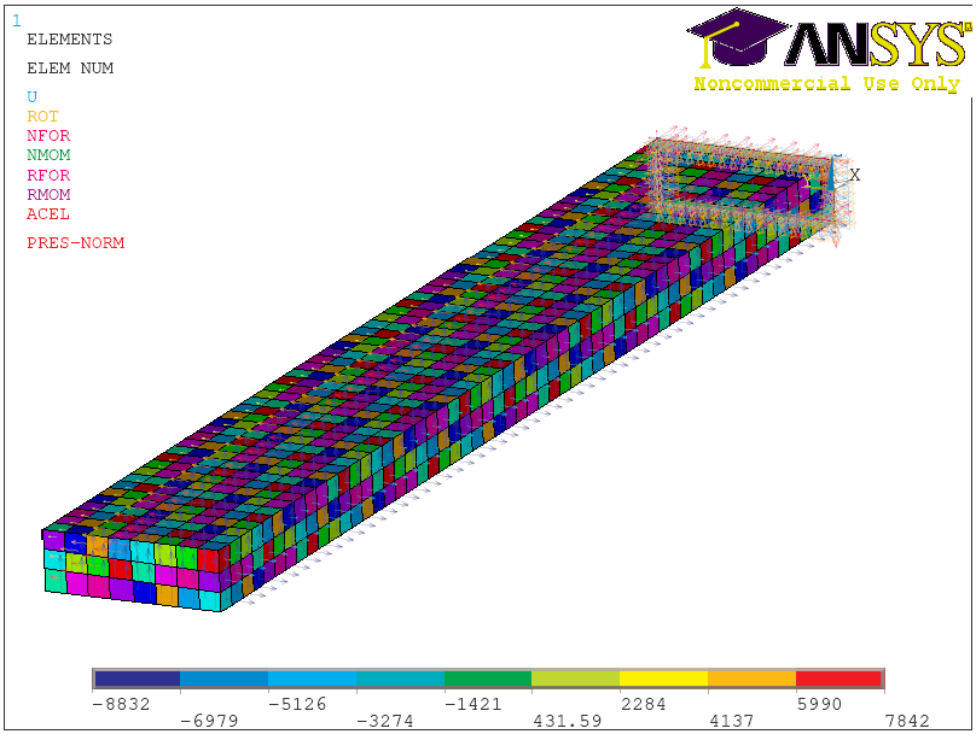

Figure 4.18: Quasi Composite Box Beam, Wing Length, Fuel Pressure Sides

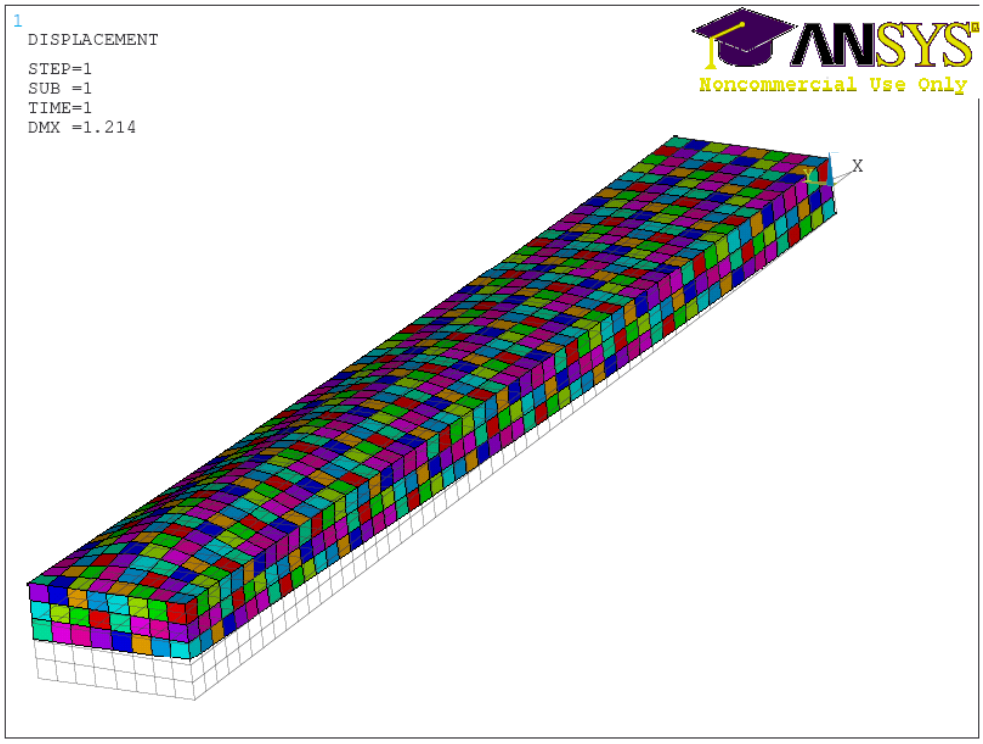

Figure 4.19: Quasi Composite Box Beam, Wing Length, FLUID80 Elements, Deformed

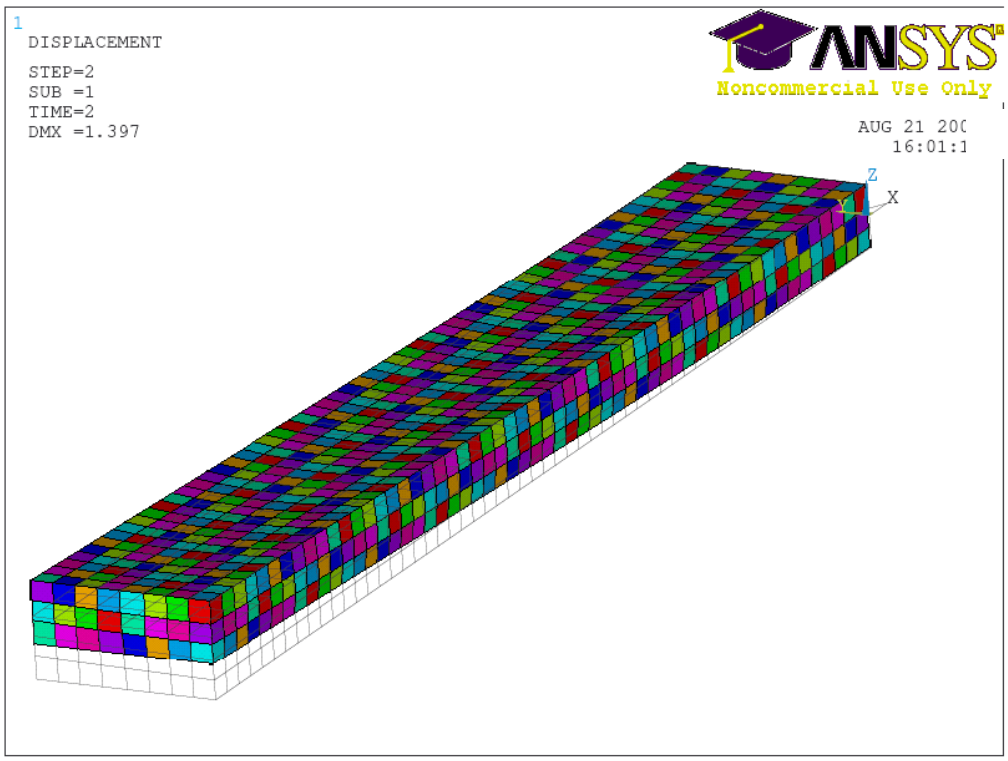

Figure 4.20: Quasi Composite Box Beam, Wing Length, Surface Pressures, Deformed

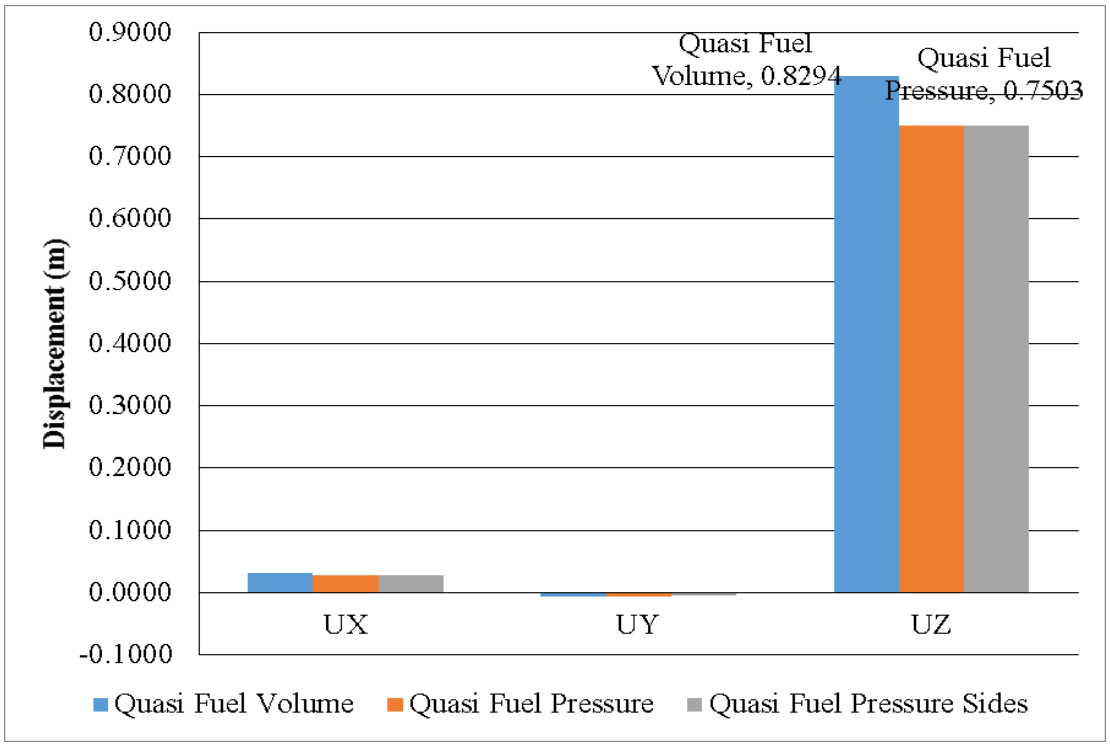

Figure 4.21: Comparison of Displacements for Fuel Weight Modeling on Box Beam

4.3.3 Composite Wing Design Finite Element Modeling

The solid model of the composite wing was generated in SolidWorks and imported to ANSYS using an IGES file. Once there, the geometry was "cleaned up" and the wing leading and trailing edge reaction, aerodynamic, and fuel pressure loads were added. The side-of-body boundary condition in the finite element model is imposed using springs; the stiffness of these root springs is very high (3.0647×10^7 N/m) compared with wing stiffness, practically cantilevering the wing [415]. An advantage of this approach is that the results of a structural model can be matched to experiments, taking the flexibility of the experimental setup supports into account [416]. These springs are COMBIN14 elements and are applied at all nodes of the upper and lower skin panels and front and rear spars at the side-of-body rib. The model was then meshed using SHELL99 8-noded composite shell elements [417]. There are 3,902 shell elements, 86 spring elements, and 11,098 nodes in the model (see Figure 4.22). The point masses specified in Table 4.6 are shown applied to the wing model in Figure 4.23. The fuel inside the wing exerts pressures on the internal structures. These pressures are translated into nodal loads, which vary spanwise along the wing and from the lower to upper wing panels. Fuel bay pressures are shown graphically in Figure 4.24, and a typical fuel bay ANSYS model applied load is shown in Figure 4.25. Figure 4.26 are the fuel loads for the wing model. The mass of the current wing model is 16,320 kg. This finite element model is sufficiently detailed to enable structural optimization algorithms that incorporate flutter and divergence, aeroelastic tailoring, buckling and post buckling, vibration and natural frequency, and bolted joint analyses. This study focuses on the aeroelastic cycle, bolted joint analyses, and composite laminate strength constraints.

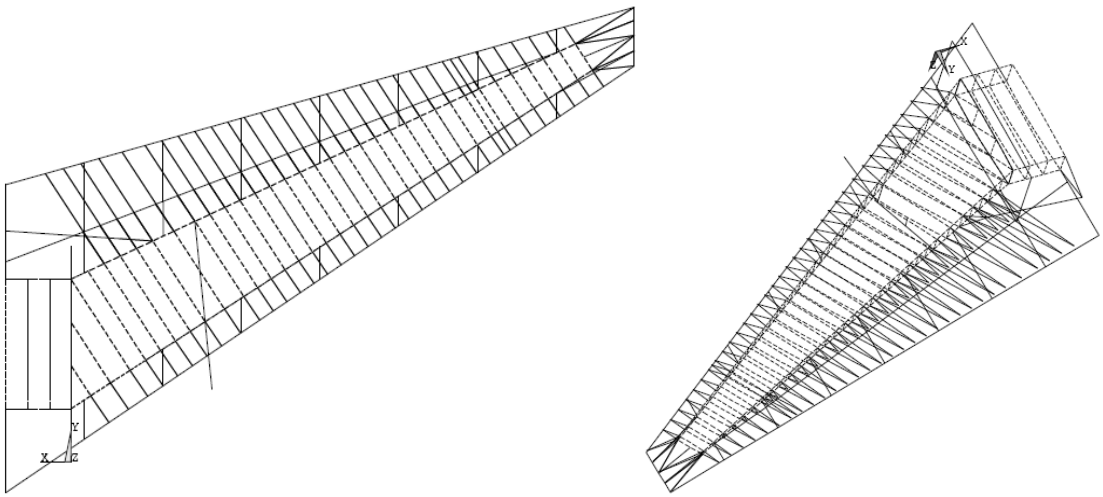

Figure 4.22: Two Views of the ANSYS Finite Element Wing Model Showing the Leading and Trailing Edge Masses, Power Plant, and Landing Gear Attachment Points

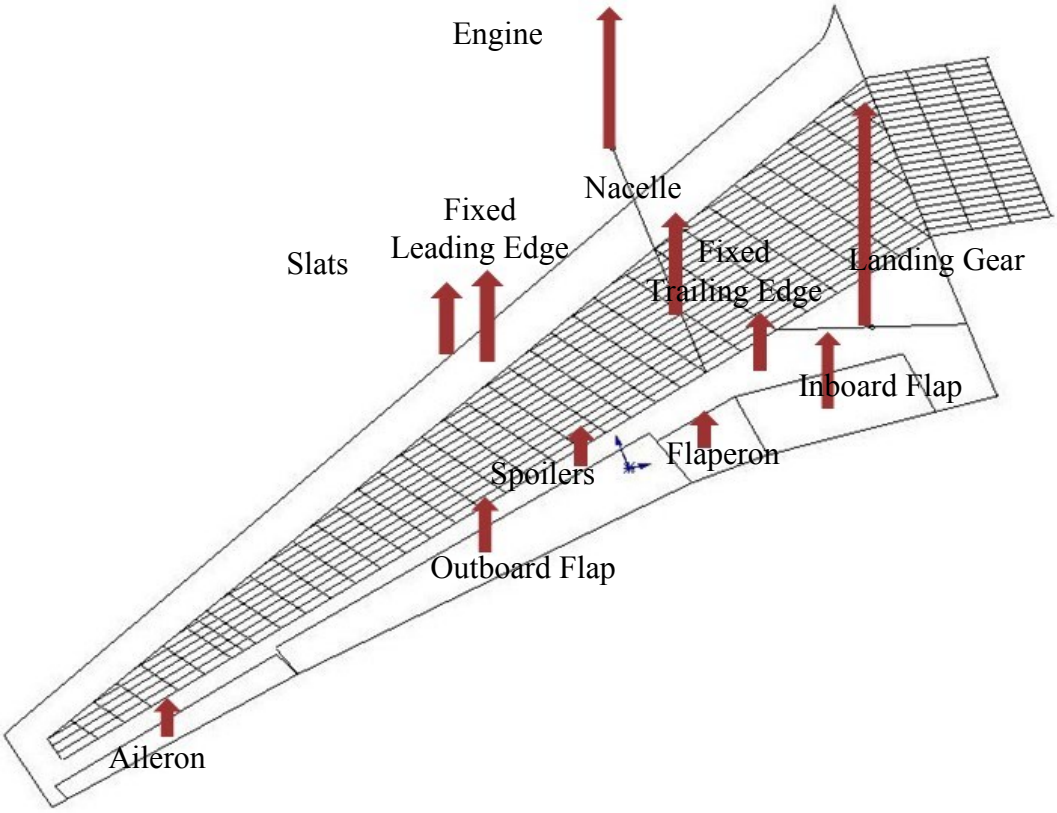

Figure 4.23: Secondary Structure, Power Plant, and Landing Gear Masses Applied to Wing Model

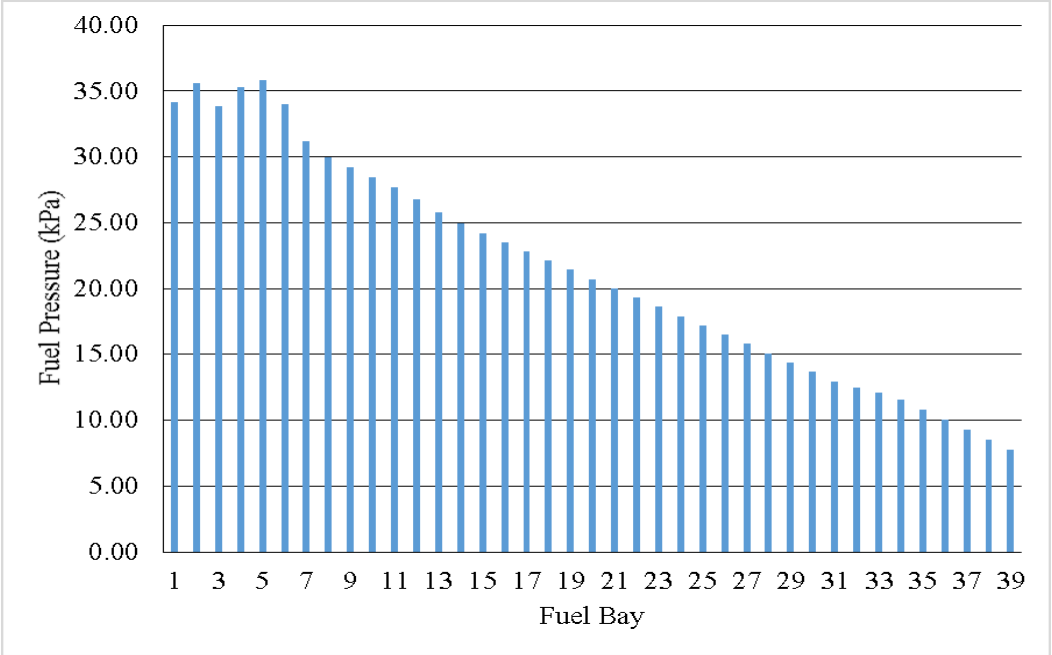

Figure 4.24: Fuel Pressures in Each Fuel Bay, 3.75G

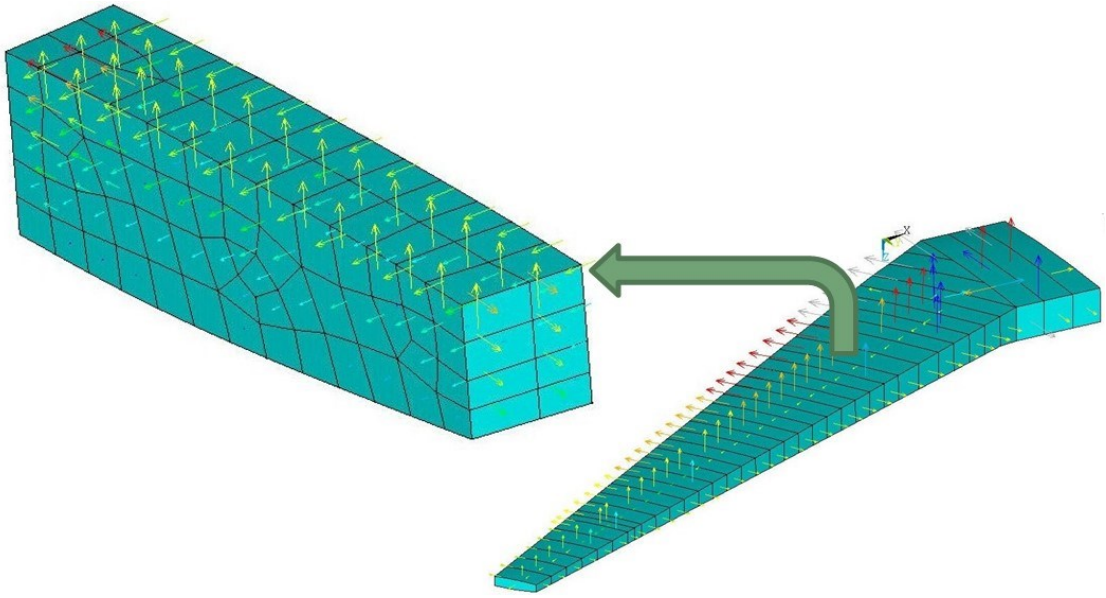

Figure 4.25: Typical Fuel Bay with Downward Acceleration Pressure Loads

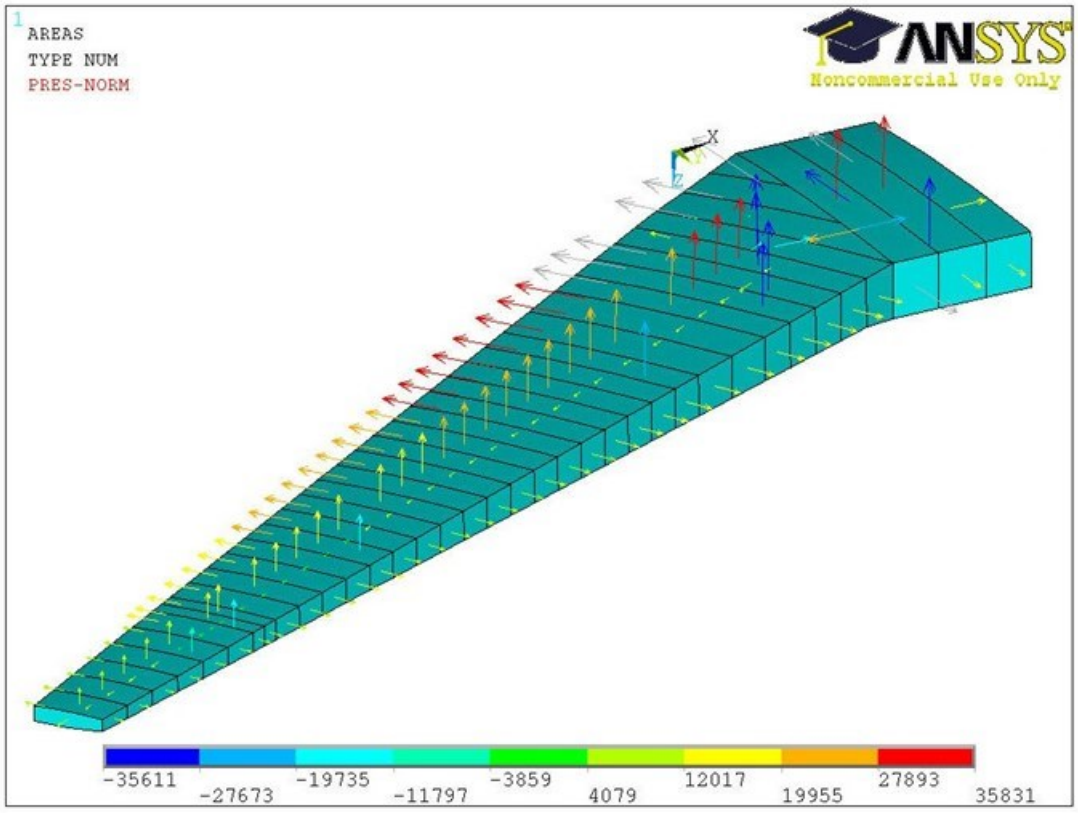

Figure 4.26: Applied Fuel Loads to Wing Model

Fourteen load cases were applied to the wing model; these are listed in Table 4.14. These include two critical loading conditions based on the design cruise speed Vc and the limit load factors (2.5 G and -1.0 G) [418]. With the ultimate load factor of 1.5, these loading conditions become 3.75 G up bending and -1.5 G down bending. Results from the aerodynamic, mass, and fuel loads, applied separately and in combination, are shown to more fully understand the performance of this wing model. The emergency landing loads were chosen to be 6G downward, 9G forward, and 3G outboard [419].

Only the mass of the structural box and the power plant were considered in this case. It should be noted that these load cases do not include all the cases that are included in the structural design of the wing, and are not the critical load case for the entire wing acreage. Figure 4.27 shows the loads applied for case 12, all 3.75G loads, including aerodynamic pressures and moments, fuel pressures, and point mass loads. The tip deflection in the z-axis direction for loads case 12 are shown in Figure 4.28. The twist induced in the wing model caused by the non-linear geometry is illustrated in Figure 4.29 (shown scaled ten times the actual displacements). The tip deflection in the z-axis direction for load case 13 (all –1.5G loads) is shown in Figure 4.30. All load cases show similar trends in z-axis deflections. Figure 4.31 shows all the tip deflection results, and Figure 4.32 shows the results for the strains in the x-axis direction at mid-chord of the upper skin at the wing joint (bay five). Note that a negative deflection is upwards.

The tip deflections that these load cases produce can be seen to be very small. The expected deflection for a wing of this type would be something on the order of five meters. It is important to remember that the idea behind this wing model is that the laminate design of the wing root joint is used for the entire wing structural box. The model is over designed for the purpose of providing a starting point for structural optimization. During the process of an optimization algorithm it is expected that unnecessary plies in the skins, spars, ribs, and I-stringers will be dropped.

Table 4.14: Wing Model Load ANSYS Results

Load No.	Load Type	Tip Deflection UZ (m)	Bay 5 EPSX
1	Aerodynamic Loads	-0.1042	-2.93E-04
2	3.75G Mass Loads	-0.2066	-3.99E-04
3	-1.5G Mass Loads	0.0827	1.60E-04
4	3.75G Fuel Loads	-0.4363	-8.65E-03
5	-1.5G Fuel Loads	0.1793	3.27E-04
6	Aerodynamic & 3.75G Mass Loads	-0.3063	-6.27E-04
7	Aerodynamic & -1.5G Mass Loads	-0.0272	-1.58E-04
8	Aerodynamic & 3.75G Fuel Loads	-0.5402	-1.17E-02
9	Aerodynamic & -1.5G Fuel Loads	0.1671	3.69E-04
10	3.75G Fuel & Mass Loads	-0.4979	-9.40E-04
11	-1.5G Fuel & Mass Loads	0.2040	3.94E-04
12	All 3.75G Loads	-0.5975	-1.21E-03
13	All -1.5G Loads	0.1952	4.32E-04
14	Emergency Landing Loads	0.2430	5.33E-04

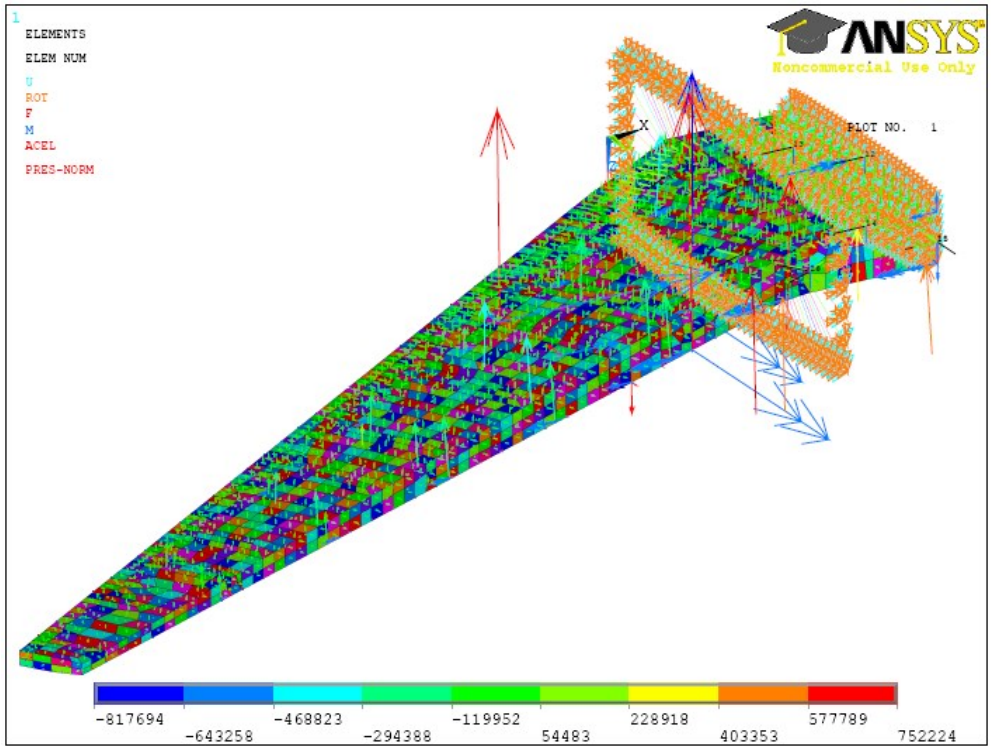

Figure 4.27: ANSYS Finite Element Wing Model Showing Load Case 12, All 3.75G Loads

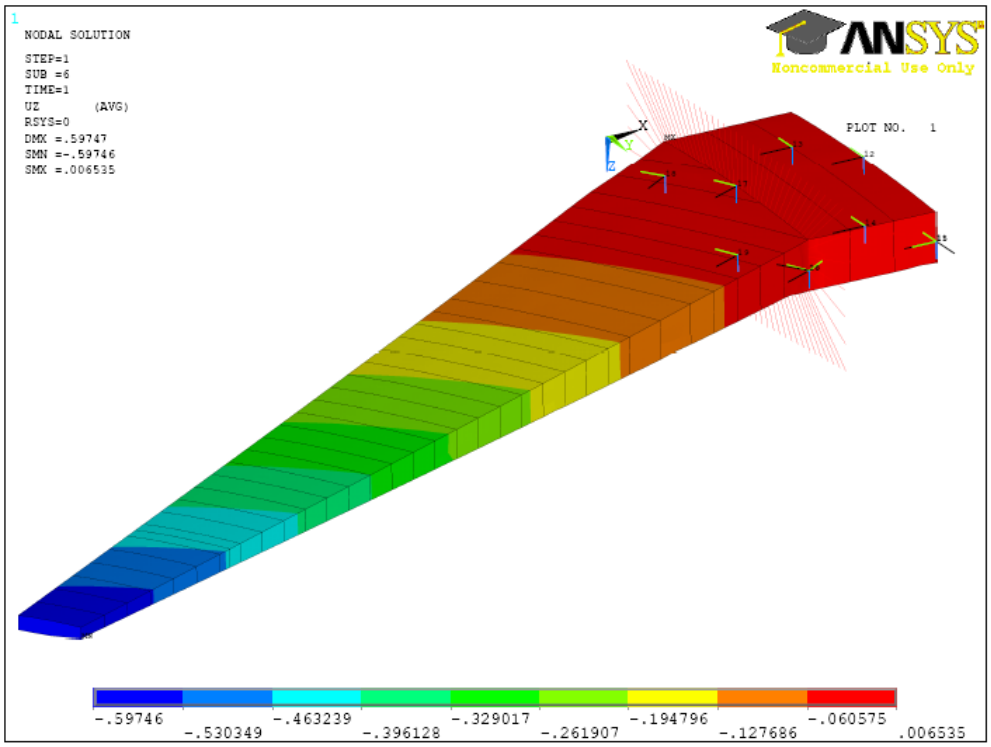

Figure 4.28: Z-axis Deflection Result for Load Case 12, All 3.75G Loads (UZ in m)

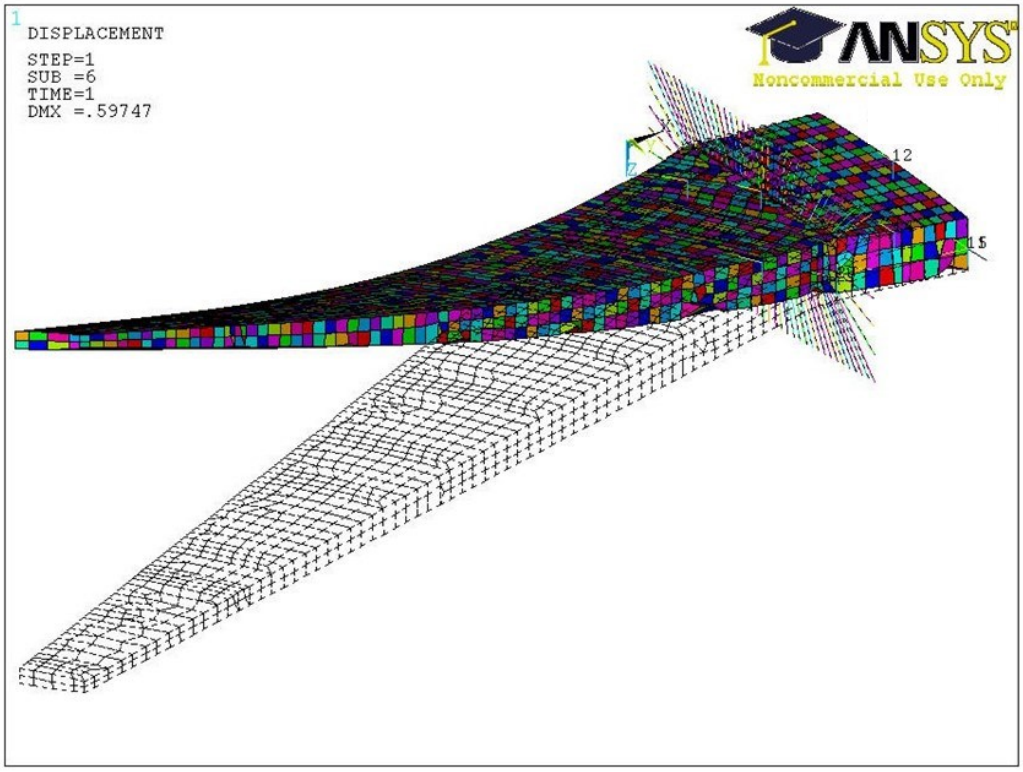

Figure 4.29: Typical Displacement of All 3.75G Loads (Scaled 10X)

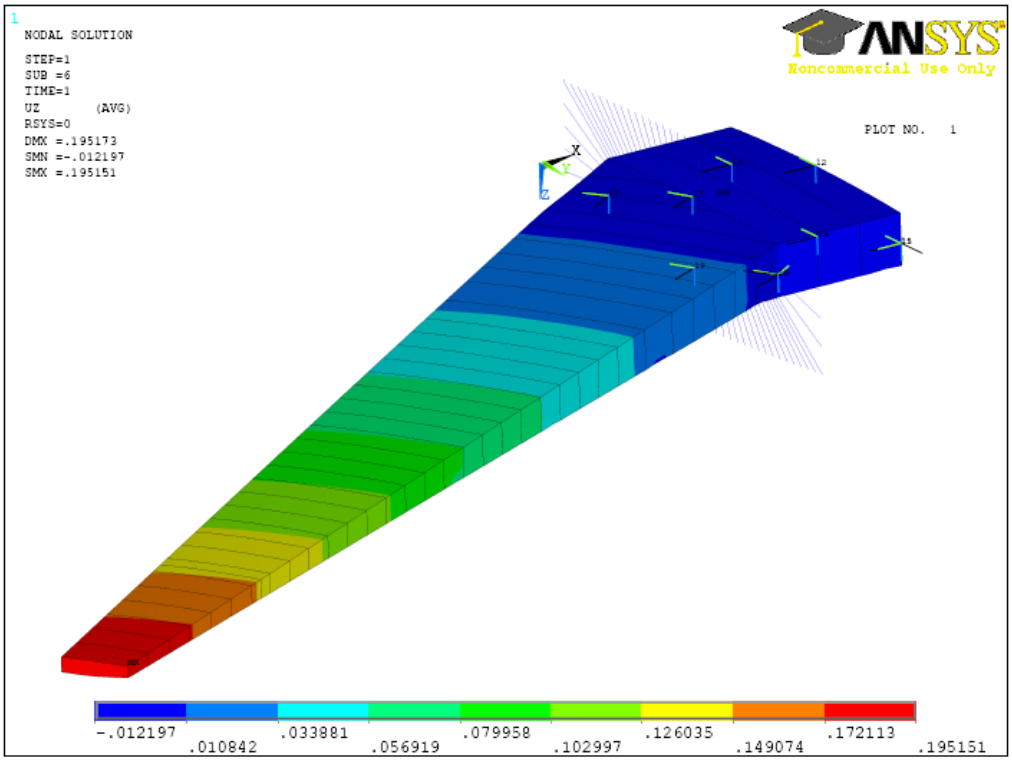

Figure 4.30: Z-axis Deflection Result for Load Case 13, All –1.5G Loads (UZ in m)

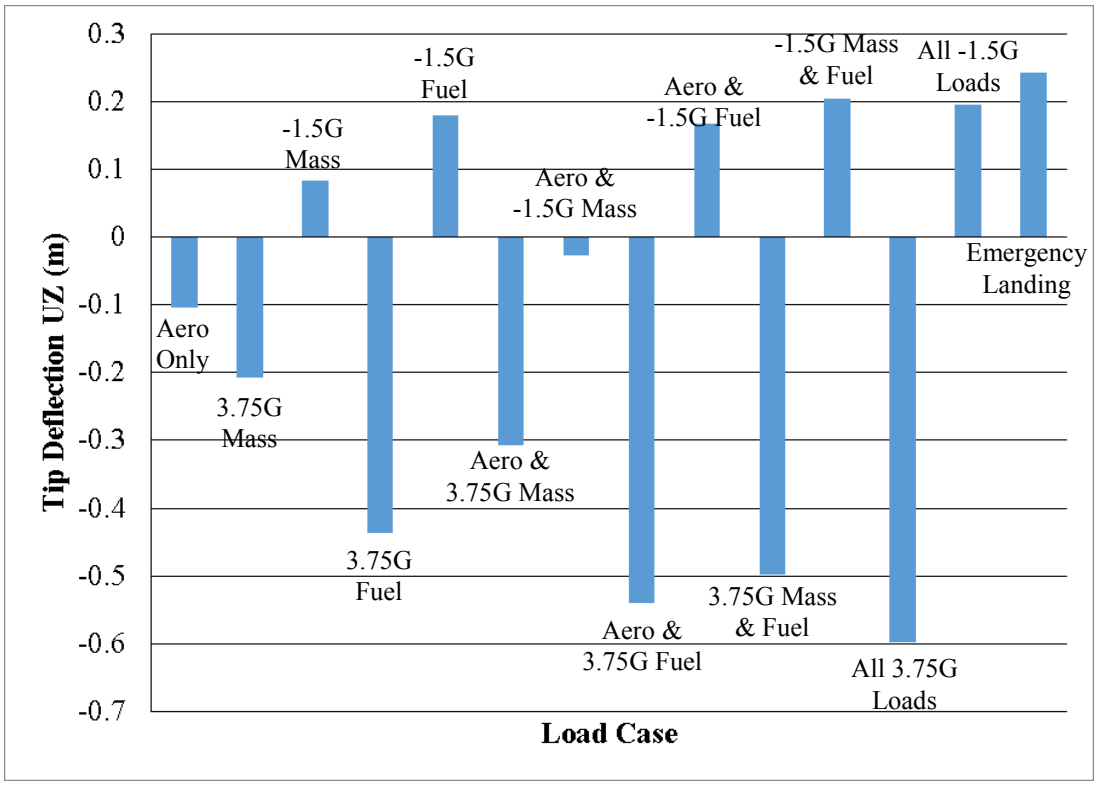

Figure 4.31: Tip Deflection Results for Wing Model Load Cases

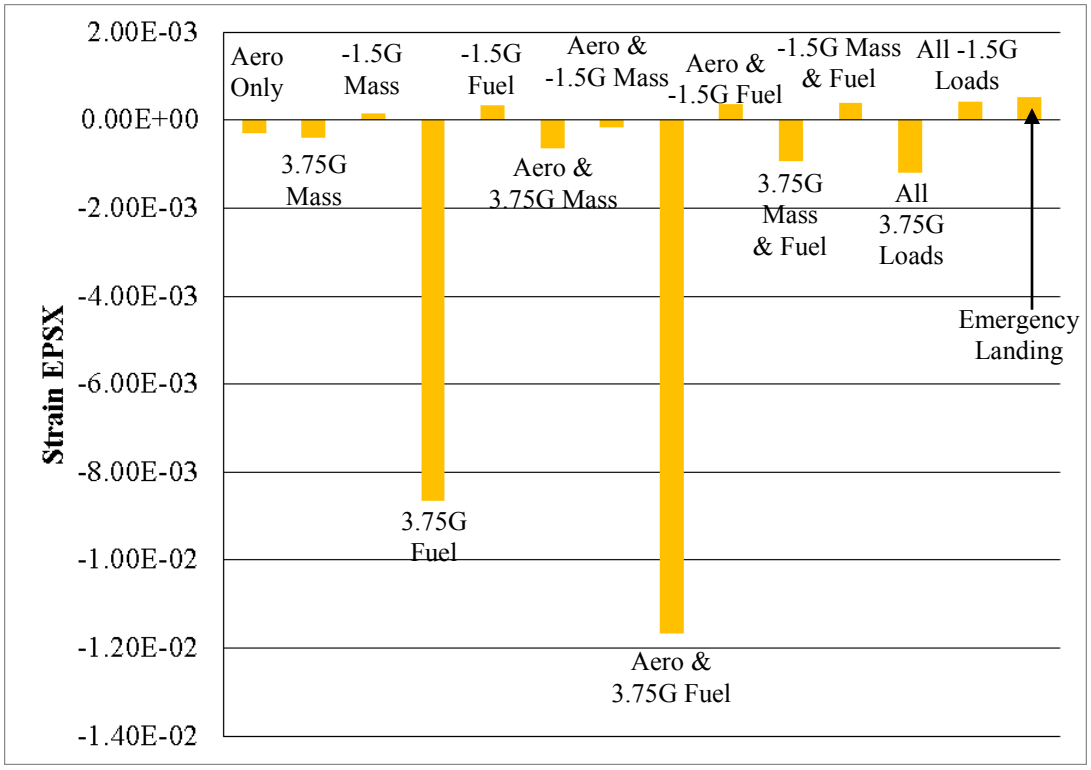

Figure 4.32: X-axis Strain Results for Bay Five for Wing Model Load Cases

Appendix C.1 contains details of the preliminary wing design, including geometry; airfoil thickness; initial stringer panel property calculations; the applied mass loads; applied fuel pressures; and the emergency landing loads. The contents of the title page of the University of Washington Subsonic Transport Composite Wing Model is shown in Appendix C.2.

4.4 Composite Wing Design – Initial Joint Configurations

All joints in the model composite wing are bolted. These are the rib-to-skin, rib-to-spar joints, and spar-to-skin joints. The upper panel of the benchmark composite wing model includes 278 individual joints. Figure 4.33 shows the upper panel joint positions and Table 4.15 provides some joint numbering definitions.

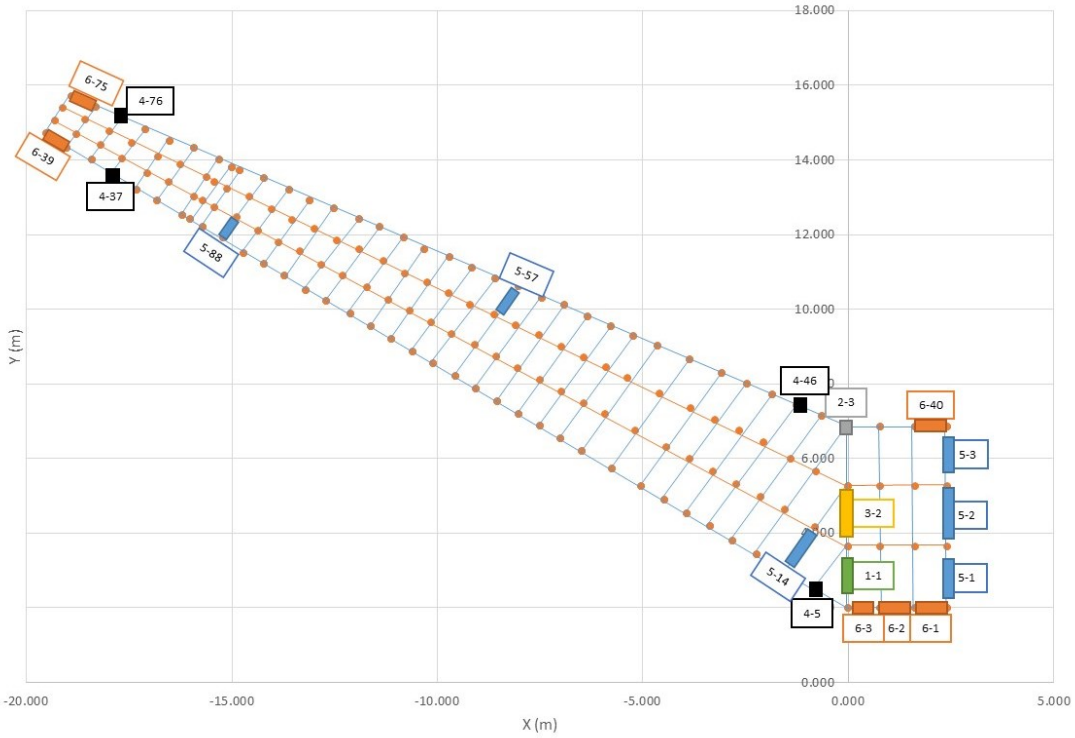

Figure 4.33: Upper Wing Panel Joint Identification

Table 4.15: Upper Wing Panel Joint Designations

Joint Designation	Joint Description	Number of Joints
1	Side-of-Body Skin/Stringer	3
2	Side-of-Body Skin/Spar	2
3	Side-of-Body Rib	3
4	Rib/Spar	78
5	Rib/Skin	117
6	Spar/Skin	75

Nelson et al. [372] was used as the major reference for joint design. As discussed previously, the side-of-body joint used in that study is the same one that is used here. In order to develop that joint (and analyze with ANSYS), the composite material properties must be determined. Table 4.16 lists the material properties used in this study and their sources. It should be noted that some of the composite fabric properties were estimated by comparing similar materials and calculating a knockdown factor; these are noted in the table. Some information about structural composite fastening systems was obtained from the Hi-Shear Corp. (Torrance, CA) is used here to provide proper sizing of Hi-Lok fasteners; information about these fasteners is shown in Table 4.17 [420-423].

Nelson et al. [372] provide laminate stacking sequence rules that were used to develop the initial laminate for the wing model. These are: 1. changes of only 45° are allowed between interior plies, 2. no stacked plies except at the midplane, 3. symmetry is required, and 4. the laminate should be of the "hard" type, i.e., 37.5% 0° / 50% 45° / 12.5% 90°. Table 4.18 shows the resulting 98-ply laminate design.

Next, notional composite bolted joints were drawn to illustrate the general lay-out and geometry of each of the joints in the wing. The side-of-body joint is shown in Figures 4.34 and 4.35. It should be noted that the spar-to-skin and rib-to-skin joints are similar in that they are double-shear joints; however, they have two fastener rows per joint instead of three. A generic rib-to-spar joint is shown in Figures 4.36 and 4.37. These are single-shear joints and have only one row of fasteners. Based on fasteners sizes, joint strip widths, the number of fastener rows, and joint lengths the number of fasteners required for all of the bolted joints in the model wing were determined. These are shown in Figures 4.38-4.42 for the front spar-rib, rear spar-rib, upper skin-rib, lower skin-rib, and all of the spar-skin joints, respectively. Further, Table 4.19 shows the details of how the side-of-body joint was developed using methods proposed by Hart-Smith [424, 376] and Nelson et al. [372]. The other joints in the wing were designed in a similar way. The preliminary procedure for the conceptual design of joints include:

1. The allowable strain should not exceed 0.005.
2. Find average bolt size dav for the load Pw in a strip w wide. Double shear splicing. Bolt diameter should equal the thickness of the central member in a double shear joint. Number of bolts satisfy Pav = Pw / k*n, where Pav is the bolt load, n is the number of bolts per strip, and k is the bolt efficiency factor not to exceed zero.
3. The resulting w / dav should be compared with bearing and bypass interactions. Usually $3.5 < w / dav < 5.0$ depending on n.
4. First bolt entering the joint should be made smaller than the average diameter, the last bolt larger.
5. Splice plate taper and bearing thicknesses should be established to accommodate the bolt load distributions.
6. Bearing stresses vary from 30 to 100% of the ultimate bearing allowable stress in a tailored multirow joint if fatigue is not considered.
7. Side edge distance is 2.5d and the end distance is 3d to prevent shear-out.

Table 4.16: Composite and Titanium Material Properties

Property	Value	Units	Source
T800HB / 3900-2 Carbon/Epoxy Unidirectional Laminate			
E11	155.8	GPa	[408]
E22	8.89	GPa	[408]
E33	8.89	GPa	[177]
ν12	0.3		[408]
ν13	0.3		[177]
ν23	0.3675		[177]
G12	5.14	GPa	[408]
G13	5.14	GPa	[177]
G23	3.517	GPa	[177]
t	0.0001905	m	[409]
density	1550	kg/m^3	[409]
T700S / 3900-2 Carbon/Epoxy Plain Weave Laminate			
*E11t	73.65	GPa	[409]
*E11c	70.82	GPa	[409]
*E22t	60.38	GPa	[409]
*E22c	70.82	GPa	[177]
E33	10.26	GPa	[177]
*G12	5.52	GPa	[409]
G13	3.83	GPa	[177]
G23	3.83	GPa	[177]
*ν12	0.046		[177]
ν13	0.4		[177]
ν23	0.4		[177]
t	0.000201	m	[409]
density	1530	kg/m^3	[409]
Titanium 6Al4V Plate			
Et	116.52	GPa	[425]
Ec	118.59	GPa	[425]
ν	0.31		[425]
G	44.82	GPa	[425]
density	4428.78	kg/m^3	[425]

* Knockdown factors based on material MIL-HDB-17 Section 4.2.29, T650-35 12K / 976 Uni Tape vs. 4.2.35, T650-35 3K / 976 Plain Weave Fabric

Table 4.17: Hi-Lok/Hi-Tigue and Hi-Lok Fastening System, Hi-Lok HL10 Pin, 6AL-4V Titanium [420-421]

Tensile Strength = 1103 MPa				
Shear Strength = 655 MPa				
Fastener ID	**Dash Number**	**Diameter (m)**	**Double Shear Load (N)**	**Tensile Load (N)**
1	5	0.00396875	17,837.4	8,629.5
2	6	0.00476250	23,931.4	11,120.6
3	8	0.00635000	41,368.5	19,127.4
4	10	0.00793750	64,944.0	28,023.8
5	12	0.00952500	93,412.7	38,699.5
6	14	0.01111250	127,219.1	53,823.5
7	16	0.01270000	165,918.7	68,057.8
8	18	0.01428750	209,956.1	84,516.2
9	20	0.01587500	259,331.3	102,309.1
10	24	0.01905000	373,205.8	136,560.4
11	28	0.02222500	507,097.3	200,170.0
12	32	0.02540000	662,785.0	270,896.7

Table 4.18: Composite Joint Laminate Design

Ply Number	Orientation (°)	0° plies	45° plies	90° plies
Plain Weave	45			
1	45		1	
2	0	1		
3	0	1		
4	-45		1	
5	90			1
6	-45		1	
7	0	1		
8	45		1	
9	45		1	
10	0	1		
11	0	1		
12	-45		1	
13	90			1
14	-45		1	
15	0	1		
16	45		1	
17	45		1	
18	0	1		
19	0	1		
20	-45		1	
21	90			1
22	-45		1	
23	0	1		
24	45		1	
25	45		1	
26	0	1		
27	0	1		
28	-45		1	
29	90			1
30	-45		1	
31	0	1		
32	45		1	
33	45		1	
34	0	1		
35	0	1		
36	-45		1	
37	90			1
38	-45		1	
39	0	1		
40	45		1	
41	45		1	
42	0	1		
43	0	1		
44	-45		1	
45	90			1
46	-45		1	
47	0	1		
48	45		1	
98	Count	18	24	6
	%	0.375	0.5	0.125

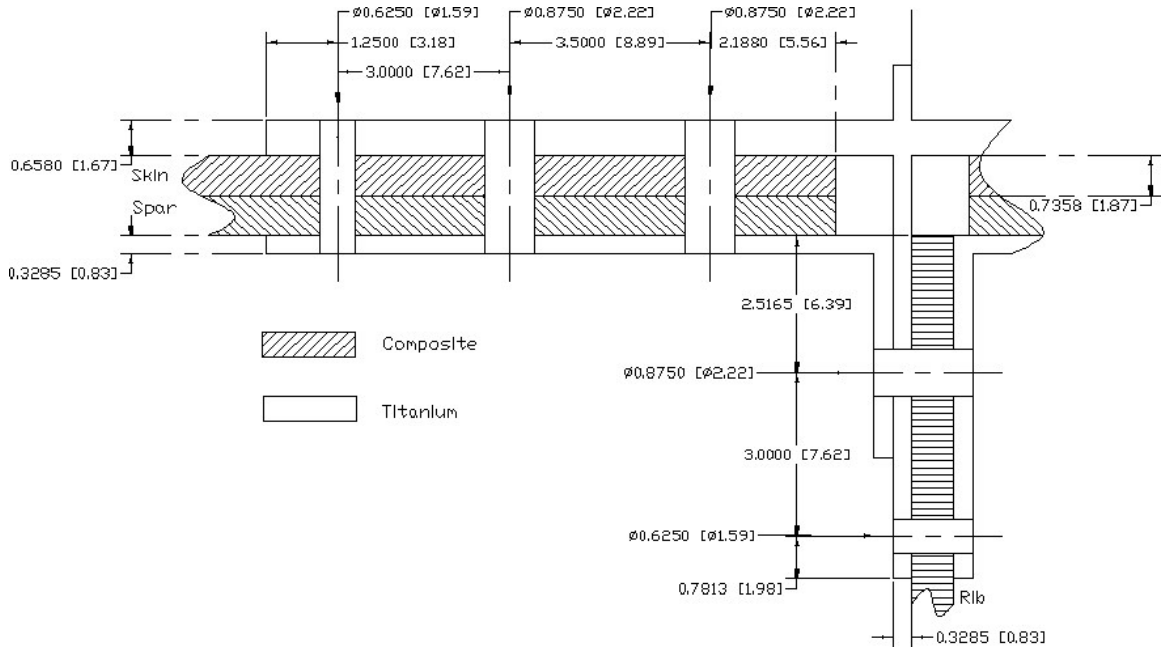

Figure 4.34: Side-of-Body Joint General Arrangement, Cross-sectional View. All Dimensions are in inches [cm]

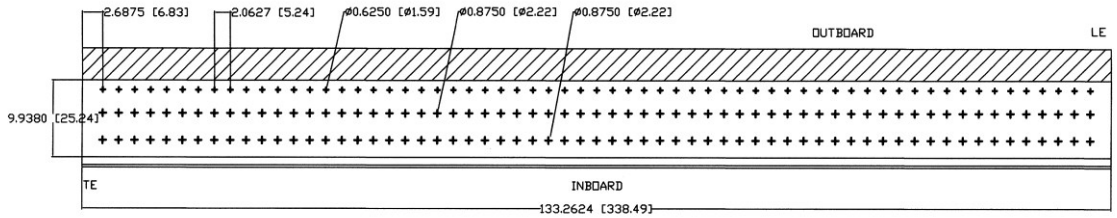

Figure 4.35: Side-of-Body Joint General Arrangement, Plan View. All Dimensions are in inches [cm].

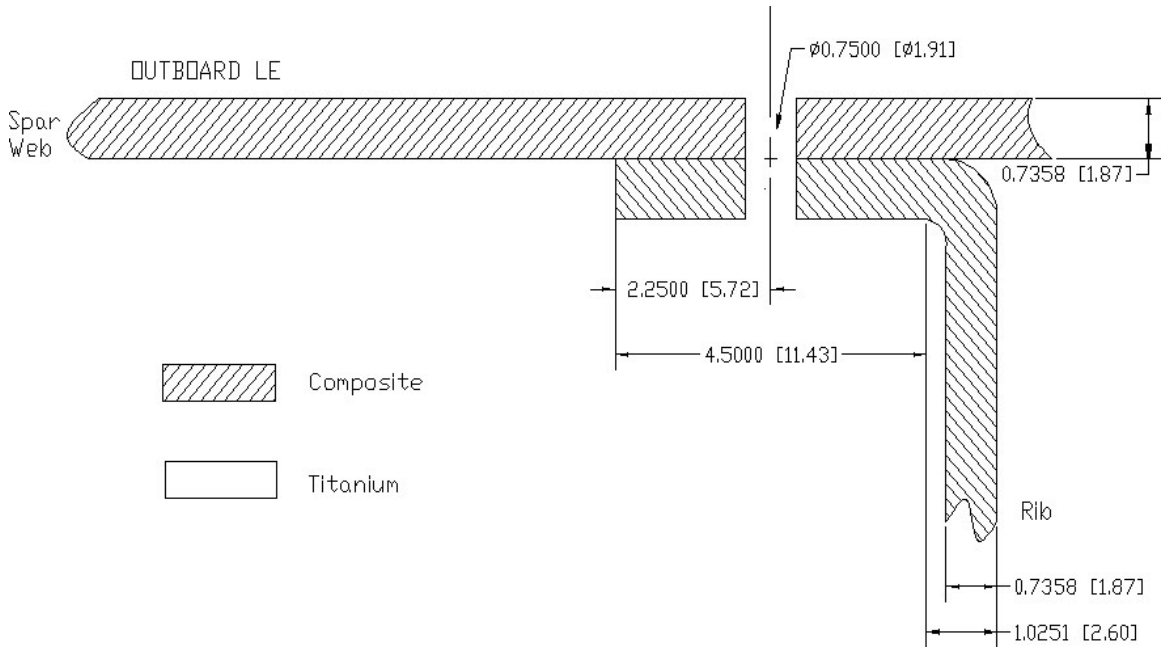

Figure 4.36: Rib-to-Spar Joint General Arrangement, Cross-sectional View. All Dimensions are in inches [cm]

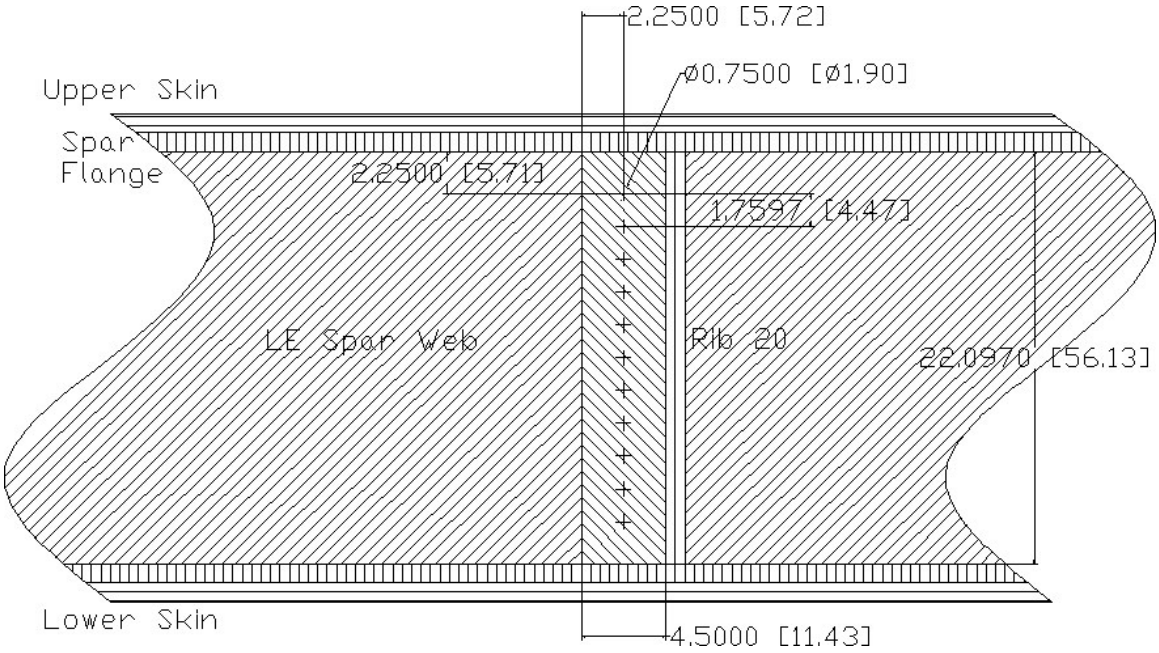

Figure 4.37: Rib-to-Spar Joint General Arrangement, Rib 20, Plan View. All Dimensions are in inches [cm]

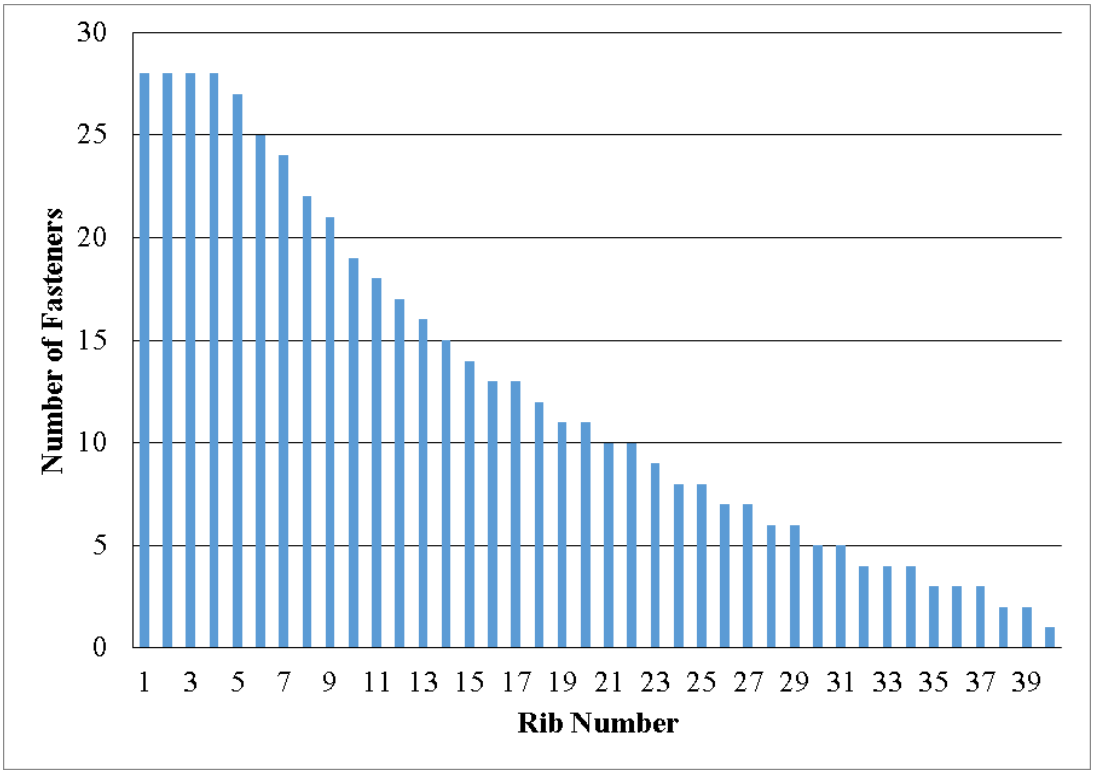

Figure 4.38: Front Spar-Rib Joints, Number of Bolts/Row

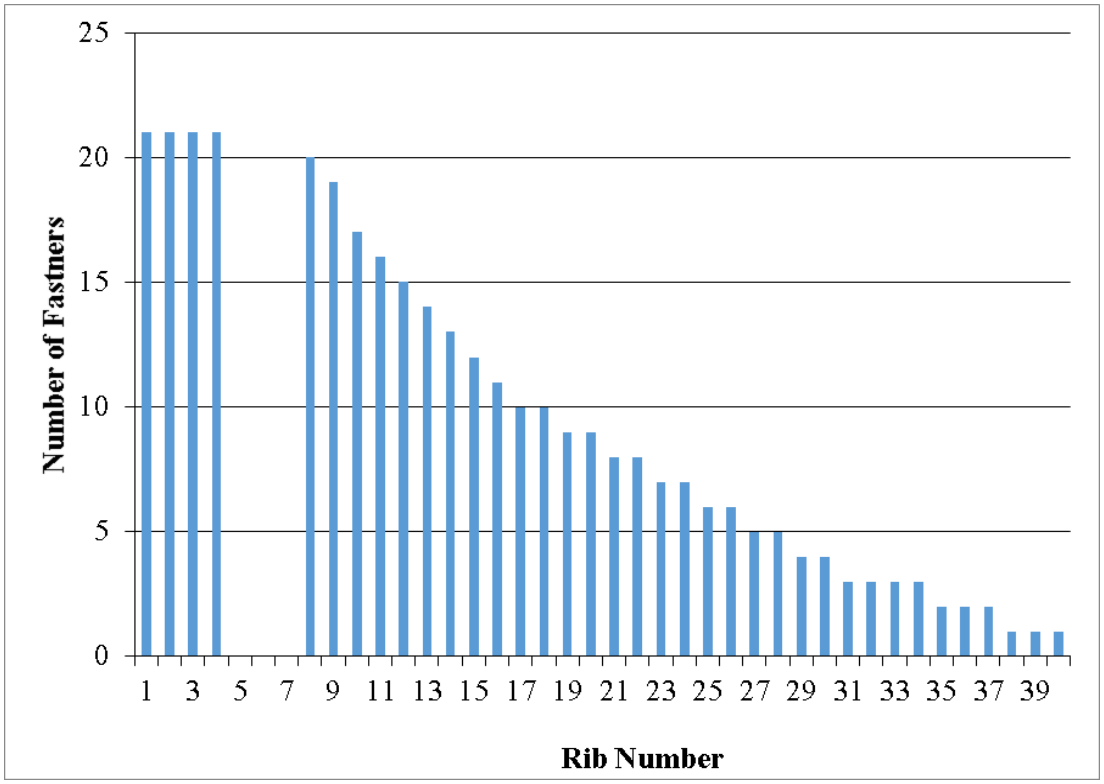

Figure 4.39: Rear Spar-Rib Joints, Number of Bolts/Row

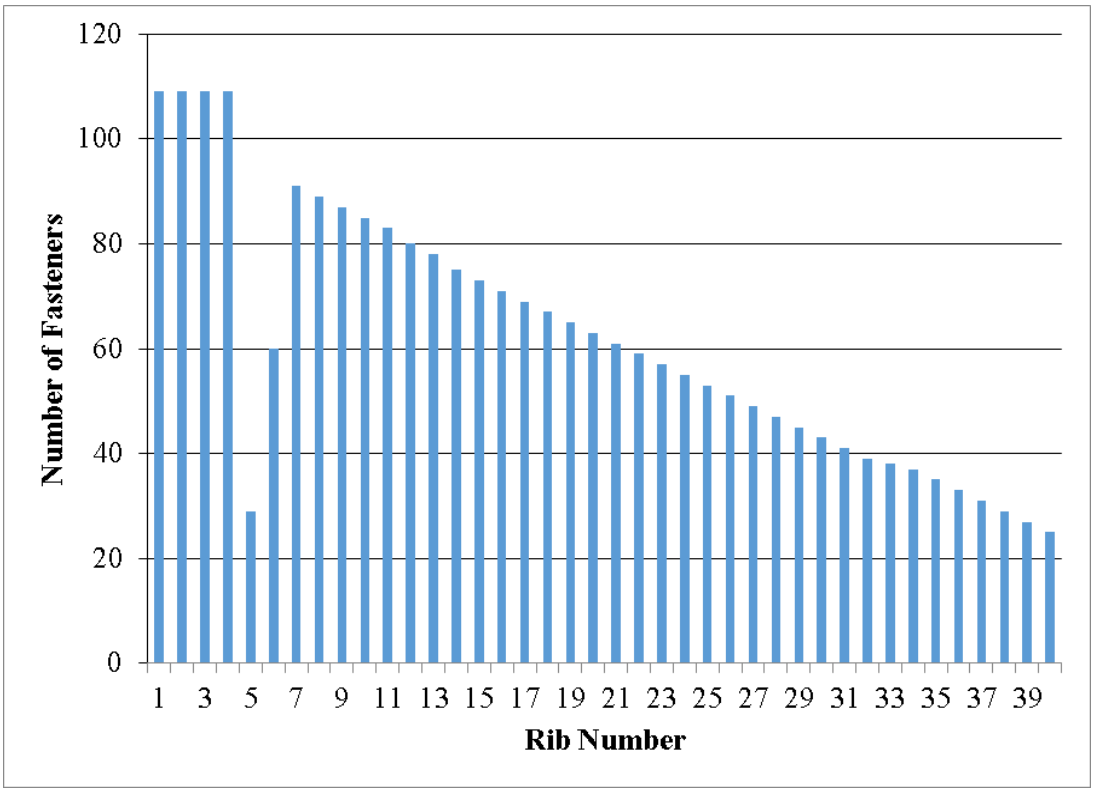

Figure 4.40: Upper Skin-Rib Joints, Number of Bolts/Row

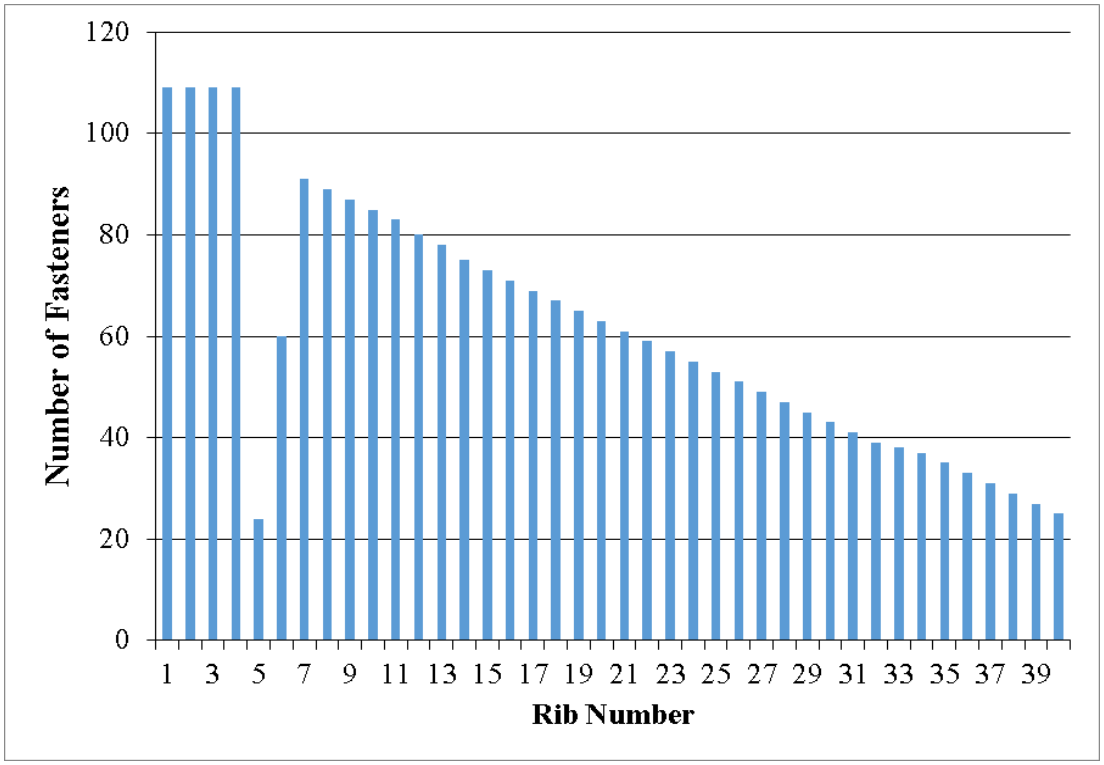

Figure 4.41: Lower Skin-Rib Joints, Number of Bolts/Row

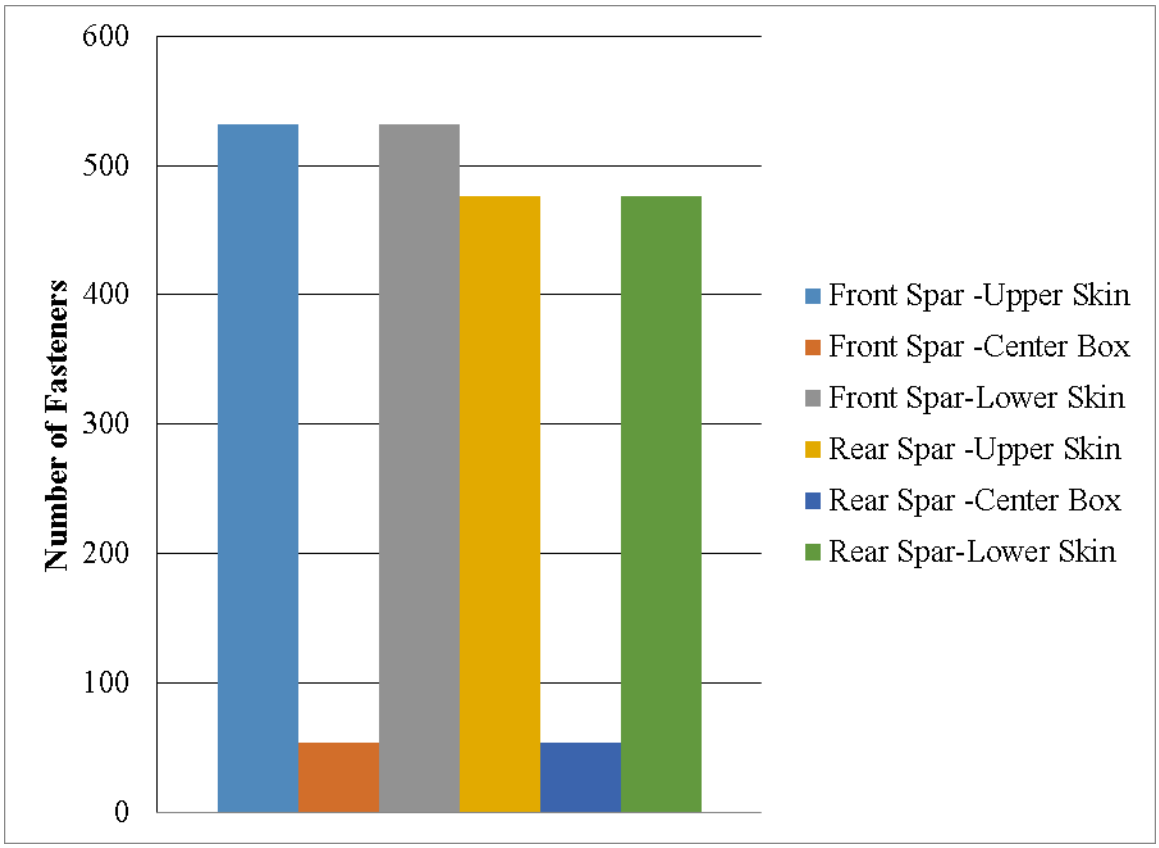

Figure 4.42: Skin-Spar Joints, Number of Bolts/Row

4.5 Finite Element Analysis and Load Redistribution

A finite element analysis code has been developed for the specific purpose of accounting for the changes in internal loads of the wing as the structures are optimized. This section will discuss the methods and elements used in the code developed for this study.

The internal finite element analysis for this optimization algorithm would be performed thousands of times; therefore, a relatively simple, four-node composite plate element was selected for implementation to minimize computational expense. The element has four nodes and is a C^1, conforming plate element, with six degrees of freedom per node and four integration points in the element as described by Ochoa and Reddy [426].

In addition to nodal loads, this finite element program can include both element pressures and fixed displacements. Fixed displacements were not used for the optimization algorithm; however, the pressure loads calculated during the aeroelastic cycle (see Section 4.2) were applied to the finite element model. The function in the program computes the equivalent nodal forces from a transverse pressure applied to a composite plate. It can work with both constant and linearly-varying transverse pressures [426-427]. The Hermite functions for pressure-induced nodal loads are shown in Appendix A.

Table 4.19: Side-of-Body Wing Joint Preliminary Design

Wing Load Intensity (N/m)		Max Load Intensity (N/m)		Strip Width w (m)		Strip Load Pw (N)		Laminate Thickness t (m)
6.36E+07		9.54E+06 1.5(load intensity)		0.076962		7.34E+05 max load intensity*w		0.03737864
No. of Bolts per Strip n		**w/dav**		**Side Edge Distance (m)**		**End Distance e (m)**		**Average Bolt Size dav (m)**
3.00		4.04		0.047625		0.05715		0.01905
Pw/(Pav*k)				2.5*dav		3.0*dav		
Joint Width (m)		**Bolt Pitch p (m)**		**Joint Length l (m)**		**No. of Bolts/Row**		Note: Chord-wise and Span-wise bolt pitch p are equal
0.2524252		0.052391733 (w-2*2.5*dav)/n (transverse)		4.8602		91 (l-2*e)/p		
Hole Diameter d (m)		**e/p**		**k_{te} = σmax/σave**		**k_{tb} = σmax/σbrg**		[424]
0.015875	1	1.090820944		3.30026667	1	0.85765766		
0.022225	2			2.35733333	2	0.95715391		
				p/d		kte/((w/d)-1)		
Average Stress σ_{ave} (MPa)		**Peak Stress σmax (MPa)**		**Bearing Stress σbrg (MPa)**		**Bearing Load P (N)**		**Bolt Rated Double Shear Strength Pav (N)**
77.83		256.85	1	299.48	1	1.58E+09	1	373,206
		183.47	2	191.68	2	1.13E+09	2	Dash 24--3/4 in pin
Pw/(w*t)		kte*σave		σmax/ktb		(4*strip load)/(π*d*t)		

To increase the efficiency of the solution of the finite element model the structure matrices are typically assembled in such a way that only nonzero coefficients are stored and used for the solution. These correspond to the element degrees-of-freedom. This is accomplished through a skyline scheme; the skyline is simply the bounds of the uppermost nonzero coefficient in each column of the stiffness matrix [363]. The compacted element stiffness matrix (of the order of the global number of degrees-of-freedom) is matched with a vector that relates the element degrees-of-freedom to the corresponding assembled, global degrees-of-freedom. This means that an entry i in this connectivity vector gives the equation number of that corresponds to the element degree-of-freedom i [428]. The method presented in Smith and Griffiths is most closely followed here [427].

The global equilibrium equation (equation A.18) is solved through linear algebra. Finite element solvers generally use some form of a Gauss elimination. Here, the Cholesky factorization is used [429]. Cholesky factorization usually requires fewer operations than direct Gaussian elimination, especially as the size of the system increases [430]. The method requires that all diagonal elements of the stiffness matrix be positive, i.e., the system must be positive definite [428], so the node numbering scheme must be correct. If [K] is a symmetric, positive definite matrix there exists a real, non-singular, lower-triangular matrix [L] such that [431]

$$[K] = [L][L]^T = [\tilde{L}][D][\tilde{L}]^T \tag{4.4}$$

An algorithm can be found in Numerical Recipes [432]; however, the algorithm in Smith and Griffiths was utilized [427].

Once the nodal values of the displacements are solved for the strains and stresses can be found. However, although the strains can be computed at any point in the element, they are most accurate if they are computed at the Barlow points [433, 434]. This is because only the displacements are continuous across the element boundaries, and strain continuity is not ensured. The Barlow points are the (N-1) x (N-1) Gauss points, were N x N is the Gauss quadrature rule used to evaluate the stiffness coefficients above. This reduced integration rule indicates that a one-point integration should be used to calculate the stresses and strains [426]. For WINGJOTA the mid-plane strains are calculated at these points in each element.

The last aspect of this implementation of the finite element method is the calculation of nodal loads. These are necessary here for application to the joint analyses discussed in Chapter 3. The direct stiffness method [435] was applied to derive these loads. To do this an uncondensed global stiffness matrix and displacement vector had to be generated using an assignment vector. These had to include the fixed nodal displacements of the boundary conditions, and were produced alongside the condensed analogs. The nodal loads are simply the product of the uncondensed global stiffness matrix and displacement vector.

4.6 Summary and Conclusions

The wing design used in this study was developed as a preliminary design exercise that involved multiple sources of data and design methodologies. Once the planform, masses, aerodynamic

loading, smeared skin/I-stringer composite laminate design, and fuel volumes were determined a finite element model was built in ANSYS. A simple composite plate was modeled first to verify that the ANSYS model was performing as expected. Second, a more challenging design, a box beam, was modeled and evaluated for performance with spring elements and pressure loadings that would be needed for the full wing model. Finally, the wing was modeled and 14 different load cases applied, yielding baseline wing behavior. Following on from the wing preliminary design was the initial lay-out of all of the bolted joints contained in the wing. These designs are of sufficient detail to allow the composite bolted joint constraint analysis presented in Chapter 3 to be applied to the structural optimization algorithm in WINGJOTA discussed in the next chapter.

Chapter 5

GLOBAL COMPOSITE WING JOINT OPTIMIZATION AND ANALYSIS

(WINGJOTA)

The approach taken in this work follows closely that taken by the University of Washington Optimal Design of Composite Structures Group during the 1990's for the development of COSTADE (see Section 2.1.3). One of the innovations made by Neogi et al. [24] was that load distribution in a structure needs to be redistributed at every iteration of the optimization algorithm, because the distribution changes every time the design changes during the optimization process. To demonstrate this, Neogi et al. made use of the simple three-bar truss; this was a familiar example in the structural optimization literature [55, 41]. If load redistribution is not performed at every iteration the design turns out to be infeasible [31]. The approach taken here follows this research by performing a finite element analysis during every iteration of the optimization algorithm based on a relatively coarse mesh to minimize computational expense. A detailed (fine mesh) finite element analysis is performed at the beginning of the optimization analysis to develop boundary conditions. Chapter 4 provides details of the detailed wing analysis for internal loads.

Different global optimization formulations can be applied to a composite wing with consideration for bolted joints. The composite structural optimization algorithm by Graesser et al. [233] and modified by Neogi et al. [31, 24] forms the basis of the software package presented here, WINGJOTA. The benchmark composite wing design described in Chapter 4 is a challenging problem for any optimization algorithm; a global optimization algorithm is certainly required because the design space has many local suboptimal points. A relatively well-known algorithm, the Improving Hit-and-Run (IHR), was chosen to implement due to its success in the past with composite fuselage design problems. A second algorithm, Multi-Particle Simulated Annealing (MPSA), was also implemented to explore its utility for this design problem. Assumptions, design variables, design parameters, an objective function, constraints, and outputs are discussed in the following sections.

5.1 Assumptions

Assumptions for the optimization and design analyses can be divided into those for material behavior, geometry and mechanical behavior, and failure criteria. Material behavior assumptions are as follows. First, we consider only solid laminates, i.e., there is no honeycomb core sandwich composite structure. Second, the fibers in a given ply are straight and not steered. The fiber angles are considered to be continuous and not incremented at discrete angles. Third, the assumptions for the Classical Lamination Theory (CLT) are applied [436]. The laminates are balanced and symmetric; Chapter 3 discusses this assumption in more detail. Fourth, the

stiffness E is constant, i.e., there are no viscoelastic or hygrothermal effects considered [377]. Further, given the plate, strap, and bolt moduli E_p, E_s, and E_b, respectively, assume the following relationships [326, 316]:

$$E_{pbr} = E_p \tag{5.1}$$
$$E_{sbr} = E_s \tag{5.2}$$
$$E_{bbr} = E_{bb} = E_b \tag{5.3}$$

Geometric and mechanical behavior assumptions include the following [339]:

1. Stress in the joint is uniformly distributed
2. Friction is negligible
3. Laminates are not damaged with bolt insertion
4. Joints are symmetric with respect to load direction
5. Load on a plate is transferred by flexible, frictionless fasteners over half of the hole edges along the primary loading direction
6. Secondary bending of the plates due to load eccentricity is negligible compared to the in-plane deformations
7. Fasteners are modeled as elastic beams with fixed end conditions
8. Transverse rows of fasteners are equally loaded and have the same fastener type
9. Clamp up is not considered
10. Bearing bypass after Tate and Rosenfeld [324]
11. No stringer run-outs

Failure modes assumptions for the laminates and bolted joints are that tension, shear, and bearing failures are the primary causes of failure. Cleavage and fastener pull-out failure are not considered due to the following assumptions about fastener diameter-to-joint thickness ratios and diameter-to-edge margin [313]:

$$\frac{d}{tn} \geq \frac{1}{3} \tag{5.4}$$

$$\frac{e}{d} \geq 3 \tag{5.5}$$

where d is the fastener diameter, tn is the joint thickness, and e is the edge margin. Crippling is not considered. Lastly, there is no fatigue analysis in this study; a critical strain is chosen as a constraint that is below the level generally considered critical for fatigue.

5.2 Optimal Design Problem Statement

The optimal design problem for the stiffened panel can be stated mathematically as follows: find a set of design variables **X**, that will

$$\text{Minimize } f(\mathbf{X}) \tag{5.6a}$$
$$\text{Subject to } g_j(\mathbf{X}) \geq 0 \tag{5.6b}$$
$$\mathbf{x}^l \leq \mathbf{x} \leq \mathbf{x}^u \tag{5.6c}$$

Here, the objective function f(**X**) is the panel weight, which includes the skin, stringers, and bolted joints. The inequality constraints $g_j(\mathbf{X})$ are measures of the mechanical performance of the structure under the given loading conditions. Side constraints are given as upper and lower bounds $\mathbf{x}^l \leq \mathbf{x} \leq \mathbf{x}^u$ on the design variables.

5.2.1 Design Variables

The composite panel optimized in this research program is a laminated skin stiffened with stringers with an I-cross-sections. Each stringer is composed of three sections: the bottom flange, and top flange, and the web. The panel skin laminate is made from n_{sk} plies, each having an orientation of θ_i^{sk}. The stringers are made from n_{bf} bottom flange plies with θ_i^{bf} fiber angles; n_{tf} top flange plies with θ_i^{tf} fiber angles; and n_w web plies with θ_i^{w} fiber angles. The complete design description of the panel also includes the bottom flange width bbf, the top flange width ttf, and the web height hw. The design variables and their lower and upper bounds are shown in Table 5.1.

Both the IHR and MPSA optimization algorithms used in this study can be made to deal with a mixed continuous and discrete design space. However, WINGJOTA treats all design variables as continuous. The per ply thickness of the composite material is a constant. The number of plies in each design iteration for the skins, I-stringer bottom and top flanges, and web are rounded to the nearest integer. The total thickness of the structural components is then the number of plies multiplied by the per ply thickness. The ply angles and I-stringer geometric dimensions are treated as continuous variables. A method of treating the ply angles as discrete variables can be found in Graesser [30].

Table 5.1: Panel Design Variables and Lower and Upper Bounds

Design Variable	Design Variable	Lower Bound	Upper Bound
1	Number of Skin Plies n_{sk}	16	48
2	Number of I-stringer Bottom Flange Plies n_{bf}	16	48
3	I-stringer Bottom Flange Width bbf (m)	0.0508	0.0889
4	Number of I-stringer Top Flange Plies n_{tf}	16	48
5	I-stringer Top Flange Width btf (m)	0.0508	0.0889
6	Number of I-stringer Web Plies n_w	16	48
7	I-stringer Web Height hw (m)	0.0508	0.0762
8-56	Skin Laminate Ply Angles θ_i^{sk}	-90°	90°
57-105	I-stringer Bottom Flange Laminate Ply Angles θ_i^{bf}	-90°	90°
106-154	I-stringer Top Flange Laminate Ply Angles θ_i^{tf}	-90°	90°
155-203	I-stringer Web Laminate Ply Angles θ_i^{w}	-90°	90°

To say that composite design problems are global in nature implies that there are large, probably disconnected, feasible regions in the design space. The optimization routine must choose one design from this feasible set, and design and manufacturing rules associated with composite laminates help guide the solution. Here the purpose of these "rules of thumb" are twofold: one, they provide an acceptable design for engineering, and two, they can reduce the number of design variables in the optimization process. The bolted joint analysis utilized here assumes balanced and symmetric laminates. This means that for every ply angle θ_i, there must be a corresponding ply angle - θ_i, and for every ply angle on one side of the laminate midplane there is a corresponding ply angle on the opposite side of the laminate. A laminate therefore may have at most n/2 distinct ply angles if n is even and n/2 + 1 if n is odd. Further, in the case of an odd number of plies, the middle ply must be a 0° or 90° ply. For example, if n_{sk} is 20 plies, WINGJOTA uses the first 20 θ_i^{sk} to generate a balanced and symmetric laminate of 40 total plies. If n_{sk} is an odd number of plies a 0° ply is added to the center of the laminate to maintain the balanced and symmetric assumption. Manufacturing guidelines provided by Niu [276] were also applied in this analysis. One of these was to not allow more than six plies of the same (approximate) orientation to be adjacent in the laminate stack. These design and manufacturing rules help provide feasible laminate designs for engineering application.

5.2.2 Design Parameters

The design parameters for the stiffened panel and associated joints is shown in Table 5.2. These include loading conditions, geometries, material properties, and optimization algorithm parameters.

Table 5.2: Design Parameters for WINGJOTA

Loading Conditions:	**Description**
Nx, Ny, Nxy	In-plane loads (axial, transverse, and shear)
Mx, My, Mxy	Bending moments
P	Load
R_i	Load in individual bolt i
Geometric Parameters:	**Description**
t	Per ply thickness
w	Panel skin width
l	Panel skin length
wj	Joint width
lj	Joint height
d	Hole diameter
e	Edge margin
r	Number of bolts
N_i	Number of bolts in ith row
p	Fastener pitch
t_p, t_s	Thickness, plate and strap, respectively

Table 5.2: Design Parameters for WINGJOTA (continued)

Material Properties:	Description
E_1	Young's modulus
E_2	Transverse modulus
G_{12}	Shear modulus
ν_{12}	Poisson's ratio
ε_1^{cr}	Critical axial strain
ε_2^{cr}	Critical transverse strain
γ_{12}^{cr}	Critical shear strain
X_T	Critical axial stress, tensile
X_C	Critical axial stress, compressive
Y_T	Critical transverse stress, tensile
Y_C	Critical transverse stress, compressive
S	Critical shear stress
G_b	Bolt shear modulus
E_p	Plate modulus
E_s	Strap modulus
E_{pbr}	Bearing modulus for plate
E_{sbr}	Bearing modulus for strap
E_{bb}	Bolt bending modulus
E_b	Bolt modulus
E_{bbr}	Bolt bearing modulus
R_{0t}	Characteristic length in tension
R_{0c}	Characteristic length in compression
ρ	Composite material density
ρ_b	Fastener material density
Optimization Parameters:	**Description**
maxrun	Maximum number of restarts
maxiter	Maximum number of iterations
ifeas	Maximum number of non-improving iterations (IHR)
Ngen	Number of particles (MPSA)
maxstop	Maximum number of non-improving iterations (MPSA)
jfeas	Maximum number of infeasible point iterations (MPSA)

5.2.3 Objective Function

The objective function f(**X**) in this study is the panel weight. The panel and the joints are included in the weight, which is the weight of the panel, plus the weight of the joint area, minus the weight of the composite material removed for fastener holes, plus the weight of the fasteners. Note that there are six I-stringers in the panel, two rib-to-skin joints, and a spar-to-skin joint.

The objective function is given as

$$f(\mathbf{X}) = \rho(\text{volume of panel}) + \rho(\text{volume of joints}) - \rho(\text{volume of holes}) + \rho_b(\text{volume of fasteners}) \tag{5.7}$$

where

$$\text{Volume of panel} = w*l*t*n_{sk} + 6*l*t*(bbf*n_{bf} + btf*n_{tf} + hw*n_w) \tag{5.8a}$$
$$\text{Volume of joint area} = Vrib1 + Vrib2 + Vspar \tag{5.8b}$$
$$\text{Volume of holes} = \text{Volume of fasteners} = Vribholes1 + Vribholes2 + Vsparholes \tag{5.8c}$$

Further, the volumes of the joints and fastener holes are specified as follows, noting that the rib flange is always half the thickness of the skin and the spar flange is always the same thickness as the skin:

$$Vrib1 = t*(n_{sk} + n_{tf} + n_{sk}/2)*wj_{rib1}*lj_{rib1} \tag{5.9a}$$
$$Vrib2 = t*(n_{sk} + n_{tf} + n_{sk}/2)*wj_{rib2}*lj_{rib2} \tag{5.9b}$$
$$Vspar = t*(n_{sk} + n_{sk})*wj_{spar}*lj_{spar} \tag{5.9c}$$
$$Vribholes1 = r_{rib1}*\pi*(d_{rib1}/2)^2* t*(n_{sk} + n_{tf} + n_{sk}/2) \tag{5.9d}$$
$$Vribholes2 = r_{rib2}*\pi*(d_{rib2}/2)^2* t*(n_{sk} + n_{tf} + n_{sk}/2) \tag{5.9e}$$
$$Vsparholes = r_{spar}*\pi*(d_{spar}/2)^2* t*(n_{sk} + n_{sk}) \tag{5.9f}$$

where the variables are defined in Table 5.2 above. It can be seen that the objective function is dependent on the design variables for the skin, I-stringer bottom flange, top flange and web thicknesses (number of plies), and on the I-stringer geometry (bottom flange and top flange widths, and web height). As described in Chapter 3, these design variables drive the design of the bolted joints, which WINGJOTA automatically creates. The number of bolts and the diameters of the bolts in each joint is calculated and included in the objective function for weight. The width and length of the panel and the joints is fixed geometry.

5.2.4 Constraints

The inequality constrains $g_j(\mathbf{X}) \geq 0$ are defined in terms of structural mechanical performance. These constraints are described by margin of safety calculations and strength criteria. As discussed in Chapter 3, the major mechanical performance criteria investigated in this study are those associated with the bolted composite joints. These included maximum strain, Tsai-Wu, Yamada, and bolt failure. Additionally, the maximum strain and Tsai-Wu criteria were applied to the acreage panel skin and stringers. There are a total of 45 different checks on structural performance for each iteration of WINGJOTA. Table 5.3 summarizes the constraints applied in this study and Table 5.2 shows the parameters needed for these constraints.

Table 5.3: Structural Performance Constraints Applied in Wing Panel Optimization

Criterion	Structures	Failure	Number of Constraints
Modified Tsai-Wu	Acreage skin, I-stringer bottom flange, top flange, and web laminates	tws < 1 twbf < 1 twtf < 1 tww < 1	4
Modified Tsai-Wu	Skin-rib joints skin, I-stringer top flange, and rib laminates	tws5 < 1 twtf5 < 1 twr5 < 1	3
Modified Tsai-Wu	Skin-spar joint skin and spar laminates	tws6 < 1 twsp6 < 1	2
Modified Tsai-Wu	Skin-rib joints, holes in bolt rows A and B and skin, top flange, and rib laminates	twaa < 1 twab < 1 twba < 1 twbb < 1 twca < 1 twcb < 1	6
Modified Tsai-Wu	Skin-spar joint, holes in bolt rows A and B, skin and spar laminates	twaa < 1 twab < 1 twba < 1 twbb < 1	4
Yamada	Skin-rib joints, holes in skin, top flange, and rib laminates	es5 < 1 etf5 < 1 er5 < 1	3
Yamada	Skin-spar joint, holes in skin and spar laminates	es6 < 1 esp6 < 1	2
Maximum Strain	Acreage skin, I-stringer bottom flange, top flange, and web laminates	msfs > 0 msfbf > 0 msftf > 0 msfw > 0	4
Maximum Strain	Skin-rib joints skin, I-stringer top flange, and rib laminates	msfs5 > 0 msftf5 > 0 msfr5 > 0	3
Maximum Strain	Skin-spar joint skin and spar laminates	msfs6 > 0 msfsp6 > 0	2
Maximum Strain	Skin-rib joints, holes in bolt rows A and B and skin, top flange, and rib laminates	msfaa > 0 msfab > 0 msfba > 0 msfbb > 0 msfca > 0 msfcb > 0	6

Table 5.3: Structural Performance Constraints Applied in Wing Panel Optimization (continued)

Criterion	Structures	Failure	Number of Constraints
Maximum Strain	Skin-spar joint, holes in bolt rows A and B, skin and spar laminates	msfaa > 0 msfab > 0 msfba >0 msfbb > 0	4
Bolt Failure	Skin-rib joints	bfail5 > 0	1
Bolt Failure	Skin-spar joint	bfail6 > 0	1

5.2.5 Outputs

The software package generates a large amount of information about the stiffened panel structure, the bolted joints, and the operations of the optimization algorithms. The main output of the program is the optimum laminate design with laminate ply orientations and number of plies and the resulting objective function (weight) for each design. Structural information, such as maximum ply strains and stresses in both the acreage of the panel and the joints, the bearing-bypass loads, and the critical stress concentration factors is also generated. During the optimization information such as the best objective function for each iteration and run, the number of iterations, the number of function evaluations, and the CPU time are stored and available as outputs.

5.3 Flow of WINGJOTA

The flow of WINGJOTA is illustrated in Figures 5.1 and 5.2. Figure 5.1 shows the flowchart for the baseline design development and initial finite element analysis. These are independent and manual processes, using commercial software for computer-aided design and finite element analysis. Input step 1 is the development of the benchmark composite wing design and associated bolted joints, as described in Chapter 4. Next, the aerodynamic loads are found and assigned to the wing model. Step 3 is the creation of the ANSYS fine mesh FE model, including the geometries, material properties, boundary conditions, and external loads. That model is analysed in step 4. In step 5 the constraint analyses are performed for the joints, skins, spars, and ribs as shown in Chapter 3. Note that the fine mesh, ANSYS wing model is designed and analyzed for feasibility (step 6) prior to utilizing the internal load set generated as boundary conditions for the wing panel chosen for optimization in this study. If the initial wing design is infeasible it would be redesigned until it was feasible (step 7), i.e., only a feasible design will be the starting point for WINGJOTA.

The feasible, benchmark composite wing design is now available for use as a basis for the boundary conditions for the wing panel to be optimized. First, the ANSYS-generated internal loads for the designated panel must be translated and transformed into boundary conditions for the FEM in WINGJOTA (step 8). Step 9 is the creation of the coarse mesh FEM model of the wing panel to be optimized, including the geometries, material properties, boundary conditions,

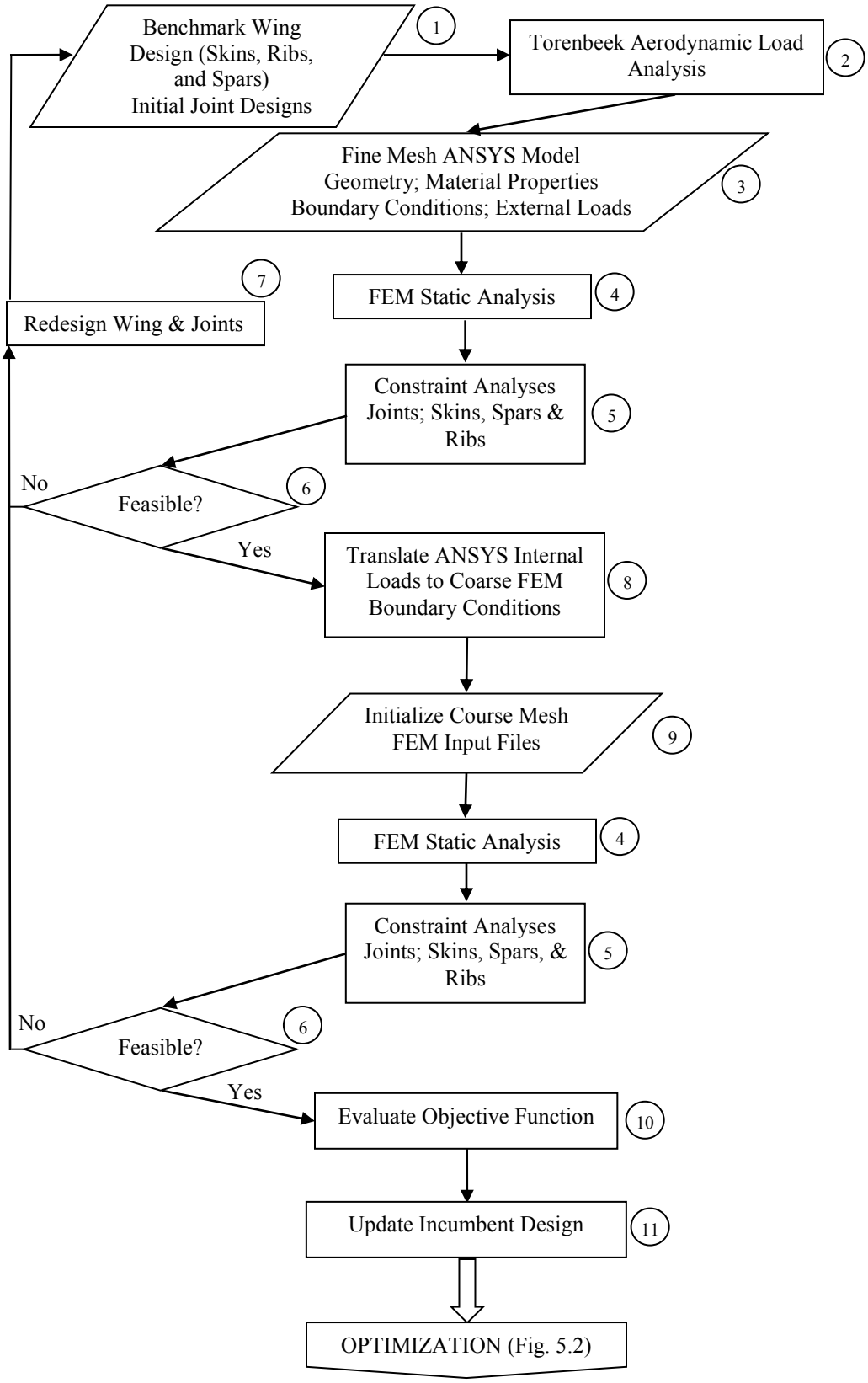

Figure 5.1: Baseline Design Initial Finite Element Model and Constraint Analysis. The Numbered Circles Represent Processes and Decision Gates.

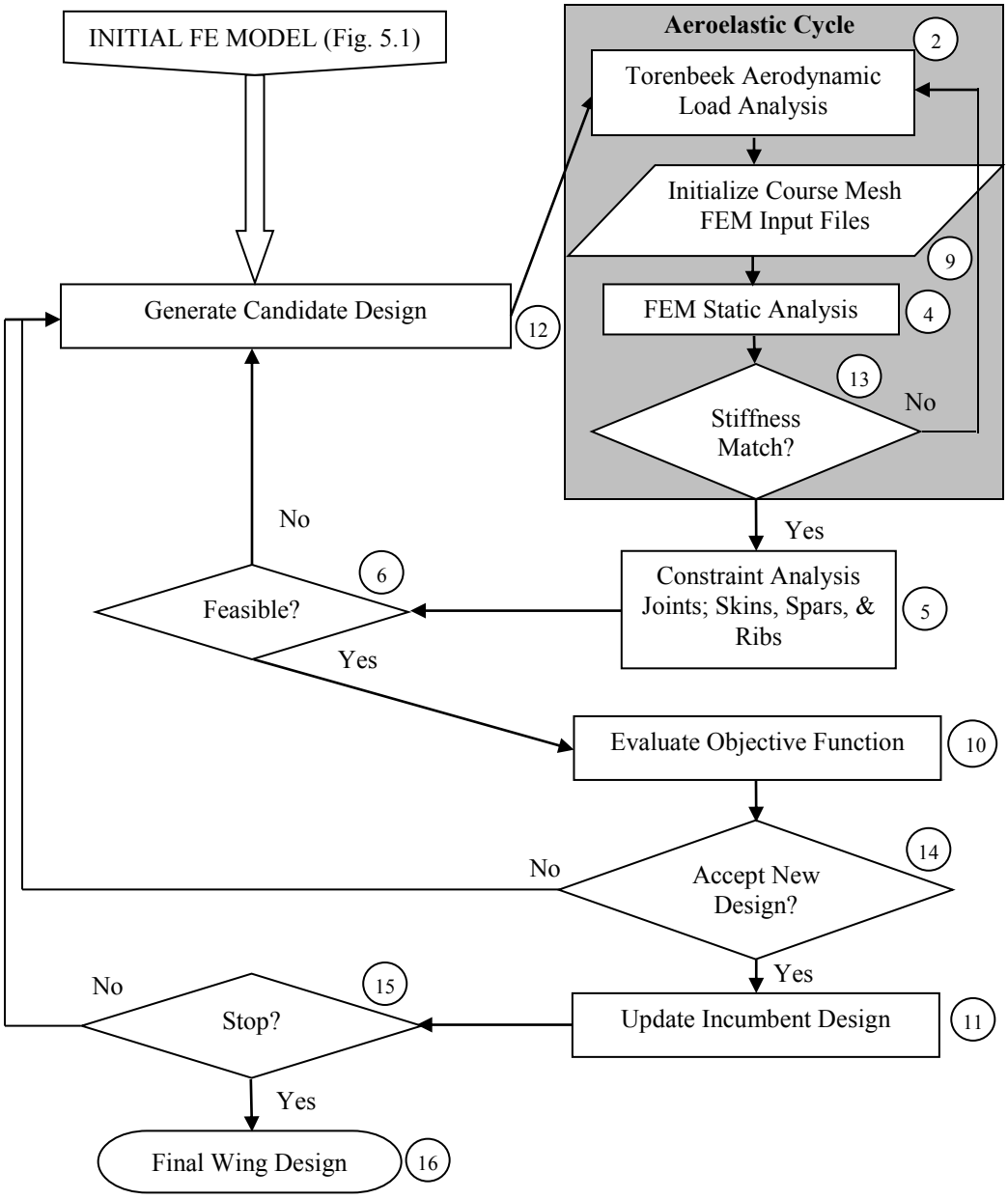

Figure 5.2: WINGJOTA Composite Wing Global Optimization Algorithm. The Numbered Circles Represent Processes and Decision Gates.

and external loads. The coarse mesh FEM of the wing panel was chosen such that it would be approximately comparable to the ANSYS model of the same panel through a mesh convergence study (see Appendix A). This model is then analysed, and the constraint analyses are completed. If the resulting initial panel design is feasible, the objective function is evaluated (step 10). The initial design variables are updated in step 11, and the design at the bottom of Figure 5.1 is used as the initial design to start off the optimization algorithm. The wing panel optimized using WINGJOTA uses the benchmark composite wing presented in Chapter 4 as the initial design for the optimization results discussed in Chapter 6.

Figure 5.2 shows the flowchart for WINGJOTA. This is the automated design point selection, analyses, and optimization algorithm to arrive at the final wing design. First, a candidate design is generated in step 12. This involves generating a random direction d_k and a random point on the line set λ_k. WINGJOTA uses the hyperspherical direction (HD) generator [231] to determine d_k. This is done by generating 203 independent values, one for each design variable, from a standard normal distribution from zero to one [432]. These values are then scaled to determine a unit direction vector [437]:

$$DV = (d_1, d_2, \ldots, d_n)\left(\sum_{i=1}^{n} d_i^2\right)^{1/2} \tag{5.10}$$

The random points λ_k are determined as [438]

$$\lambda \leq \lambda_{max} = \min\left\{\begin{matrix}\frac{U_k - x_k}{DV_k} & \text{for k such that } DV_k > 0 \\ \frac{L_k - x_j}{DV_k} & \text{for k such that } DV_k < 0\end{matrix}\right\} \tag{5.11a}$$

$$\lambda \leq \lambda_{min} = \max\left\{\begin{matrix}\frac{L_k - x_k}{DV_k} & \text{for k such that } DV_k > 0 \\ \frac{U_k - x_j}{DV_k} & \text{for k such that } DV_k < 0\end{matrix}\right\} \tag{5.11b}$$

where U_k and L_k are the upper and lower limits on the design variables, respectively.

Earlier work has shown that using simple box constraints to define the upper and lower bounds on design variables in IHR can allow ply angle design variables to "jam" in the corner points of the box constraints [30, 228]. Two different mapping rules were used in both algorithms in this study. These rules modify the design variables chosen as the next step in an attempt to avoid this issue. The first rule is called reflective mapping, and is used for the stringer geometry variables.

In equation form:

$$x_i^{rect} = \begin{cases} x_i^{max} - \left(x_i - x_i^{max}\right) \text{if } x_i > x_i^{max} \\ x_i^{min} + \left(x_i^{min} - x_i\right) \text{if } x_i < x_i^{min} \\ x_i \qquad\qquad \text{otherwise} \end{cases} \tag{5.12}$$

where x_i^{max} and x_i^{min} are the upper and lower bounds of the box constraints, respectively, for the ith design variable. The fiber angle design variables are mapped using circular mapping rules:

$$x_i^{circ} = \begin{cases} x_i - \left(x_i^{max} - x_i^{min}\right) \text{if } x_i > x_i^{max} \\ \left(x_i^{max} - x_i^{min}\right) - x_i \text{ if } x_i < x_i^{min} \\ x_i \qquad\qquad \text{otherwise} \end{cases} \tag{5.13}$$

This rule keeps the fiber angles between 90° and -90° by reflecting a point chosen outside the bounds of the original box off the side and back to the interior [30].

Using the ply angles generated by the Markov kernel above, WINGJOTA generates a balanced and symmetric laminate by pairing ply angles and assigning them to the laminate stack until the number of plies for that design point is reached. The stack is then made to be symmetric, adding a 0° ply at the plane of symmetry if the number of plies is odd. The effective stiffnesses of the skin, I-stringer bottom flange, top flange, and web laminates are determined using CLT. Next, the I-stringer laminates are smeared into a single equivalent laminate as described in Chapter 4 and Appendix B. These smeared properties are used in the finite element module as part of the aeroelastic cycle. The smeared panel properties are recalculated for each iteration of a design point or particle.

The aeroelastic cycle identified in Figure 5.2 begins with a switch that determines if aerodynamic loads are part of the current load case. If they are, the aerodynamic loads are generated using the Torenbeek analysis described in Chapter 4. The FEM is initialized for the new effective panel properties and the aerodynamic loads are applied as needed in step 9. The FEM analysis is completed, and in step 13 a determination is made if the structural deflection is within 0.01° of the initial angle-of-attack at the wing root; this represents about 1% of the normal range of the angle-of-attack. If the deflection changes more than this tolerance, the aerodynamic loads are recalculated and the FEM re-run until the criterion is met.

The skin and stringer loads that are the output from the FEM in step 4 are used for the original, non-smeared skin / I-stringer acreage panel, rib-to-skin joints, and spar-to-skin joint calculations and MS determination in step 5. The joint constraint analysis includes the generation of the bolted joint design for the candidate point. Although the joint design is not a design variable, it is dependent on the composite panel design to determine the diameter and number of fasteners in each joint, as described in Chapter 3. If the candidate point design is feasible as determined in step 6, the objective function is evaluated in step 10. If the point is infeasible, a new candidate point is generated in step 12, and a new aeroelastic cycle is started. The new objective function is compared to the incumbent best objective function in step 14. IHR and MPSA are different

during this step. IHR will accept any improving point. MPSA, as discussed in Chapter 2, tends to select candidate points with high Metropolis ratios. The probability that the particle will be moved to a new location is dependent on the current points, candidate points, and the current temperature (see Equation 2.5). If the new design point is not accepted, a new candidate point is generated (step 12). If it is accepted, the incumbent design is updated in step 11.

An important consideration for any stochastic optimization algorithm is the stopping criteria (step 15). WINGJOTA uses different maximum numbers of iterations, restarts, and function evaluations as stopping criteria for IHR and MPSA. Both optimization algorithms used a maximum of 10 restarts. After some experimentation with the design problem maxiter was set to 100 for IHR. Another iteration limit for IHR was maximum number of non-improving point iterations, ifeas. If the improvement of the objective function does not improve by at least an ε-optimum after 10 iterations of the Markov kernel the iteration step is terminated and a new direction vector is chosen. ε-optimum was set to 0.01 kgf for this study. For MPSA, the number of particles Ngen was 100. The maximum number of non-improving point iterations, maxstop, was set to 10. A limit on the number of feasibility check loops that could be performed on any given particle, jfeas, was limited to 10 as well. If the stopping criteria in step 15 is met, WINGJOTA reports the final wing design variables, objective function, and the other outputs in step 16.

5.4 Summary and Conclusions

WINGJOTA optimizes a composite transport wing with consideration of bolted joints. The formulation and flow of the software package was described. IHR and MPSA were the two optimization algorithms implemented in the software. Assumptions, design variables, design parameters, an objective function, constraints, and outputs were discussed. The flow of the wing panel design and optimization process was described, including the aeroelastic cycle, design point generation, and stopping criteria. The next chapter presents a wing panel design optimization using both optimization algorithms in WINGJOTA.

Chapter 6

GLOBAL COMPOSITE WING JOINT OPTIMIZATION AND ANSYSIS (WINGJOTA)

RESULTS AND DISCUSSION

WINGJOTA, discussed in Chapter 5, was used to optimize a wing panel structure for 14 different load cases using both IHR and MPSA. Section 6.1 describes the wing panel design problem, details of its structure, and the finite element model used with WINGJOTA. Section 6.2 shows the results from optimization with the IHR algorithm and the MPSA algorithm. The results are discussed in Section 6.3. Section 6.4 offers a summary and conclusions. Note that a test problem was run using both IHR and MPSA that has been utilized to demonstrate effectivity of various stochastic, global optimization algorithms; results are shown in Appendix D.

6.1 Upper Wing Panel 18 Model

A single sub-panel of the upper wing panel of the benchmark composite wing model was chosen to exercise WINGJOTA. There were 114 such panels identified on the upper wing panel (see Figure 6.1). Panel 18 is located at the juncture of the rear spar and the side-of-body. The panel has six I-stringers, and is 1.42 x 0.70 m. A finite element model of this panel was created using the elements described in Appendix A. There are 50 nodes and 36 elements in the model (see Figure 6.2). This model geometry was rotated from the ANSYS wing model; the internal loads of the fine mesh model were also rotated to the new, Panel 18 coordinate system. It can be seen that there are three joints in the FEM of the panel: two rib-to-skin joints and one spar-to-skin joint. The geometries of these joints are described in Table 6.1.

The fixed degrees of freedom (dof) in the model are as follows. The single node at the side-of-body is completely fixed in all six dof. The nodes along the rear spar are fixed but are allowed to rotate about the span (Y) axis. Similarly, the nodes along the ribs are fixed but are allowed to rotate about the chord (X) axis. The remaining edge, which is attached to the skin of the adjoining panel, is fixed in UX and UY only.

As only the upper wing panel 18 would be analyzed, designs for the rib and spar flanges needed to be designed to provide the joint analyses a full design to work with. It was assumed here that the rib flange number of plies is half that of the corresponding skin laminate; the spar flange has the same number of plies as the skin laminate. Both of these laminates are assumed to be quasi-isotropic and utilize only [0°/±45°/90°] ply angles. These laminates were created by WINGJOTA for each design point generated by the optimization algorithm.

Appendix C.3 contains the loads applied to the Panel 18 FEM.

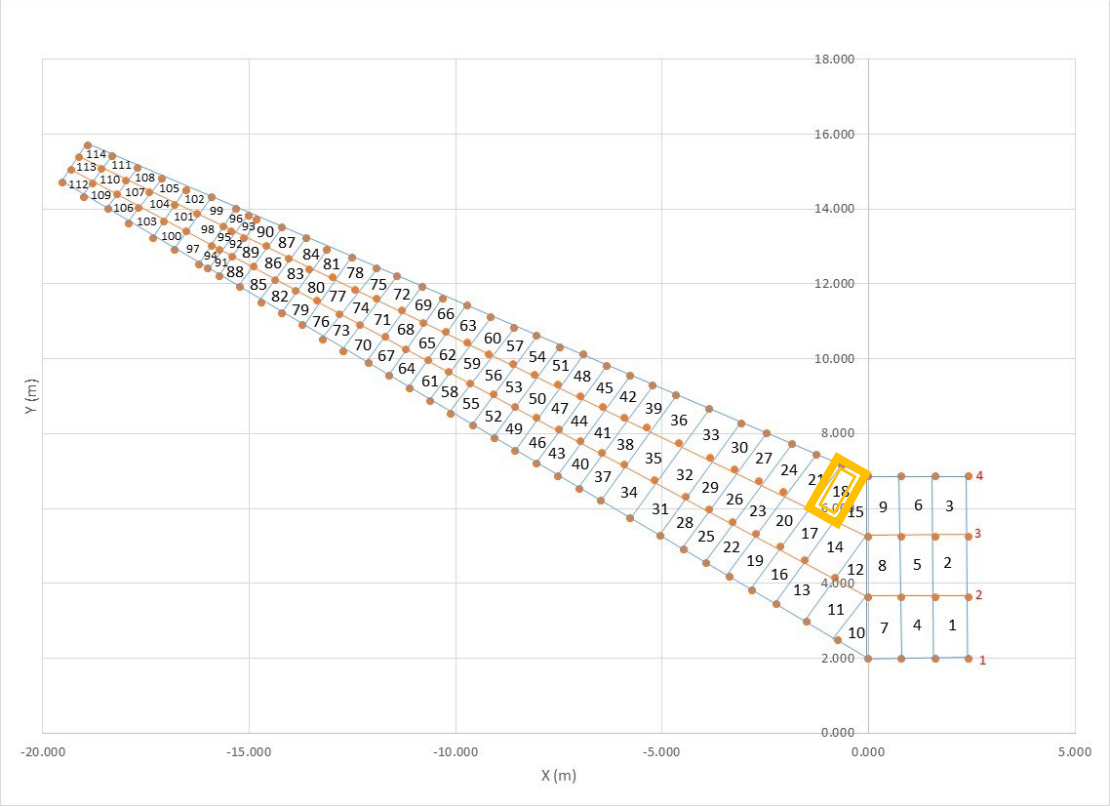

Figure 6.1: Upper Wing Skin FEM Panels. Panel 18 is Highlighted

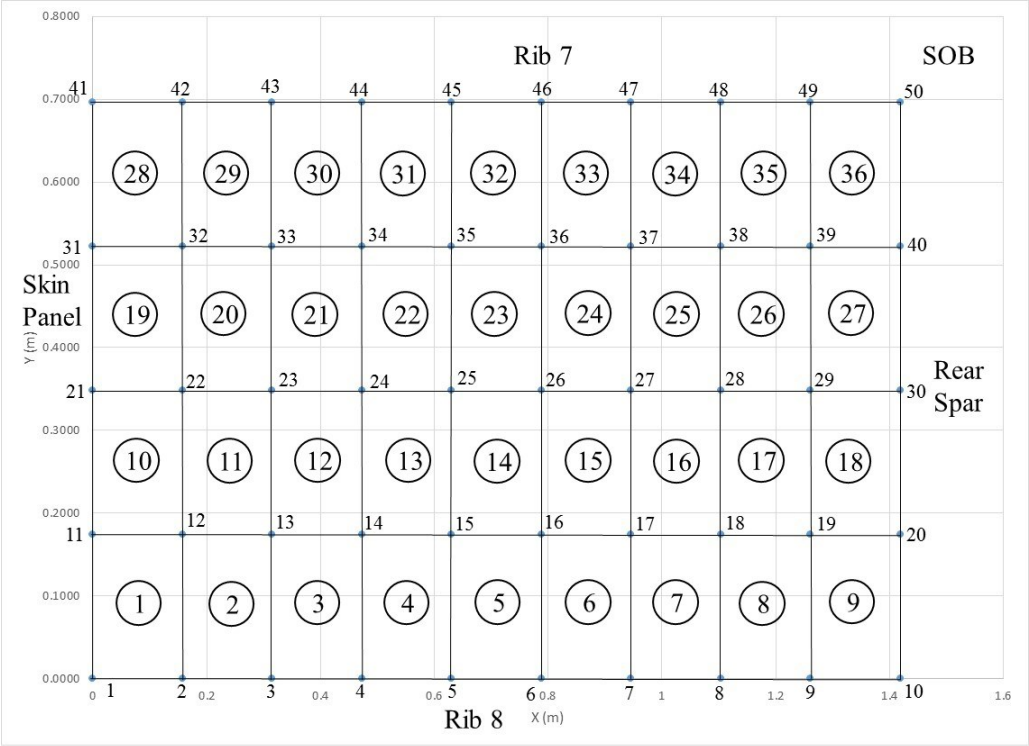

Figure 6.2: Panel 18 Finite Element Model Mesh. Element Numbers are Circled

Table 6.1: Joint Geometries for Panel 18

Joint Number	X (m)	Y (m)	Length (m)	Width (m)
518 (Rib 7)	-8.54	7.53	1.3400	0.1143
	-6.89	10.10		
521 (Rib 8)	-10.10	8.53	1.3100	0.1143
	-8.58	10.80		
634 (Rear Spar)	-16.20	12.50	0.7211	0.1143
	-16.80	12.90		

6.2 WINGJOTA Results

Wing panel 18 was analyzed using the structural properties calculations, FEM, and failure criteria described previously. IHR was implemented as the baseline optimization algorithm to solve the design problem within WINGJOTA. MPSA was also implemented to compare performance for this design problem. WINGJOTA is a C++ program with approximately 26,000 lines of code. It was run on a computer with an Intel Core© i7-4700MQ CPU running at 2.40 GHz.

6.2.1 IHR Results

Table 6.2 shows the design variable and objective function results from the 14 load cases. Figure 6.3 shows the panel weights. The joint designs associated with the optimal points for each load case are shown in Table 6.3.

The highest panel weight is found for the -1.5G Mass load case (3) at 70.10 kgf. This is very nearly the initial value of 75.88 kgf. The load case for aerodynamic loads with 3.75G fuel (8) is found to have the lowest weight at 42.14 kgf. The average objective function for all 14 load cases is 53.33 kgf. This average is approximately 30% less than the maximum value. The standard deviation for the IHR-generated panel weights is 7.36 kgf. Considering the bolted joint design shown in Table 6.3, it can be seen that the largest fastener diameters for the rib joints (0.0127 m) are needed for the -1.5G Mass load case (3) and the All -1.5G loads case (13). The smallest fastener diameter for the rib joints is 0.0079375 m for load case (8), the minimum weight case. The spar joint also needs the largest fastener (0.0111125 m) for load case (3). The smallest fastener (0.00635 m) was common to load cases (4), (5), (8), (9), and (12). Note that for load cases (10) and (11) (mass and fuel only) the ribs and spar joints have the same fastener diameter of 0.009525 m.

Table 6.2: Wing Panel Design IHR Results

Loadcase	Skin Laminate nskin	I-stringer Bottom Flange Width bbf (m)	I-stringer Bottom Flange Laminate nbf	I-stringer Top Flange Width btf (m)	I-stringer Top Flange Laminate ntf	I-stringer Web Height hw (m)	I-stringer Web Laminate nweb	Weight (kgf)
(1) Aerodynamic Loads Only	[±64/±23/±69/ ±81/±56/±26/ ±76/±79/±36/ ±30/±57/±89/ ±75/±12/±22/ ±9/±51/±37]S 72 plies	0.060	[±77/±62/±33/ ±56/±29/±37/ ±52/±19/±48/ ±64/±66/$\bar{0}$[1]]S 45 plies	0.058	[0/0/±88/±21/ ±86/±38/±74/ ±3/±42/±18/ ±49/±44/±31/ ±82/±55/±23/ ±46/±58/±89/ ±37/±11/$\bar{0}$]S 81 plies	0.051	[0/0/±13/±61/ ±85/±11/±22/ ±19/±27/±13/ ±49/±30/±22/ ±10/±53/$\bar{0}$]S 47 plies	55.36
(2) 3.75G Mass	[±64/±49/±76/ ±75/±76/±13/ ±44/±44/±31/ ±62/±89/±25/ ±46/±71/±56/ ±17/±33/±25/ ±79/±64/±50/ $\bar{0}$]S 85 plies	0.056	[±14/±28/±48/ ±77/±54/±74/ ±21/±86/±74/ ±19/±42/±60/ ±66]S 52 plies	0.044	[0/0/±48/±39/ ±33/±65/±67/ ±77/±44/±19/ ±53/±84/±54/ ±8/±22/±41]S 60 plies	0.056	[0/0/±86/±71/ ±2/±70/±65/ ±39/±46/±17/ ±25/$\bar{0}$]S 41 plies	56.67

[1] $\bar{0}$ is used to indicate that the midplane passes through the zero degree ply

Table 6.2: Wing Panel Design IHR Results (continued)

Loadcase	nskin	bbf (m)	nbf	btf (m)	ntf	hw (m)	nweb	Weight (kgf)
(3) -1.5G Mass	[±15/±24/±64/ ±37/±87/±55/ ±60/±17/±81 /±22/±20/±70/ ±69/±79/±41/ ±4/±29/±1/±56/ ±67/±6/±10/ ±21]S 72 plies	0.050	[±34/±2/±18/±1/ ±58/±66/±2/±74/ ±43/±63/±47/ ±60/±46/±24/ ±82/±65/±78/ ±48/$\bar{0}$]S 73 plies	0.044	[0/0/±79/±44/ ±21/±33/±11/ ±38/±74/±42/ ±14/±49/±18/ ±54/±17/±11/ ±80/±71/±37/ ±71/±64/±44/ ±49/±64/±87]S 96 plies	0.056	[0/0/±60/±34/ ±51/±32/±43/ ±82/±7/±39/ ±16/±71/±7/ ±58/±60/±35/ 0/0/±89/±56/ ±33/±70/±32/ $\bar{0}$]S 86 plies	70.10
(4) 3.75G Fuel	[±48/±85/±40/ ±69/±14/±49/ ±13/±61/±65/ ±88/±36/±73/ ±26/$\bar{0}$]S 53 plies	0.053	[±14/±8/±82/±87/ ±22/±31/±40/ ±22/±85/±32/ ±82/±58/±78/ ±67/$\bar{0}$]S 57 plies	0.040	[0/0/±54/±62/ ±33/±50/±15/ ±16/±82/±25/ ±32/±62/±65/ ±27/v16/±27/ ±69/±58/±36]S 72 plies	0.067	[0/0/±6/±34/±7 2/±41/±15/±18 /±20/±87/±19/ ±41/±55/$\bar{0}$]S 49 plies	43.43

Table 6.2: Wing Panel Design IHR Results (continued)

Loadcase	nskin	bbf (m)	nbf	btf (m)	ntf	hw (m)	nweb	Weight (kgf)
(5) -1.5G Fuel	[±45/±28/±69/ ±68/±11/±61/ ±59/±60/±1/ ±87/±23/±66/ ±8/±5/±72/$\bar{0}$]S 61 plies	0.051	[±46/±44/±72/ ±69/±84/±30/±7/ ±38/±71/0/0/±22/ ±2/±3/±10/$\bar{0}$]S 57 plies	0.051	[0/0/±60/0/0/ ±56/±76/±46/ ±56/±50/±75/ ±84/±30/±17/ ±11/±82/±82/ ±54/±27/±63/ ±30/±65/±10]S 84 plies	0.051	[0/0/±56/±1/ ±52/±69/±75/ ±55/±27/±24/ ±72/±6/±60/ ±42/±36/±47/ ±42/±42/±43/ ±86/±89/±10/ ±82/±26]S 88 plies	51.63
(6) Aero & 3.75G Mass	[±1/±24/±34/ ±4/±86/±3/±36/ ±44/±55/±39/ ±14/±25/±26/ ±6/±69/±80/±2/ ±12/$\bar{0}$]S 73 plies	0.052	[±49/±67/±86/ ±88/±43/±36/ ±67/±45/±14/$\bar{0}$]S 37 plies	0.053	[±78/±30/±75/ ±78/±46/±22/ ±50/±10/±60/ ±66/±52/±27/ ±58/±83/±49/ ±85/±10]S 68 plies	0.056	[±30/±79/±3/ ±10/±15/±70/ ±53/±40/±18/ ±30/±65/±37/ ±7/±59/±13/ ±85/±29/±2/ ±86/±12/±58/ ±27]S 88 plies	54.60

Table 6.2: Wing Panel Design IHR Results (continued)

Loadcase	nskin	bbf (m)	nbf	btf (m)	ntf	hw (m)	nweb	Weight (kgf)
(7) Aero & -1.5G Mass	[±86/±32/±54/ ±8/±36/±10/ ±55/±47/±40/ ±72/±79/±6/ ±30/±59/±2/ ±25/±67/±31/ $\bar{0}$]S 73 plies	0.064	[±65/±4/±61/±55/ ±32/±5/±26/±60/ ±38/±58/$\bar{0}$]S 41 plies	0.051	[0/0/±77/±36/ ±82/±54/±59/ ±19/±58/±52/ ±14/±36/±14/ ±69/±87/±60/ ±4/±26/$\bar{0}$]S 69 plies	0.053	[0/0/±14/±89/ ±8/90/90/±26/ ±3/±2/±32/ ±65/±69/±73/ $\bar{0}$]S 49 plies	52.72
(8) Aero & 3.75G Fuel	[±75/±29/±40/ ±65/±46/±42/ ±38/±75/±53/ ±16/±69/±17/ ±56/$\bar{0}$]S 53 plies	0.054	[±85/±31/±48/ ±32/±53/90/90/ ±76/±2/±64/±36/ ±33/±3/±86/±8/ ±1/±88/±32/±28/ ±32/±17/±25]S 84 plies	0.054	[0/0/±16/±6/ ±78/±3/±19/ ±82/±32/±78/ ±12/±57/$\bar{0}$]S 45 plies	0.051	[0/0/±88/±25/ ±52/±27/±79/ ±25/±31/±57/ ±30/±88/±33/ ±85/±73/±3/ ±49/±21]S 68 plies	42.14
(9) Aero & -1.5G Fuel	[±83/±28/±32/ ±18/±5/±63/ ±58/±63/±58/ ±14/±33/±41/ ±45/$\bar{0}$]S 53 plies	0.053	[±57/±23/±74/ ±17/±88/±15/±1/ ±45/±4/±74/±25/ ±66/±45/±50/ ±41/±41/±14/ ±56]S 72 plies	0.061	[0/0/±15/±44/ ±83/±37/±56/ ±58/±34/±56/ ±58/±55/±15/ ±76/±68/90/90/ ±46/±52/±13/0/ 0/±76/±51/$\bar{0}$]S 85 plies	0.057	[0/0/±77/±8/ ±46/±32/±73/ ±45/±22/±79/ ±58/±55/±16/ ±8/±81/±6/ ±58/±51/±85/ ±63/$\bar{0}$]S 77 plies	50.04

Table 6.2: Wing Panel Design IHR Results (continued)

Loadcase	nskin	bbf (m)	nbf	btf (m)	ntf	hw (m)	nweb	Weight (kgf)
(10) 3.75G Mass & Fuel	[±1/±54/±73/ ±89/±69/±46/ ±60/±9/±38/±5/ ±80/±12/±83/ ±81/±45/±81/ ±36/±66/±76/ $\bar{0}$]S 77 plies	0.052	[±36/±54/±82/ ±62/±29/±55/ ±26/±87/±39/ ±12/±88/±41/ ±22/±44/±34]S 60 plies	0.052	[0/0/±11/±6/ ±32/±83/±4/ ±17/±55/±6/ ±63/±21/±16/ $\bar{0}$]S 49 plies	0.052	[0/0/±7/±70/ ±27/±5/±80/ ±73/±73/±36/ ±83]S 40 plies	51.21
(11) -1.5G Mass & Fuel	[±75/±74/±4/ ±55/±8/±47/ ±38/±8/±80/ ±48/±71/±77/ ±46/±14/±22/ ±2/$\bar{0}$]S 65 plies	0.040	[±29/±65/±28/ ±23/±80/±53/ ±56/±22/±34/ ±69/±17/±49/ ±16/±78/±45/ ±27/±32/±81/ ±68/±24/±9/$\bar{0}$]S 85 plies	0.053	[0/0/±70/±20/ ±78/±6/±6/±75/ ±77/±7/±9/±13/ ±58/±6/$\bar{0}$]S 53 plies	0.057	[0/0/±62/±26/ ±20/±84/±53/ ±32/±65/±38/ ±23/±32/±28/ ±39/±67/±20/ ±45/±12/±60/ ±29/±50/±1]S 84 plies	49.79
(12) All 3.75G Loads	[±16/±54/±39/ ±67/±79/±65/ ±2/±17/±81/ ±53/±50/±7/ ±36/$\bar{0}$]S 53 plies	0.053	[±74/±65/±66/ ±23/±24/±73/ ±29/±50/±68/ ±62/±54/±47/ ±61/±83/±57/$\bar{0}$]S 61 plies	0.060	[0/0/±57/±17/ ±79/±33/±21/ ±88/±58/±51/ ±20/±46/±63/ ±72/±37/±63/ ±10/±78/±58/ ±51/±61/$\bar{0}$]S 81 plies	0.053	[0/0/±88/±18/ ±73/±16/±6/ ±84/±17/±29/ ±52/±44/±4/ ±54/±42/±3/ ±87/±55/±19/ $\bar{0}$]S 73 plies	47.80

Table 6.2: Wing Panel Design IHR Results (continued)

Loadcase	nskin	bbf (m)	nbf	btf (m)	ntf	hw (m)	nweb	Weight (kgf)
(13) All -1.5G Loads	[±84/±19/±4/ ±86/±52/±75/ ±6/±73/±74/ ±16/±45/±87/ ±32/±15/±56/ ±58/±84/±42/ ±11/±19/±6/ ±75/±32/±4]S 96 plies	0.051	[±70/±62/±88/ ±47/±56/±76/ ±43/±21/±44/ ±76]S 40 plies	0.055	[0/0/±56/±53/ ±56/±67/±84/ ±10/±63/±62/ ±8/±20/±8/±21/ ±63/±28/±21/ ±49/±6/±8]S 76 plies	0.055	[0/0/±22/±79/ ±66/±72/±79/ ±33/±52/±62/ ±30/±80/±66/ ±41/±77/±45/ ±54/±84/$\bar{0}$]S 69 plies	66.55
(14) Emergency Landing	[±58/±10/±85/ ±73/±41/±30/ ±77/±84/±49/ ±6/±67/±86/ ±36/±4/±78/ ±73/±48/±27/ ±29/$\bar{0}$]S 77 plies	0.052	[±41/±50/±82/ ±29/±87/±31/ ±77/±63/±77/ ±55/±63/±46/±3/ ±72/±68/±62/$\bar{0}$]S 65 plies	0.054	[0/0/±82/±29/ ±85/±59/±52/ ±59/±63/±5/±8/ ±28/±75/±84/ ±20/±52/±21]S 64 plies	0.054	[0/0/±48/±62/ ±41/±39/±43/ ±68/±17/±28/ ±23/±33]S 44 plies	54.58

Table 6.3: Wing Panel Joint Design IHR Results

Loadcase	Joint	Joint Number of Plies	Fastener Diameter (m)	Number of Fasteners
(1) Aerodynamic Loads Only	518 (Rib 7)	189	0.0111125	78
	521 (Rib 8)	189	0.0111125	76
	634 (Spar)	144	0.0079375	56
(2) 3.75G Mass	518 (Rib 7)	188	0.0111125	78
	521 (Rib 8)	188	0.0111125	76
	634 (Spar)	170	0.009525	46
(3) -1.5G Mass	518 (Rib 7)	204	0.0127	68
	521 (Rib 8)	204	0.0127	66
	634 (Spar)	144	0.0079375	56
(4) 3.75G Fuel	518 (Rib 7)	152	0.009525	92
	521 (Rib 8)	152	0.009525	90
	634 (Spar)	106	0.00635	72
(5) -1.5G Fuel	518 (Rib 7)	176	0.0111125	78
	521 (Rib 8)	176	0.0111125	76
	634 (Spar)	122	0.00635	72
(6) Aero & 3.75G Mass	518 (Rib 7)	178	0.0111125	78
	521 (Rib 8)	178	0.0111125	76
	634 (Spar)	146	0.0079375	56
(7) Aero & -1.5G Mass	518 (Rib 7)	179	0.0111125	78
	521 (Rib 8)	179	0.0111125	76
	634 (Spar)	146	0.0079375	56
(8) Aero & 3.75G Fuel	518 (Rib 7)	125	0.0079375	110
	521 (Rib 8)	125	0.0079375	108
	634 (Spar)	106	0.00635	72
(9) Aero & -1.5G Fuel	518 (Rib 7)	165	0.009525	92
	521 (Rib 8)	165	0.009525	90
	634 (Spar)	106	0.00635	72
(10) 3.75G Mass & Fuel	518 (Rib 7)	165	0.009525	92
	521 (Rib 8)	165	0.009525	90
	634 (Spar)	154	0.009525	46
(11) -1.5G Mass & Fuel	518 (Rib 7)	151	0.009525	92
	521 (Rib 8)	151	0.009525	90
	634 (Spar)	130	0.009525	46
(12) All 3.75G Loads	518 (Rib 7)	161	0.009525	92
	521 (Rib 8)	161	0.009525	90
	634 (Spar)	112	0.00635	72
(13) All -1.5G Loads	518 (Rib 7)	220	0.0127	68
	521 (Rib 8)	220	0.0127	66
	634 (Spar)	192	0.0111125	40
(14) Emergency Landing	518 (Rib 7)	180	0.0111125	78
	521 (Rib 8)	180	0.0111125	76
	634 (Spar)	154	0.009525	46

6.2.2 MPSA Results

Table 6.4 shows the design variable and objective function results from the 14 load cases. Figure 6.3 shows the panel weights. The joint designs associated with the optimal points for each load case are shown in Table 6.5.

As Figure 6.3 shows that the highest weight is associated with the 3.75G mass load case (2) at 33.32 kgf. This is about 56% lower than the maximum, initial value of 75.88 kgf. The lowest weight is given by the 3.75G fuel and mass load case (10) at 27.73 kgf. The average objective function for these 14 load cases is 30.20 kgf, and the standard deviation is 1.22 kgf. The average is approximately 60% less than the maximum value. Table 6.5 shows that the largest fastener diameters for the rib joints (0.0142875 m) are needed for the All 3.75G load case (12). The smallest fastener diameter for the rib joints (0.0047625 m) is shared by two load cases, (6) and (8) (the lowest weight case). The spar joint needs the largest fastener (0.0111125 m) for load cases (9), (10), and (12), which are not the same cases as the for the rib joints. The smallest fastener (0.00396875 m) was common to load cases (8) and (14). Note that for load cases (10) and (13) the ribs and spar joints have the same fastener diameters, albeit of two different sizes.

Table 6.4: Wing Panel Design MPSA Results

Loadcase	Skin Laminate nskin	I-stringer Bottom Flange Width bbf (m)	I-stringer Bottom Flange Laminate nbf	I-stringer Top Flange Width btf (m)	I-stringer Top Flange Laminate ntf	I-stringer Web Height hw (m)	I-stringer Web Laminate nweb	Weight (kgf)
(1) Aerodynamic Loads Only	[±18/±17/±33/ ±55/±86/±27/ ±44/±79/±51/ ±23/±30/±32/ ±82/±27/±84/ ±41/$\bar{0}$]S 73 plies	0.071	[±63/±69/±6/±22/ ±17/±49/±33/ ±10/±12/±17/$\bar{0}$]S 41 plies	0.073	[±75/±43/±5/ ±63/±1/±12/ ±74/±8/±39/ ±24/±72/±48/ ±29/±81/±48/ ±23/±43/±86/ ±70/±45/±87/ ±72/±38/±44/ $\bar{0}$]S 97 plies	0.068	[±42/±29/±17/ ±38/±34/90/ 90/0/0/±13/ ±40/±4/±87/ ±72]S 48 plies	30.47
(2) 3.75G Mass	[±7/±31/±41/ ±47/±1/±6/±22/ ±26/±78/±69/ $\bar{0}$]S 41 plies	0.060	[±87/±14/±87/ ±13/±39/±75/ ±23/±64/±7/ ±35]S 40 plies	0.053	[±55/±29/±81/ ±15/±50/±33/ ±70/±26/±9/ ±77/±71/±76/ ±23/$\bar{0}$]S 53 plies	0.052	[±3/±77/±65/ ±19/±21/±23/ ±68/±47/±83/ ±7/±26/±79/ ±78/±10/$\bar{0}$]S 57 plies	33.32

Table 6.4: Wing Panel Design MPSA Results (continued)

Loadcase	nskin	bbf (m)	nbf	btf (m)	ntf	hw (m)	nweb	Weight (kgf)
(3) -1.5G Mass	[±2/±36/±83/ ±88/±5/±61/ ±37/±2/±84/ ±84/±2/±79/ ±23/$\bar{0}$]S 53 plies	0.054	[±34/±70/±28/ ±20/±23/±30/ ±22/±25/±4/±78/ ±8/±73]S 48 plies	0.083	[±57/±53/±2/ ±71/±36/±34/ ±33/±2/±19/ ±49/±76/±50/ ±39/±26/±38/ ±36/±66/±33/ ±48]S 76 plies	0.063	[±24/±54/±59/ ±20/±17/±31/ ±70/±33/±25/ ±81/±17/±15/ ±9/±35/±74/ ±81/±86/±62/ ±2/±87]S 80 plies	29.88
(4) 3.75G Fuel	[±24/±16/±9/ ±27/±30/±40/ ±82/±1/±15/±9/ ±8/±2/±34]S 52 plies	0.068	[±23/±77/±37/ ±22/±50/±80/ ±75/±20/±39/ ±84/±81/±54/ ±8/±89]S 56 plies	0.075	[±8/±65/±36/ ±25/±53/±19/ ±76/±44/±39/ ±16/±67/±81/ ±82/±38/±61/ ±54/±82/±35/ ±82/±41/±56/ ±69/±64/±25]S 96 plies	0.095	[±64/±60/±73/ ±2/±16/±6/ ±76/±50/±20/ ±26/±33/±31/ ±18/±36/±88/ ±69/±49/±85/ ±9/±89/±55/ ±81/±52]S 92 plies	29.28
(5) -1.5G Fuel	[±26/±71/±52/ ±5/±68/±51/ ±87/±31/±25/ ±73/±28/±16/ ±34/±79/$\bar{0}$]S 57 plies	0.056	[±33/±21/±36/ ±48/±62/±65/ ±55/±24/±16/ ±46/±85/±12/ ±65/$\bar{0}$]S 53 plies	0.076	[±17/±42/±40/ ±77/±22/±20/ ±59/±54/±35]S 36 plies	0.092	[±84/±71/±18/ ±60/±35/±38/ ±45/±8/±58/ ±63]S 40 plies	30.54

Table 6.4: Wing Panel Design MPSA Results (continued)

Loadcase	nskin	bbf (m)	nbf	btf (m)	ntf	hw (m)	nweb	Weight (kgf)
(6) Aero & 3.75G Mass	[±83/±55/±48/ ±23/±53/±73/ ±88/±52/±56/ ±55]S 40 plies	0.060	[±59/±58/±71/ ±50/±40/±24/ ±87/±75/±36/$\bar{0}$]S 37 plies	0.061	[±2/±37/±51/ ±60/±86/±56/ ±12/±48/±68/ $\bar{0}$]S 37 plies	0.062	[±56/±82/±77/ ±51/±67/0/0/ ±61/±56/±56/ ±68/±6/±88/ ±73/$\bar{0}$]S 53 plies	30.12
(7) Aero & -1.5G Mass	[±71/±52/±15/ ±26/±51/±44/ ±70/±79/±10/ ±56/±45/±81/ $\bar{0}$]S 49 plies	0.066	[±78/±18/±88/ ±28/±89/±41/ ±40/±88/±66/ ±68]S 40 plies	0.057	[±70/±27/±83/ ±79/±60/±85/ ±4/±9/±9/$\bar{0}$]S 37 plies	0.074	[±48/±16/±61/ ±65/±14/±52/ ±60/±10/0/0/ ±54/±36/$\bar{0}$]S 45 plies	31.81
(8) Aero & 3.75G Fuel	[±88/±88/±60/ ±13/±8/±25/ ±76/±68/±68]S 36 plies	0.056	[±79/±45/±56/ ±18/±46/±2/±50/ ±81/±68/$\bar{0}$]S 37 plies	0.054	[±25/±62/±7/ ±19/±45/±76/ ±85/±87/2±3/ ±64/±24]S 44 plies	0.066	[±65/±21/±22/ ±11/±85/±36/ ±69/±38/±5/ ±78/±83/±10/ ±56/±1]S 56 plies	29.16

Table 6.4: Wing Panel Design MPSA Results (continued)

Loadcase	nskin	bbf (m)	nbf	btf (m)	ntf	hw (m)	nweb	Weight (kgf)
(9) Aero & -1.5G Fuel	[±1/±67/±32/ ±18/±39/±4/ ±12/±73/±27/ ±53/±81/±39/ ±85/±79/±86/ ±11/±48/±43/ ±35/±78/90/90/ ±30/±84]S 92 plies	0.051	[±80/±36/±52/ ±21/±87/±88/ ±46/±24/±33/ ±39/±86]S 44 plies	0.065	[±24/±29/±10/ ±8/±76/±67/ ±57/±86/±74/ ±52/±50/±5/ ±68/±65]S 72 plies	0.064	[±85/±58/±9/ ±81/±80/±26/ ±42/±33/±59/ ±38/±82/±1/ ±60/±7/±79]S 60 plies	30.40
(10) 3.75G Mass & Fuel	[±35/±51/±29/ ±62/±67/±71/ ±22/±49/±43/ ±20/±86/±36/ ±53/±10/±27/ ±3/±26/±52/ ±87/±78/±22/ ±15/±66/$\bar{0}$]S 93 plies	0.073	[±80/±38/±17/±3/ ±64/±52/±69/ ±80/±72/±15/$\bar{0}$]S 41 plies	0.061	[±79/±61/±73/ ±59/±73/±20/ ±28/±18/±53/ ±36/±52/±18/ ±5/±55]S 56 plies	0.079	[±8/±46/±66/ ±48/±30/±43/ ±45/±42/±72/ ±86/±74/±19/ ±22/±82/±76/ ±17/±45/±72/ ±23/±30/±18]S 84 plies	27.73

Table 6.4: Wing Panel Design MPSA Results (continued)

Loadcase	nskin	bbf (m)	nbf	btf (m)	ntf	hw (m)	nweb	Weight (kgf)
(11) -1.5G Mass & Fuel	[±42/±17/±89/ ±58/±18/±52/ ±87/±77/±64/ ±3/±32/±71/ ±22/±75/±73/ ±89/±18]S 68 plies	0.073	[±42/±16/±68/ ±11/±59/±27/ ±30/±33/±72/ ±89/±16]S 44 plies	0.053	[±55/±65/±41/ ±46/±24/±56/ ±79/±72/±33/ ±14/±16/±10/ ±89/±38/±79/ ±31/±25/±49/ ±79/±29/±13/ ±22/$\bar{0}$]S 89 plies	0.067	[±23/±36/±38/ ±11/±72/±12/ ±17/±33/±84/ ±9]S 40 plies	30.12
(12) All 3.75G Loads	[±24/±47/±56/ ±6/±57/±39/ ±41/±89/±88/ ±12/±21/±60/ ±34/±79/±36/ ±12/±7/±43/ ±84/±56/±28/ ±45/±9/±38/ $\bar{0}$]S 97 plies	0.088	[±6/±17/±20/±59/ ±13/±11/±16/ ±89/±31/±75/ ±67/±5/±64/±84/ ±84/±66/$\bar{0}$]S 65 plies	0.075	[±76/±87/±37/ ±76/±57/±5/ ±88/±62/±64/ ±87/±20/±61/ ±16/±27/±50/ ±24/±75/±16/ ±48/±25/$\bar{0}$]S 81 plies	0.084	[±87/±73/±88/ ±59/±8/±47/ ±81/±1/±23/ ±75/±40/±19/ ±10/±14/±82/ ±55]S 64 plies	29.93

Table 6.4: Wing Panel Design MPSA Results (continued)

Loadcase	nskin	bbf (m)	nbf	btf (m)	ntf	hw (m)	nweb	Weight (kgf)
(13) All -1.5G Loads	[±65/±76/±84/ ±28/±48/±30/ ±33/±7/±25/ ±20/±44/±7/ ±65/±78/±86/0/ 0/±18/±1/$\bar{0}$]S 73 plies	0.085	[±41/±56/±81/±3/ ±87/±59/0/0/±13/ ±20/±82/±49/ ±53/±62/±21/ ±83/±50/±15/ ±87/±34/±53]S 80 plies	0.083	[±74/±8/±51/ ±56/±65/±76/ ±17/±59/±20/ $\bar{0}$]S 37 plies	0.052	[±67/±58/±68/ ±17/±67/±82/ ±17/±66/±46/ ±77/±50/±51]S 48 plies	30.32
(14) Emergency Landing	[±65/±37/±33/ ±39/±45/±29/ ±6/±67/±78/ $\bar{0}$]S 37 plies	0.087	[±17/±34/±23/ ±34/±54/±21/ ±17/±78/±40/±6/ ±57/±89/±3/±68/ ±80/±79/±39/$\bar{0}$]S 69 plies	0.065	[±29/±70/±30/ ±78/±63/±72/ ±63/±37/±5/ ±82/±61/±40/ ±59/±33/$\bar{0}$]S 57 plies	0.072	[±81/±76/±17/ ±87/±81/±20/ ±9/±80/±31/ ±57/±52/±15/ ±50/±11/±8/ ±61/±75/±81]S 72 plies	29.79

Table 6.5: Wing Panel Joint Design MPSA Results

Loadcase	Joint	Joint Number of Plies	Fastener Diameter (m)	Number of Fasteners
(1) Aerodynamic Loads Only	518 (Rib 7)	207	0.0127	68
	521 (Rib 8)	207	0.0127	66
	634 (Spar)	146	0.0079375	56
(2) 3.75G Mass	518 (Rib 7)	115	0.00635	138
	521 (Rib 8)	115	0.00635	136
	634 (Spar)	82	0.0047625	96
(3) -1.5G Mass	518 (Rib 7)	156	0.009525	92
	521 (Rib 8)	156	0.009525	90
	634 (Spar)	106	0.00635	72
(4) 3.75G Fuel	518 (Rib 7)	174	0.009525	92
	521 (Rib 8)	174	0.009525	90
	634 (Spar)	104	0.00635	72
(5) -1.5G Fuel	518 (Rib 7)	122	0.00635	138
	521 (Rib 8)	122	0.00635	136
	634 (Spar)	114	0.00635	72
(6) Aero & 3.75G Mass	518 (Rib 7)	97	0.0047625	186
	521 (Rib 8)	97	0.0047625	182
	634 (Spar)	80	0.0047625	96
(7) Aero & -1.5G Mass	518 (Rib 7)	111	0.00635	138
	521 (Rib 8)	111	0.00635	136
	634 (Spar)	98	0.0047625	96
(8) Aero & 3.75G Fuel	518 (Rib 7)	98	0.0047625	186
	521 (Rib 8)	98	0.0047625	182
	634 (Spar)	72	0.00396875	116
(9) Aero & -1.5G Fuel	518 (Rib 7)	210	0.0127	68
	521 (Rib 8)	210	0.0127	66
	634 (Spar)	184	0.0111125	40
(10) 3.75G Mass & Fuel	518 (Rib 7)	196	0.0111125	78
	521 (Rib 8)	196	0.0111125	76
	634 (Spar)	186	0.0111125	40
(11) -1.5G Mass & Fuel	518 (Rib 7)	191	0.0111125	78
	521 (Rib 8)	191	0.0111125	76
	634 (Spar)	136	0.0079375	56
(12) All 3.75G Loads	518 (Rib 7)	227	0.0142875	60
	521 (Rib 8)	227	0.0142875	58
	634 (Spar)	194	0.0111125	40
(13) All -1.5G Loads	518 (Rib 7)	147	0.0079375	110
	521 (Rib 8)	147	0.0079375	108
	634 (Spar)	146	0.0079375	56
(14) Emergency Landing	518 (Rib 7)	113	0.00635	138
	521 (Rib 8)	113	0.00635	136
	634 (Spar)	74	0.00396875	116

6.3 Discussion of WINGJOTA Results

A comparison of the objective functions obtained by both the IHR and MPSA algorithms is shown in Figure 6.3. The optimum weight designs found by IHR were higher than those found using MPSA. The difference in weight between the load cases was also much smaller using the MPSA algorithm. This may indicate that the use of many simultaneous particles is better able to find a minimum point in this complex design space.

Both algorithms show the highest weight for the mass only load cases (2) (3.75G up load) and (3) (-1.5G down load) but differ which direction of bending is critical. Both panel designs feature moderate thickness skin and bottom flange laminates; however, the IHR solution shows the maximum number of plies for the top flange. The IHR algorithm for load case (3) likely did not find a design point that could withstand the shear forces induced in the rib joints. A better design may have been found with more iterations. The lightest panel weights using the two optimization algorithms differed as well. For IHR it was load case (8), aerodynamic loads with 3.75G fuel. The 3.75G fuel and mass load case (10) was the lightest for MPSA.

The joint designs are independent of the optimization algorithm and are dependent only on the design variables. Since the joint design does contribute to the objective function there is an influence on which panel geometries are chosen as optimal designs. As can be seen in Tables 6.3 and 6.5 the total joint thickness (given as the number of plies) determines the fastener diameter. The diameter drives the number of fasteners in the joint as the geometry is fixed, which in turn affects weight. A successful panel design must balance the I-stringer geometry to provide bending stiffness to the panel and be capable of passing the structural constraints for the rib joints. For instance, an I-stringer with a very thick bottom flange may have good section modulus and bending capability, but the top flange may be too small and thin to handle the loads in the rib joint. The tradeoff is similar for the skin. This is especially true for the spar joint, as the only design variable driving the bolt diameter is the skin thickness.

There may be a few different ways to determine a preliminary design for this wing panel from the results presented. One way would be to choose the load case that included all the loads for a single gravity acceleration, i.e., either All 3.75G or All -1.5G loads. That design would then undergo detail design with many more load cases and more accurate analyses. Another way to use these results would be to choose the maximum diameter fastener for each joint and hold that parameter fixed. Then the optimization algorithm could be re-run to explore the design space for variations in the four laminate thicknesses.

During the course of these analyses it was noticed that the Tsai-Wu criterion for the joints was causing design points to be infeasible most often. This was particularly true for the load cases that included the aerodynamic loads. This wing panel has eight elements that have pressure loads applied to simulate the aerodynamic forces, and the boundary conditions and resulting in-plane loads at the joints drove the thicknesses higher to reduce the stresses. Another effect may be caused by the use of discrete fastener sizes with discrete ply thicknesses in the joints. There may have been situations where the design point would dictate some joint thickness and WINGJOTA would choose an appropriate fastener size given the thickness-to-diameter ratio

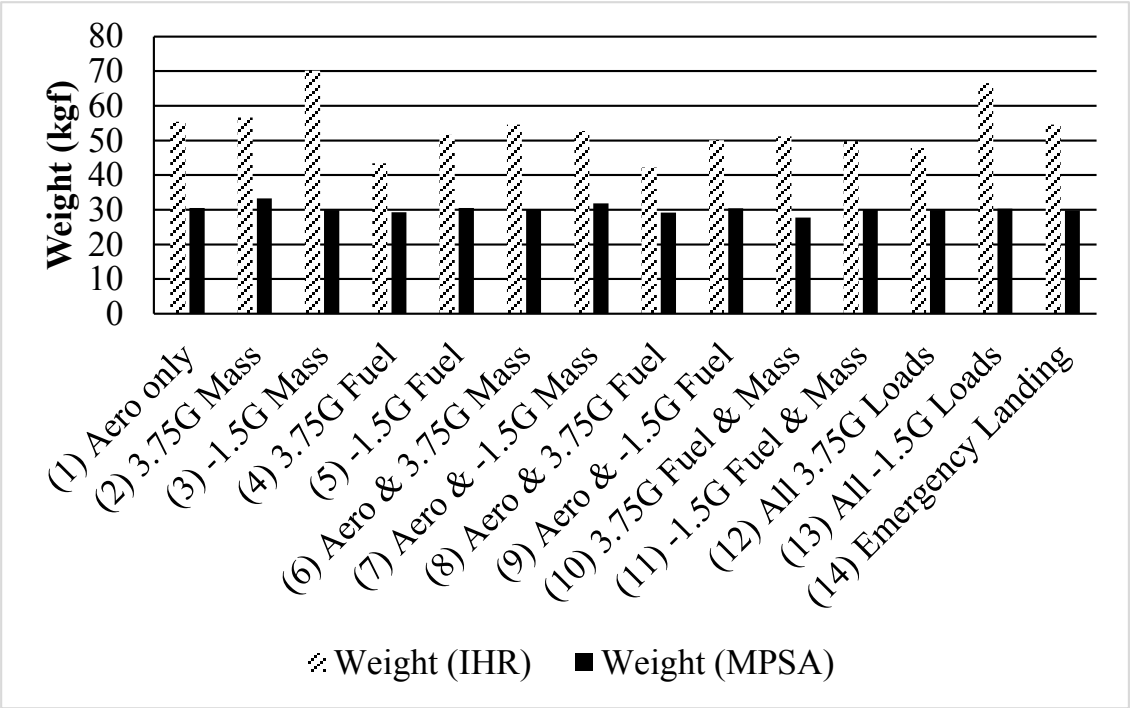

Figure 6.3: Optimized Weights of Wing Panel 18 with IHR and MPSA

required, causing the stresses to be too high in the laminate. Note that the bolted joint design rules applied were successful; there were no failures of the fasteners themselves.

Both algorithms showed similar behavior with respect to which load cases were more difficult to optimize. Figure 6.4 shows the CPU times for both algorithms. Clearly the IHR algorithm was taking less computational time. It can also be seen that the load cases with aerodynamic loads took less time; these cases tended to generate infeasible design points more often than the other load cases. Run times for IHR optimization varied by load case. Load cases that have many infeasible regions, generally those that include the aerodynamic loads, run quickly, typically taking about a half hour. Those load cases with many feasible design points took longer, generally between five and six hours. A similar trend can be observed for MPSA, although the run times were much longer, sometimes as long as ten hours.

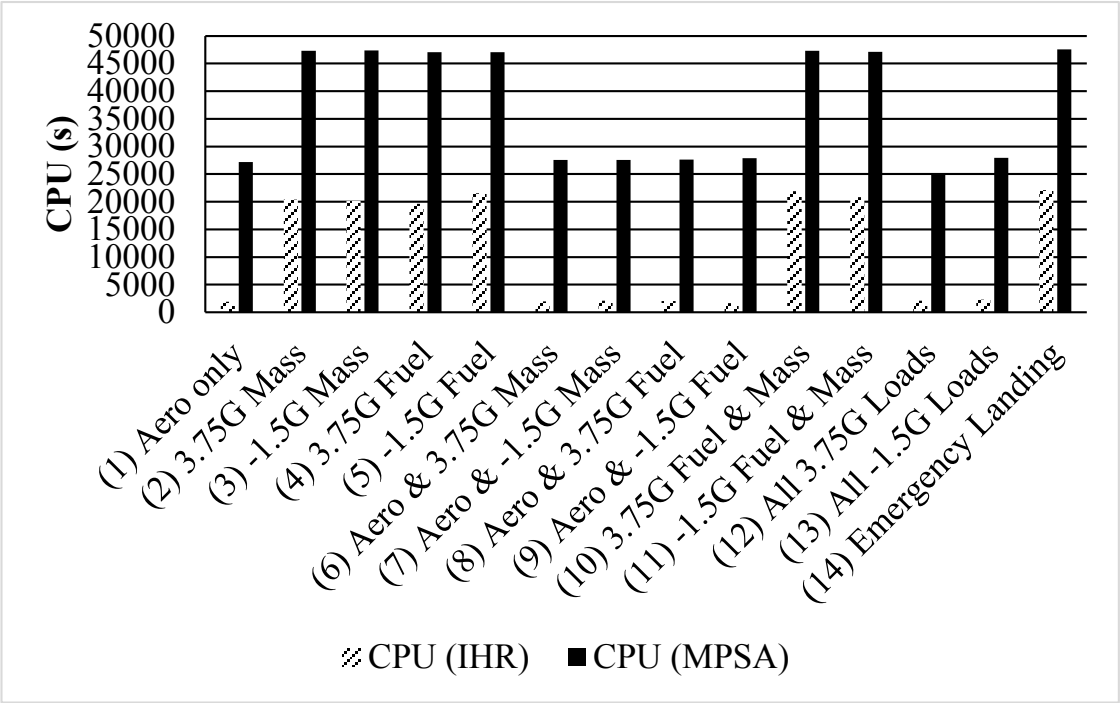

Figure 6.4: CPU Times for IHR and MPSA WINGJOTA Optimizations

6.4 Summary and Conclusions

The integration of optimization algorithm flow, bolted joint analysis, wing design and resulting loads, finite element analysis, and stochastic optimization algorithms were integrated into a full program called WINGJOTA for the analysis of an I-stringer stiffened wing panel. The two optimization algorithms, IHR and MPSA, were incorporated and used to optimize a panel from the upper panel of the benchmark composite wing design, labeled panel 18. A finite element model of this panel was developed and provided as an input for WINGJOTA.

The results show a marked difference between IHR and MPSA in objective functions achieved and the number of function iterations necessary to find that optimum. IHR was able to find reasonable panel weights in relatively short times. MPSA, with its much larger number of design points to iterate, was able to find lower weights but with a much longer run time.

Chapter 7

SUMMARY AND CONCLUSIONS

7.1 Summary and Conclusions

A composite wing panel software package, named WING Joint OpTimization and Analysis (WINGJOTA) featuring bolted joint analysis, was presented in this research. Three areas of focus were the development of an analytic composite bolted joint analysis suitable for fast evaluation; a more realistic wing design than what has been considered in the open literature; and the application of two optimization algorithms for composite wing design.

The composite bolted joint analysis consists of an elasticity solution that provides the stress state at a characteristic distance away from the bolt holes. The stresses at the characteristic distance are compared to a failure criterion on a ply-by-ply basis that not only determines first ply failure but also the failure mode. The loads in the multi-fastener joints used in this study were determined by an iterative scheme that provides the bearing-bypass loads to the elasticity analysis.

A preliminary design of a composite subsonic transport wing was developed, based around a mid-size, twin-aisle aircraft. The benchmark design includes the leading and trailing edge structures and the center box inside the fuselage. Wing masses were included as point loads, and fuel loads were incorporated as distributed loads. The side-of-body boundary condition was modeled using high stiffness springs, and the aerodynamic loads were applied using an approximate point load scheme. The entire wing structure was modeled using the finite element code ANSYS to provide the internal loads needed as boundary conditions for the wing panel analyzed by WINGJOTA.

The software package WINGJOTA combines the composite bolted joint analysis, a composite plate finite element analysis, a wing aeroelastic cycle, and two optimization algorithms to form the basis of a computer code for analysis and optimization. Both the Improving Hit-and-Run (IHR) and the Multi-Particle Simulated Annealing (MPSA) algorithms were coded and used as the optimization routines in WINGJOTA.

Based on this study, the following conclusions can be made:

- The two-dimensional composite bolted joint analysis developed provides a sufficiently accurate analysis for wing panel preliminary design
- The benchmark composite wing design proposed contains enough design detail to serve as a vehicle for optimization algorithm trials with various constraints

- WINGJOTA captures the interplay between wing stiffened panel geometry, effective laminate properties, loading conditions, and composite bolted joint behavior for wing preliminary design
- The MPSA algorithm was able to find wing panel designs with lighter weights than IHR at the expense of computation time.

7.2 Future Work

There are a few categories of future work that could be performed from this basic algorithm and approach. They include changes to the bolted joint analysis, more specialized wing analyses, structural analyses, and changes to the optimization routine. First, the bolted joint analysis could be expanded to general laminates by incorporation of the Jenkins-Traub three-stage algorithm for the solution of polynomials with complex roots. A more detailed bolted joint analysis that includes three-dimensional effects could be more accurate than the two-dimensional analysis used in WINGJOTA. A question would be whether it could be made fast enough to run in a stochastic optimization algorithm.

A constraint not considered in this study that applies to wing structures is flutter speed. Such a constraint could be easily incorporated into the algorithm; however, a computational fluid dynamics solution would be difficult to use during the optimization. Therefore, an iterative solution, such as the V, g method, may be utilized to develop the constraint. Alternatively, a gradient projection search could be used. A further wing constraint is that of natural frequency; the dynamic stiffness matrix method could be developed for the algorithm. As an alternative to the approximate, point-load aerodynamic solution of Torenbeek the more accurate Doublet-Lattice method could be used to develop the aerodynamic loads introduced in the finite element model.

The wing panel design analysis could be modified to incorporate different stringer shapes, such as hat and blades, as has been done in the past. Another avenue could be to use a more detailed bending and torsion theory for I-stringer analysis and I-stringer specific manufacturing constraints. Structural constraints for the panel around buckling and postbuckling of upper wing skin panels and ribs could be developed. A postbuckling analysis may be utilized for the upper wing skins.

A two phase optimization strategy could be used to improve the performance of the optimization algorithms by allowing the algorithm to traverse the infeasible regions of the design space while searching for a feasible design point. A secondary objective function would be established that is related to the mechanical performance failure criteria ($f_m(X)$) and defined by the minimum of the inequality constraints:

$$f_m(X) = \min[g_j(X)] \text{ for } j = 1, 2, \ldots \tag{7.1}$$

It was found in this study that the design space contains many infeasible regions; in the initial phases of the optimization process it is likely that the candidate point is infeasible. Therefore, the mechanical performance function $f_m(X)$ is maximized until all the constraints are satisfied.

The algorithm then would move to the primary, weight objective function while the design points are feasible [30]. Another important opportunity is to optimize the composite joints first, then blend the resulting laminates into the rest of the wing panels. The blending rules developed by Kristinsdottir et al. [439, 32] could be utilized.

In conclusion, the goals of this study, to develop a fast-running composite bolted joint analysis and incorporate it into a composite wing design optimization algorithm, have been accomplished. Further work is necessary to develop a useful wing structure preliminary design tool. However, the algorithm flow and architecture created here can accommodate many of these changes.

BIBLIOGRAPHY

1. Anonymous, *Boeing Completes First 7E7 Compostie Fuselage Section*, *JEC Composites Magazine*. 2005, Journal and Exhibitions on Composites (JEC) Group: Paris, France.
2. Griffiths, B., *Boeing Sets Pace for Composite Usage in Large Civil Aircraft*, *High-Performance Composites*. 2005, Gardner Publications, Inc.: Cincinnati, OH.
3. Black, S., *Very Light Jets Creating a Demand for Composites*, *High-Performance Composites*. 2006, Gardner Publications, Inc.: Cincinnati, OH.
4. Gates, D., *Boeing Builds its Case for Using Composites for 7E7*, *Seattle Times*. 2004, Seattle Times Co.: Seattle, WA.
5. Butterworth-Hayes, P., *European Investments Lift Aerodynamic Research*, *Aerospace America*. 2007, American Institute of Aeronautics and Astronautics: Reston, VA. p. 4-6.
6. Schrauf, G. *KATnet: Key Aerodynamic Technologies for Aircraft Performance Improvement*. in *Proceedings of the 5th Community Aeronautical Days*. 2006. Vienna, Austria: Deutsche Gesellschaft für Luft- und Raumfahrt (DGLR).
7. Choudhari, M., and Piomelli, U., *Aerospace Sciences: Fluid Dynamics*, *Aerospace America*. 2006, American Institute of Aeronautics and Astronautics: Reston, VA. p. 20-21.
8. Shifrin, C., *787: Expect Something Different*, *Overhaul and Maintenance*. 2005, McGraw-Hill: Washington, DC. p. 35-40.
9. Green, J.E., *Air Travel - Greener by Design: Mitigating the Environmental Impact of Aviation: Opportunities and Priorities*, *Greener by Design Science and Technology Sub-Group*. 2005, Royal Aeronautical Society: London, UK.
10. Wilson, J.R., *Quiet Plans for Tomorrow's Jet Engines*, *Aerospace America*. 2005, American Institute of Aeronautics and Astronautics: Reston, VA. p. 38-42.
11. Laurenzo, R., *Hushing the Roar of Air Traffic Growth*, *Aerospace America*. 2006, American Institute of Aeronautics and Astronautics: Reston, VA. p. 38-42.
12. Brosius, D., *Boeing 787 Update*, *High-Performance Composites*. 2007, Gardner Publications, Inc.: Cincinnati, OH. p. 56-59.
13. Neill, D.J., Johnson, E. H., and Canfield, R., *ASTROS: A Multidisciplinary Automated Structural Design Tool.* Journal of Aircraft, 1990. **27**(12): p. 1021-1027.
14. Lamar, W.E. *The Role of Preliminary Design in Reducing Development, Production, and Operational Cost of Aircraft Systems*. *AGARD Conference Proceedings on Aircraft Design Integration and Optimization*. 1973. North Atlantic Treaty Organization (NATO). p. 1-1-1-7.
15. De Baets, P.W.G., Mavris, D. N., and Sobieszczanski-Sobieski, J. *Aeroelastic Design by Combining Conventional Practice with Bi-Level Integrated System Synthesis (BLISS)*. *Proceedings of the 10th AIAA/ISSMO Symposium on Multidisciplinary Analysis and Optimization*. 2004. Albany, NY: American Institute of Aeronautics and Astronautics. AIAA 2004-4431.
16. Kirsch, U., *Structural Optimization: Fundamentals and Applications*. 1993, Berlin, Germany: Springer-Verlag.

17. Foye, R.L., *Advanced Design Concepts for Advanced Composite Airframes*. 1968, AFML-TR-68-91 Volume I, Air Force Materials Laboratory, Air Force Systems Command: Wright-Patterson Air Force Base, OH. p. 4-19, 26-37, 245-269, 282-285.
18. Lansing, W., Dwyer, W., Emerton, R., and Ranalli, E., *Application of Fully Stressed Design Procedures to Wing and Empennage Structures.* Journal of Aircraft, 1971. **8**(9): p. 683-688.
19. Starnes, J.H.J., and Haftka, R. T., *Preliminary Design of Composite Wings for Buckling, Strength, and Displacement Constraints.* Journal of Aircraft, 1979. **16**(8): p. 564-570.
20. Giles, G.L., *Equivalent Plate Analysis of Aircraft Wing Box Structures with General Platform Geometry.* Journal of Aircraft, 1986. **23**(11): p. 859-864.
21. Livne, E., *Analytic Sensitivities for Shape Optimization in Equivalent Plate Structural Wing Models.* Journal of Aircraft, 1994. **31**(4): p. 961-969.
22. Mabson, G.E., Flynn, B. W., Ilcewicz, L. B., and Graesser, D. L. *The Use of COSTADE in Developing Composite Commercial Aircraft Fuselage Structures*. *Proceedings of the 35th AIAA/ASME/ASCE/AHS/ASC 35th Structures, Structural Dynamics, and Materials Conference*. 1994. Hilton Head, SC: American Institute of Aeronautics and Astronautics. p. 1384-1393.
23. Kim, G.-I., and Tuttle, M. E. *Buckling Analysis for a Stiffened Panel*. in *Proceedings of the 35th AIAA/ASME/ASCE/AHS/ACS Structures, Structural Dynamics, and Materials Conference*. 1994. Hilton Head, SC: American Institute of Aeronautics and Astronautics. p. 1423-1433.
24. Neogi, S., Tuttle, M. E., Zabinsky, Z. B., and Kristinsdottir, B. P. *Load Redistribution Issues in Optimal Design of Composite Airplane Structures*. in *Proceedings of the ICCE/2 Conference*. 1995. New Orleans, LA. p. 539-540.
25. Graesser, D.L., Zabinsky, Z. B., Tuttle, M. E., and Kim, G. I., *Optimal Design of Composite Structures.* Composite Structures, 1993. **24**(4): p. 273-281.
26. Chang, F.-K., Scott, R. A., and Springer, G. S., *Strength of Mechanically Fastened Composite Joints.* Journal of Composite Materials, 1982. **16**(November): p. 470-494.
27. Savin, G.N., *Stress Distribution Around Holes*, NASA TT F-607. 1970, National Aeronautics and Space Administration: Washington, DC.
28. Yamada, S.E., and Sun, C. T., *Analysis of Laminate Strength and Its Distribution.* Journal of Composite Materials, 1978. **12**(July): p. 275-284.
29. Whitney, J.M., and Nuismer, R. J., *Stress Fracture Criteria for Laminated Composites Containing Stress Concentrations.* Journal of Composite Materials, 1974. **8**(7): p. 253-265.
30. Graesser, D.L., *Design of Laminated Composite Panels Optimized for Damage Tolerance*, Ph.D., *Mechanical Engineering*. 1993, University of Washington: Seattle, WA.
31. Neogi, S., *Design of Large Composite Structures Using Global Optimization and Finite Element Analysis*, Ph.D. *Mechanical Engineering*. 1997, University of Washington: Seattle, WA.
32. Kristinsdottir, B.P., *Analysis and Development of Random Search Algorithms*, Ph.D. *Mechanical Engineering*. 1997, University of Washington: Seattle, WA.
33. Savic, V., *Design Optimization of Thin-Walled Composite Beams*, Ph.D. *Mechanical Engineering*. 2000, University of Washington: Seattle, WA.

34. Molvalioglu, O., Zabinsky, Z. B., and Kohn, W., *Multi-Particle Simulated Annealing*, *Models and Algorithms for Global Optimization: Essays Dedicated to Antanas Žilinskas on the Occasion of His 60th Birthday*, A. Törn, and Žilinskas, J., Editors. 2007, Springer Science + Business Media, LLC: New York, NY. p. 215-222.
35. Garcelon, J.H., Balabanov, V. O., and Sobieski, J. *Multidisciplinary Optimization of a Transport Aircraft Wing Using VisualDOC*. *Proceedings of the 40th AIAA/ASME/ASCE/AHS/ASC Structures, Structural Dynamics, and Materials Conference*. 1999. St. Louis, MO: American Institute of Aeronautics and Astronautics. p. 1306-1313.
36. Schmit, L.A.J., *Structural Synthesis: Its Genesis and Development.* AIAA Journal, 1981. **19**(10): p. 1249-1263.
37. Haftka, R.T., and Gürdal, Z., *Elements of Structural Optimization*. 3rd ed. Solid Mechanics and Its Applications, ed. G.M.L. Gladwell. 1992, Dordrecht, The Netherlands: Kluwer Academic Publishers.
38. Venkayya, V.B., *Structural Optimization: A Review and Some Recommendations.* International Journal for Numerical Methods in Engineering, 1978. **13**(2): p. 203-228.
39. Schmit, L.A. Jr., *Chapter 2: A Basis for Assessing the State-of-the-Art*, Structural Design Applications of Mathematical Programming Techniques, AGARDograph No. 149, AGARD-AG-149-71. G.G. Pope, and Schmit, L. A. Jr., Editors. 1971, Advisory Group for Aerospace Research and Development, North Atlantic Treaty Organization: Neuilly-Sur-Seine, France. p. 14-29.
40. Schmit, L.A. Jr., and Mallett, R. H., *Structural Synthesis and Design Parameter Hierarchy.* Journal of the Structural Division, 1963. **89**(4): p. 269-299.
41. Haug, E.J., and Arora, J. S., *Applied Optimal Design: Mechanical and Structural Systems*. 1979, New York, NY: John Wiley and Sons.
42. Niordson, F.I., and Pedersen, P., *A Review of Optimal Structure Design*, *Proceedings of the 13th International Congress of Theoretical Applied Mechanics*. 1973: Moscow University, Moscow, Soviet Union. p. 264-278.
43. Eschenauer, H.A., Koski, J., and Osyczka, A., *Chapter 1: Multicriteria Optimization--Fundamentals and Motivation*, *Multicriteria Design Optimization: Procedures and Applications*, H.A. Eschenauer, Koski, J., and Osyczka, A., Editors. 1990, Springer-Verlag: Berlin, Germany. p. 1-32.
44. Gill, P.E., Murray, W., and Wright, M. H., *Practical Optimization*. 1981, New York, NY: Academic Press.
45. Schmit, L.A.J., and Fox, R. L., *An Integrated Approach to Structural Synthesis and Analysis.* AIAA Journal, 1965. **3**(6): p. 1104-1112.
46. Fox, R.L., and Schmit, L. A. Jr., *Advances in the Integrated Approach to Structural Synthesis.* Journal of Spacecraft and Rockets, 1966. **3**(6): p. 858-866.
47. Maxwell, J.C., *XXXIX: On Reciprocal Figures, Frames, and Diagrams of Forces*, in *The Scientific Papers of James Clerk Maxwell*, W.D. Niven, Editor. 1890, Cambridge University Press: Cambridge, England. p. 161-207.
48. Michell, A.G.M., *The Limits of Economy of Material in Frame Structures.* Philosophical Magazine, Series VI, 1904. **8**(47): p. 589-597.
49. Zahorski, A., *Effects of Material Distribution on Strength of Panels.* Journal of the Aeronautical Sciences, 1944. **2**(3): p. 247-253.

50. Gerard, G., *Minimum Weight Analysis of Compression Structures*. 1956, New York, NY: New York University Press.
51. Shanley, F.R., *Weight-Strength Analysis of Aircraft Structures*. 2 ed. 1960, New York, NY: Dover Publications, Inc.
52. Heyman, J., *Plastic Design of Beams and Frames for Minimum Material Consumption.* Quarterly of Applied Mathematics, 1951. **8**(4): p. 373-381.
53. Klein, B., *Direct Use of Extremal Principles in Solving Certain Optmization Problems Involving Inequalities.* Journal of the Operations Research Society of America, 1955. **3**: p. 168-175.
54. Pearson, C.E. *Structural Design by High-Speed Computing Machines*. in *Proceedings of the 1st Conference on Electronic Computation*. 1958. Kansas City, MO: American Society of Civil Engineers. p. 417-436.
55. Schmit, L.A. Jr. *Structural Design by Systematic Synthesis*. in *Proceedings of the 2nd Conference on Electronic Computation*. 1960. Pittsburgh, PA: American Society of Civil Engineering. p. 105-122.
56. Fox, R.L., *Constraint Surface Normals for Structural Synthesis Techniques.* AIAA Journal, 1965. **3**(8): p. 1517-1518.
57. Haug, E.J., Choi, K. K., and Komkov, V., *Design Sensitivity Analysis of Structural Systems*. Mathematics in Science and Engineering, ed. W.F. Ames. 1986, Orlando, FL: Academic Press, Inc.
58. Razani, R., *The Behavior of the Fully-Stressed Design of Structures and its Relationship to Minimum-Weight Design.* AIAA Journal, 1965. **3**(12): p. 2262-2268.
59. Prager, W., and Taylor, J. E., *Problems of Optimal Structural Design.* Journal of Applied Mechanics, 1968. **35**(3): p. 102-106.
60. Prager, W., and Shield, R. T., *Optimal Design of Multi-Purpose Structures.* International Journal of Solids and Structures, 1968. **4**(4): p. 469-475.
61. Venkayya, V.B., Khot, N. S., and Reddy, V. S., *Energy Distribution in an Optimum Structure Design*. AFFDL-TR-68-156. 1969, Air Force Flight Dynamics Laboratory, Air Force Systems Command: Wright-Patterson Air Force Base, OH.
62. Vanderplaats, G.N., *Thirty Years of Modern Structural Optimization.* Advances in Engineering Software, 1993. **16**(2): p. 81-88.
63. Noor, A.K., and Lowder, H. E., *Approximate Techniques of Structural Reanalysis.* Computers and Structures, 1974. **4**(4): p. 801-812.
64. Bhatia, K.G., *Rapid Iterative Reanalysis for Automated Design*. NASA TN D-7357. 1973, NASA Langely Research Center: Hampton, VA.
65. Schmit, L.A. Jr., and Miura, H., *Approximation Concepts for Efficient Structural Synthesis*. NASA CR-2552. 1976, NASA Langley Research Center: Langley, VA.
66. Wolfe, P., *A Duality Theorem for Non-Linear Programming.* Quarterly of Applied Mathematics, 1963. **19**(3): p. 239-244.
67. Falk, J.E., *Lagrange Multipliers and Nonlinear Programming.* Journal of Mathematical Analysis and Applications, 1967. **19**: p. 141-159.
68. Fleury, C., and Sander, G. *Relations Between Optimality Criteria and Mathematical Programming in Structural Optimization*. *Proceedings of the Symposium on Applications of Computer Methods in Engineering*. 1977. Los Angeles, CA: University of Southern California. p. 507-520.

69. Fleury, C., *A Unified Approach to Structural Weight Minimization.* Computer Methods in Applied Mechanics and Engineering, 1979. **20**(1): p. 17-38.
70. Schmit, L.A. Jr., and Fleury, C., *Structural Synthesis by Combining Approximation Concepts and Dual Methods.* AIAA Journal, 1980. **18**(10): p. 1252-1260.
71. Vanderplaats, G.N., *CONMIN: A Fortran Program for Constrained Function Minimization, User's Manual*. NASA TM X-62282. 1973, NASA Ames Research Center and U. S. Army Air Mobility R&D Laboratory: Moffett Field, CA.
72. Dwyer, W.J., Emerton, R. K., and Ojalvo, I. U., *An Automated Procedure for the Optimization of Practical Aerospace Structures, Volume I: Theoretical Development and User's Information*. AFFDL-TR-70-118. 1971, Air Force Flight Dynamics Laboratory: Wright-Patterson Air Force Base, OH.
73. Dwyer, W.J., *An Improved Automated Structural Optimization Program*. AFFDL-TR-74-96. 1974, Air Force Flight Dynamics Laboratory: Wright-Patterson AFB, OH.
74. Isakson, G., and Pardo, H., *ASOP-3: A Program for the Minimum-Weight Design of Structures Subjected to Strength and Deflection Constraints*. AFFDL-TR-76-157. 1976, Air Force Flight Dynamics Laboratory: Wright-Patterson Air Force Base, OH.
75. Williams, F.W., *Computation of Natural Frequencies and Initial Buckling Stresses of Prismatic Plate Assemblies.* Journal of Sound and Vibration, 1972. **21**(1): p. 87-106.
76. Williams, F.W., and Anderson, M. E., *User's Guide to VIPASA (Vibration and Instability of Plate Assemblies Including Shear and Anisotropy)*. 1973, University of Birmingham: Birmingham, England, UK.
77. Wittrick, W.H., and Williams, F. W., *Buckling and Vibration of Anisotropic or Isotropic Plate Assemblies Under Combined Loadings.* International Journal of Mechanical Sciences, 1974. **16**(4): p. 209-239.
78. Williams, F.W., *Approximations in Complicated Critical Buckling and Free Vibration Analyses of Prismatic Plate Structures.* The Aeronautical Quarterly, 1974. **25**(3): p. 180-185.
79. Anderson, M.S., Hennessy, K. W., and Heard, W. L. Jr., *Addendum to User's Guide to VIPASA (Vibration and Instability of Plate Assemblies Including Shear and Anisotropy)*. NASA TM X-73914. 1976, National Aeronautics and Space Administration: Washington, DC.
80. Almroth, B.O., and Brogan, F. A., *The STAGS Computer Code*. NASA CR-2950. 1978, NASA Langley Research Center: Hampton, VA.
81. Moore, R.E., *Interval Analysis*. Prentice-Hall Series in Automatic Computation, ed. G. Forsythe. 1966, Englewood Cliffs, NJ: Prentice-Hall, Inc.
82. Ratschek, H., *Inclusion Functions and Global Optimization.* Mathematical Programming, 1985. **33**(3): p. 300-317.
83. Moore, R.E., and Ratschek, H., *Inclusion Functions and Global Optimization II.* Mathematical Programming, 1988. **41**(3): p. 341-356.
84. Törn, A., and Zilinskas, A., *Global Optimization*. Lecture Notes in Computer Science, ed. G. Goos, and Hartmanis, J. 1989, Berlin, Germany: Springer-Verlag.
85. Brooks, S.H., *A Discussion of Random Methods for Seeking Maxima.* Operations Research, 1958. **6**(2): p. 244-251.
86. Rastrigin, L.A., *Sequential Binary Random Search in Problems of Stochastic Programming.* Soviet Journal of Computer and Systems Science, 1987. **25**(5): p. 163-172.

87. Rinnooy Kan, A.H.G., and Timmer, G. T., *Stochastic Methods for Global Optimization.* American Journal of Mathematical and Management Sciences, 1984. **4**(1-2): p. 7-40.
88. Metropolis, N., Rosenbluth, A., Rosenbluth, M., Teller, A., and Teller, E., *Equation of State Calculations by Fast Computing Machines.* Journal of Chemical Physics, 1953. **21**(6): p. 1087-1090.
89. Pincus, M., *A Monte Carlo Method for the Approximate Solution of Certain Types of Constrained Optimization Problems.* Operations Research, 1970. **18**(6): p. 1225-1228.
90. Kirkpatrick, S., Gelatt, C. D., Jr., and Vecchi, M. P., *Optimization by Simulated Annealing.* Science, 1983. **220**(4598): p. 671-680.
91. Černý, V., *Thermodynamical Approach to the Traveling Salesman Problem: An Efficient Simulation Algorithm.* Journal of Optimization: Theory and Applications, 1985. **45**(1): p. 41-52.
92. Aarts, E., and Korst, J., *Simulated Annealing and Boltzmann Machines - A Stochastic Approach to Combinatorial Optimization and Neural Computers*. Wiley-Interscience Series in Discrete Mathematics and Optimization, ed. R.L. Graham, Lenstra, J. K., and Tarjan, R. E. 1989, New York, NY: John Wiley & Sons Ltd.
93. van Laarhoven, P.J.M., and Aarts, E. H. L., *Simulated Annealing: Theory and Applications*. Mathematics and Its Applications, ed. M. Hazewinkel. 1987, Dordrecht, The Netherlands: D. Reidel Publishing Co.
94. Dekkers, A., and Aarts, E., *Global Optimization and Simulated Annealing.* Mathematical Programming, 1991. **50**(3): p. 367-393.
95. Collins, N.E., Egelese, R. W., and Golden, B. L., *Simulated Annealing--An Annotated Bibliography.* American Journal of Mathematical and Management Sciences, 1988. **8**(3-4): p. 209-307.
96. Darwin, C., *On The Origin of Species by Means of Natural Selection*. 1st ed. 2003, New York, NY: Everyman's Library, Alfred A. Knopf.
97. Engelbrecht, A.P., *Fundamentals of Computational Swarm Intelligence*. 2005, Chichester, England: John Wiley & Sons, Ltd.
98. Reynolds, R.G. *An Introduction to Cultural Algorithms*. in *Proceedings of the 3rd Annual Conference on Evolutionary Programming*. 1994. San Diego, CA: World Scientific Publishing Co. p. 131-139.
99. Holland, J.H., *Adaptation of Natural and Artificial Systems: An Introductory Analysis with Applications to Biology, Control, and Artificial Intelligence*. 1992, Cambridge, MA: The MIT Press.
100. Michalewicz, Z., and Janikow, C. Z., *Genetic Algorithms for Numerical Optimization.* Statics and Computing, 1991. **1**(2): p. 75-91.
101. Michalewicz, Z., *Genetic Algorithms + Data Structures = Evolution Programs*. 3rd ed. 1996, Berlin, Germany: Springer-Verlag.
102. Mühlenbein, H., Gorges-Schleuter, M., and Krämer, O., *New Solutions to the Mapping Problem of Parallel Systems: The Evolution Approach.* Parallel Computing, 1987. **4**(3): p. 269-279.
103. Stroud, W.J., and Anderson, M. S., *PASCO: Structural Panel Analysis and Sizing Code, Capability and Analytical Foundations*. NASA TM-80181. 1981, NASA Langley Research Center: Hampton, VA.

104. Anderson, M.S., Stroud, W. J., Durling, B. J., and Hennessy, K. W., *PASCO: Structural Panel Analysis and Sizing Code, User's Manual*. NASA TM-80182. 1981, NASA Langley Research Center: Hampton, VA.
105. Dickson, J.N., and Biggers, S. B., *POSTOP: Postbuckled Open-Stiffened Optimum Panels--Theory and Capability*. NASA-CR-172259. 1984, National Aeronautics and Space Administration: Hampton, VA.
106. Biggers, S.B., and Dickson, J. N., *POSTOP: Postbuckled Open-Stiffened Optimum Panels--User's Manual*. NASA CR-172260. 1984, National Aeronautics and Space Administration: Hampton, VA.
107. Vanderplaats, G.N., *ADS: A Fortran Program for Automated Design Synthesis--Version 1.10*. 1985.
108. Anonymous, *Design Optimization Tools (DOT) User's Manual*, in *DOT User's Manual, Version 5.0*. 1999, Vanderplaats Research & Development, Inc.: Colorado Springs, CO.
109. Bushnell, D., *PANDA2: Program for Minimum Weight Design of Stiffened, Composite, Locally Buckled Panels.* Computers and Structures, 1987. **25**(4): p. 469-605.
110. Bushnell, D., *BOSOR4: Program for Stress, Buckling, and Vibration of Complex Shells of Revolution*, *Structural Mechanics Software Series*, N. Perrone, Pilkey, W., and Pilkey, B., Editors. 1977, University Press of Virginia: Charolttesville, VA. p. 11-131.
111. Bushnell, D., *Computerized Buckling Analysis of Shells*. Mechanics of Elastic Stability, ed. H.H.E. Leipholz, and Oravas, G. Æ. 1985, Dordrecht, The Netherlands: Martinus Nijhoff Publishers.
112. Bushnell, D., *PANDA--Interactive Program for Minimum Weight Design of Stiffened Cylindrical Panels and Shells.* Computers and Structures, 1983. **16**(1-4): p. 167-185.
113. Bushnell, D., *Theoretical Basis of the PANDA Computer Program for Preliminary Design of Stiffened Panels Under Combined In-Plane Loads.* Computers and Structures, 1987. **27**(4): p. 541-563.
114. Bushnell, D., and Rankin, C. *Optimization of Perfect and Imperfect Ring and Stringer Stiffened Cylindrical Shells with PANDA2 and Evaluation of the Optimum Designs with STAGS*. *Proceedings of the 43rd AIAA/ASME/ASCE/AHS/ASC Structures, Structural Dynamics, and Materials Conference*. 2002. Denver, CO: American Institute of Aeronautics and Astronautics. AIAA Paper 2002-1408.
115. Hartmanis, J., and Stearns, R. E., *On the Computational Complexity of Algorithms.* Transactions of the American Mathematical Society, 1965. **117**: p. 285-306.
116. Nemirovsky, A.S., and Yudin, D. B., *Chapter 2: Convex Programming. Linearly Convergent Methods for Classes of General Convex Problems*, *Problem Complexity and Method Efficiency in Optimization*, E.R. Dawson, Editor. 1983, John Wiley & Sons, Inc.: Chichester, UK. p. 42-82.
117. Vavasis, S.A., *Nonlinear Optimization: Complexity Issues*. The International Series of Monographs on Computer Science, ed. D.M. Gabbay, Hopcroft, J. E., Plotkin, G. D., Schwartz, J. T., Scott, D. S., and Vuillemin, J. 1991, New York, NY: Oxford University Press.
118. Vavasis, S.A., *Complexity Issues in Global Optimization: A Survey*, in *Handbook of Global Optimization*, R. Horst, and Pardalos, P. M., Editor. 1995, Kluwer Academic Publishers: Dordrecht, The Netherlands. p. 27-41.
119. Stephens, C.P., and Baritompa, W., *Global Optimization Requires Global Information.* Journal of Optimization: Theory and Applications, 1998. **96**(3): p. 575-588.

120. Zabinsky, Z.B., Smith, R. L., McDonald, J. F., Romeijn, H. E., and Kaufman, D. E., *Improving Hit-and-Run for Global Optimization.* Journal of Global Optimization, 1993. **3**(2): p. 171-192.
121. Zabinsky, Z.B. *Global Optimization for Composite Structural Design*. *Proceedings of the 35th AIAA/ASME/ASCE/AHS/ACS Structures, Structural Dynamics, and Materials Conference*. 1994. Hilton Head, SC: American Institute of Aeronautics and Astronautics. p. 1406-1412.
122. Ingber, L., *Simulated Annealing: Practice versus Theory.* Mathematical and Computer Modelling, 1993. **18**(11): p. 29-57.
123. Bonomi, E., and Lutton, J.-L., *The N-City Travelling Saleman Problem: Statistical Mechanics and the Metropolis Algorithm.* SIAM Review, 1984. **26**(4): p. 551-568.
124. Peterson, C., and Söderberg, B., *Chapter 7: Artificial Neural Networks*, *Local Search in Combinatorial Optimization*, E.H.L. Aarts, and Lenstra, J. K., Editors. 1997, John Wiley & Sons: Chichester, West Sussex, UK. p. 173-213.
125. Bohr, H., and Brunak, S., *A Travelling Salesman Approach to Protein Conformation.* Complex Systems, 1989. **3**(1): p. 9-28.
126. Rothman, D.H., *Nonlinear Inversion, Statistical Mechanics, and Residual Statics Estimation.* Geophysics, 1985. **50**(12): p. 2784-2796.
127. Goffe, W.L., Ferrier, G. D., and Rogers, J., *Global Optimization of Statistical Functions with Simulated Annealing.* Journal of Econometrics, 1994. **60**(1-2): p. 65-99.
128. Kuperman, W.A., Collins, M. D., Perkins, J. S., and Davis, N. R., *Optimal Time-Domain Beamforming with Simulated Annealing Including Application of a priori Information.* Journal of the Acoustical Society of America, 1990. **88**(4): p. 1802-1810.
129. Romeijn, H.E., and Smith, R. L., *Simulated Annealing and Adaptive Search in Global Optimization.* Probability in the Engineering and Informational Sciences, 1994. **8**(4): p. 571-590.
130. Romeijn, H.E., and Smith, R. L., *Simulated Annealing for Constrained Global Optimization.* Journal of Global Optimization, 1994. **5**: p. 101-126.
131. Smith, R.L., *Efficient Monte Carlo Procedures for Generating Points Uniformly Distributed Over Bounded Regions.* Operations Research, 1984. **32**(6): p. 1296-1308.
132. Romeijn, H.E., Zabinsky, Z. B., Graesser, D. L., and Neogi, S., *New Reflection Generator for Simulated Annealing in Mixed Integer/Continuous Global Optimization.* Journal of Optimization: Theory and Applications, 1999. **101**(2): p. 403-427.
133. Ingber, L., and Rosen, B., *Genetic Algorithms and Very Fast Simulated Annealing: A Comparison.* Mathematical and Computer Modelling, 1992. **16**(11): p. 87-100.
134. Ingber, L., *Very Fast Simulated Re-Annealing.* Mathematical and Computer Modelling, 1989. **12**(8): p. 967-973.
135. Fox, B.L., *Integrating and Accelerating Tabu Search, Simulated Annealing, and Genetic Algorithms.* Annals of Operations Research, 1993. **41**(1-4): p. 47-67.
136. Glover, F., *Tabu Search--Part I.* ORSA Journal on Computing, 1989. **1**(3): p. 190-206.
137. Glover, F., *Tabu Search--Part II.* ORSA Journal on Computing, 1990. **2**(1): p. 4-32.
138. Glover, F., and Laguna, M., *Chapter 3: Tabu Search*, in *Modern Heuristic Techniques for Combinatorial Problems*, C.R. Reeves, Editor. 1993, Halsted Press: New York, NY. p. 70-150.
139. Koehler, G.J., *New Directions in Genetic Algorithm Theory.* Annals of Operations Research, 1997. **75**: p. 49-68.

140. Wolpert, D.H., and Macready, W. G., *No Free Lunch Theorems for Search*. 95-02-010. 1995, Santa Fe Institute: Santa Fe, NM.
141. Wolpert, D.H., and Macready, W. G., *No Free Lunch Theorems for Optimization.* IEEE Transactions on Evolutionary Computation, 1997. **1**(1): p. 67-82.
142. Vose, M.D., *The Simple Genetic Algorithm: Foundations and Theory*. Complex Adaptive Systems, ed. J.H. Holland, Langton, C. G., and Wilson, S. W. 1999, Cambridge, MA: MIT Press.
143. Roy, R., and Parmee, I. C., *An Overview of Evolutionary Computing for Multimodal Function Optimisation*, *Soft Computing in Engineering Design and Manufacturing: Proceedings of the 2nd World Conference on Soft Computing*, P.K. Chawdhry, Roy, R., and Pant, R. K., Editors. 1998, Springer-Verlag. p. 30-39.
144. Kennedy, J., and Eberhart, R. *Particle Swarm Optimization*. *Proceedings of the 1995 IEEE International Conference on Neural Networks*. 1995. Perth, Western Australia: Institute of Electrical and Electronics Engineers. p. 1942-1948.
145. Eberhart, R.C., and Kennedy, J. *A New Optimizer Using Particle Swarm Theory*. *Proceedings of the 6th International Symposium on Micro Machine and Human Science*. 1995. Nagoya, Japan: Institute of Electrical and Electronics Engineers. p . 39-43.
146. Reynolds, C.W., *Flocks, Herds, and Schools: A Distributed Behavioral Model.* Computer Graphics, 1987. **21**(4): p. 25-34.
147. Heppner, F., and Grenander, U., *A Stochastic Nonlinear Model for Coordinated Bird Flocks*, *The Ubiquity of Chaos*, S. Krasner, Editor. 1990, American Association for the Advancement of Science: Washington, DC.
148. Millonas, M.M., *Swarms, Phase Transitions, and Collective Intelligence*, *Artificial Life III: Proceedings of the Workshop on Artificial Life*, C.G. Langton, Editor. 1994, Addison Wesley Publishing Co.: Santa Fe, NM. p. 417-445.
149. Reeves, W.T., *Particle Systems - A Technique for Modeling a Class of Fuzzy Objects.* ACM Transactions on Graphics, 1983. **2**(2): p. 91-108.
150. Schutte, J.F., and Groenwold, A. A. *Optimal Sizing Design of Truss Structures Using the Particle Swarm Optimization Algorithm*. *Proceedings of the 9th AIAA/ISSMO Symposium and Exhibit on Multidisciplinary Analysis and Optimization*. 2002. Atlanta, GA: American Institute of Aeronautics and Astronautics. AIAA 2002-5639.
151. Venter, G., and Sobieszczanski-Sobieski, J. *Multidisciplinary Optimization of a Transport Aircraft Wing Using Particle Swarm Optimization*. *Proceedings of the 9th AIAA/ISSMO Symposium and Exhibit on Multidisciplinary Analysis and Optimization*. 2002. Atlanta, GA: American Institute of Aeronautics and Astronautics. AIAA 2002-5644.
152. Venter, G., and Sobieszczanski-Sobieski, J., *Multidisciplinary Optimization of a Transport Aircraft Wing Using Particle Swarm Optimization.* Structural and Multidisciplinary Optimization, 2004. **26**(1-2): p. 121-131.
153. AIAA Technical Committee on Multidisciplinary Design Optimization (MDO), *Current State of the Art: Multidisciplinary Design Optimization*. 1991, American Institute of Aeronautics and Astronautics: Washington, DC.
154. Sobieszczanski-Sobieski, J., and Haftka, R. T., *Multidisciplinary Design Optimization: Survey of Recent Developments.* Structural Optimization, 1997. **14**(1): p. 1-23.

155. Morris, A.J. *Distributed MDO: The Way of the Future*. *Proceedings of the CEAS Conference on Multidisciplinary Aircraft Design and Optimisation*. 2001. Köhn, Germany.
156. Marler, R.T., and Arora, J. S., *Survey of Multi-Objective Optimization Methods for Engineering.* Structural and Multidisciplinary Optimization, 2004. **26**(6): p. 369-395.
157. Kortanek, K.O., *Chapter 1: On the 1962-1972 Decade of Semi-Infinite Programming: A Subjective View*, *Semi-Infinite Programming: Recent Advances*, M.Á. Goberna, and López, M. A., Editors. 2001, Kluwer Academic Publishers: Dordrecht, The Netherlands. p. 3-41.
158. Geletu, A., and Hoffmann, A., *A Conceptual Method for Solving Generalized Semi-Infinite Programming Problems via Global Optimization by Exact Discontinuous Penalization.* European Journal of Operations Research, 2004. **157**(1): p. 3-15.
159. Wolkowicz, H., Saigal, R., and Vandenberghe, L., *Chapter 1: Introduction*, *Handbook of Semidefinite Programming: Theory, Algortihms, and Applications*, H. Wolkowicz, Saigal, R., and Vandenberghe, L., Editors. 2000, Kluwer Academic Publishers: Boston, MA. p. 1-8.
160. Ben-Tal, A., and Nemirovski, A., *Chapter 15: Structural Design*, *Handbook of Semidefinite Programming: Theory, Algortihms, and Applications*, H. Wolkowicz, Saigal, R., and Vandenberghe, L., Editors. 2000, Kluwer Academic Publishers: Boston, MA. p. 443-467.
161. Box, G.E.P., Hunter, W. G., and Hunter, J. S., *Statistics for Experimenters: An Introduction to Design, Data Analysis, and Model Building*. Wiley Series in Probability and Mathematical Statistics, ed. R.A. Bradley, Hunter, J. S., Kendall, D. G., and Watson, G. S. 1978, New York, NY: John Wiley & Sons.
162. Myers, R.H., and Montgomery, D. C., *Response Surface Methodology: Process and Product Optimization Using Design Experiments*. 2nd ed. Wiley Series in Probability and Statistics, ed. P. Bloomfield, Cressie, N. A. C., Fisher, N. I., Johnstone, I. M., Kadane, J. B., Ryan, L. M., Scott, D. W., Silverman, B. W., Smith, A. F. M., and Teugels, J. L. 2002, New York, NY: John Wiley & Sons, Inc.
163. Booker, A.J., Dennis, J. E. Jr., Frank, P. D., Serafini, D. B., Torczon, V., and Trosset, M. W., *A Rigorous Framework for Optimization of Expensive Functions by Surrogates.* Structural Optimization, 1999. **17**(1): p. 1-13.
164. Simpson, T.W., Mauery, T. M., Korte, J. J., and Mistree, F. *Comparison of Resonse Surface and Kriging Models for Multidisciplinary Design Optimization*. in *Proceedings of the 7th AIAA/USAF/NASA/ISSMO Symposium on Multidisciplinary Analysis and Optimization*. 1998. St. Louis, MO: American Institute of Aeronautics and Astronautics. p. 381-391.
165. Engelund, S., and Rackwitz, R., *A Benchmark Study on Importance Sampling Techniques in Structural Reliability.* Structural Safety, 1993. **12**: p. 255-276.
166. Venter, G., Haftka, R. T., and Starnes, J. H. Jr. *Construction of Response Surfaces for Design Optimization Applications*. *Proceedings of the 6th AIAA/NASA/ISSMO Symposium on Multidisciplinary Analysis and Optimization*. 1996. Bellevue, WA: American Institute of Aeronautics and Astronautics. p. 548-564.
167. Chen, M.-H., and Schmeiser, B. W., *General Hit-and-Run Monte Carlo Sampling for Evaluating Multidimensional Integrals.* Operations Research Letters, 1996. **19**(4): p. 161-169.

168. Jin, R., Chen, W., and Simpson, T. W., *Comparative Studies of Metamodelling Techniques under Multiple Modelling Criteria.* Structural and Multidisciplinary Optimization, 2001. **23**(1): p. 1-13.
169. Barthelemy, J.-F.M., and Haftka, R. T., *Approximation Concepts for Optimum Structural Design--A Review.* Structural Optimization, 1993. **5**(3): p. 129-144.
170. Williams, F.W., Kennedy, D., and Anderson, M. S. *Analysis Features of VICONOPT, an Exact Buckling and Vibration Program for Prismatic Assemblies of Anisotropic Plates*. *Proceedings of the 31st AIAA/ASME/ASCE/AHS Structures, Structural Dynamics, and Materials Conference*. 1990. Long Beach, CA: American Institute of Aeronautics and Astronautics. p. 920-929.
171. Butler, R., and Williams, F. W. *Optimum Design Features of VICONOPT, an Exact Buckling Program for Prismatic Assemblies of Anisotropic Plates*. *Proceedings of the 31st AIAA/ASME/ASCE/AHS Structures, Structural Dynamics, and Materials Conference*. 1990. Long Beach, CA: American Institute of Aeronautics and Astronautics. p. 1289-1299.
172. Williams, F.W., Kennedy, D., Butler, R., and Anderson, M. S., *VICONOPT: Program for Exact Vibration and Buckling Analysis or Design of Prismatic Plate Assemblies.* AIAA Journal, 1991. **29**(11): p. 1927-1928.
173. Butler, R., and Williams, F. W., *Optimum Design Using VICONOPT, a Buckling and Strength Constraint Program for Prismatic Assemblies of Anisotropic Plates.* Computers and Structures, 1992. **43**(4): p. 699-708.
174. Butler, R., and Williams, F. W., *Optimum Buckling Design of Compression Panels Using VICONOPT.* Structural Optimization, 1993. **6**(3): p. 160-165.
175. Fischer, M., Kennedy, D., and Featherston, C. A. *Multilevel Optimization of a Composite Aircraft Wing Using VICONOPT MLO*. *Proceedings of the 9th AIAA/ISSMO Symposium and Exhibit on Multidisciplinary Analysis and Optimization*. 2002. Atlanta, GA: American Institute of Aeronautics and Astronautics. AIAA 2002-5511.
176. Mabson, G.E., Ilcewicz, L. B., Graesser, D. L., Metschan, S. L., Proctor, M. R., Tervo, D. K., Tuttle, M. E., and Zabinsky, Z. B., *Cost Optimization Software for Transport Aircraft Design Evaluation (COSTADE)--Overview*. NASA CR-4736. 1996, NASA Langley Research Center: Hampton, VA.
177. Mabson, G.E., and Graesser, D. L., *Cost Optimization Software for Transport Aircraft Design Evaluation (COSTADE)--User's Manual*. NASA CR-4738. 1996, NASA Langley Research Center: Hampton, VA.
178. Ilcewicz, L.B., Mabson, G. E., Metschan, S. L., Swanson, G. D., Proctor, M. R., Tervo, D. K., Fredrikson, H. G., Gutowski, T. G., Neoh, E. T., and Polgar, K. C., *Cost Optimization Software for Transport Aircraft Design Evaluation (COSTADE)--Design Cost Methods*. NASA CR-4737. 1996, NASA Langley Research Center: Hampton, VA.
179. Proctor, M.R., Metschan, S. L., and Klein, H. S., *Cost Optimization Software for Transport Aircraft Design Evaluation (COSTADE)--Process Cost Analysis Database (PCAD) v. 2.0 User's Manual*. NASA CR-4739. 1996, NASA Langley Research Center: Hampton, VA.
180. Moore, G.J., *Nastran Design Sensitivity and Optimization*, *MSC/Nastran Design Sensitivity and Optimization*. 1994, MacNeal-Schwendler Corp.: Los Angeles, CA.

181. Barker, D.K., Johnson, J. C., Johnson, E. H., and Layfield, D. P. *Integration of External Design Criteria with MSC.Nastran Structural Analysis and Optimization*. *Proceedings of the MSC 3rd Worldwide Aerospace Users Conference and Technology Showcase*. 2001.
182. Anonymous, *Genesis User's Manual*, in *GENESIS User's Manual, Vol. 1*. 2001, Vanderplaats Research & Development, Inc.: Colorado Springs, CO.
183. Leiva, J.P., Ghosh, D. K., and Rastogi, N. *A New Approach in Stacking Sequence Optimization of Composite Laminates Using GENESIS Structural Analysis and Optimization Software*. *Proceedings of the 9th AIAA/ISSMO Symposium and Exhibit on Multidisciplinary Analysis and Optimization*. 2002. Atlanta, GA: American Institute of Aeronautics and Astronautics. AIAA 2002-5451.
184. Leiva, J.P., Watson, B. C., Kosaka, I., and Vanderplaats, G. N. *Dynamic Finite Element Analysis and Optimization in GENESIS*. *Proceedings of the 9th AIAA/ISSMO Symposium and Exhibit on Multidisciplinary Analysis and Optimization*. 2002. Atlanta, GA: American Institute of Aeronautics and Astronautics. AIAA 2002-5645.
185. Rastogi, N., Ghosh, D. K., and Vanderplaats, G. N. *Discrete Optimization Capabilities in GENESIS Structural Analysis and Optimization Software*. *Proceedings of the 9th AIAA/ISSMO Symposium and Exhibit on Multidisciplinary Analysis and Optimization*. 2002. Atlanta, GA: American Institute of Aeronautics and Astronautics. AIAA 2002-5646.
186. Anonymous, *Formal vs. Discrete Optimization and HyperSizer*. 1997, Collier Research Corp.: Hampton, VA.
187. Collier, C.S. *Next Generation Structural Optimization Today*. in *Proceedings of the MSC 1997 Aerospace Users' Conference*. 1997. MacNeal-Schwendler Corp.
188. Collier, C.S., Yarrington, P., and Pickenheim, M. *Design Optimization Using HyperSizer™*. in *Proceedings of the MSC 1998 Americas Users' Conference*. 1998. MacNeal-Schwendler Corp.
189. Collier, C.S., Yarrington, P., and Pickenheim, M. *The HyperSizing Method for Structures*. *Proceedings of the NAFEMS World Congress '99*. 1999. International Association for the Engineering Analysis Community.
190. Collier, C.S., Yarrington, P., and Pickenheim, M., *2000 HyperSizer Method Paper: Analysis and Optimization of the Grid-Stiffened Family of Panel Concepts*. 2000.
191. Anonymous, *HyperSizer® Pro 3.0 Brochure*, in *HyperSizer® Pro 3.0 Brochure*. 2000, Collier Research Corp.: Hampton, VA.
192. Anonymous, *HyperSizer Integrated TPS--Structure Sizing*. 2000, Collier Research Corp.: Hampton, VA.
193. Anonymous, *HyperSizer Version 3.0 Presentation*. 2000, Collier Research Corp.: Hampton, VA.
194. Anonymous, *HyperSizer® Basic and Pro v. 3.0 Specifications*. 2000, Collier Research Corp.: Hampton, VA.
195. Anonymous, *HyperSizer Presentation: Optimization Approach*. 2002, Collier Research Corp.: Hampton, VA.
196. Anonymous, *HyperSizer Presentation: Coupling to FEA*. 2002, Collier Research Corp.: Hampton, VA.
197. Collier, C., *Consistent Structural Integrity and Efficient Certification with Analysis, Volume 1: Executive Summary, Implemented Solution, and Industry Applications*.

AFRL-VA-WPTR-2005-3033. 2005, Air Force Research Laboratory: Wright-Patterson AFB, OH.
198. Collier, C., *Consistent Structural Integrity and Efficient Certification with Analysis, Volume 2: Detailed Report on Innovative Research Developed, Applied, and Commercially Available*. AFRL-VA-WPTR-2005-3034. 2005, Air Force Research Laboratory: Wright-Patterson AFB, OH.
199. Collier, C., Veley, D., and Owens, S. *Virtual Testing with Validated Analysis Tools*. *Proceedings of the NATO AVT Symposium*. 2002. Paris, France.
200. Collier, C., and Yarrington, P. *Consistent Structural Integrity in Preliminary Design Using Experimentally Validated Analysis*. *Proceedings of the 46th AIAA/ASME/ASCE/AHS/ASC Structures, Structural Dynamics, and Materials Conference*. 2005. Austin, TX: American Institute of Aeronautics and Astronautics. AIAA Paper 2005-2366.
201. Bednarcyk, B.A., Yarrington, P. W., Collier, C. S., and Arnold, S. M. *Progressive Failure Analysis of Composite Stiffened Panels*. *Proceedings of the 47th AIAA/ASME/ASCE/AHS/ASC Structures, Structural Dynamics, and Materials Conference*. 2006. Newport, RI: American Institute of Aeronautics and Astronautics. AIAA Paper No. 06-1643.
202. Collier, C., Yarrington, P., Pickenheim, M., and Bednarcyk, B. *An Approach to Preliminary Design and Analysis*. *Proceedings of the 48th AIAA/ASME/ASCE/AHS/ASC Structures, Structural Dynamics, and Materials Conference*. 2007. Honolulu, HI: American Institute of Aeronautics and Astronautics. AIAA Paper No. 2007-2176.
203. Bednarcyk, B.A., Aboudi, J., Yarrington, P. W., and Collier, C. S. *Simplified Shear Solution for Determination of the Shear Stress Distribution in a Composite Panel from the Applied Shear Resultant*. *Proceedings of the 49th AIAA/ASME/ASCE/AHS/ASC Structures, Structural Dynamics, and Materials Conference*. 2008. Schaumburg, IL: American Institute of Aeronautics and Astronautics. AIAA Paper No. 2008-2168.
204. Anonymous. *HyperFEATM Brochure*. 2006. Accessed January 21, 2008. Available from: http://www.hypersizer.com/documents/brochure_HyperFEA.pdf.
205. Anonymous. *HyperSizer® Structural Analysis and Sizing Approach*. 2006. Accessed January 21, 2008. Available from: http://www.hypersizer.com/pdf/brochure_Progressive_Design.pdf.
206. Anonymous. *VisualDOC: VR&D's Next Generation Design Optimization Software System*. version 5.1. 2006. Accessed October 25, 2006. Available from: http://www.vrand.com/visualDOC.html.
207. Koch, P.N., Evans, J. P., and Powell, D., *Interdigitation for Effective Design Space Exploration using iSIGHT*. Structural and Multidisciplinary Optimization, 2002. **23**(2): p. 111-126.
208. Anonymous. *iSIGHT Version 9.0 Product Overview*. version 9.0. 2006. Accessed October 25, 2006. Available from: http://www.engineous.com/product_iSIGHT.htm.
209. Anonymous. *LMS Solutions Guide: LMS Virtual.Lab Optimization*. 2006. Accessed October 25, 2006. Available from: http://www.lmsintl.com/simulation/virtuallab/optimization.
210. Leary, S.J., Birtwell, P. M., Holden, H., and Johnson, G. A. *The Efficient Multi-Objective Design of Air-Vehicle Configurations using ModelCenter*. *Proceedings of the 11th AIAA/ISSMO Multidisciplinary Analysis and Optimization Conference*. 2006.

Portsmouth, VA: American Institue of Aeronautics and Astronautics. AIAA Paper No. 2006-6946.
211. Hong, U.P., Hwang, K. H., and Park, G. J., *A Comparative Study of Software Systems from the Optimization Viewpoint.* Structural and Multidisciplinary Optimization, 2004. **27**(6): p. 460-468.
212. Su, J., and Renaud, J., *Automatic Differentiation in Robust Optimization.* AIAA Journal, 1997. **35**(6): p. 1072.
213. Allen, M., and Maute, K. *Reliability-Based Design Optimization of Aeroelastic Structures*. *Proceedings of the 9th AIAA/ISSMO Symposium and Exhibit on Multidisciplinary Analysis and Optimization*. 2002. Atlanta, GA: American Institute of Aeronautics and Astronautics. AIAA 2002-5560.
214. Vittal, S., and Hajela, P. *Approaches to Reliability Based Multicriteria Optimization*. *Proceedings of the 9th AIAA/ISSMO Symposium and Exhibit on Multidisciplinary Analysis and Optimization*. 2002. Atlanta, GA: American Institute of Aeronautics and Astronautics. AIAA 2002-5583.
215. Qu, X., and Haftka, R. T. *A Reliability-Based Design Optimization using Probabilistic Safety Factor*. *Proceedings of the 44th AIAA/ASME/ASCE/AHS/ASC Structures, Structural Dynamics, and Materials Conference*. 2003. Norfolk, VA: American Institute of Aeronautics and Astronautics. AIAA Paper 2003-1657.
216. Qu, X., Singer, T., and Haftka, R. T. *Reliability-Based Global Optimization of Stiffened Panels Using Probabilisitc Sufficiency Factor*. *Proceedings of the 45th AIAA/ASME/ASCE/AHS/ACS Structures, Structural Dynamics, and Materials Conference*. 2004. Palm Springs, CA: American Institute of Aeronautics and Astronautics. AIAA Paper 2004-1898.
217. Jones, D.R., Perttunen, C. D., and Stuckman, B. E., *Lipschitzian Optimization without the Lipschitz Constant.* Journal of Optimization: Theory and Applications, 1993. **79**(1): p. 157-181.
218. Cox, S.E., Hart, W. E., Haftka, R. T., and Watson, L. T. *DIRECT Algorithm with Box Penetration for Improved Local Convergence*. *Proceedings of the 9th AIAA/ISSMO Symposium and Exhibit on Multidisciplinary Analysis and Optimization*. 2002. Atlanta, GA: American Institute of Aeronautics and Astronautics. AIAA 2002-5581.
219. Singer, T.N., Qu, X., and Haftka, R. T. *Global Optimization of a Composite Tank Structure using the DIRECT Algorithm*. *Proceedings of the 18th Technical Conference of the American Society for Composites*. 2003. Gainesville, FL. Paper No. 2496.
220. Haftka, R.T. *Reflections on Jim Starnes' Technical Contributions*. *Proceedings of the 46th AIAA/ASME/ASCE/AHS/ASC Structures, Structural Dynamics, and Materials Conference*. 2005. Austin, TX: American Institute of Aeronautics and Astronautics. AIAA Paper 2005-1872.
221. Qu, X., Venkataraman, S., Haftka, R. T., and Johnson, T. F. *Response Surface Options for Reliability-Based Optimization of Composite Laminate*. *Proceedings of the 8th ASCE Specialty Conference on Probabilistic Mechanics and Structural Reliability*. 2000. South Bend, IN: University of Notre Dame.
222. Simpson, T.W., Toropov, V., Balabanov, V., and Viana, F. A. C. *Design and Analysis of Computer Experiments in Multidisciplinary Design Optimization: A Review of How Far We Have Come - Or Not*. *Proceedings of the 12th AIAA/ISSMO Multidisciplinary*

Analysis and Optimization Conference. 2008. Victoria, British Columbia, Canada: American Institute of Aeronautics and Astronautics. AIAA Paper No. 2008-5802.
223. Bach, T., Dähne, S., Heinrich, L., and Hühne, C., *Structural Optimization of Composite Wings in an Automated Multi-Disciplinary Environment*, *Proceedings of the 15th AIAA/ISSMO Multidisciplinary Analysis and Optimization Conference*. 2014, American Institute of Aeronautics and Astronautics: Atlanta, GA. AIAA 2014-2295.
224. Kennedy, G.J., Kenway, G. K. W., and Martins, J. R. R. A., *Towards Gradient-Based Design Optmization of Flexible Transport Aircraft with Flutter Constraints*, *Proceedings of the 15th AIAA/ISSMO Multidisciplinary Analysis and Optimization Conference*. 2014, American Institute of Aeronautics and Astronautics: Atlanta, GA. AIAA 2014-2726.
225. Kenway, G.K.W., and Martins, J. R. R. A., *Multipoint High-Fidelity Aerostructural Optimization of a Transport Aircraft Configuration.* Journal of Aircraft, 2014. **51**(1): p. 144-160.
226. Patel, N.R., Smith, R. L., and Zabinsky, Z. B., *Pure Adaptive Search in Monte Carlo Optimization.* Mathematical Programming, 1988. **43**(3): p. 317-328.
227. Zabinsky, Z.B., and Smith, R. L., *Pure Adaptive Search in Global Optimization.* Mathematical Programming, 1992. **53**(3): p. 323-338.
228. Zabinsky, Z.B., *Stochastic Adaptive Search for Global Optimization*. Nonconvex Optimization and Its Applications, ed. P. Pardalos. 2003, Boston, MA: Kluwer Academic Publishers. 1-224.
229. Zabinsky, Z.B., Graesser, D. L., Tuttle, M. E., and Kim, G. I., *Global Optimization of Composite Laminate Using Improving Hit and Run*, *Recent Advances in Global Optimization*, C.A. Floudas, and Pardalos, P. M., Editors. 1992, Princeton University Press: Princeton, NJ.
230. Bélisle, C.J.P., Romeijn, H. E., and Smith, R. L., *Hit-and-Run Algorithms for Generating Multivariate Distributions.* Mathematics of Operations Research, 1993. **18**(2): p. 255-266.
231. Berbee, H.C.P., Boender, C. G. E, Rinnoay Kan, A. H. G., Scheffer, C. L., Smith, R. L., and Telgen, J., *Hit-and-Run Algorithms for the Identification of Nonredundant Linear Inequalities.* Mathematical Programming, 1987. **37**(2): p. 184-207.
232. Neogi, S., Zabinsky, Z. B., and Tuttle, M. E. *Optimal Design of Composites Using Mixed Discrete and Continuous Variables*. *Processing, Design, and Performance of Composite Materials, Proceedings of the 1994 International Mechancial Engineering Congress and Exhibition*. 1994. Chicago, IL: American Society of Mechanical Engineers. p. 91-107.
233. Graesser, D.L., Zabinsky, Z. B., Tuttle, M. E., and Kim, G. I., *Designing Laminated Composites Using Random Search Techniques.* Composite Structures, 1991. **18**(4): p. 311-325.
234. Heglund, D.A., *Methodology for Efficient Random Search in the Optimization of Composite Laminate Designs*, MS Thesis, *Industrial Engineering*. 1992, University of Washington: Seattle, WA.
235. Del Moral, P., *Feynman-Kac Formulae: Genealogical and Interacting Particle Systems with Applications*. 2004, New York, NY: Springer-Verlag.
236. Feynman, R.P., *The Principle of Least Action in Quantum Mechanics*, Ph.D. Thesis, *Physics*. 1942, Princeton University: Princeton, NJ.
237. Kac, M., *On Distributions of Certain Wiener Functionals.* Transactions of the American Mathematical Society, 1949. **65**(1): p. 1-13.

238. Molvalioglu, O., *Interacting-Particle Algorithm and Meta-Control of Temperature Parameter*, Ph.D. Thesis, *Industrial Engineering*. 2007, University of Washington: Seattle, WA.
239. Hazen, M., and Gupta, M. R. *A Multiresolutional Estimated Gradient Architecture for Global Optimization*. *IEEE Congress on Evolutionary Computation (CEC '06)*. 2006. Vancouver, BC, Canada: Institute of Electrical and Electronics Engineers. p. 3013-3020.
240. Hazen, M.U., *Search Strategies for Global Optimization*, Ph.D. Thesis, *Electrical Engineering*. 2008, University of Washington: Seattle, WA.
241. Nelson, J.K., Hazen, M. U., and Gupta, M. R. *Global Optimization for Multiple Transmitter Localization*. *IEEE Military Communications Conference (MILCOM 2006)*. 2006. Washington, DC: Institute of Electrical and Electronics Engineers.
242. Hazen, M.U., and Gupta, M. R. *Gradient Estimation in Global Optimization Algorithms*. *IEEE Congress on Evolutionary Computation (CEC '09)*. 2009. Trondheim, Norway: Institute of Electrical and Electronics Engineers. p. 1841-1848.
243. Dolan, E.D., and Moré, J. J., *Benchmarking Optimization Software with Performance Profiles.* Mathematical Programming Series A, 2002. **A91**(2): p. 201-213.
244. Foye, R.L., *Advanced Design Concepts for Advanced Composite Airframes*. 1968, Air Force Materials Laboratory, Air Force Systems Command: Wright-Patterson Air Force Base, OH. p. 36-87.
245. Woods, W.J., and Sams III, J. H. *Geometric Optimization in the Theory of Structural Synthesis*. *Proceedings of the 9th AIAA/ASME Structures, Structural Dynamics, and Materials Conference*. 1968. Palm Springs, CA: American Institute of Aeronautics and Astronautics. AIAA 68-330.
246. Waddoups, M.E., *Structural Airframe Application of Advanced Composite Materials--Analytical Methods*. AFML-TR-69-101. 1969, Air Force Materials Laboratory, Research and Technology Division, Air Force Systems Command: Wright-Patterson Air Force Base, OH.
247. Waddoups, M.E., Jackson, S. K., and Rogers, C. W., *The Integration of Composite Structures into Aircraft Design.* Journal of Composite Materials, 1972. **6**(April): p. 174-190.
248. Schmit, L.A.J., and Farshi, B., *Optimum Laminate Design for Strength and Stiffness.* International Journal for Numerical Methods in Engineering, 1973. **7**(4): p. 519-536.
249. Baldur, R., *Structural Optimization by Inscribed Hyperspheres.* Journal of the Engineering Mechanics Division, ASCE, 1972. **98**(EM3): p. 503-518.
250. McCullers, L.A., and Lynch, R. W., *Dynamic Characteristics of Advanced Filamentary Composite Structures, Vol. II: Aeroelastic Synthesis Procedure Development*. AFFDL-TR-73-111. 1974, Air Force Flight Dynamics Laboratory, Vehicle Dynamics Division, Air Force Systems Command: Wright-Patterson Air Force Base, OH.
251. Vanderplaats, G.N., Weisshaar, T. A., *Optimum Design of Composite Structures.* International Journal for Numerical Methods in Engineering, 1989. **27**(2): p. 437-448.
252. Le Riche, R., and Haftka, R. T., *Optimization of Laminate Stacking Sequence for Buckling Load Maximization by Genetic Algorithm.* AIAA Journal, 1993. **31**(5): p. 951-956.
253. Kogiso, N., Watson, L. T., Gürdal, Z., Haftka, R. T., and Nagendra, S., *Design of Composite Laminates by a Genetic Algorithm with Memory.* Mechanics of Composite Materials and Structures, 1994. **1**(1): p. 95-117.

254. Soremekun, G., Gürdal, Z., Kassapoglou, C., and Toni, D., *Stacking Sequence Blending of Multiple Composite Laminates Using Genetic Algorithms.* Composite Structures, 2002. **56**(1): p. 53-62.
255. Gürdal, Z., Haftka, R. T., and Hajela, P., *Design and Optimization of Laminated Composite Materials*. 1999, New York, NY: John Wiley & Sons, Inc.
256. Jones, R.M., *Mechanics of Composite Materials*. 1975, New York, NY: McGraw-Hill Book Co.
257. Kirchhoff, G.R., *Vorlesungen über Mathematische Physik, Mechanik*. Landmarks of Science Series of Microcards, University of Oklahoma, Norman, OK, 1969. 1876, Leipzig, Germany: B. G. Teubner.
258. Vinson, J.R., and Sierakowski, R. L., *The Behavior of Structures Composed of Composite Materials*. Mechanics of Structural Systems. 1987, Dordrecht, The Netherlands: Kluwer Academic Publishers.
259. Lamberti, L., Venkataraman, S., Haftka, R. T., and Johnson, T. F., *Preliminary Design Optimization of Stiffened Panels using Approximate Analysis Models.* International Journal for Numerical Methods in Engineering, 2003. **57**(10): p. 1351-1380.
260. Stroud, W.J., and Agranoff, N., *Minimum-mass Design of Filamentary Composite Panels Under Combined Loadings: Design Procedure Based on Simplified Buckling Equations*. NASA TN D-8257. 1976, NASA Langley Research Center: Hampton, VA.
261. Stroud, W.J., Agranoff, N., and Anderson, M. S., *Minimum-Mass Design of Filamentary Composite Panels Under Combined Loads: Design Procedure Based on a Rigorous Buckling Analysis*. NASA TN D-8417. 1977, National Aeronautics and Space Administration: Washington, DC.
262. Stroud, W.J., Greene, W. H., and Anderson, M. S., *Buckling Loads for Stiffened Panels Subjected to Combined Longitudinal Compression and Shear: Results Obtained with PASCO, EAL, and STAGS Computer Programs*. NASA TP-2215. 1984, National Aeronautics and Space Administration: Washington, DC.
263. Leissa, A.W., *Buckling of Laminated Composite Plates and Shell Panels*. AFWAL-TR-85-3069. 1985, Flight Dynamics Laboratory, Air Force Wright Aeronautical Laboratories: Wright-Patterson Air Force Base, OH.
264. Eisenmann, J.R., *Advanced Composite Panel Optimization*. FZM-6118. 1973, Advanced Filaments and Composites Division, Air Force Materials Laboratory, Air Force Systems Command: Wright-Patterson Air Force Base, OH.
265. Timoshenko, S.P., and Woinowsky-Krieger, S., *Theory of Plates and Shells*. 2nd ed. Engineering Societies Monographs. 1959, New York, NY: McGraw-Hill Book Co.
266. Wu, Z.M., Raju, G., and Weaver, P. M., *Feasible Region of Lamination Parameters for Optimization of Variable Angle Tow (VAT) Composite Plates*, *Proceedings of the 54th AIAA/ASME/ASCE/AHS/ASC Structures, Structural Dynamics, and Materials Conference*. 2013, American Institute of Aeronautics and Astronautics: Boston, MA. AIAA 2013-1481.
267. Jensen, D.W., and Lagace, P. A., *Influence of Mechanical Couplings on the Buckling and Postbuckling of Anisotropic Plates.* AIAA Journal, 1988. **26**(10): p. 1269-1277.
268. Minguet, P.J., Dugundji, J., and Lagace, P., *Postbuckling Behavior of Laminated Plates Using a Direct Energy-Minimization Technique.* AIAA Journal, 1989. **27**(12): p. 1785-1792.

269. DiNardo, M.T., and Lagace, P. A., *Buckling and Postbuckling of Laminated Composite Plates with Ply Dropoffs.* AIAA Journal, 1989. **27**(10): p. 1392-1398.
270. Adali, S., Verijenko, V. E., and Walker, M., *Optimal Laminate Configurations with Symmetric Lay-ups for Maximum Postbuckling Stiffness.* Composites Engineering, 1994. **4**(11): p. 1119-1127.
271. Adali, S., Walker, M., and Verijenko, V. E., *Multiobjective Optimization of Laminated Plates for Maximum Prebuckling, Buckling, and Postbuckling Strength using Continuous and Discrete Ply Angles.* Composite Structures, 1996. **35**(1): p. 117-130.
272. Walker, M., Adali, S., and Verijenko, V. E., *Optimization of Symmetric Laminates for Maximum Buckling Load Including the Effects of Bending-Twisting Coupling.* Computers and Structures, 1996. **58**(2): p. 313-319.
273. Wang, B.P., and Costin, D. P. *Optimum Design of a Composite Structure with Ply-Interleaving Constraints*. *Proceedings of the 3rd Air Force / NASA Symposium on Recent Advances in Multidisciplinary Analysis and Optimization*. 1990. San Francisco, CA: Wright Research and Development Center. p. 553-561.
274. Kristinsdottir, B.P., *Incorporating Manufacturing Tolerances in Optimal Design of Composite Structures*, Ph.D. Thesis, *Mechanical Engineering*. 1993, University of Washington: Seattle, WA.
275. Bare, J.M., Kapur, K. C., and Zabinsky, Z. B., *Optimization Methods for Tolerance Design Using a First-Order Approximation for System Variance.* Engineering Design and Automation, 1996. **2**(3): p. 203-214.
276. Niu, C.Y.M., *Composite Airframe Structures: Practical Design Information and Data*. 2nd ed. 1993, Hong Kong: Conmilit Press Ltd.
277. Blasi, L., and Del Core, G., *Particle Swarm Approach in Finding Optimum Aircraft Configuration.* Journal of Aircraft, 2007. **44**(2): p. 679-683.
278. Tayal, M., and Wang, B. P. *Particle Swarm Optimization for Mixed Discrete, Integer, and Continuous Variables*. *Proceedings of the 10th AIAA/ISSMO Symposium on Multidisciplinary Analysis and Optimization*. 2004. Albany, NY: American Institute of Aeronautics and Astronautics. AIAA Paper 2004-4500.
279. Kathiravan, R., and Ganguli, R., *Strength Design of Composite Beam Using Gradient and Particle Swarm Optimization.* Composite Structures, 2007. **81**(4): p. 471-479.
280. Suresh, S., Sujit, P. B., and Rao, A. K., *Particle Swarm Optimization Approach for Multi-Objective Composite Box-Beam Design.* Composite Structures, 2007. **81**(4): p. 598-605.
281. Omkar, S.N., Mudigere, D., Narayana Naik, G., and Gopalakrishnan, S., *Vector Evaluated Particle Swarm Optimization (VESPO) for Multi-Objective Design Optimization of Composite Structures.* Computers and Structures, 2008. **86**(1-2): p. 1-14.
282. Turner, M.J., *Design of Minimum Mass Structures with Specified Natural Frequencies.* AIAA Journal, 1967. **5**(3): p. 406-412.
283. Dwyer, W.J., Emerton, R. K., and Sabatelli, P. L., *An Automated Procedure for the Optimization of Practical Aerospace Structures, Volume II: Programmer's Manual*, AFFDL-TR-70-118. 1971, Air Force Flight Dynamics Laboratory: Wright-Patterson AFB, OH.
284. Lynch, R.W., Rogers, W. A., Brayman, W. W., and Hertz, T. J., *Aeroelastic Tailoring of Advanced Composite Structures for Military Aircraft, Vol. III: Modifications and User's Guide for Procedure TSO*. AFFDL-TR-76-100. 1978, Air Force Fight Dynamics Laboratory: Wright-Patterson Air Force Base, OH.

285. Markowitz, J., and Isakson, G., *FASTOP-3: A Strength, Deflection, and Flutter Optimization Program for Metallic and Composite Structures*. AFFDL-TR-78-50, Vol. I: Theory and Application. 1978, Air Force Flight Dynamics Laboratory, Air Force Wright Aeronautical Laboratories: Wright-Patterson Air Force Base, OH.
286. Markowitz, J., and Isakson, G., *FASTOP-3: A Strength, Deflection, and Flutter Optimization Program for Metallic and Composite Structures*. AFFDL-TR-78-50, Vol. II: Program User's Guide. 1978, Air Force Flight Dynamics Laboratory, Air Force Wright Aeronautical Laboratories: Wright-Patterson Air Force Base, OH.
287. Moon, Y.I., *Geodesic Wing Structural Optimization and Dynamic Analysis*. ASIAC-TR-96-02. 1996, Flight Dynamics Directorate: Wright-Patterson AFB, OH.
288. Moon, Y.I., *Design Studies of Intermediate Complexity Wings*. ASIAC-TR-98-01. 1998, Flight Dynamics Directorate: Wright-Patterson AFB, OH.
289. Haftka, R.T., *Automated Procedure for Design of Wing Structures to Satisfy Strength and Flutter Requirements*. NASA TN D-7264. 1973, NASA: Washington, DC.
290. Wilkinson, K., Markowitz, J., Lerner, E., Chipman, R., George, D., et al., *An Automated Procedure for Flutter and Strength Analysis and Optimization of Aerospace Vehicles, Vol. I: Theory and Application*. AFFDL-TR-75-137. 1975, Air Force Flight Dynamics Laboratory: Wright-Patterson AFB, OH. p. 1-186.
291. Striz, A.G., and Lee, W. T. *Multidisciplinary Optimization of a Transport Aircraft Wing*. *Proceedings of the 5th AIAA/USAF/NASA/ISSMO Symposium on Multidisciplinary Analysis and Optimization*. 1994. Panama City Beach, FL: American Institute of Aeronautics and Astronautics. p. 1369-1376.
292. Yan, S., and Striz, A. G. *Comparative Evaluation of Two MDO Codes in Aircraft Wing Analysis and Optimization*. in *Proceedings of the 6th AIAA/NASA/ISSMO Symposium on Multidisciplinary Analysis and Optimization*. 1996. Bellevue, WA: American Institute of Aeronautics and Astronautics. p. 459-468.
293. Livne, E., *Integrated Multidisciplinary Optimization of Actively Controlled Fiber Composite Wings*, Ph.D. Thesis. *Aerospace Engineering*. 1990, University of California: Los Angeles, CA.
294. Livne, E., *Integrated Multidisciplinary Aeroservoelastic Synthesis: Background, Progress, and Challenges*, in *Multidisciplinary Design Optimization: State of the Art. Proceedings of the ICASE/NASA Langley Workshop on Multidisciplinary Design Optimization*, N.M. Alexandrov, and Hussaini, M. Y., Editors. 1997, Society of Industrial and Applied Mathematics: Hampton, VA. p. 45-76.
295. Engelsen, F., and Livne, E. *Design-Oriented Principal Stress/Strain Criteria Constraints for Actively Controlled Structures Subjected to Random Excitation*. *Proceedings of the 9th AIAA/ISSMO Symposium and Exhibit on Multidisciplinary Analysis and Optimization*. 2002. Atlanta, GA: American Institute of Aeronautics and Astronautics. AIAA 2002-5525.
296. Ragon, S.A., Gürdal, Z., Haftka, R. T., and Tzong, T. J. *Global/Local Structural Wing Design Using Response Surface Techniques*. *Proceedings of the 38th AIAA/ASME/ASCE/AHS/ASC Structures, Structural Dynamics, and Materials Conference*. 1997. Kissimmee, FL: American Institute of Aeronautics and Astronautics. p. 1204-1214.
297. Liu, B., and Haftka, R. T. *Composite Wing Structural Design Optimization with Continuity Constraints*. *Proceedings of the 42nd AIAA/ASME/ASCE/AHS/ASC*

Structures, Structural Dynamics, and Materials Conference. 2001. Seattle, WA: American Institute of Aeronautics and Astronautics. AIAA 01-1205.
298. Seresta, O., Gürdal, Z., Adams, D. B., and Watson, L. T. *Optimal Design of Composite Wing Structures with Blended Laminates*. *Proceedings of the 10th AIAA/ISSMO Symposium on Multidisciplinary Analysis and Optimization*. 2004. Albany, NY: American Institute of Aeronautics and Astronautics. AIAA Paper 2004-4349.
299. Seresta, O., Gürdal, Z., Adams, D. B., and Watson, L. T., *Optimal Design of Composite Wing Structures with Blended Laminates.* Composites, Part B: Engineering, 2007. **38**(4): p. 469-480.
300. Giles, G.L., *Further Generalization of an Equivalent Plate Representation for Aircraft Structural Synthesis.* Journal of Aircraft, 1989. **26**(1): p. 67-74.
301. Barthelemy, J.-F.M., and Hall, L. E. *Automatic Differentiation as a Tool in Engineering Design*. *Proceedings of the 4th AIAA/USAF/NASA/OAI Symposium on Multidisciplinary Analysis and Optimization*. 1992. Cleveland, OH: American Institute of Aeronautics and Astronautics. p. 424-432.
302. Bendsøe, M.P., *Optimization of Structural Topology, Shape, and Material*. 1995, Berlin, Germany: Springer-Verlag.
303. Samareh, J.A., *Survey of Shape Parameterization Techniques for High-Fidelity Multidisciplinary Shape Optimization.* AIAA Journal, 2001. **39**(5): p. 877-884.
304. Wilson, E.G.J., *Static Aeroelasticity in the Design of Modern Fighters*, *Static Aeroelasticity in Combat Aircraft, AGARD Report No. 725*. 1986, Advisory Group for Aerospace Research and Development, North Atlantic Treaty Organization: Neuilly sur Seine, France. p. 1-1--1-8.
305. Hajela, P. *A Root Locus Based Flutter Synthesis Procedure*. *Proceedings of the 21st AIAA Aerospace Sciences Meeting*. 1983. Reno, NV: American Institute of Aeronautics and Astronautics.
306. Snee, J.M.D., Zimmermann, H., Schierenbeck, D., and Heinze, P., *Simulataneous Stress and Flutter Optimization for the Wing of a Transport Aircraft Equipped with Four Engines*, *Proceedings of the 72nd Meeting of the Advisory Group for Aerospace Research and Development (AGARD) Structures and Materials Panel*. 1992, North Atlantic Treaty Organization: Bath, UK. p. 13-1--13-12.
307. Collar, A.R., *The First Fifty Years of Aeroelasticity*, *Aerospace*. 1978. p. 12-20.
308. Garrick, I.E., and Reed, W. H. III. *Historical Development of Flutter*. *Proceedings of the 22nd AIAA/ASME/ASCE/AHS Structures, Structural Dynamics, and Materials Conference*. 1981. Atlanta, GA: American Institute of Aeronautics and Astronautics. p. 381-401.
309. MIL-HDBK-17, *Composite Materials Handbook, Vol. 3: Polymer Matrix Composites Materials Usage, Design, and Analysis, Chapter 6: Structural Behavior of Joints, Section 6.3: Mechanically Fastned Joints*. 2002, Department of Defense, United States of America: Washington, DC. p. 6-49--6-71.
310. Whitman, B., Shyprykevich, P., and Whiteside, J. B., *Design of the B-1 Composite Horizontal Stabilizer Joints*, *Proceedings of the 3rd NASA/USAF Conference on Fibrous Composites in Flight Vehicles Design*. 1976, National Aeronautics and Space Administration: Williamsburg, VA. NASA TM X-3377.
311. Masters, J.E., *Introduction to Symposium on Bolted and Bonded Joints in Composite Materials.* Journal of Composites Technology and Research, 1995. **17**(3): p. 235.

312. Cohen, D., Hyer, M. W., Shuart, M. J., Griffin, O. H. Jr., Prasad, C. B., and Yalamanchili, S. R., *Failure Criterion for Thick Multifastener Graphite-Epoxy Composite Joints.* Journal of Composites Technology and Research, 1995. **17**(3): p. 237-248.
313. Collings, T.A., *Experimentally Determined Strength of Mechanically Fastened Joints*, in *Joining Fibre-Reinforced Plastics*, F.L. Matthews, Editor. 1987, Elsevier Applied Science: London, England. p. 9-63.
314. Shroff, S., and Kassapoglou, C., *Designing Highly Loaded Connections in a Composite Fuselage.* Journal of Aircraft, 2014. **51**(3): p. 833-840.
315. Matthews, F.L., *Theoretical Stress Analysis of Mechanically Fastened Joints*, in *Joining Fibre-Reinforced Plastics*, F.L. Matthews, Editor. 1987, Elsevier Applied Science: London, England. p. 65-103.
316. Hart-Smith, L.J., *Design and Experimental Analysis of Bolted or Rivited Joints*, in *Joining Fibre-Reinforced Plastics*, F.L. Matthews, Editor. 1987, Elsevier Applied Science: London, England. p. 227-269.
317. Lekhnitskii, S.G., *Anisotropic Plates*. 2nd ed, ed. S.W. Tsai, and Cheron, T. 1968, New York, NY: Gordon and Breach Science Publishers.
318. Stroh, A.N., *Dislocations and Cracks in Anisotropic Elasticity.* Philosophical Magazine, 1958. **3**(30): p. 625-646.
319. Stroh, A.N., *Steady State Problems in Anisotropic Elasticity.* Journal of Mathematics and Physics, 1962. **41**(2): p. 77-103.
320. Lekhnitskii, S.G., *Teoriya Uprugosti Anizotropnogo Tela (Theory of Elasticity of an Anisotropic Elastic Body)*, ed. J.J. Brandstatter. 1963, San Francisco, CA: Holden-Day, Inc.
321. Savin, G.N., *Stress Concentration Around Holes*. International Series of Monographs in Aeronautics and Astronautics, Division I: Solid and Structural Mechanics, ed. T. Von Kármán, and Dryden, H. L. Vol. 1. 1961, New York, NY: Pergamon Press.
322. Savin, G.N., Kosmodamianskii, A. S., and Guz, A. N., *Stress Concentration Near Holes.* Prikladnaya Mekhanika, 1967. **3**(10): p. 23-37.
323. Muskhelishvili, N.I., *Some Basic Problems of the Mathematical Theory of Elasticity*. 3rd ed. 1953, Groningen, the Netherlands: P. Noordhoff.
324. Tate, M.B., and Rosenfeld, S. J., *Preliminary Investigation of the Loads Carried by Individual Bolts in Bolted Joints*. NACA Technical Note No. 1051. 1946, National Advisory Committee for Aeronautics: Washington, DC.
325. Bhachu, K.S., Waycaster, G., Haftka, R. T., and Kim, N.-H., *Aircraft Tolerance Optimization Considering Quality, Manufacturing, and Performance*, *Proceedings of the 54th AIAA/ASME/ASCE/AHS/ASC Structures, Structural Dynamics, and Materials Conference*. 2013, American Institute of Aeronautics and Astronautics: Boston, MA. AIAA 2013-1465.
326. Hart-Smith, L.J., *Mechanically-Fastened Joints for Advanced Composites--Phenomenological Considerations and Simple Analyses*, *Proceedings of the Fourth Conference on Fibrous Composites in Structural Design*, E.M. Lenoe, Oplinger, D. W., and Burke, J. J., Editors. 1980, Plenum Press: San Diego, CA. p. 543-574.
327. Collings, T.A., *The Strength of Bolted Joints in Multi-Directional CFRP Laminates.* Composites, 1977. **8**(1): p. 43-55.

328. Collings, T.A., *On the Bearing Strengths of CFRP Laminates.* Composites, 1982. **12**(3): p. 241-252.
329. Ramkumar, R.L., Saether, E. S., and Cheng, D., *Design Guide for Bolted Joints in Composite Structures*. AFWAL-TR-86-3035. 1986, Flight Dynamics Laboratory, Air Force Wright Aeronautical Laboratories: Wright-Patterson Air Force Base, OH. p. 1-261.
330. Collings, T.A. *The Use of Bolted Connections as a Means of Joining Carbon Fibre Reinforced Plastics*. *Designing with Fibre Reinforced Materials*. 1977. London, England: Institution of Mechanical Engineers.
331. Collings, T.A., and Beauchamp, M. J., *Bearing Deflection Behaviour of a Loaded Hole in CFRP.* Composites, 1984. **15**(1): p. 33-38.
332. Oplinger, D.W., *On The Structural Behavior of Mechanically Fastened Joints In Composite Structures*, *Proceedings of the Fourth Conference on Fibrous Composites in Structural Design*, E.M. Lenoe, Oplinger, D. W., and Burke, J. J., Editors. 1980, Plenum Press: San Diego, CA. p. 575-602.
333. Naik, R.A., and Crews, J. H. Jr., *Stress Analysis Method for a Clearance-Fit Bolt Under Bearing Loads.* AIAA Journal, 1986. **24**(8): p. 1348-1353.
334. Crews, J.H.J., and Naik, R. A., *Combined Bearing and Bypass Loading on a Graphite/Epoxy Laminate.* Composite Structures, 1986. **6**(1-3): p. 21-40.
335. Harris, H.G., Ojalvo, I. U., and Hooson, R. E., *Stress and Deflection Analysis of Mechanically Fastened Joints*. AFFDL-TR-70-49. 1970, Air Force Flight Dynamics Laboratory: Wright-Patterson Air Force Base, OH.
336. Waddoups, M.E., Eisenmann, J. R., and Kaminski, B. E., *Macroscopic Fracture Mechanics of Advanced Composite Materials.* Journal of Composite Materials, 1971. **5**(10): p. 446-454.
337. Eisenmann, J.R., *Bolted Joint Static Strength Model for Composite Materials*, *Proceedings of the 3rd Conference on Fibrous Composites in Flight Vehicle Design*. 1976, NASA: Williamsburg, VA. p. 563-602.
338. Cruse, T.A., and Osias, J. R., *Exploratory Development on Fracture Mechanics of Composite Materials*. AFML-TR-74-111. 1974, Air Force Materials Laboratory, Air Force Systems Command: Wright-Patterson Air Force Base, OH.
339. Xiong, Y., *An Analytical Method for Failure Prediction of Multi-Fastener Composite Joints.* International Journal of Solids and Structures, 1996. **33**(29): p. 4395-4409.
340. Timoshenko, S.P., and Goodier, J. N., *Theory of Elasticity*. 3 ed. McGraw-Hill Classic Textbook Reissue Series. 1970, New York, NY: McGraw-Hill Book Co.
341. Kradinov, V., Madenci, E., and Ambur, D. R. *Combined In-Plane and Through-the-Thickness Analysis for Failure Prediction of Bolted Composite Joints*. *Proceedings of the 45th AIAA/ASME/ASCE/AHS/ACS Structures, Structural Dynamics, and Materials Conference*. 2004. Palm Springs, CA: American Institute of Aeronautics and Astronautics. AIAA Paper 2004-1703.
342. Kradinov, V., Madenci, E., and Ambur, D. R., *Combined In-Plane and Through-the-Thickness Analysis for Failure Prediction of Bolted Composite Joints.* Composite Structures, 2007. **77**(2): p. 127-147.
343. Kradinov, V., *Optimum Design of Bolted Composite Lap Joints Under Mechanical and Thermal Loading, Ph.D. Dissertation, Aerospace Engineering*. 2003, University of Arizona: Tuscon, AZ.

344. Chern, S.-M., *Analysis of Notched Composite Plates Under In-Plane Loading*. 1999, University of Washington: Seattle, WA. Ph.D. Mechanical Engineering.
345. Chern, S.M., and Tuttle, M. E., *On Displacement Fields in Orthotropic Laminates Containing an Elliptical Hole.* Journal of Applied Mechanics, 2000. **67**(3): p. 527-539.
346. Ogonowski, J.M., *Effect of Variances and Manufacturing Tolerances on the Design Strength and Life of Mechanically Fastened Composite Joints*. AFWAL-TR-81-3041. 1981, Flight Dynamics Laboratory, Air Force Wright Aeronautical Laboratories: Wright-Patterson Air Force Base, OH.
347. Bohlmann, R.E., Renieri, G. D., Horton, D. K., *Bolted Repair Analysis Methodology*. NADC-081063-60. 1982, Naval Air Development Center: Warminster, PA.
348. Chang, F.-K., Scott, R. A., and Springer, G. S., *Strength of Bolted Joints in Laminated Composites*. AFWAL-TR-84-4029. 1984, Materials Laboratory, Air Force Wright Aeronautical Laboratores: Wright-Patterson Air Force Base, OH.
349. Ramkumar, R.L., Saether, E. S., and Appa, K., *Strength Analysis of Laminated and Metallic Plates Bolted Together by Many Fasteners*. AFWAL-TR-86-3034. 1986, Flight Dynamics Laboratory, Air Force Wright Aeronautical Laboratories: Wright-Patterson Air Force Base, OH.
350. Sawicki, A.J., Rogoff, P., and Minguet, P. J. *Comparison of Experiments and Nonlinear Analysis for Post-Buckled Composite Shear Panels with Holes*. *Proceedings of the 43rd AIAA/ASME/ASCE/AHS/ASC Structures, Structural Dynamics, and Materials Conference*. 2002. Denver, CO: American Institute of Aeronautics and Astronautics. AIAA Paper 2002-1405.
351. Eisenmann, J.R., and Rousseau, C. Q., *IBOLT: A Composite Bolted Joint Static Strength Prediction Tool*, *Joining and Repair of Composite Structures*, K.T. Kedward, and Kim, H., Editors. 2004, ASTM International: West Conshohocken, PA. p. 161-181.
352. Thoppul, S.D., Finegan, J., and Gibson, R. F., *Mechanics of Mechanically Fastened Joints in Polymer-Matrix Composite Structures - A Review.* Composites Science and Technology, 2009. **69**(3-4): p. 301-329.
353. Garbo, S.P., and Ogonowski, J. M., *Effect of Variances and Manufacturing Tolerances on the Design Strength and Life of Mechanically Fastened Composite Joints, Vol. 1: Methodology Development and Data Evaluation*. AFWAL-TR-81-3041. 1981, Air Force Wright Aeronautical Laboratories: Wright-Patterson AFB, OH.
354. Kim, R.Y., and Whitney, J. M., *Effect of Temperature and Moisture on Pin Bearing Strength of Composite Laminates.* Journal of Composite Materials, 1976. **10**(April): p. 149-155.
355. Qing, X., Sun, H.-T., Dagba, L., and Chang, F.-K., *Damage-Tolerance-Based Design of Bolted Composite Joints*, *Composite Structures: Theory and Practice*, P. Grant, and Rousseau, C. Q., Editors. 2000, American Society for Testing and Materials: West Conshohocken, PA. p. 243-272.
356. Sawicki, A.J., and Minguet, P. J., *The Influence of Fastener Clearance Upon the Failure of Compression-Loaded Composite Bolted Joints*, *Composite Structures: Theory and Practice*, P. Grant, and Rousseau, C. Q., Editors. 2000, American Society for Testing and Materials: West Conshohocken, PA. p. 293-308.
357. Anlas, G., and Tüzer, Ö, *Design of Laminated Composite Plates Containing a Hole Under In-Plane Loadings.* Journal of Reinforced Plastics and Composites, 2001. **20**(12): p. 1024-1035.

358. Shivakumar, K.N., and Crews, J. H. Jr., *Bolt Clampup Relaxation in a Graphite/Epoxy Laminate*. NASA TM 83268. 1982, NASA Langley Research Center: Hampton, VA.
359. Ramkumar, R.L., and Tossavainen, E. W., *Bolted Joints in Composite Structures: Design, Analysis, and Verification*. AFWAL-TR-84-3047. 1984, Flight Dynamics Laboratory, Air Force Wright Aeronautical Laboratories: Wright-Patterson Air Force Base, OH.
360. Walter, R.W., and Tuttle, M. M., *Investigation of Static and Cyclic Failure Mechanisms for GR/EP Laminates*, *Proceedings of the 9th DoD/NASA/FAA Conference on Fibrous Composites in Structural Design*, J.R. Soderquist, Neri, L. M., and Bohon, H. L., Editors. 1992, FAA Technical Center: Lake Tahoe, NV. p. 167-184.
361. McCarthy, M.A., Lawlor, V. P., and Stanley, W. F., *An Experimental Study of Bolt-Hole Clearance Effects in Single-Lap, Multibolt Composite Joints.* Journal of Composite Materials, 2005. **39**(9): p. 799-825.
362. Thomas, F.P., and Zhao, Y. *Torque Limit for Composites Joined with Mechanical Fasteners*. *Proceedings of the 46th AIAA/ASME/ASCE/AHS/ASC Structures, Structural Dynamics, and Materials Conference*. 2005. Austin, TX: American Institute of Aeronautics and Astronautics. AIAA Paper 2005-2351.
363. Cook, R.D., Malkus, D. S., and Plesha, M. E., *Concepts and Applications of Finite Element Analysis*. 3rd ed. 1989, New York, NY: John Wiley and Sons, Inc.
364. Galerkin, B.G., *Series-Solutions of Some Cases of Equilibrium of Elastic Beams and Plates.* Vestnik Inshenernov i Tekhnikov, 1915. **1**: p. 897-908.
365. Ritz, W., *Über eine neue Methode zur Lösung gewisser Varationsprobleme der mathematischen Physik.* Journal für die reine und angewandte Mathematik, 1909. **135**: p. 1-61.
366. Turner, M.J., Clough, R. W., Martin, H. C., and Topp, L. J., *Stiffness and Deflection Analysis of Complex Structures.* Journal of the Aeronautical Sciences, 1956. **23**(9): p. 805-823; 854.
367. Argyris, J.H., *Energy Theorems and Structural Analysis, Part I: General Theory.* Aircraft Engineering, 1954. **26**(308): p. 347-356.
368. Zienkiewicz, O.C., and Cheung, Y. K., *The Finite Element Method for Analysis of Elastic Isotropic and Orthotropic Slabs.* Proceedings of the Institution of Civil Engineers, 1964. **28**: p. 471-488.
369. Zienkiewicz, O.C., and Taylor, R. L., *The Finite Element Method, Volume 1: The Basis*. 5th ed. Vol. 1. 2000, Oxford, England: Butterworth Heinemann.
370. Zienkiewicz, O.C., *The Birth of the Finite Element Method and of Computational Mechanics.* International Journal for Numerical Methods in Engineering, 2004. **60**(1): p. 3-10.
371. Chang, F., Scott, R. A., and Springer, G. S., *Strength of Mechanically Fastened Composite Joints*. AFWAL-TR-82-4095. 1982, Materials Laboratory, Air Force Wright Aeronautical Laboratories: Wright-Patterson Air Force Base, OH.
372. Nelson, W.D., Bunin, B. L., and Hart-Smith, L. J., *Critical Joints in Large Composite Aircraft Structure*. NASA CR 3710. 1983, National Aeronautics and Space Administration: Washington, DC.
373. Yeh, H.-Y., Lee, J. J., Yang, D. Y. T., and Yeh, H.-L., *Study of Multirow Highly Loaded Bolt Joints in Composite Wing Structure.* Journal of Aircraft, 2004. **41**(2): p. 380-385.

374. Lee, J.J., *Design and Analysis of Multirow Highly Loaded Bolt Joints in Composite Wing Structures*, MS Thesis, *Mechanical Engineering*. 2000, California State University, Long Beach: Long Beach, CA.
375. Hart-Smith, L.J., *Bolted Joints in Graphite-Epoxy Laminates*. NASA CR-144899. 1977, National Aeronautics and Space Administration: Washington, DC.
376. Hart-Smith, L.J., *Bolted Joint Analyses for Composite Structures - Current Empirical Methods and Future Scientific Prospects*, *Joining and Repair of Composite Structures*, K.T. Kedward, and Kim, H., Editors. 2004, ASTM International: West Conshohocken, PA. p. 127-160.
377. Niklewicz, J., Ferriss, D. H., Nunn, G. J., and Sims, G. D., *The Use of Pin Bearing Data for the Preliminary Design of "Bolted" Joints*. 1999, National Physical Laboratory: Teddington, Middlesex, UK.
378. Gauss, C.F., *Gauss an Gerling, Göttingen, 26 December 1823*, in *Carl Friedrich Gauss Werke*. 1903, Herausgegeben von der Königlichen Gesellschaft der Wissenschaften: Göttingen, Germany. p. 278-281.
379. von Seidel, P.L., *Über ein Verfahren, die Gleichungen, auf welche die Methode der kleinsten Quadrate führt, sowie lineare Gleichungen überhaupt, durch successive Annäherung aufzulösen.* Abhandlungen der Mathematisch-Physikalischen Classe der Königlich Bayerischen Akademie der Wissenschaften, 1874. **11**(3): p. 81-108.
380. Tuttle, M.E., *Structural Analysis of Polymeric Composite Materials*. 2nd ed. 2013, Boca Raton, FL: CRC Press, Taylor and Francis Group.
381. Jenkins, M.A., and Traub, J. F., *A Three-Stage Variable-Shift Iteration for Polynomial Zeros and Its Relation to Generalized Rayleigh Iteration.* Numerische Mathematik, 1970. **14**(3): p. 252-263.
382. Jenkins, M.A., and Traub, J. F., *Algorithm 419: Zeros of a Complex Polynomial [C2]*. Communications of the ACM, 1972. **15**(2): p. 97-99.
383. Ting, T.C.T., *Anisotropic Elasticity: Theory and Applications*. Oxford Engineering Science Series. 1996, New York, NY: Oxford University Press.
384. Tung, T.K., *On Computation of Stresses Around Holes in Anisotropic Plates.* Journal of Composite Materials, 1987. **21**(2): p. 100-104.
385. Camanho, P.M.P.R.d.C., *Application of Numerical Methods to the Strength Prediction of Mechanically Fastened Joints in Composite Laminates*. 1999, Ph.D. Thesis, Imperial College of Science, Technology, and Medicine: London, UK.
386. Nuismer, R.J., and Whitney, J. M. *Uniaxial Failure of Composite Laminates Containing Stress Concentrations*. *Fracture Mechanics of Composites: Proceedings of the Symposium*. ASTM STP 593. 1974. Gaithersburg, MD: American Society for Testing and Materials. p. 117-142.
387. Camanho, P.P., and Lambert, M., *A Design Methodology for Mechanically Fastened Joints in Laminated Composite Materials.* Composites Science and Technology, 2006. **66**(15): p. 3004-3020.
388. Tsai, S.W., and Wu, E. M., *A General Theory of Strength for Anisotropic Materials.* Journal of Composite Materials, 1971. **5**(1).
389. Tsai, S.W., and Hahn, H. T., *Introduction to Composite Materials*. 1980, Lancaster, PA: Technomic Publishing Co., Inc.
390. Gere, J.M., and Timoshenko, S. P., *Mechanics of Materials*. 3rd ed. 1990, Boston, MA: PWS-Kent Publishing Co.

391. Bunin, B.L., *Critical Composite Joint Subcomponent--Analysis and Test Results*. NASA CR-3711. 1983, National Aeronautics and Space Administration: Washington, DC.
392. Hart-Smith, L.J., *Expanding the Capabilities of the Ten-Percent Rule for Predicting the Strength of Fibre-Polymer Composites.* Composites Science and Technology, 2002. **62**(12-13): p. 1515-1544.
393. Albers, R.G., Tuttle, M. E., and Avery, W. B. *Subsonic Transport Composite Wing Model for Optimization Studies*. *Proceedings of the 12th AIAA/ISSMO Multidisciplinary Analysis and Optimization Conference*. 2008. Victoria, British Columbia, Canada: American Institute of Aeronautics and Astronautics. AIAA Paper No. 2008-6016.
394. Brown, D.A., *Advanced Airfoils Studied for Transports*, *Aviation Week and Space Technology*. 1970, McGraw-Hill: New York, NY. p. 55-57; 60.
395. Anderton, D., *Dateline America: Supercritical Wing*, *Flight International*. 1971. p. 23-26.
396. Selig, M. *UIUC Airfoil Coordinates Database, Version 2.0*. 2006 Accessed March 13, 2006. Available from: http://www.ae.uiuc.edu/m-selig/ads/coord_database.html#B.
397. Jenkinson, L.R., Simpkin, P., and Rhodes, D., *Civil Jet Aircraft Design*. AIAA Education Series, ed. J.S. Przemieniecki. 1999, Reston, VA: American Institute of Aeronautics and Astronautics.
398. Anonymous. *Boeing 767*. September 11, 2001. Accessed March 13, 2006; Available from: http://www.janes.com/aerospace/civil/news/jawa/boeing_767.shtml.
399. Badrocke, M., and Gunston, B., *Boeing Aircraft Cutaways: The History of the Boeing Aircraft Company*. 1998, Osprey Publishing: Oxford, UK.
400. Niu, M.C.-Y., *Airframe Structural Design: Practical Design Information and Data on Aircraft Structures*. 1988, Conmilit Press Ltd.: Hong Kong.
401. Anonymous, *SolidWorks Education Edition*. 2005, SolidWorks Corp.: Concord, MA.
402. Torenbeek, E., *Development and Application of a Comprehensive, Design-Sensitive Weight Prediction Method for Wing Structures for Transport Category Aircraft*. 1992, Delft University of Technology: Delft, The Netherlands.
403. Torenbeek, E., *Synthesis of Subsonic Airplane Design: An Introduction to the Preliminary Design of Subsonic General Aviation and Transport Aircraft, with Emphasis on Layout, Aerodynamic Design, Propulsion, and Performance*. 1982, Delft, The Netherlands: Delft University Press.
404. Roskam, J., *Airplane Design, Part 5: Component Weight Estimation*. Vol. 5. 1989, Ottawa, KS: Roskam Aviation and Engineering Corp.
405. Anonymous, *Pratt & Whitney Models PW 4062 Type Certificate Data Sheet*. 2002, Federal Aviation Administration: Washington, DC.
406. Anonymous. *Model CF6-80C2 Engine Overview*. 2006. Accessed March 27, 2006; Available from: http://www.geae.com/engines/commercial/cf6/cf6-80c2.html.
407. Coordinating Research Council, *Handbook of Aviation Fuel Properties*. 1983, Society of Automotive Engineers, Inc.: Warrendale, PA. p. 20-32, 84-87.
408. Swanson, S.R., and Qian, Y., *Multiaxial Characterization of T800/3900-2 Carbon/Epoxy Composites.* Composites Science and Technology, 1992. **43**(2): p. 197-203.
409. MIL-HDBK-17, *Composite Materials Handbook, Vol. 2: Polymer Matrix Composites Materials Properties, Section 4.2.33: T700S 12k/3900-2 Plain Weave Fabric and Section 4.2.34: T800HB 12k/3900-2 Unidirectional Tape*. 2002, Department of Defense, United States of America: Washington, DC. p. 4-243--4-254.

410. Gimmestad, D. *An Aeroelastic Optimization Procedure for Composite High Aspect Ratio Wings*. *Proceedings of the 20th AIAA/ASME/ASCE/AHS Structures, Structural Dynamics, and Materials Conference*. 1979. St. Louis, MO: American Institute of Aeronautics and Astronautics. p. 79-86
411. Shah, G.H., Cunningham, K., Foster, J. V., Fremaux, C. M., Stewart, E. C., Wilborn, J. E., Gato, W., and Pratt, D. W. *Wind-Tunnel Investigation of Commercial Transport Aircraft Aerodynamics at Extreme Flight Conditions*. *Proceedings of the SAE World Aviation Congress and Display: SAE Transactions, Journal of Aerospace*. 2002. Phoenix, AZ: Society of Automotive Engineers. SAE Paper No. 2002-01-2912.
412. Cunningham, K., Foster, J. V., Shah, G. H., Stewart, E. C., Wilborn, J. E., and Gato, W. *Simulation Study of a Commercial Transport Airplane During Stall and Post-Stall Flight*. *Proceedings of the SAE World Aviation Congress: SAE 2004 Transactions, Journal of Aerospace*. 2004. Reno, NV: Society of Automotive Engineers.
413. Anonymous, *ANSYS Academic Research*. 2007, ANSYS, Inc.: Canonsburg, PA.
414. Anonymous, *ANSYS Elements Reference*. 2007, ANSYS, Inc.: Canonsburg, PA.
415. Livne, E., Sels, R. A., and Bhatia, K. G., *Lessons from Application of Equivalent Plate Structural Modeling to an HSCT Wing.* Journal of Aircraft, 1994. **31**(4): p. 953-960.
416. Gallagher, R.H., Rattinger, I., and Archer, J. S., *A Correlation Study of Methods of Matrix Structural Analysis: Report to the 14th Meeting of the Structures and Materials Panel, Advisory Group for Aeronautical Research and Development (AGARD), NATO, Paris, France, July 6, 1962*, *AGARDograph*. 1964, Macmillan Co.: New York, NY.
417. Anonymous, *Chapter 13: Composites, ANSYS Structural Analysis Guide*. 2007, ANSYS, Inc.: Canonsburg, PA. p. 337-350.
418. Niu, M.C.-Y., *Airframe Stress Analysis and Sizing*. 1997, Hong Kong: Hong Kong Conmilit Press Ltd.
419. Howe, D., *Aircraft Loading and Structural Layout*. AIAA Education Series, ed. J.A. Schetz. 2004, Reston, VA: American Institute of Aeronautics and Astronautics.
420. Cawley, M., *Product Specification: Hi-Lok®/Hi-Tigue® and Hi-Lok® Fastening System, Hi-Lok®/Hi-Tigue® and Hi-Lok® Pin*. 2003, Hi-Shear Corp.: Torrance, CA.
421. Thompson, K., *Product Specification: Hi-Lok®/Hi-Tigue® and Hi-Lok® Fastening System, Hi-Lok®/Hi-Tigue® and Hi-Lok® Collars*. 2004, Hi-Shear Corp.: Torrance, CA.
422. Anonymous, *Drawing No. HL97: Hi-Lok® Collar, A-286 High Temperature Alloy, 1/16 Grip Variation, Shear Application*, *Rev. 39*. 2005, Hi-Shear Corp.: Torrance, CA.
423. Anonymous, *Drawing No. HL10: Hi-Lok® Pin, Protruding Shear Head, Titanium, 1/16 Grip Variation*, *Rev. 40*. 2006, Hi-Shear Corp.: Torrance, CA.
424. Hart-Smith, L.J., *Analysis Methods for Bolted Composite Joints Subjected to In-Plane Shear Loads*, *Proceedings of the AGARD 83rd Structures and Materials Panel, Bolted/Bonded Joints in Polymeric Composites Specialist Meeting*. 1997, North Atlantic Treaty Organization Advisory Group for Aerospace Research and Development (AGARD): Florence, Italy. p. 8-1--8-11.
425. MIL-HDBK-5, *Metallic Materials and Elements for Aerospace Vehicle Structures, Section 5.4: Alpha-Beta Titanium Alloys*. 2003, Department of Defense, United States of America: Washington, DC. p. 5-51--5-58.
426. Ochoa, O.O., and Reddy, J. N., *Finite Element Analysis of Composite Laminates*. Solid Mechanics and its Applications, ed. G.M.L. Gladwell. 1992, Dordrecht, The Netherlands: Kluwer Academic Publishers.

427. Smith, I.M., and Griffiths, D. V., *Programming the Finite Element Method*. 4th ed. 2006, Chichester, UK: John Wiley & Sons, Ltd.
428. Bathe, K.-J., *Finite Element Procedures in Engineering Analysis*. 1982, Englewood Cliffs, NJ: Prentice-Hall, Inc.
429. Benoit, C., *Note sur une méthode de résolution des équations normales provenant de l'application de la méthode des moindres carrés à un système d'équations linéaires en nombre inférieur à celui des inconnues.--Application de la méthode a la résolution d'un système defini d'équations linéaires (Procédé du Commandant Cholesky).* Bulletin Géodésique, 1924. **2**: p. 67-77.
430. Burden, R.L., and Faires, J. D., *Numerical Analysis*. 5th ed. Prindle, Weber, and Schmidt Series in Mathematics. 1993, Boston, MA: PWS Publishing Co.
431. Martin, R.S., Peters, G., and Wilkinson, J. H., *Handbook Series Linear Algebra: Symmetric Decomposition of a Positive Definite Matrix.* Numerische Mathematik, 1965. **7**(5): p. 362-383.
432. Press, W.H., Teukolsky, S. A., Vetterling, W. T., and Flannery, B. P., *Numerical Recipes in FORTRAN: The Art of Scientific Computing*. 2nd ed. 1992, Cambridge, England: Cambridge University Press.
433. Barlow, J., *Optimal Stress Locations in Finite Element Models.* International Journal for Numerical Methods in Engineering, 1976. **10**(2): p. 243-251.
434. Barlow, J., *More on Optimal Stress Points--Reduced Integration, Element Distortions and Error Estimation.* International Journal for Numerical Methods in Engineering, 1989. **28**(7): p. 1487-1504.
435. Logan, D.L., *A First Course in the Finite Element Method*. 2nd ed. The PWS Series in Engineering. 1993, Boston, MA: PWS Publishing Co.
436. Tsai, S.W., and Hahn, H. T., *Introduction to Composite Materials*. 1980, Technomic Publishing Co., Inc.: Lancaster, PA.
437. Knuth, D.E., *The Art of Computer Programming*. Addison-Wesley Series in Computer Science and Information Processing, ed. R.S. Varga, and Harrison, M. A. Vol. 2: Seminumerical Algorithms. 1969, Addison-Wesley Publishing Co.: Reading, PA. 100-118.
438. Zabinsky, Z.B., *Stochastic Adaptive Search for Global Optimization*. Nonconvex Optimization and Its Applications, ed. P. Pardalos. 2003, Kluwer Academic Publishers: Boston, MA.
439. Kristinsdottir, B.P., Zabinsky, Z. B., Tuttle, M. E., and Neogi, S., *Optimal Design of Large Composite Panels with Varying Loads.* Composite Structures, 2001. **51**(1): p. 93-102.
440. Ambartsumyan, S.A., *Teoriia Anizotropnykh Plastin*. Progress in Materials Science. 1970, Stamford, CT: Technomic Publishing Co., Inc.
441. Ugural, A.C., *Stresses in Plates and Shells*. 1981, New York, NY: McGraw-Hill Book Co.
442. Kirchhoff, G., *Über das Gleichgwich und die Bewegung einer Elastischen Scheibe.* Journal für die reine und angewandte Mathematik, 1850. **40**: p. 51-88.
443. Love, A.E.H., *A Treatise on the Mathematical Theory of Elasticity*. 4th ed. 1944, New York, NY: Dover Publications, Inc.
444. Whitney, J.M., *Structural Analysis of Laminated Anisotropic Plates*. 1987, Lancaster, PA: Technomic Publishing Co., Inc.

445. Reddy, J.N., *Mechanics of Laminated Composite Plates and Shells: Theory and Analysis*. 2nd edition ed. 2004, Boca Raton, FL: CRC Press, Inc.
446. Reddy, J.N., *Energy Principles and Variational Methods in Applied Mechanics*. 2002, Hoboken, NJ: John Wiley & Sons, Inc.
447. Edwards, C.H., Jr., and Penny, D. E., *Calculus and Analytic Geometry*. 2nd ed. 1986, Englewood Cliffs, NJ: Prentice-Hall, Inc.
448. Reddy, J.N., *Introduction to the Finite Element Method*. 3rd ed. McGraw-Hill Series in Mechanical Engineering. 2006, New York, NY: McGraw-Hill.
449. Lindsey, C.H., *Structure Charts: A Structured Alternative to Flowcharts.* SIGPLAN Notices / ACM Special Interest Group on Programming Languages, 1977. **12**(11): p. 36-49.
450. Ergatoudis, J., Irons, B. M., and Zienkiewicz, O. C., *Curved, Isoparametric, "Quadrilateral" Elements for Finite Element Analysis*. International Journal of Solids and Structures, 1968. **4**(1): p. 31-42.
451. Gauss, C.F., *Methodus nova integralium valores per approximationen inveniendi.* Commentationes Societatis Regiae Scientiarum Gottingensis Recentiores, 1814. **3**(Classis Mathematicae): p. 39-76.
452. Legendre, A.M., *Sur l'attraction des Sphéroïdes Homogènes.* Mémoires mathématique et de physique, présentés à l'Académie royale des. sciences par divers savants, 1785. **10**: p. 411-435.
453. Irons, B.M., *Engineering Applications of Numerical Integration in Stiffness Methods.* AIAA Journal, 1966. **4**(11): p. 2035-2037.
454. Bickford, W.B., *A First Course in the Finite Element Method*. 2nd ed. 1994, Burr Ridge, IL: Richard D Irwin, Inc.
455. Jacobi, C.G.J., *Ueber die functionaldeterminanten (De determinantibus functionalibus).* Journal für die reine und angewandte Mathematik, 1841. **22**: p. 319-352.
456. Lowan, A.N., Davids, N., and Levenson, A., *Table of the Zeros of the Legendre Polynomials of Order 1-16 and the Weight Coefficients for Gauss' Mechanical Quadrature Formula.* Bulletin of the American Mathematics Society, 1942. **48**(10): p. 739-743.
457. Holsapple, K.A., *FRED Input Instructions, Dept. of Aeronautics and Astronautics, University of Washington, Seattle, WA*. 1991.
458. Halpin, J.C., *Primer On Composite Materials Analysis*. 2nd, Revised ed. 1992, Lancaster, PA: Technomic Publishing Co., Inc.
459. Almroth, B.O., *Influence of Edge Conditions on the Stability of Axially Compressed Cylindrical Shells.* AIAA Journal, 1966. **4**(1): p. 134-140.
460. Bourke, P. *Calculating the Area and Centroid of a Polygon*. July, 1988. Accessed April 3, 2009; Available from: http://local.wasp.uwa.edu.au/~pbourke/geometry/polyarea/.
461. Khompatraporn, C., *Analysis and Development of Stopping Criteria for Stochastic Global Optimization Algorithms*, Ph.D. Thesis *Industrial Engineering*. 2004, University of Washington: Seattle, WA.

Appendix A

FINITE ELEMENT ANALYSIS

A finite element analysis code has been developed for the specific purpose of accounting for the changes in internal loads of the wing as the structures are optimized. This appendix will discuss the methods and elements used in WINGJOTA.

A.1 Composite Plate FEA Implementation

The internal finite element analysis for this optimization algorithm would be performed thousands of times; therefore, a relatively simple, four-node composite plate element was selected for implementation to minimize computational expense. The element has four nodes and is a C^1, conforming plate element, with six degrees of freedom per node and four integration points in the element.

Although balanced and symmetric laminates are being utilized in this work, laminates in the future should be allowed to be more general. Accordingly a generalized Hooke's law is adopted from the full tensor form [440] for the constitutive relations:

$$\sigma_k = C_{kj}\varepsilon_j, \text{ k} = 1, 2, \ldots, 6 \tag{A.1}$$

$$\begin{gathered}\sigma_1 = \sigma_{11},\ \sigma_2 = \sigma_{22},\ \sigma_3 = \sigma_{33},\ \sigma_4 = \sigma_{23},\ \sigma_5 = \sigma_{13},\ \sigma_6 = \sigma_{12} \\ \varepsilon_1 = \varepsilon_{11},\ \varepsilon_2 = \varepsilon_{22},\ \varepsilon_3 = \varepsilon_{33},\ \varepsilon_4 = 2\varepsilon_{23},\ \varepsilon_5 = 2\varepsilon_{13},\ \varepsilon_6 = 2\varepsilon_{12}\end{gathered} \tag{A.2}$$

where σ_1, σ_2, and σ_3 represent the normal stresses, σ_4, σ_5, and σ_6 represent the shear stresses; σ_1, σ_2, and σ_6 represent the in-plane stresses, σ_3, σ_4, and σ_5 represent the out-of-plane stresses. The strains ε are defined in a similar way. C_{kj} are the elastic coefficients. This can also be written as

$$\begin{Bmatrix}\sigma_1\\ \sigma_2\\ \sigma_3\\ \sigma_4\\ \sigma_5\\ \sigma_6\end{Bmatrix} = \begin{bmatrix} C_{11} & C_{12} & C_{13} & C_{14} & C_{15} & C_{16} \\ & C_{22} & C_{23} & C_{24} & C_{25} & C_{26} \\ & & C_{33} & C_{34} & C_{35} & C_{36} \\ & & & C_{44} & C_{45} & C_{46} \\ & \textit{symm} & & & C_{55} & C_{56} \\ & & & & & C_{66} \end{bmatrix} \begin{Bmatrix}\varepsilon_1\\ \varepsilon_2\\ \varepsilon_3\\ \varepsilon_4\\ \varepsilon_5\\ \varepsilon_6\end{Bmatrix} \tag{A.3}$$

for anisotropic materials [426].

Classical laminated plate theory is used for the composite finite elements. It has been found to be useful in applications where the thickness of the plate is small compared to the in-plane dimensions by two orders of magnitude [265, 441]. This theory assumes the Kirchhoff-Love hypothesis for small deformations: a straight line perpendicular to the midplane remains straight and perpendicular after deformation and is inextensible [442-443]. This implies that the plates are infinitely rigid in the transverse direction, which for small deformations is acceptable. Whitney [444], Reddy [445], and Tuttle [380] have published texts that cover this theory.

Following from these assumptions the displacement field becomes

$$\begin{aligned} u_1 &= u - z\frac{\partial w}{\partial x} \\ u_2 &= v - z\frac{\partial w}{\partial y} \\ u_3 &= w \end{aligned} \tag{A.4}$$

where u_1, u_2, and u_3 are the components of the displacement vector; u, v, and w are the displacements of a point on the midplane of the laminate. This field assumes that the strain through the thickness is continuous layer to layer, i.e., the laminate is replaced with a single layer. Therefore global responses can be found from finite elements based on this theory, but not ply-by-ply interlaminar stresses and strains.

The equations of motion are derived using the principle of virtual displacements. This states that if a body is in static equilibrium, the total virtual work done by all externally applied and internally-generated forces must be zero in moving through all their respective virtual displacements [446]. Using this principle and applying it to the classical laminated plate theory the equilibrium equations can be found to be

$$-\left(\frac{\partial N_1}{\partial x} + \frac{\partial N_6}{\partial y}\right) = 0 \tag{A.5a}$$

$$-\left(\frac{\partial N_6}{\partial x} + \frac{\partial N_2}{\partial y}\right) = 0 \tag{A.5b}$$

$$-\left(\frac{\partial^2 M_1}{\partial x^2} + 2\frac{\partial^2 M_6}{\partial x \partial y} + \frac{\partial^2 M_2}{\partial^2 y} + N(\omega) + q\right) = 0 \tag{A.5c}$$

where q is the transverse (out-of-plane) loading on the plate, N_1, N_2, and N_3 are the force resultants and M_1, M_2, and M_3 are the moment resultants, defined by

$$\begin{Bmatrix} N_1 \\ N_2 \\ N_6 \end{Bmatrix} = \int_{\frac{-h}{2}}^{\frac{h}{2}} \begin{Bmatrix} \sigma_1 \\ \sigma_2 \\ \sigma_6 \end{Bmatrix} dz, \quad \begin{Bmatrix} M_1 \\ M_2 \\ M_6 \end{Bmatrix} = \int_{\frac{-h}{2}}^{\frac{h}{2}} \begin{Bmatrix} \sigma_1 \\ \sigma_2 \\ \sigma_6 \end{Bmatrix} z dz \tag{A.6}$$

where h is the thickness of the plate, and N(ω) is

$$N(\omega) = \frac{\partial}{\partial x}\left(N_1 \frac{\partial w}{\partial x} + N_6 \frac{\partial w}{\partial y} \right) + \frac{\partial}{\partial y}\left(N_6 \frac{\partial w}{\partial x} + N_2 \frac{\partial w}{\partial y} \right) \tag{A.7}$$

Note that the nonlinear term N(ω) will not be used to develop the linear finite element model from these equations. This is a valid assumption if the maximum out-of-plane displacement is less than half the plate thickness, i.e., $w_{max} < h/2$ [380].

To develop the linear finite element model the weighted-integral statements, known as the weak form, of the equilibrium equations (A.5) are constructed. They are known as the weak form because they require less differentiability of the dependent variables u, v, and w than the original equilibrium equations. Each equation is multiplied by a weight, or virtual variation, for each coordinate direction (here δu, δv, and δw) and integrated over the element domain Ω^e [426]:

$$0 = \int_{\Omega^e} \delta u \left[-\left(\frac{\partial N_1}{\partial x} + \frac{\partial N_6}{\partial y} \right) \right] dxdy \tag{A.8a}$$

$$0 = \int_{\Omega^e} \delta v \left[-\left(\frac{\partial N_6}{\partial x} + \frac{\partial N_2}{\partial y} \right) \right] dxdy \tag{A.8b}$$

$$0 = \int_{\Omega^e} \delta w \left[-\left(\frac{\partial^2 M_1}{\partial x^2} + 2\frac{\partial^2 M_6}{\partial x \partial y} + \frac{\partial^2 M_2}{\partial^2 y} + q \right) \right] dxdy \tag{A.8c}$$

The differentiation on N_1 and N_6 in equation (A.8a) are transferred to the weight function δu by integration-by-parts [447]:

$$0 = \int_{\Omega^e} \left(\frac{\partial \delta u}{\partial x} N_1 + \frac{\partial \delta u}{\partial y} N_6 \right) dxdy - \int_{\Gamma^e} \left(N_1 n_x + N_6 n_y \right) \delta u ds \tag{A.9}$$

where n_x and n_y are the direction cosines of the unit normal on the boundary Γ^e of the element. Noting that the in-plane normal force is given by

$$N_1 n_x + N_6 n_y = N_n \tag{A.10}$$

the weak form of equation (A.8a) becomes

$$0 = \int_{\Omega^e} \left(\frac{\partial \delta u}{\partial x} N_1 + \frac{\partial \delta u}{\partial y} N_6 \right) dxdy - \int_{\Gamma^e} \delta u N_n ds \tag{A.11a}$$

Similarly, for equations (A.8b) and (A.8c) the weak forms are [426]

$$0 = \int_{\Omega^e} \left(\frac{\partial \delta v}{\partial x} N_6 + \frac{\partial \delta v}{\partial y} N_2 \right) dxdy - \int_{\Gamma^e} \delta v N_{ns} ds \tag{A.11b}$$

$$\begin{aligned} 0 = -\int_{\Omega^e} \left(\frac{\partial^2 \delta w}{\partial x^2} M_1 + 2 \frac{\partial^2 \delta w}{\partial x \partial y} M_6 + \frac{\partial^2 \delta w}{\partial y^2} M_2 + \delta w q \right) dxdy \\ - \int_{\Gamma^e} \left(\delta w V_n + \frac{\partial \delta w}{\partial n} M_n \right) ds \end{aligned} \tag{A.11c}$$

The nodal displacements and rotations are generalized over the element Ω^e by interpolations of the form

$$u = \sum_{j=1}^{n} u_j \psi_j (x, y) \tag{A.12a}$$

$$v = \sum_{j=1}^{n} v_j \psi_j (x, y) \tag{A.12b}$$

$$w = \sum_{j=1}^{m} \Delta_j \phi_j (x, y) \tag{A.12c}$$

where u_j and v_j are the nodal values of u and v, and Δ_j are the nodal values of w and its derivatives. Interpolations of the function only are called Lagrange interpolation functions, ψ_j. Those interpolations of both the function and its derivatives are called Hermite interpolation functions, ϕ_j. From the order of differentiation seen in equations (A.11), it is shown that u and v are linear interpolations (Lagrange) and w are cubic interpolations (Hermite) when considering these weak forms of the classical plate theory [448].

Considering a four-node rectangular finite element there are n = 4 and m = 16 degrees of freedom in the element in equations (A.12), i.e., four for u, four for v, and 16 for w, for a total of 24. This geometric description is called subparametric as the approximation of the dependent variable is higher-order than the geometric approximation. The four nodal values associated with w at each node are

$$\text{w, } \frac{\partial w}{\partial x}\text{, } \frac{\partial w}{\partial xy}\text{, and } \frac{\partial^2 w}{\partial x \partial y} \tag{A.13}$$

Using this interpolation of u, v, and w insures continuity of u, v, w, and the first derivatives of w at the interface of the elements. Such elements are called conforming elements, and as noted above they have six degrees of freedom per node [448].

The interpolation or shape functions for the linear Lagrange rectangular elements are, for variables u and v,

$$¼(1 + \xi_0)(1 + \eta_0), \text{ node i} = 1, 2, 3, 4 \tag{A.14}$$

The interpolation functions for the cubic Hermite rectangular elements (for variable w and its derivative) are

$$\phi_I = \tfrac{1}{16}(\xi+\xi_i)^2(\xi_0-2)(\eta+\eta_i)^2(\eta_0-2) \text{ for w;} \tag{A.15a}$$

$$\phi_{I+1} = -\tfrac{1}{16}\xi_i(\xi+\xi_i)^2(\xi_0-1)(\eta+\eta_i)^2(\eta_0-2) \text{ for } \frac{\partial w}{\partial x}, \tag{A.15b}$$

$$\phi_{I+2} = -\tfrac{1}{16}(\xi+\xi_i)^2(\xi_0-2)\eta_i(\eta+\eta_i)^2(\eta_0-1) \text{ for } \frac{\partial w}{\partial xy} \tag{A.15c}$$

$$\phi_{I+3} = \tfrac{1}{16}\xi_i(\xi+\xi_i)^2(\xi_0-1)\eta_i(\eta+\eta_i)^2(\eta_0-1) \text{ for } \frac{\partial^2 w}{\partial x \partial y} \tag{A.15d}$$

where

$$I = 4(i-1)+1, \text{ node } i = 1, 2, 3, 4 \tag{A.16a}$$

$$\xi_0 = \xi^*\xi_i \text{ and } \eta_0 = \eta^*\eta_i \tag{A.16b}$$

$$\xi = (x - x_c)/a \text{ and } \eta = (y - y_c)/b \tag{A.16c}$$

and (ξ, η) are the natural coordinates of the element, (x_c, y_c) are the global coordinates of the center of the element, and 2a and 2b are the sides of the rectangular element (Figure A.1) [448]. It is interesting to note that the Hermite functions for the conforming plate element are found by taking the tensor product of the same functions for the Euler-Bernoulli beam element [446].

Substituting the interpolations for u, v, and w (equations A.12) and letting the virtual displacements δu, δv, and δw equal the Lagrange and Hermite interpolations in the weak form (equations A.11) yields the i-th algebraic equations for the equilibrium equations:

$$0 = \int_{\Omega^e}\left(\frac{\partial \psi_i}{\partial x}N_1 + \frac{\partial \psi_i}{\partial y}N_6\right)dxdy - \int_{\Gamma^e}\psi_i N_n ds \tag{A.17a}$$

$$0 = \int_{\Omega^e}\left(\frac{\partial \psi_i}{\partial x}N_6 + \frac{\partial \psi_i}{\partial y}N_2\right)dxdy - \int_{\Gamma^e}\psi_i N_{ns} ds \tag{A.17b}$$

$$\begin{aligned} 0 = &-\int_{\Omega^e}\left(\frac{\partial^2 \phi_i}{\partial x^2}M_1 + 2\frac{\partial^2 \phi_i}{\partial x \partial y}M_6 + \frac{\partial^2 \phi_i}{\partial y^2}M_2 + \phi_i q\right)dxdy \\ &- \int_{\Gamma^e}\left(\phi_i V_n + \frac{\partial \phi_i}{\partial n}M_n\right)ds \end{aligned} \tag{A.17c}$$

Equations (A.17) can be expressed in a more programming-friendly form as typical global equilibrium equation:

$$\sum_{\beta=1}^{3}\sum_{j=1}^{n(\beta)} K_{ij}^{\alpha\beta}\Delta_j^\beta - F_i^\alpha = 0, \text{ i} = 1, 2, \ldots, \text{n}(\alpha) \tag{A.18a}$$

$$\text{or } \{K^e\}\{\Delta^e\} - \{F^e\} = \{0\} \tag{A.18b}$$

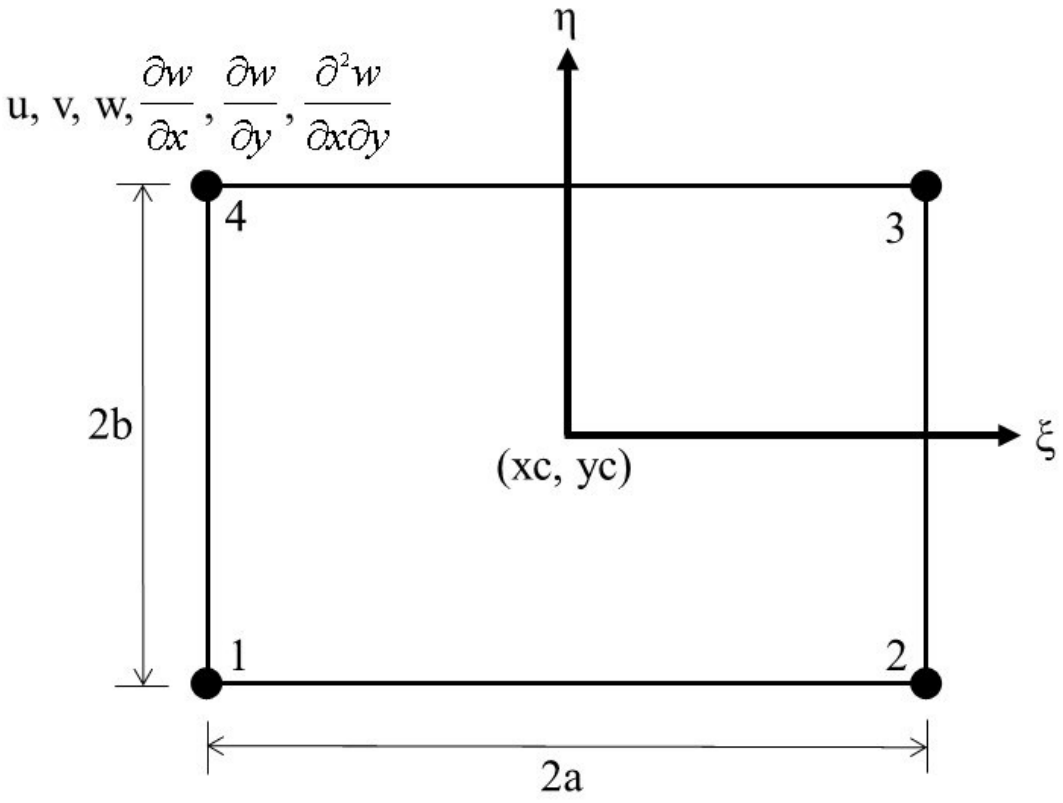

Figure A.1: Classical Laminated Theory Conforming, Subparametric, Rectangular Plate Finite Element

where α = 1, 2, 3; n(1) = n (2) = 4, and n(3) = 16. The stiffness coefficients $K_{ij}^{\alpha\beta}$ and Δ_j^{β} are given by

$$\Delta_j^1 = u_j,\ \Delta_j^2 = v_j,\ \Delta_j^3 = \Delta_j \tag{A.19}$$

$$K_{ij}^{1\alpha} = \int_{\Omega^e} \left(\frac{\partial \psi_i}{\partial x} N_{1j}^{\alpha} + \frac{\partial \psi_i}{\partial y} N_{6j}^{\alpha} \right) dxdy \tag{A.20a}$$

$$K_{ij}^{2\alpha} = \int_{\Omega^e} \left(\frac{\partial \psi_i}{\partial x} N_{6j}^{\alpha} + \frac{\partial \psi_i}{\partial y} N_{2j}^{\alpha} \right) dxdy \tag{A.20b}$$

where

$$N_{1j}^1 = A_{11} \frac{\partial \psi_i}{\partial x} + A_{16} \frac{\partial \psi_i}{\partial y} \tag{A.20c}$$

$$N_{1j}^2 = A_{16} \frac{\partial \psi_i}{\partial x} + A_{12} \frac{\partial \psi_i}{\partial y} \tag{A.20d}$$

$$N_{1j}^{3} = -\left(B_{11}\frac{\partial^2 \phi_i}{\partial x^2} + 2B_{16}\frac{\partial^2 \phi_i}{\partial x \partial y} + B_{12}\frac{\partial^2 \phi_i}{\partial y^2} \right) \tag{A.20e}$$

$$N_{2j}^{1} = A_{12}\frac{\partial \psi_i}{\partial x} + A_{26}\frac{\partial \psi_i}{\partial y} \tag{A.20f}$$

$$N_{2j}^{2} = A_{26}\frac{\partial \psi_i}{\partial x} + A_{22}\frac{\partial \psi_i}{\partial y} \tag{A.20g}$$

$$N_{2j}^{3} = -\left(B_{12}\frac{\partial^2 \phi_i}{\partial x^2} + 2B_{26}\frac{\partial^2 \phi_i}{\partial x \partial y} + B_{22}\frac{\partial^2 \phi_i}{\partial y^2} \right) \tag{A.20h}$$

$$N_{6j}^{1} = A_{16}\frac{\partial \psi_i}{\partial x} + A_{66}\frac{\partial \psi_i}{\partial y} \tag{A.20i}$$

$$N_{6j}^{2} = A_{66}\frac{\partial \psi_i}{\partial x} + A_{26}\frac{\partial \psi_i}{\partial y} \tag{A.20j}$$

$$N_{6j}^{3} = -\left(B_{16}\frac{\partial^2 \phi_i}{\partial x^2} + 2B_{66}\frac{\partial^2 \phi_i}{\partial x \partial y} + B_{26}\frac{\partial^2 \phi_i}{\partial y^2} \right) \tag{A.20k}$$

and

$$K_{ij}^{3\alpha} = -\int_{\Omega^e}\left(\frac{\partial^2 \phi_i}{\partial x^2} M_{1j}^{\alpha} + 2\frac{\partial^2 \phi_i}{\partial x \partial y} M_{6j}^{\alpha} + \frac{\partial^2 \phi_i}{\partial y^2} M_{2j}^{\alpha} \right) dxdy \tag{A.21a}$$

where

$$M_{1j}^{1} = B_{11}\frac{\partial \psi_i}{\partial x} + B_{16}\frac{\partial \psi_i}{\partial y} \tag{A.21b}$$

$$M_{1j}^{2} = B_{16}\frac{\partial \psi_i}{\partial x} + B_{12}\frac{\partial \psi_i}{\partial y} \tag{A.21c}$$

$$M_{1j}^{3} = -\left(D_{11}\frac{\partial^2 \phi_i}{\partial x^2} + 2D_{16}\frac{\partial^2 \phi_i}{\partial x \partial y} + D_{12}\frac{\partial^2 \phi_i}{\partial y^2} \right) \tag{A.21d}$$

$$M_{2j}^{1} = B_{12}\frac{\partial \psi_i}{\partial x} + B_{26}\frac{\partial \psi_i}{\partial y} \tag{A.21e}$$

$$M_{2j}^{2} = B_{26}\frac{\partial \psi_i}{\partial x} + B_{22}\frac{\partial \psi_i}{\partial y} \tag{A.21f}$$

$$M_{2j}^{3} = -\left(D_{12}\frac{\partial^2 \phi_i}{\partial x^2} + 2D_{26}\frac{\partial^2 \phi_i}{\partial x \partial y} + D_{22}\frac{\partial^2 \phi_i}{\partial y^2} \right) \tag{A.21g}$$

$$M_{6j}^{1} = B_{16}\frac{\partial \psi_i}{\partial x} + B_{66}\frac{\partial \psi_i}{\partial y} \tag{A.21h}$$

$$M_{6j}^{2} = B_{66}\frac{\partial \psi_i}{\partial x} + B_{26}\frac{\partial \psi_i}{\partial y} \tag{A.21i}$$

$$M_{6j}^{3} = -\left(D_{16}\frac{\partial^2 \phi_i}{\partial x^2} + 2D_{66}\frac{\partial^2 \phi_i}{\partial x \partial y} + D_{26}\frac{\partial^2 \phi_i}{\partial y^2} \right) \tag{A.21j}$$

Finally,

$$F_i^1 = \int_{\Gamma^e} \psi_i N_n ds \tag{A.22a}$$

$$F_i^2 = \int_{\Gamma^e} \psi_i N_{ns} ds \tag{A.22b}$$

$$F_i^3 = \int_{\Gamma^e} \left(\phi_i V_n + \frac{\partial \phi_i}{\partial n} M_n \right) ds - \int_{\Omega^e} (\phi_i q) dx dy \tag{A.22c}$$

These equations require evaluation of integrals over each element domain; with rectangular elements this is exact. Triangular elements would require numerical integration methods to compute the coefficients [426].

Now that the finite element model of classical laminated plate theory is complete the finite element method can be applied to determine displacements, strains, stresses, and loads in a composite plate structure. First, the equations of (A.18) are assembled using the two basic tenants of 1) continuity of nodal displacements between elements, and 2) balance of nodal forces [369]. The finite element mesh is formed through a scheme given by Smith and Griffiths [427], using a global node number assembly array, a nodal degree-of-freedom assembly array, and a global steering vector. Note that this particular mesh generation removes "zero freedoms" from the assembly process; later, these will have to be included for the calculation of nodal loads through the direct stiffness method.

Figure A.2 shows a "structure chart" [449] of the finite element program as coded for this work. It conveys the nested structure of the program in a visual way that is easy to understand. It can be seen that after the geometric mesh, and material properties are input the global problem size is determined; this is done via the methods briefly outlined above. The next step is to loop through all the elements to develop the element stiffness matrix. First, the nodal coordinates and the steering vector must be determined. Second, using Gauss-Legendre quadrature, the shape functions and derivatives are found in local, element coordinates. These functions must then be transformed from local to global coordinates. The element stiffness matrix is then calculated. Once all element stiffness matrices have been found they are assembled into the global stiffness matrix representing the entire structure. Externally applied point loads, element pressures, and fixed displacements are input. The equilibrium equation is then solved via factorization of the global stiffness matrix; this yields nodal displacements. To find strains and stresses the strain-displacement equations must be reconstituted. Stresses can be calculated at mathematically valid points within the element [427].

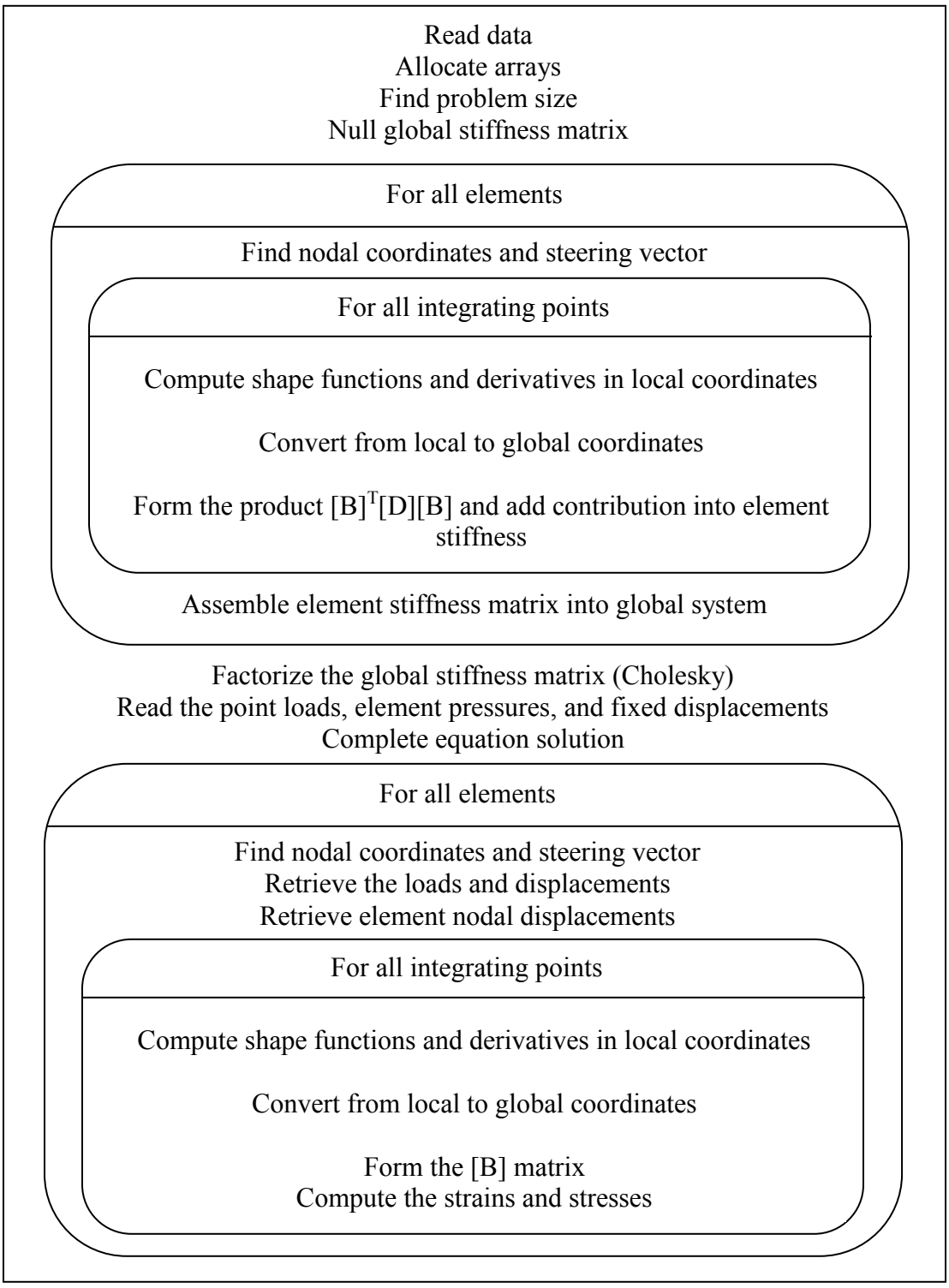

Figure A.2: Structure Chart for Finite Element Model (after [427])

The element stiffness matrix terms described above contain integrals that are not easy to determine analytically due to complexity and non-rectangular shapes of elements [450]. A numerical integration, or quadrature, must be used to evaluate these integrals. The most common quadrature for finite element analysis is called the Gauss-Legendre quadrature [451-453]. The basic idea is that the area under the curve is approximated by a weighted sum; in the Gauss-Legendre quadrature the sampling points (where the weights are taken) and the weights are chosen such that the exact value of the integral is found when using [454]

$$N = (p + 1) / 2 \tag{A.23}$$

where N is the number of weighted values evaluated and p is the degree of the polynomial to be integrated. Here, N is four. To convert one coordinate system (local element) to another (global model) one uses the chain rule of partial differentiation, expressed in matrix form as

$$\begin{Bmatrix} \frac{\partial}{\partial \xi} \\ \frac{\partial}{\partial \eta} \end{Bmatrix} = \begin{bmatrix} \frac{\partial x}{\partial \xi} & \frac{\partial y}{\partial \xi} \\ \frac{\partial x}{\partial \eta} & \frac{\partial y}{\partial \eta} \end{bmatrix} \begin{Bmatrix} \frac{\partial}{\partial x} \\ \frac{\partial}{\partial y} \end{Bmatrix} = [J] \begin{Bmatrix} \frac{\partial}{\partial x} \\ \frac{\partial}{\partial y} \end{Bmatrix} \tag{A.24}$$

where [J] is known as the Jacobian matrix [455]. Using this relation with the quadrature gives a general equation for quadrilateral elements:

$$\int_{-1}^{1}\int_{-1}^{1} f(\xi,\eta)\det|J|d\xi d\eta \approx \sum_{i=1}^{n}\sum_{j=1}^{n} w_i w_j f(\xi_i,\eta_j) \approx \sum_{i=1}^{nip} W_i f(\xi,\eta)_i \tag{A.25}$$

where nip is the number of integrating points (equal to n^2), w_i and w_j (or $W_i = w_i w_j$) are weighting coefficients. In this case, n is 2 and nip is 4. Therefore, Gauss-Legendre quadrilateral integration requires the values shown in Table A.1.

The next step is to calculate the element stiffness matrix through analysis at each integration point. The derivatives of the shape functions must be determined (see Section A.3). Next, the direction cosines for the orthogonal coordinates in the plane of and normal to the 2-D plate element are determined. The local (not natural) coordinates of the element are then found from the global coordinates by first shifting the coordinates to node 1 as specified by the direction cosines. An algorithm developed by Holsapple is utilized for this transformation [457].

The element stiffness matrix is then calculated using an expression derived from either the equilibrium, constitutive, and strain-displacement relations or through an energy approach for element strain energy per unit thickness:

Table A.1: Gauss-Legendre Quadrature for Linear Quadrilateral Elements ([456])

n	nip	(ξ_i, η_j)	w_i, w_j	W_i
2	4	$\left(\pm\sqrt{1/3}, \pm\sqrt{1/3}\right)$	(1, 1)	1

$$[KM] = \iint [B]^T [D][B] dxdy \tag{A.26}$$

Here [B] is the strain-displacement matrix and [D] is the stress-strain matrix as shown in equations (A.27) and (A.28).

In the strain-displacement matrix B the symbol following Yi (i = 1, 2, 3, 4) denotes the first derivative with respect to that variable, e.g., Y1ξ represents the derivative of Y1 with respect to ξ. Similarly the symbols following Fi (i = 1, 2, …, 16) denotes the derivatives with respect to those variables, e.g., F1 ξ ξ represents the second derivative of F1 with respect to ξξ. Section A.3 contains all the shape function derivatives.

$$B^T = \begin{bmatrix}
Y1x & 0 & Y1y & 0 & 0 & 0 \\
Y2x & 0 & Y2y & 0 & 0 & 0 \\
Y3x & 0 & Y3y & 0 & 0 & 0 \\
Y4x & 0 & Y4y & 0 & 0 & 0 \\
0 & Y1y & Y1x & 0 & 0 & 0 \\
0 & Y2y & Y2x & 0 & 0 & 0 \\
0 & Y3y & Y3x & 0 & 0 & 0 \\
0 & Y4y & Y4x & 0 & 0 & 0 \\
0 & 0 & 0 & F1xx & F1yy & F1xy^2 \\
0 & 0 & 0 & F2xx & F2yy & F2xy^2 \\
0 & 0 & 0 & F3xx & F3yy & F3xy^2 \\
0 & 0 & 0 & F4xx & F4yy & F4xy^2 \\
0 & 0 & 0 & F5xx & F5yy & F5xy^2 \\
0 & 0 & 0 & F6xx & F6yy & F6xy^2 \\
0 & 0 & 0 & F7xx & F7yy & F7xy^2 \\
0 & 0 & 0 & F8xx & F8yy & F8xy^2 \\
0 & 0 & 0 & F9xx & F9yy & F9xy^2 \\
0 & 0 & 0 & F10xx & F10yy & F10xy^2 \\
0 & 0 & 0 & F11xx & F11yy & F11xy^2 \\
0 & 0 & 0 & F12xx & F12yy & F12xy^2 \\
0 & 0 & 0 & F13xx & F13yy & F13xy^2 \\
0 & 0 & 0 & F14xx & F14yy & F14xy^2 \\
0 & 0 & 0 & F15xx & F15yy & F15xy^2 \\
0 & 0 & 0 & F16xx & F16yy & F16xy^2
\end{bmatrix} \tag{A.27}$$

$$D = \begin{bmatrix} A_{11} & A_{12} & A_{16} & 0 & 0 & 0 \\ A_{12} & A_{22} & A_{26} & 0 & 0 & 0 \\ A_{16} & A_{26} & A_{66} & 0 & 0 & 0 \\ 0 & 0 & 0 & D_{11} & D_{12} & D_{16} \\ 0 & 0 & 0 & D_{12} & D_{22} & D_{26} \\ 0 & 0 & 0 & D_{16} & D_{26} & D_{66} \end{bmatrix} \tag{A.28}$$

The stress-strain matrix D is calculated using the formulation provided by Halpin [458] based on the material invariants and geometric factors of the laminate. The material invariants are functions of the reduced stiffness matrix in local coordinates, $\overline{Q}$ [380]:

$$U_1 = \frac{1}{8}\left(3\overline{Q}_{11} + 3\overline{Q}_{22} + 2\overline{Q}_{12} + 4\overline{Q}_{66}\right) \tag{A.29a}$$

$$U_1 = \frac{1}{2}\left(\overline{Q}_{11} - \overline{Q}_{22}\right) \tag{A.29b}$$

$$U_3 = \frac{1}{8}\left(\overline{Q}_{11} + \overline{Q}_{22} - 2\overline{Q}_{12} - 4\overline{Q}_{66}\right) \tag{A.29c}$$

$$U_4 = \frac{1}{8}\left(\overline{Q}_{11} + \overline{Q}_{22} + 6\overline{Q}_{12} - 4\overline{Q}_{66}\right) \tag{A.29d}$$

$$U_5 = \frac{1}{8}\left(\overline{Q}_{11} + \overline{Q}_{22} - 2\overline{Q}_{12} + 4\overline{Q}_{66}\right) \tag{A.29e}$$

The geometric factors are functions of the ply angles θ and ply thicknesses h. For the extensional stiffness these are given by

$$V_{0A} = \sum_{k=1}^{n} h_k \tag{A.30a}$$

$$V_{1A} = \sum_{k=1}^{n} \cos(2\theta_k)(h_k - h_{k-1}) \tag{A.30b}$$

$$V_{2A} = \sum_{k=1}^{n} \sin(2\theta_k)(h_k - h_{k-1}) \tag{A.30c}$$

$$V_{3A} = \sum_{k=1}^{n} \cos(4\theta_k)(h_k - h_{k-1}) \tag{A.30d}$$

$$V_{4A} = \sum_{k=1}^{n} \sin(4\theta_k)(h_k - h_{k-1}) \tag{A.30e}$$

Similarly, for the bending stiffnesses,

$$V_{0D} = \frac{\left(\sum_{k=1}^{n} h_k\right)^3}{12} \tag{A.31a}$$

$$V_{1D} = \frac{1}{3}\sum_{k=1}^{n}\cos(2\theta_k)\left(h_k^3 - h_{k-1}^3\right) \tag{A.32b}$$

$$V_{2D} = \frac{1}{3}\sum_{k=1}^{n}\sin(2\theta_k)\left(h_k^3 - h_{k-1}^3\right) \tag{A.32c}$$

$$V_{3D} = \frac{1}{3}\sum_{k=1}^{n}\cos(4\theta_k)\left(h_k^3 - h_{k-1}^3\right) \tag{A.32d}$$

$$V_{4D} = \frac{1}{3}\sum_{k=1}^{n}\sin(4\theta_k)\left(h_k^3 - h_{k-1}^3\right) \tag{A.32e}$$

The invariant form of the [A] and [D] matrices can now be expressed as [458]

$$A_{11} = U_1 V_{0A} + U_2 V_{1A} + U_3 V_{3A} \tag{A.33a}$$

$$A_{22} = U_1 V_{0A} - U_2 V_{1A} + U_3 V_{3A} \tag{A.33b}$$

$$A_{12} = U_4 V_{0A} - U_3 V_{3A} \tag{A.33c}$$

$$A_{66} = U_5 V_{0A} - U_3 V_{3A} \tag{A.33d}$$

$$A_{16} = \frac{1}{2} U_2 V_{2A} + U_3 V_{4A} \tag{A.33e}$$

$$A_{26} = \frac{1}{2} U_2 V_{2A} - U_3 V_{4A} \tag{A.33f}$$

for the extensional stiffnesses and

$$D_{11} = U_1 V_{0D} + U_2 V_{1D} + U_3 V_{3D} \tag{A.34a}$$

$$D_{22} = U_1 V_{0D} - U_2 V_{1D} + U_3 V_{3D} \tag{A.34b}$$

$$D_{12} = U_4 V_{0D} - U_3 V_{3D} \tag{A.34c}$$

$$D_{66} = U_5 V_{0D} - U_3 V_{3D} \tag{A.34d}$$

$$D_{16} = \frac{1}{2} U_2 V_{2D} + U_3 V_{4D} \tag{A.34e}$$

$$D_{26} = \frac{1}{2} U_2 V_{2D} - U_3 V_{4D} \tag{A.34f}$$

for the bending stiffnesses.

The element stiffness matrix can now be algebraically determined as

$$[KM] \approx \sum_{i=1}^{4} W_i \det|J|_i \left([B]^T [D][B]\right)_i \tag{A.35}$$

where det|J| is the Jacobian previously described [427].

A.2 Composite Plate FEA Results

The C++ finite element code developed for this project was compared to both an ANSYS model and the computer program SYMM [380]. SYMM solves thin, symmetric composite plate problems approximately using the Ritz method. Two sizes of plates, two mesh densities, and both point load at the center of the plate and a transverse pressure load were explored. In all cases simple-support boundary conditions S4 [459] were applied along the edge x = a:

$$\text{S4: } w(a,y)=0 \qquad M_{xx}^{*}(a,y)=0 \qquad N_{xx}^{*}(a,y)=N_{xx}^{+x}(y) \qquad N_{xy}^{*}(a,y)=N_{xy}^{+x}(y) \tag{A.36}$$

Here M^* and N^* denote moment and stress resultants at any arbitrary interior point of the plate.

Table A.2 shows the composite plates analyzed and their displacements in z(w) results. All plates were square, i.e., the size specified denotes both the a and b lengths. Also, all plates compared were 16 plies with a quasi-isotropic [0/45/-45/90] layup and used the same material properties as shown in Chapter 5. Not all plate examples were analyzed with ANSYS, but those that were used the same elements used in Chapter 5, SHELL99. Figures A.3 and A.4 show the results of center point loads for large and small plates, respectively. Figure A.5 shows the results of pressure load on the small plate. It can be seen that higher mesh densities approximate the plate behavior more effectively than small numbers of elements, as would be expected. The results of WINGJOTA match very closely to that of the analytic, numerical analysis of SYMM and that of the ANSYS model. Approximately the same mesh density is used in the optimization program and provides sufficient accuracy to track load redistribution during the analysis.

A.3 Composite Four-Node Conforming Plate Finite Element Shape Function Derivatives and Equivalent Nodal Forces due to Transverse Element Pressure

A.3.1 Lagrange Shape Functions and Derivatives

In the following formulas the centroid of a general, non-overlapping closed polygon (element) defined by n vertices (xi, yi) must be found. The area of the polygon can be calculated as [460]

$$A=\frac{1}{2}\sum_{i=0}^{n-1}\left(x_i y_{i+1}-x_{i+1}y_i\right) \tag{A.37}$$

and its centroid is C = (xc, yc) where

$$xc=\frac{1}{6A}\sum_{i=0}^{n-1}\left(x_i+x_{i+1}\right)\left(x_i y_{i+1}-x_{i+1}y_i\right) \tag{A.38a}$$

$$yc=\frac{1}{6A}\sum_{i=0}^{n-1}\left(y_i+y_{i+1}\right)\left(x_i y_{i+1}-x_{i+1}y_i\right) \tag{A.38b}$$

Table A.2: Composite Plate Analysis Results

Plate	Size (m)	Elements	Load P (N)	Load Application	SYMM Result w (m)	C++ Result w (m)	Error (%) (SYMM to C++)	ANSYS Result w (m)
1	3.41	4	100	center	0.0852	0.0993	-16.6	
2	3.41	16	100	center	0.0852	0.0833	2.2	
3	0.5	4	100	center	0.00183	0.00182	0.66	0.00233
4	0.5	16	100	center	0.00183	0.00176	3.9	0.00197
5	0.5	4	400	pressure	0.000636	0.000741	-16.5	
6	0.5	16	400	pressure	0.000636	0.000666	-4.7	0.000682

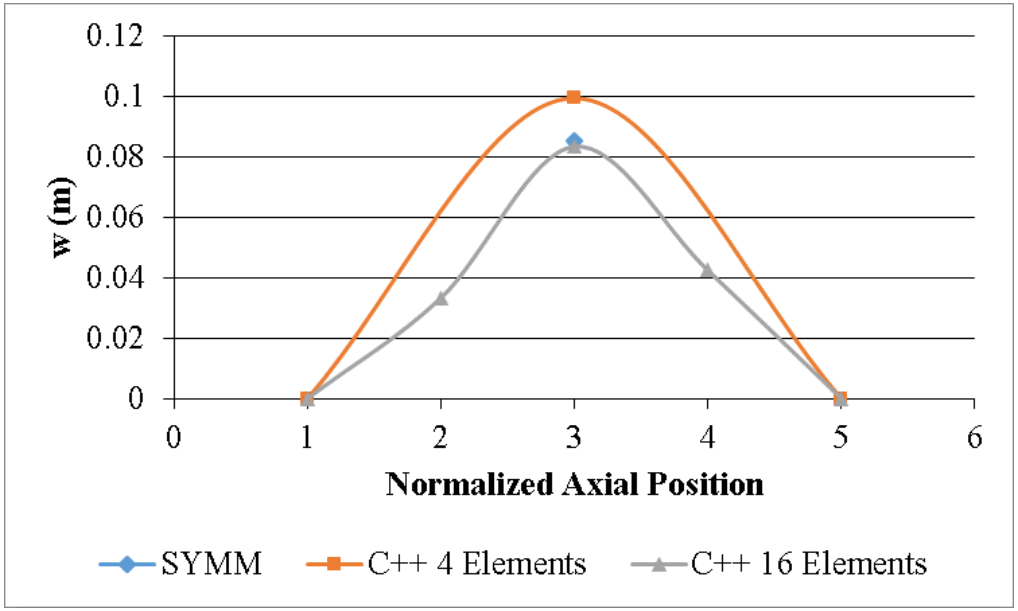

Figure A.3: Large Composite Plate, Center Point Load Results

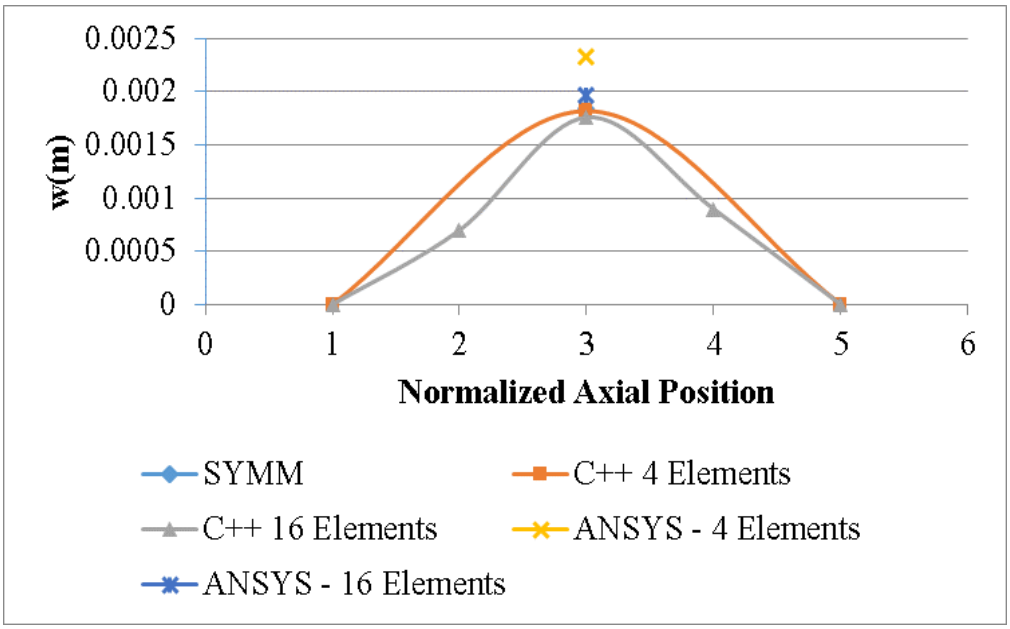

Figure A.4: Small Composite Plate, Center Point Load Results

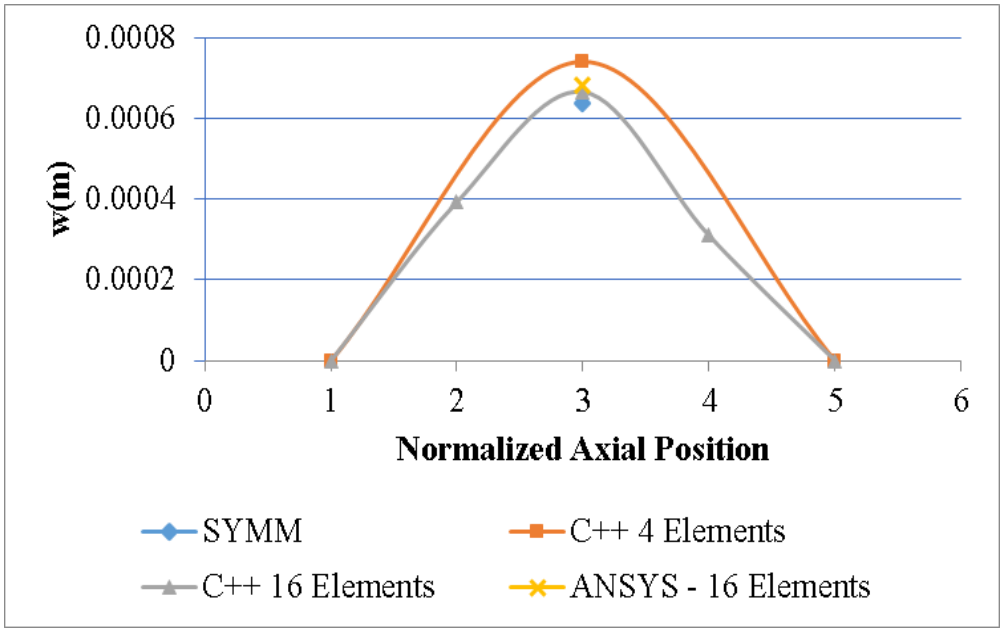

Figure A.5: Small Composite Plate, Pressure Load Results

Note: the symbol following Yi (i = 1, 2, 3, 4) denotes the first derivative with respect to that variable, e.g., Y1ξ represents the derivative of Y1 with respect to ξ.

$$Y1 = \tfrac{1}{4}(\xi - 1)(\eta - 1) = \tfrac{1}{4}\left(\frac{x - x_c}{a} - 1\right)\left(\frac{y - y_c}{b} - 1\right) \tag{A.39a}$$

$$Y1\xi = -\tfrac{1}{4}(1-\eta)$$

$$Y1x = -\tfrac{1}{4a}\left(1-\frac{y-y_c}{b}\right) \tag{A.39b}$$

$$Y1\eta = -\tfrac{1}{4}(1-\xi)$$

$$Y1y = -\tfrac{1}{4b}\left(1-\frac{x-x_c}{a}\right) \tag{A.39c}$$

$$Y2 = \tfrac{1}{4}(\xi-1)(\eta+1) = \tfrac{1}{4}\left(\frac{x-x_c}{a}-1\right)\left(\frac{y-y_c}{b}+1\right) \tag{A.40a}$$

$$Y2\xi = \tfrac{1}{4}(1-\eta)$$

$$Y1x = \tfrac{1}{4a}\left(1-\frac{y-y_c}{b}\right) \tag{A.40b}$$

$$Y2\eta = -\tfrac{1}{4}(1+\xi)$$

$$Y2y = -\tfrac{1}{4b}\left(1+\frac{x-x_c}{a}\right) \tag{A.40c}$$

$$Y3 = \tfrac{1}{4}(\xi+1)(\eta+1) = \tfrac{1}{4}\left(\frac{x-x_c}{a}+1\right)\left(\frac{y-y_c}{b}+1\right) \tag{A.41a}$$

$$Y3\xi = \tfrac{1}{4}(1+\eta)$$

$$Y3x = \tfrac{1}{4a}\left(1+\frac{y-y_c}{b}\right) \tag{A.41b}$$

$$Y3\eta = \tfrac{1}{4}(1+\xi)$$

$$Y3y = \tfrac{1}{4b}\left(1+\frac{x-x_c}{a}\right) \tag{A.41c}$$

$$Y4 = \tfrac{1}{4}(\xi+1)(\eta-1) = \tfrac{1}{4}\left(\frac{x-x_c}{a}+1\right)\left(\frac{y-y_c}{b}-1\right) \tag{A.42a}$$

$$Y4\xi = -\tfrac{1}{4}(1+\eta)$$

$$Y4x = -\tfrac{1}{4a}\left(1+\frac{y-y_c}{b}\right) \tag{A.42b}$$

$$Y4\eta = \tfrac{1}{4}(1-\xi)$$

$$Y4y = \tfrac{1}{4b}\left(1-\frac{x-x_c}{a}\right) \tag{A.42c}$$

A.3.2 Hermite Shape Functions and Derivatives

Note: the symbols following Fi (i = 1, 2, …, 16) denotes the derivatives with respect to those variables, e.g., F1ξξ represents the second derivative of F1 with respect to ξξ.

$$F1 = \tfrac{1}{16}(\xi-1)^2(-\xi-2)(\eta-1)^2(-\eta-2)$$
$$= \tfrac{1}{16}\left(\frac{x-x_c}{a}-1\right)^2\left(-\frac{x-x_c}{a}-2\right)\left(\frac{y-y_c}{b}-1\right)^2\left(-\frac{y-y_c}{b}-2\right) \quad \text{(A.43a)}$$

$$F1\xi\xi = \frac{(-\xi-2)(\eta-1)^2(-\eta-2)}{8} - \frac{(\xi-1)(\eta-1)^2(-\eta-2)}{4}$$

$$F1xx = \frac{\left(-\frac{x-x_c}{a}-2\right)\left(\frac{y-y_c}{b}-1\right)^2\left(-\frac{y-y_c}{b}-2\right)}{8a^2} - \frac{\left(\frac{x-x_c}{a}-1\right)\left(\frac{y-y_c}{b}-1\right)^2\left(-\frac{y-y_c}{b}-2\right)}{4a^2} \quad \text{(A.43b)}$$

$$F1\eta\eta = \frac{(\xi-1)^2(-\xi-2)(-\eta-2)}{8} - \frac{(\xi-1)^2(-\xi-2)(\eta-1)}{4}$$

$$F1yy = \frac{\left(\frac{x-x_c}{a}-1\right)^2\left(-\frac{x-x_c}{a}-2\right)\left(-\frac{y-y_c}{b}-2\right)}{8b^2} - \frac{\left(\frac{x-x_c}{a}-1\right)^2\left(-\frac{x-x_c}{a}-2\right)\left(\frac{y-y_c}{b}-1\right)}{4b^2} \quad \text{(A.43c)}$$

$$F1\xi\eta = \frac{(\xi-1)(-\xi-2)(\eta-1)(-\eta-2)}{4} - \frac{(\xi-1)(-\xi-2)(\eta-1)^2}{8} - \frac{(\xi-1)^2(\eta-1)(-\eta-2)}{8} + \frac{(\xi-1)^2(\eta-1)^2}{16}$$

$$F1xy = \frac{\left(\frac{x-x_c}{a}-1\right)\left(-\frac{x-x_c}{a}-2\right)\left(\frac{y-y_c}{b}-1\right)\left(-\frac{y-y_c}{b}-2\right)}{4ab} - \frac{\left(\frac{x-x_c}{a}-1\right)\left(-\frac{x-x_c}{a}-2\right)\left(\frac{y-y_c}{b}-1\right)^2}{8ab} \quad \text{(A.43d)}$$
$$- \frac{\left(\frac{x-x_c}{a}-1\right)^2\left(\frac{y-y_c}{b}-1\right)\left(-\frac{y-y_c}{b}-2\right)}{8ab} + \frac{\left(\frac{x-x_c}{a}-1\right)^2\left(\frac{y-y_c}{b}-1\right)^2}{16ab}$$

$$F2 = \tfrac{1}{16}(\xi-1)^2(-\xi-1)(\eta-1)^2(-\eta-2)$$
$$= -\tfrac{1}{16}\left(\frac{x-x_c}{a}-1\right)^2\left(1+\frac{x-x_c}{a}\right)\left(\frac{y-y_c}{b}-1\right)^2\left(-\frac{y-y_c}{b}-2\right) \quad \text{(A.44a)}$$

$$F2\xi\xi = \frac{(-\xi-1)(\eta-1)^2(-\eta-2)}{8} - \frac{(\xi-1)(\eta-1)^2(-\eta-2)}{4}$$

$$F2xx = -\frac{\left(1+\frac{x-x_c}{a}\right)\left(\frac{y-y_c}{b}-1\right)^2\left(-\frac{y-y_c}{b}-2\right)}{8a^2} - \frac{\left(\frac{x-x_c}{a}-1\right)\left(\frac{y-y_c}{b}-1\right)^2\left(-\frac{y-y_c}{b}-2\right)}{4a^2} \quad \text{(A.44b)}$$

$$F2\eta\eta = \frac{(\xi-1)^2(-\xi-1)(-\eta-2)}{8} - \frac{(\xi-1)^2(-\xi-1)(\eta-1)}{4}$$

$$F2yy = -\frac{\left(\frac{x-x_c}{a}-1\right)^2\left(1+\frac{x-x_c}{a}\right)\left(-\frac{y-y_c}{b}-2\right)}{8b^2} + \frac{\left(\frac{x-x_c}{a}-1\right)^2\left(1+\frac{x-x_c}{a}\right)\left(\frac{y-y_c}{b}-1\right)}{4b^2} \quad \text{(A.44c)}$$

$$F2\xi\eta = \frac{(\xi-1)(-\xi-1)(\eta-1)(-\eta-2)}{4} - \frac{(\xi-1)(-\xi-1)(\eta-1)^2}{8} - \frac{(\xi-1)^2(\eta-1)(-\eta-2)}{8} + \frac{(\xi-1)^2(\eta-1)^2}{16}$$

$$F2xy = -\frac{\left(\frac{x-x_c}{a}-1\right)\left(1+\frac{x-x_c}{a}\right)\left(\frac{y-y_c}{b}-1\right)\left(-\frac{y-y_c}{b}-2\right)}{4ab} + \frac{\left(\frac{x-x_c}{a}-1\right)\left(1+\frac{x-x_c}{a}\right)\left(\frac{y-y_c}{b}-1\right)^2}{8ab} \quad \text{(A.44d)}$$
$$- \frac{\left(\frac{x-x_c}{a}-1\right)^2\left(\frac{y-y_c}{b}-1\right)\left(-\frac{y-y_c}{b}-2\right)}{8ab} + \frac{\left(\frac{x-x_c}{a}-1\right)^2\left(\frac{y-y_c}{b}-1\right)^2}{16ab}$$

$$F3 = \tfrac{1}{16}(\xi-1)^2(-\xi-2)(\eta-1)^2(-\eta-1)$$
$$= -\tfrac{1}{16}\left(\frac{x-x_c}{a}-1\right)^2\left(-\frac{x-x_c}{a}-2\right)\left(\frac{y-y_c}{b}-1\right)^2\left(1+\frac{y-y_c}{b}\right) \quad \text{(A.45a)}$$

$$F3\xi\xi = \frac{(-\xi-2)(\eta-1)^2(-\eta-1)}{8} - \frac{(\xi-1)(\eta-1)^2(-\eta-1)}{4}$$

$$F3xx = -\frac{\left(-\frac{x-x_c}{a}-2\right)\left(\frac{y-y_c}{b}-1\right)^2\left(1+\frac{y-y_c}{b}\right)}{8a^2} + \frac{\left(\frac{x-x_c}{a}-1\right)\left(\frac{y-y_c}{b}-1\right)^2\left(1+\frac{y-y_c}{b}\right)}{4a^2} \quad \text{(A.45b)}$$

$$F3\eta\eta = \frac{(\xi-1)^2(-\xi-2)(-\eta-1)}{8} - \frac{(\xi-1)^2(-\xi-2)(\eta-1)}{4}$$

$$F3yy = -\frac{\left(\frac{x-x_c}{a}-1\right)^2\left(-\frac{x-x_c}{a}-2\right)\left(1+\frac{y-y_c}{b}\right)}{8b^2} - \frac{\left(\frac{x-x_c}{a}-1\right)^2\left(-\frac{x-x_c}{a}-2\right)\left(\frac{y-y_c}{b}-1\right)}{4b^2} \quad \text{(A.45c)}$$

$$F3\xi\eta = \frac{(\xi-1)(-\xi-1)(\eta-1)(-\eta-2)}{4} - \frac{(\xi-1)(-\xi-1)(\eta-1)^2}{8} - \frac{(\xi-1)^2(\eta-1)(-\eta-2)}{8} + \frac{(\xi-1)^2(\eta-1)^2}{16}$$

$$F3xy = -\frac{\left(\frac{x-x_c}{a}-1\right)\left(-\frac{x-x_c}{a}-2\right)\left(\frac{y-y_c}{b}-1\right)\left(1+\frac{y-y_c}{b}\right)}{4ab} - \frac{\left(\frac{x-x_c}{a}-1\right)\left(-\frac{x-x_c}{a}-2\right)\left(\frac{y-y_c}{b}-1\right)^2}{8ab} \quad \text{(A.45d)}$$
$$+ \frac{\left(\frac{x-x_c}{a}-1\right)^2\left(\frac{y-y_c}{b}-1\right)\left(1+\frac{y-y_c}{b}\right)}{8ab} + \frac{\left(\frac{x-x_c}{a}-1\right)^2\left(\frac{y-y_c}{b}-1\right)^2}{16ab}$$

$$F4 = \tfrac{1}{16}(\xi-1)^2(-\xi-1)(\eta-1)^2(-\eta-1)$$
$$= \tfrac{1}{16}\left(\frac{x-x_c}{a}-1\right)^2\left(1+\frac{x-x_c}{a}\right)\left(\frac{y-y_c}{b}-1\right)^2\left(1+\frac{y-y_c}{b}\right) \quad \text{(A.46a)}$$

$$F4\xi\xi = \frac{(-\xi-1)(\eta-1)^2(-\eta-1)}{8} - \frac{(\xi-1)(\eta-1)^2(-\eta-1)}{4}$$

$$F4xx = -\frac{\left(1+\frac{x-x_c}{a}\right)\left(\frac{y-y_c}{b}-1\right)^2\left(1+\frac{y-y_c}{b}\right)}{8a^2} + \frac{\left(\frac{x-x_c}{a}-1\right)\left(\frac{y-y_c}{b}-1\right)^2\left(1+\frac{y-y_c}{b}\right)}{4a^2} \quad \text{(A.46b)}$$

$$F4\eta\eta = \frac{(\xi-1)^2(-\xi-1)(-\eta-1)}{8} - \frac{(\xi-1)^2(-\xi-1)(\eta-1)}{4}$$

$$F4yy = \frac{\left(\frac{x-x_c}{a}-1\right)^2\left(1+\frac{x-x_c}{a}\right)\left(1+\frac{y-y_c}{b}\right)}{8b^2} + \frac{\left(\frac{x-x_c}{a}-1\right)^2\left(1+\frac{x-x_c}{a}\right)\left(\frac{y-y_c}{b}-1\right)}{4b^2} \quad \text{(A.46c)}$$

$$F4\xi\eta = \frac{(\xi-1)(-\xi-1)(\eta-1)(-\eta-1)}{4} - \frac{(\xi-1)(-\xi-1)(\eta-1)^2}{8} - \frac{(\xi-1)^2(\eta-1)(-\eta-1)}{8} + \frac{(\xi-1)^2(\eta-1)^2}{16}$$

$$F4xy = \frac{\left(\frac{x-x_c}{a}-1\right)\left(1+\frac{x-x_c}{a}\right)\left(\frac{y-y_c}{b}-1\right)\left(1+\frac{y-y_c}{b}\right)}{4ab} + \frac{\left(\frac{x-x_c}{a}-1\right)\left(1+\frac{x-x_c}{a}\right)\left(\frac{y-y_c}{b}-1\right)^2}{8ab} \quad \text{(A.46d)}$$
$$+ \frac{\left(\frac{x-x_c}{a}-1\right)^2\left(\frac{y-y_c}{b}-1\right)\left(1+\frac{y-y_c}{b}\right)}{8ab} + \frac{\left(\frac{x-x_c}{a}-1\right)^2\left(\frac{y-y_c}{b}-1\right)^2}{16ab}$$

$$F5 = \tfrac{1}{16}(\xi-1)^2(-\xi-2)(\eta+1)^2(\eta-2)$$
$$= \tfrac{1}{16}\left(1+\frac{x-x_c}{a}\right)^2\left(\frac{x-x_c}{a}-2\right)\left(\frac{y-y_c}{b}-1\right)^2\left(-\frac{y-y_c}{b}-2\right) \quad \text{(A.47a)}$$

$$F5\xi\xi = \frac{(-\xi-2)(\eta+1)^2(\eta-2)}{8} - \frac{(\xi-1)(\eta+1)^2(\eta-2)}{4}$$

$$F5xx = \frac{\left(\frac{x-x_c}{a}-2\right)\left(\frac{y-y_c}{b}-1\right)^2\left(-\frac{y-y_c}{b}-2\right)}{8a^2} + \frac{\left(1+\frac{x-x_c}{a}\right)\left(\frac{y-y_c}{b}-1\right)^2\left(-\frac{y-y_c}{b}-2\right)}{4a^2} \tag{A.47b}$$

$$F5\eta\eta = \frac{(\xi-1)^2(-\xi-2)(\eta-2)}{8} + \frac{(\xi-1)^2(-\xi-2)(\eta+1)}{4}$$

$$F5yy = \frac{\left(1+\frac{x-x_c}{a}\right)^2\left(\frac{x-x_c}{a}-2\right)\left(-\frac{y-y_c}{b}-2\right)}{8b^2} - \frac{\left(1+\frac{x-x_c}{a}\right)^2\left(\frac{x-x_c}{a}-2\right)\left(\frac{y-y_c}{b}-1\right)}{4b^2} \tag{A.47c}$$

$$F5\xi\eta = \frac{(\xi-1)(-\xi-2)(\eta+1)(\eta-2)}{4} + \frac{(\xi-1)(-\xi-2)(\eta+1)^2}{8} - \frac{(\xi-1)^2(\eta+1)(\eta-2)}{8} - \frac{(\xi-1)^2(\eta+1)^2}{16}$$

$$F5xy = \frac{\left(1+\frac{x-x_c}{a}\right)\left(\frac{x-x_c}{a}-2\right)\left(\frac{y-y_c}{b}-1\right)\left(-\frac{y-y_c}{b}-2\right)}{4ab} - \frac{\left(1+\frac{x-x_c}{a}\right)\left(\frac{x-x_c}{a}-2\right)\left(\frac{y-y_c}{b}-1\right)^2}{8ab} \tag{A.47d}$$
$$+ \frac{\left(1+\frac{x-x_c}{a}\right)^2\left(\frac{y-y_c}{b}-1\right)\left(-\frac{y-y_c}{b}-2\right)}{8ab} - \frac{\left(1+\frac{x-x_c}{a}\right)^2\left(\frac{y-y_c}{b}-1\right)^2}{16ab}$$

$$F6 = \tfrac{1}{16}(\xi-1)^2(-\xi-1)(\eta+1)^2(\eta-2)$$
$$= \tfrac{1}{16}\left(1+\frac{x-x_c}{a}\right)^2\left(1-\frac{x-x_c}{a}\right)\left(\frac{y-y_c}{b}-1\right)^2\left(-\frac{y-y_c}{b}-2\right) \tag{A.48a}$$

$$F6\xi\xi = \frac{(-\xi-1)(\eta+1)^2(\eta-2)}{8} - \frac{(\xi-1)(\eta+1)^2(\eta-2)}{4}$$

$$F6xx = \frac{\left(1-\frac{x-x_c}{a}\right)\left(\frac{y-y_c}{b}-1\right)^2\left(-\frac{y-y_c}{b}-2\right)}{8a^2} - \frac{\left(1+\frac{x-x_c}{a}\right)\left(\frac{y-y_c}{b}-1\right)^2\left(-\frac{y-y_c}{b}-2\right)}{4a^2} \tag{A.48b}$$

$$F6\eta\eta = \frac{(\xi-1)^2(-\xi-1)(\eta-2)}{8} + \frac{(\xi-1)^2(-\xi-1)(\eta+1)}{4}$$

$$F6yy = \frac{\left(1+\frac{x-x_c}{a}\right)^2\left(1-\frac{x-x_c}{a}\right)\left(-\frac{y-y_c}{b}-2\right)}{8b^2} - \frac{\left(1+\frac{x-x_c}{a}\right)^2\left(1-\frac{x-x_c}{a}\right)\left(\frac{y-y_c}{b}-1\right)}{4b^2} \tag{A.48c}$$

$$F6\xi\eta = \frac{(\xi-1)(-\xi-1)(\eta+1)(\eta-2)}{4} + \frac{(\xi-1)(-\xi-1)(\eta+1)^2}{8} - \frac{(\xi-1)^2(\eta+1)(\eta-2)}{8} - \frac{(\xi-1)^2(\eta+1)^2}{16}$$

$$F6xy = \frac{\left(1+\frac{x-x_c}{a}\right)\left(1-\frac{x-x_c}{a}\right)\left(\frac{y-y_c}{b}-1\right)\left(-\frac{y-y_c}{b}-2\right)}{4ab} - \frac{\left(1+\frac{x-x_c}{a}\right)\left(1-\frac{x-x_c}{a}\right)\left(\frac{y-y_c}{b}-1\right)^2}{8ab} \tag{A.48d}$$
$$- \frac{\left(1+\frac{x-x_c}{a}\right)^2\left(\frac{y-y_c}{b}-1\right)\left(-\frac{y-y_c}{b}-2\right)}{8ab} + \frac{\left(1+\frac{x-x_c}{a}\right)^2\left(\frac{y-y_c}{b}-1\right)^2}{16ab}$$

$$F7 = -\tfrac{1}{16}(\xi-1)^2(-\xi-2)(\eta+1)^2(\eta-1)$$
$$= -\tfrac{1}{16}\left(1+\frac{x-x_c}{a}\right)^2\left(\frac{x-x_c}{a}-2\right)\left(\frac{y-y_c}{b}-1\right)^2\left(1+\frac{y-y_c}{b}\right) \tag{A.49a}$$

$$F7\xi\xi = -\frac{(-\xi-2)(\eta+1)^2(\eta-1)}{8} + \frac{(\xi-1)(\eta+1)^2(\eta-1)}{4}$$

$$F7xx = -\frac{\left(\frac{x-x_c}{a}-2\right)\left(\frac{y-y_c}{b}-1\right)^2\left(1+\frac{y-y_c}{b}\right)}{8a^2} - \frac{\left(1+\frac{x-x_c}{a}\right)\left(\frac{y-y_c}{b}-1\right)^2\left(1+\frac{y-y_c}{b}\right)}{4a^2} \tag{A.49b}$$

$$F7\eta\eta = -\frac{(\xi-1)^2(-\xi-2)(\eta-1)}{8} - \frac{(\xi-1)^2(-\xi-2)(\eta+1)}{4}$$

$$F7yy = -\frac{\left(1+\frac{x-x_c}{a}\right)^2\left(\frac{x-x_c}{a}-2\right)\left(1+\frac{y-y_c}{b}\right)}{8b^2} - \frac{\left(1+\frac{x-x_c}{a}\right)^2\left(\frac{x-x_c}{a}-2\right)\left(\frac{y-y_c}{b}-1\right)}{4b^2} \tag{A.49c}$$

$$F7\xi\eta = -\frac{(\xi-1)(-\xi-2)(\eta+1)(\eta-1)}{4} - \frac{(\xi-1)(-\xi-2)(\eta+1)^2}{8} + \frac{(\xi-1)^2(\eta+1)(\eta-1)}{8} + \frac{(\xi-1)^2(\eta+1)^2}{16}$$

$$F7xy = -\frac{\left(1+\frac{x-x_c}{a}\right)\left(\frac{x-x_c}{a}-2\right)\left(\frac{y-y_c}{b}-1\right)\left(1+\frac{y-y_c}{b}\right)}{4ab} - \frac{\left(1+\frac{x-x_c}{a}\right)\left(\frac{x-x_c}{a}-2\right)\left(\frac{y-y_c}{b}-1\right)^2}{8ab} \tag{A.49d}$$

$$- \frac{\left(1+\frac{x-x_c}{a}\right)^2\left(\frac{y-y_c}{b}-1\right)\left(1+\frac{y-y_c}{b}\right)}{8ab} - \frac{\left(1+\frac{x-x_c}{a}\right)^2\left(\frac{y-y_c}{b}-1\right)^2}{16ab}$$

$$F8 = -\tfrac{1}{16}(\xi-1)^2(-\xi-1)(\eta+1)^2(\eta-1)$$

$$= -\tfrac{1}{16}\left(1+\frac{x-x_c}{a}\right)^2\left(1-\frac{x-x_c}{a}\right)\left(\frac{y-y_c}{b}-1\right)^2\left(1+\frac{y-y_c}{b}\right) \tag{A.50a}$$

$$F8\xi\xi = -\frac{(-\xi-1)(\eta+1)^2(\eta-1)}{8} + \frac{(\xi-1)(\eta+1)^2(\eta-1)}{4}$$

$$F8xx = -\frac{\left(1-\frac{x-x_c}{a}\right)\left(\frac{y-y_c}{b}-1\right)^2\left(1+\frac{y-y_c}{b}\right)}{8a^2} + \frac{\left(1+\frac{x-x_c}{a}\right)\left(\frac{y-y_c}{b}-1\right)^2\left(1+\frac{y-y_c}{b}\right)}{4a^2} \tag{A.50b}$$

$$F8\eta\eta = -\frac{(\xi-1)^2(-\xi-1)(\eta-1)}{8} - \frac{(\xi-1)^2(-\xi-1)(\eta+1)}{4}$$

$$F8yy = -\frac{\left(1+\frac{x-x_c}{a}\right)^2\left(1-\frac{x-x_c}{a}\right)\left(1+\frac{y-y_c}{b}\right)}{8b^2} - \frac{\left(1+\frac{x-x_c}{a}\right)^2\left(1-\frac{x-x_c}{a}\right)\left(\frac{y-y_c}{b}-1\right)}{4b^2} \tag{A.50c}$$

$$F8\xi\eta = -\frac{(\xi-1)(-\xi-1)(\eta+1)(\eta-1)}{4} - \frac{(\xi-1)(-\xi-1)(\eta+1)^2}{8} + \frac{(\xi-1)^2(\eta+1)(\eta-1)}{8} + \frac{(\xi-1)^2(\eta+1)^2}{16}$$

$$F8xy = -\frac{\left(1+\frac{x-x_c}{a}\right)\left(1-\frac{x-x_c}{a}\right)\left(\frac{y-y_c}{b}-1\right)\left(1+\frac{y-y_c}{b}\right)}{4ab} - \frac{\left(1+\frac{x-x_c}{a}\right)\left(1-\frac{x-x_c}{a}\right)\left(\frac{y-y_c}{b}-1\right)^2}{8ab} \tag{A.50d}$$

$$+ \frac{\left(1+\frac{x-x_c}{a}\right)^2\left(\frac{y-y_c}{b}-1\right)\left(1+\frac{y-y_c}{b}\right)}{8ab} + \frac{\left(1+\frac{x-x_c}{a}\right)^2\left(\frac{y-y_c}{b}-1\right)^2}{16ab}$$

$$F9 = \tfrac{1}{16}(\xi+1)^2(\xi-2)(\eta+1)^2(\eta-2)$$

$$= \tfrac{1}{16}\left(1+\frac{x-x_c}{a}\right)^2\left(\frac{x-x_c}{a}-2\right)\left(1+\frac{y-y_c}{b}\right)^2\left(\frac{y-y_c}{b}-2\right) \tag{A.51a}$$

$$F9\xi\xi = \frac{(\xi-2)(\eta+1)^2(\eta-2)}{8} + \frac{(\xi+1)(\eta+1)^2(\eta-2)}{4}$$

$$F9xx = \frac{\left(\frac{x-x_c}{a}-2\right)\left(1+\frac{y-y_c}{b}\right)^2\left(\frac{y-y_c}{b}-2\right)}{8a^2} + \frac{\left(1+\frac{x-x_c}{a}\right)\left(1+\frac{y-y_c}{b}\right)^2\left(\frac{y-y_c}{b}-2\right)}{4a^2} \tag{A.51b}$$

$$F9\eta\eta = \frac{(\xi+1)^2(\xi-2)(\eta-2)}{8} + \frac{(\xi+1)^2(\xi-2)(\eta+1)}{4}$$

$$F9yy = \frac{\left(1+\frac{x-x_c}{a}\right)^2\left(\frac{x-x_c}{a}-2\right)\left(\frac{y-y_c}{b}-2\right)}{8b^2} + \frac{\left(1+\frac{x-x_c}{a}\right)^2\left(\frac{x-x_c}{a}-2\right)\left(1+\frac{y-y_c}{b}\right)}{4b^2} \tag{A.51c}$$

$$F9\xi\eta = \frac{(\xi+1)(\xi-2)(\eta+1)(\eta-2)}{4} + \frac{(\xi+1)(\xi-2)(\eta+1)^2}{8} + \frac{(\xi+1)^2(\eta+1)(\eta-2)}{8} + \frac{(\xi+1)^2(\eta+1)^2}{16}$$

$$F9xy = \frac{\left(1+\frac{x-x_c}{a}\right)\left(\frac{x-x_c}{a}-2\right)\left(1+\frac{y-y_c}{b}\right)\left(1+\frac{y-y_c}{b}\right)}{4ab} + \frac{\left(1+\frac{x-x_c}{a}\right)\left(\frac{x-x_c}{a}-2\right)\left(1+\frac{y-y_c}{b}\right)^2}{8ab} \tag{A.51d}$$
$$+ \frac{\left(1+\frac{x-x_c}{a}\right)^2\left(1+\frac{y-y_c}{b}\right)\left(\frac{y-y_c}{b}-2\right)}{8ab} + \frac{\left(1+\frac{x-x_c}{a}\right)^2\left(\frac{y-y_c}{b}+1\right)^2}{16ab}$$

$$F10 = -\tfrac{1}{16}(\xi+1)^2(\xi-1)(\eta+1)^2(\eta-2)$$
$$= \tfrac{1}{16}\left(1+\frac{x-x_c}{a}\right)^2\left(1-\frac{x-x_c}{a}\right)\left(1+\frac{y-y_c}{b}\right)^2\left(\frac{y-y_c}{b}-2\right) \tag{A.52a}$$

$$F10\xi\xi = -\frac{(\xi-1)(\eta+1)^2(\eta-2)}{8} - \frac{(\xi+1)(\eta+1)^2(\eta-2)}{4}$$

$$F10xx = \frac{\left(1-\frac{x-x_c}{a}\right)\left(1+\frac{y-y_c}{b}\right)^2\left(\frac{y-y_c}{b}-2\right)}{8a^2} - \frac{\left(1+\frac{x-x_c}{a}\right)\left(1+\frac{y-y_c}{b}\right)^2\left(\frac{y-y_c}{b}-2\right)}{4a^2} \tag{A.52b}$$

$$F10\eta\eta = -\frac{(\xi+1)^2(\xi-1)(\eta-2)}{8} - \frac{(\xi+1)^2(\xi-1)(\eta+1)}{4}$$

$$F10yy = \frac{\left(1+\frac{x-x_c}{a}\right)^2\left(1-\frac{x-x_c}{a}\right)\left(\frac{y-y_c}{b}-2\right)}{8b^2} + \frac{\left(1+\frac{x-x_c}{a}\right)^2\left(1-\frac{x-x_c}{a}\right)\left(1+\frac{y-y_c}{b}\right)}{4b^2} \tag{A.52c}$$

$$F10\xi\eta = -\frac{(\xi+1)(\xi-1)(\eta+1)(\eta-2)}{4} - \frac{(\xi+1)(\xi-1)(\eta+1)^2}{8} - \frac{(\xi+1)^2(\eta+1)(\eta-2)}{8} - \frac{(\xi+1)^2(\eta+1)^2}{16}$$

$$F10xy = \frac{\left(1+\frac{x-x_c}{a}\right)\left(1-\frac{x-x_c}{a}\right)\left(1+\frac{y-y_c}{b}\right)\left(\frac{y-y_c}{b}-2\right)}{4ab} + \frac{\left(1+\frac{x-x_c}{a}\right)\left(1-\frac{x-x_c}{a}\right)\left(1+\frac{y-y_c}{b}\right)^2}{8ab} \tag{A.52d}$$
$$- \frac{\left(1+\frac{x-x_c}{a}\right)^2\left(1+\frac{y-y_c}{b}\right)\left(\frac{y-y_c}{b}-2\right)}{8ab} - \frac{\left(1+\frac{x-x_c}{a}\right)^2\left(\frac{y-y_c}{b}+1\right)^2}{16ab}$$

$$F11 = -\tfrac{1}{16}(\xi+1)^2(\xi-2)(\eta+1)^2(\eta-1)$$
$$= \tfrac{1}{16}\left(1+\frac{x-x_c}{a}\right)^2\left(\frac{x-x_c}{a}-2\right)\left(1+\frac{y-y_c}{b}\right)^2\left(1-\frac{y-y_c}{b}\right) \tag{A.53a}$$

$$F11_{\xi\xi} = -\frac{(\xi-2)(\eta+1)^2(\eta-1)}{8} - \frac{(\xi+1)(\eta+1)^2(\eta-1)}{4}$$

$$F11_{xx} = \frac{\left(\frac{x-x_c}{a}-2\right)\left(1+\frac{y-y_c}{b}\right)^2\left(1-\frac{y-y_c}{b}\right)}{8a^2} + \frac{\left(1+\frac{x-x_c}{a}\right)\left(1+\frac{y-y_c}{b}\right)^2\left(1-\frac{y-y_c}{b}\right)}{4a^2} \tag{A.53b}$$

$$F11_{\eta\eta} = -\frac{(\xi+1)^2(\xi-2)(\eta-1)}{8} - \frac{(\xi+1)^2(\xi-2)(\eta+1)}{4}$$

$$F11_{yy} = \frac{\left(1+\frac{x-x_c}{a}\right)^2\left(\frac{x-x_c}{a}-2\right)\left(1-\frac{y-y_c}{b}\right)}{8b^2} - \frac{\left(1+\frac{x-x_c}{a}\right)^2\left(\frac{x-x_c}{a}-2\right)\left(1+\frac{y-y_c}{b}\right)}{4b^2} \tag{A.53c}$$

$$F11_{\xi\eta} = -\frac{(\xi+1)(\xi-2)(\eta+1)(\eta-1)}{4} - \frac{(\xi+1)(\xi-2)(\eta+1)^2}{8} - \frac{(\xi+1)^2(\eta+1)(\eta-1)}{8} - \frac{(\xi+1)^2(\eta+1)^2}{16}$$

$$F11_{xy} = \frac{\left(1+\frac{x-x_c}{a}\right)\left(\frac{x-x_c}{a}-2\right)\left(1+\frac{y-y_c}{b}\right)\left(1-\frac{y-y_c}{b}\right)}{4ab} - \frac{\left(1+\frac{x-x_c}{a}\right)\left(\frac{x-x_c}{a}-2\right)\left(1+\frac{y-y_c}{b}\right)^2}{8ab} \tag{A.53d}$$
$$+ \frac{\left(1+\frac{x-x_c}{a}\right)^2\left(1+\frac{y-y_c}{b}\right)\left(1-\frac{y-y_c}{b}\right)}{8ab} - \frac{\left(1+\frac{x-x_c}{a}\right)^2\left(\frac{y-y_c}{b}+1\right)^2}{16ab}$$

$$F12 = \tfrac{1}{16}(\xi+1)^2(\xi-1)(\eta+1)^2(\eta-1)$$
$$= \tfrac{1}{16}\left(1+\frac{x-x_c}{a}\right)^2\left(1-\frac{x-x_c}{a}\right)\left(1+\frac{y-y_c}{b}\right)^2\left(1-\frac{y-y_c}{b}\right) \tag{A.54a}$$

$$F12_{\xi\xi} = \frac{(\xi-1)(\eta+1)^2(\eta-1)}{8} + \frac{(\xi+1)(\eta+1)^2(\eta-1)}{4}$$

$$F12_{xx} = \frac{\left(1-\frac{x-x_c}{a}\right)\left(1+\frac{y-y_c}{b}\right)^2\left(1-\frac{y-y_c}{b}\right)}{8a^2} - \frac{\left(1+\frac{x-x_c}{a}\right)\left(1+\frac{y-y_c}{b}\right)^2\left(1-\frac{y-y_c}{b}\right)}{4a^2} \tag{A.54b}$$

$$F12_{\eta\eta} = \frac{(\xi+1)^2(\xi-1)(\eta-1)}{8} + \frac{(\xi+1)^2(\xi-1)(\eta+1)}{4}$$

$$F12_{yy} = \frac{\left(1+\frac{x-x_c}{a}\right)^2\left(1-\frac{x-x_c}{a}\right)\left(1-\frac{y-y_c}{b}\right)}{8b^2} - \frac{\left(1+\frac{x-x_c}{a}\right)^2\left(1-\frac{x-x_c}{a}\right)\left(1+\frac{y-y_c}{b}\right)}{4b^2} \tag{A.54c}$$

$$F12_{\xi\eta} = \frac{(\xi+1)(\xi-1)(\eta+1)(\eta-1)}{4} + \frac{(\xi+1)(\xi-1)(\eta+1)^2}{8} + \frac{(\xi+1)^2(\eta+1)(\eta-1)}{8} + \frac{(\xi+1)^2(\eta+1)^2}{16}$$

$$F12_{xy} = \frac{\left(1+\frac{x-x_c}{a}\right)\left(1-\frac{x-x_c}{a}\right)\left(1+\frac{y-y_c}{b}\right)\left(1-\frac{y-y_c}{b}\right)}{4ab} - \frac{\left(1+\frac{x-x_c}{a}\right)\left(1-\frac{x-x_c}{a}\right)\left(1+\frac{y-y_c}{b}\right)^2}{8ab} \tag{A.54d}$$
$$- \frac{\left(1+\frac{x-x_c}{a}\right)^2\left(1+\frac{y-y_c}{b}\right)\left(1-\frac{y-y_c}{b}\right)}{8ab} + \frac{\left(1+\frac{x-x_c}{a}\right)^2\left(\frac{y-y_c}{b}+1\right)^2}{16ab}$$

$$F13 = \tfrac{1}{16}(\xi+1)^2(\xi-2)(\eta-1)^2(-\eta-2)$$
$$= \tfrac{1}{16}\left(1+\frac{x-x_c}{a}\right)^2\left(-\frac{x-x_c}{a}-2\right)\left(1+\frac{y-y_c}{b}\right)^2\left(\frac{y-y_c}{b}-2\right) \tag{A.55a}$$

$$F13\xi\xi = \frac{(\xi-2)(\eta-1)^2(-\eta-2)}{8} + \frac{(\xi+1)(\eta-1)^2(-\eta-2)}{4}$$

$$F13xx = \frac{\left(-\frac{x-x_c}{a}-2\right)\left(1+\frac{y-y_c}{b}\right)^2\left(\frac{y-y_c}{b}-2\right)}{8a^2} - \frac{\left(\frac{x-x_c}{a}-1\right)\left(1+\frac{y-y_c}{b}\right)^2\left(\frac{y-y_c}{b}-2\right)}{4a^2} \tag{A.55b}$$

$$F13\eta\eta = \frac{(\xi+1)^2(\xi-2)(-\eta-2)}{8} - \frac{(\xi+1)^2(\xi-2)(\eta-1)}{4}$$

$$F13yy = \frac{\left(\frac{x-x_c}{a}-1\right)^2\left(-\frac{x-x_c}{a}-2\right)\left(\frac{y-y_c}{b}-2\right)}{8b^2} + \frac{\left(\frac{x-x_c}{a}-1\right)^2\left(-\frac{x-x_c}{a}-2\right)\left(1+\frac{y-y_c}{b}\right)}{4b^2} \tag{A.55c}$$

$$F13\xi\eta = \frac{(\xi+1)(\xi-2)(\eta-1)(-\eta-2)}{4} - \frac{(\xi+1)(\xi-2)(\eta-1)^2}{8} + \frac{(\xi+1)^2(\eta-1)(-\eta-2)}{8} - \frac{(\xi+1)^2(\eta-1)^2}{16}$$

$$F13xy = \frac{\left(\frac{x-x_c}{a}-1\right)\left(-\frac{x-x_c}{a}-2\right)\left(1+\frac{y-y_c}{b}\right)\left(\frac{y-y_c}{b}-2\right)}{4ab} + \frac{\left(\frac{x-x_c}{a}-1\right)\left(-\frac{x-x_c}{a}-2\right)\left(1+\frac{y-y_c}{b}\right)^2}{8ab} \tag{A.55d}$$
$$- \frac{\left(\frac{x-x_c}{a}-1\right)^2\left(1+\frac{y-y_c}{b}\right)\left(\frac{y-y_c}{b}-2\right)}{8ab} - \frac{\left(\frac{x-x_c}{a}-1\right)^2\left(\frac{y-y_c}{b}+1\right)^2}{16ab}$$

$$F14 = -\tfrac{1}{16}(\xi+1)^2(\xi-1)(\eta-1)^2(-\eta-2)$$
$$= -\tfrac{1}{16}\left(\frac{x-x_c}{a}-1\right)^2\left(1+\frac{x-x_c}{a}\right)\left(1+\frac{y-y_c}{b}\right)^2\left(\frac{y-y_c}{b}-2\right) \tag{A.56a}$$

$$F14\xi\xi = -\frac{(\xi-1)(\eta-1)^2(-\eta-2)}{8} - \frac{(\xi+1)(\eta-1)^2(-\eta-2)}{4}$$

$$F14xx = -\frac{\left(1+\frac{x-x_c}{a}\right)\left(1+\frac{y-y_c}{b}\right)^2\left(\frac{y-y_c}{b}-2\right)}{8a^2} - \frac{\left(\frac{x-x_c}{a}-1\right)\left(1+\frac{y-y_c}{b}\right)^2\left(\frac{y-y_c}{b}-2\right)}{4a^2} \tag{A.56b}$$

$$F14\eta\eta = -\frac{(\xi+1)^2(\xi-1)(-\eta-2)}{8} + \frac{(\xi+1)^2(\xi-1)(\eta-1)}{4}$$

$$F14yy = -\frac{\left(\frac{x-x_c}{a}-1\right)^2\left(1+\frac{x-x_c}{a}\right)\left(\frac{y-y_c}{b}-2\right)}{8b^2} - \frac{\left(\frac{x-x_c}{a}-1\right)^2\left(1+\frac{x-x_c}{a}\right)\left(1+\frac{y-y_c}{b}\right)}{4b^2} \tag{A.56c}$$

$$F14\xi\eta = -\frac{(\xi+1)(\xi-1)(\eta-1)(-\eta-2)}{4} + \frac{(\xi+1)(\xi-1)(\eta-1)^2}{8} - \frac{(\xi+1)^2(\eta-1)(-\eta-2)}{8} + \frac{(\xi+1)^2(\eta-1)^2}{16}$$

$$F14xy = -\frac{\left(\frac{x-x_c}{a}-1\right)\left(1+\frac{x-x_c}{a}\right)\left(1+\frac{y-y_c}{b}\right)\left(\frac{y-y_c}{b}-2\right)}{4ab} - \frac{\left(\frac{x-x_c}{a}-1\right)\left(1+\frac{x-x_c}{a}\right)\left(1+\frac{y-y_c}{b}\right)^2}{8ab} \tag{A.56d}$$
$$- \frac{\left(\frac{x-x_c}{a}-1\right)^2\left(1+\frac{y-y_c}{b}\right)\left(\frac{y-y_c}{b}-2\right)}{8ab} - \frac{\left(\frac{x-x_c}{a}-1\right)^2\left(\frac{y-y_c}{b}+1\right)^2}{16ab}$$

$$F15 = \tfrac{1}{16}(\xi+1)^2(\xi-2)(\eta-1)^2(-\eta-1)$$
$$= \tfrac{1}{16}\left(\frac{x-x_c}{a}-1\right)^2\left(-\frac{x-x_c}{a}-2\right)\left(1+\frac{y-y_c}{b}\right)^2\left(1-\frac{y-y_c}{b}\right) \tag{A.57a}$$

$$F15\xi\xi = \frac{(\xi-2)(\eta-1)^2(-\eta-1)}{8} + \frac{(\xi+1)(\eta-1)^2(-\eta-1)}{4}$$

$$F15xx = \frac{\left(-\frac{x-x_c}{a}-2\right)\left(1+\frac{y-y_c}{b}\right)^2\left(1-\frac{y-y_c}{b}\right)}{8a^2} - \frac{\left(\frac{x-x_c}{a}-1\right)\left(1+\frac{y-y_c}{b}\right)^2\left(1-\frac{y-y_c}{b}\right)}{4a^2} \tag{A.57b}$$

$$F15\eta\eta = \frac{(\xi+1)^2(\xi-2)(-\eta-1)}{8} - \frac{(\xi+1)^2(\xi-2)(\eta-1)}{4}$$

$$F15yy = \frac{\left(\frac{x-x_c}{a}-1\right)^2\left(-\frac{x-x_c}{a}-2\right)\left(1-\frac{y-y_c}{b}\right)}{8b^2} - \frac{\left(\frac{x-x_c}{a}-1\right)^2\left(-\frac{x-x_c}{a}-2\right)\left(1+\frac{y-y_c}{b}\right)}{4b^2} \tag{A.57c}$$

$$F15\xi\eta = \frac{(\xi+1)(\xi-2)(\eta-1)(-\eta-1)}{4} - \frac{(\xi+1)(\xi-2)(\eta-1)^2}{8} + \frac{(\xi+1)^2(\eta-1)(-\eta-1)}{8} - \frac{(\xi+1)^2(\eta-1)^2}{16}$$

$$F15xy = \frac{\left(\frac{x-x_c}{a}-1\right)\left(-\frac{x-x_c}{a}-2\right)\left(1+\frac{y-y_c}{b}\right)\left(1-\frac{y-y_c}{b}\right)}{4ab} - \frac{\left(\frac{x-x_c}{a}-1\right)\left(-\frac{x-x_c}{a}-2\right)\left(1+\frac{y-y_c}{b}\right)^2}{8ab} \tag{A.57d}$$
$$- \frac{\left(\frac{x-x_c}{a}-1\right)^2\left(1+\frac{y-y_c}{b}\right)\left(1-\frac{y-y_c}{b}\right)}{8ab} + \frac{\left(\frac{x-x_c}{a}-1\right)^2\left(\frac{y-y_c}{b}+1\right)^2}{16ab}$$

$$F16 = -\frac{1}{16}(\xi+1)^2(\xi-)(\eta-1)^2(-\eta-1)$$

$$= -\frac{1}{16}\left(\frac{x-x_c}{a}-1\right)^2\left(1+\frac{x-x_c}{a}\right)\left(1+\frac{y-y_c}{b}\right)^2\left(1-\frac{y-y_c}{b}\right) \tag{A.58a}$$

$$F16\xi\xi = -\frac{(\xi-1)(\eta-1)^2(-\eta-1)}{8} - \frac{(\xi+1)(\eta-1)^2(-\eta-1)}{4}$$

$$F16xx = -\frac{\left(1+\frac{x-x_c}{a}\right)\left(1+\frac{y-y_c}{b}\right)^2\left(1-\frac{y-y_c}{b}\right)}{8a^2} - \frac{\left(\frac{x-x_c}{a}-1\right)\left(1+\frac{y-y_c}{b}\right)^2\left(1-\frac{y-y_c}{b}\right)}{4a^2} \tag{A.58b}$$

$$F16\eta\eta = -\frac{(\xi+1)^2(\xi-1)(-\eta-1)}{8} + \frac{(\xi+1)^2(\xi-1)(\eta-1)}{4}$$

$$F16yy = -\frac{\left(\frac{x-x_c}{a}-1\right)^2\left(1+\frac{x-x_c}{a}\right)\left(1-\frac{y-y_c}{b}\right)}{8b^2} + \frac{\left(\frac{x-x_c}{a}-1\right)^2\left(1+\frac{x-x_c}{a}\right)\left(1+\frac{y-y_c}{b}\right)}{4b^2} \tag{A.58c}$$

$$F16\xi\eta = -\frac{(\xi+1)(\xi-1)(\eta-1)(-\eta-1)}{4} + \frac{(\xi+1)(\xi-1)(\eta-1)^2}{8} - \frac{(\xi+1)^2(\eta-1)(-\eta-1)}{8} + \frac{(\xi+1)^2(\eta-1)^2}{16}$$

$$F16xy = -\frac{\left(\frac{x-x_c}{a}-1\right)\left(1+\frac{x-x_c}{a}\right)\left(1+\frac{y-y_c}{b}\right)\left(1-\frac{y-y_c}{b}\right)}{4ab} + \frac{\left(\frac{x-x_c}{a}-1\right)\left(1+\frac{x-x_c}{a}\right)\left(1+\frac{y-y_c}{b}\right)^2}{8ab} \tag{A.58d}$$
$$- \frac{\left(\frac{x-x_c}{a}-1\right)^2\left(1+\frac{y-y_c}{b}\right)\left(1-\frac{y-y_c}{b}\right)}{8ab} + \frac{\left(\frac{x-x_c}{a}-1\right)^2\left(\frac{y-y_c}{b}+1\right)^2}{16ab}$$

A.3.3 Equivalent Nodal Forces for Transverse Constant Element Pressure

$$F1_{press} = \frac{q\left(a^3 - a^2xc + 3axc^2 - xc^3\right)\left(b^3 - b^2yc + 3byc^2 - yc^3\right)}{4a^2b^2} \tag{A.59}$$

$$F2_{press} = \frac{q\left(2a^3 - 3a^2xc + 6axc^2 - 3xc^3\right)\left(b^3 - b^2yc + 3byc^2 - yc^3\right)}{12a^2b^2} \quad \text{(A.60)}$$

$$F3_{press} = \frac{q\left(a^3 - a^2xc + 3axc^2 - xc^3\right)\left(2b^3 - 3b^2yc + 6byc^2 - 3yc^3\right)}{12a^2b^2} \quad \text{(A.61)}$$

$$F4_{press} = \frac{q\left(2a^3 - 3a^2xc + 6axc^2 - 3xc^3\right)\left(2b^3 - 3b^2yc + 6byc^2 - 3yc^3\right)}{36a^2b^2} \quad \text{(A.62)}$$

$$F5_{press} = \frac{q\left(3a^3 + a^2xc - 3axc^2 + xc^3\right)\left(b^3 - b^2yc + 3byc^2 - yc^3\right)}{4a^2b^2} \quad \text{(A.63)}$$

$$F6_{press} = \frac{q\left(4a^3 - 15a^2xc + 12axc^2 - 3xc^3\right)\left(b^3 - b^2yc + 3byc^2 - yc^3\right)}{12a^2b^2} \quad \text{(A.64)}$$

$$F7_{press} = \frac{q\left(3a^3 + a^2xc - 3axc^2 + xc^3\right)\left(2b^3 - 3b^2yc + 6byc^2 - 3yc^3\right)}{12a^2b^2} \quad \text{(A.65)}$$

$$F8_{press} = \frac{q\left(4a^3 - 15a^2xc + 12axc^2 - 3xc^3\right)\left(2b^3 - 3b^2yc + 6byc^2 - 3yc^3\right)}{36a^2b^2} \quad \text{(A.66)}$$

$$F9_{press} = \frac{q\left(3a^3 + a^2xc - 3axc^2 + xc^3\right)\left(3b^3 + b^2yc - 3byc^2 + yc^3\right)}{4a^2b^2} \quad \text{(A.67)}$$

$$F10_{press} = \frac{q\left(4a^3 - 15a^2xc + 12axc^2 - 3xc^3\right)\left(3b^3 + b^2yc - 3byc^2 + yc^3\right)}{12a^2b^2} \quad \text{(A.68)}$$

$$F11_{press} = \frac{q\left(3a^3 + a^2xc - 3axc^2 + xc^3\right)\left(4b^3 - 15b^2yc + 12byc^2 - 3yc^3\right)}{12a^2b^2} \quad \text{(A.69)}$$

$$F12_{press} = \frac{q\left(4a^3 - 15a^2xc + 12axc^2 - 3xc^3\right)\left(4b^3 - 15b^2yc + 12byc^2 - 3yc^3\right)}{36a^2b^2} \quad \text{(A.70)}$$

$$F13_{press} = \frac{q\left(a^3 - a^2xc + 3axc^2 - xc^3\right)\left(3b^3 + b^2yc - 3byc^2 + yc^3\right)}{4a^2b^2} \quad \text{(A.71)}$$

$$F14_{press} = \frac{q\left(2a^3 - 3a^2xc + 6axc^2 - 3xc^3\right)\left(3b^3 + b^2yc - 3byc^2 + yc^3\right)}{12a^2b^2} \quad \text{(A.72)}$$

$$F15_{press} = \frac{q\left(a^3 - a^2xc + 3axc^2 - xc^3\right)\left(4b^3 - 15b^2yc + 12byc^2 - 3yc^3\right)}{12a^2b^2} \quad \text{(A.73)}$$

$$F16_{press} = \frac{q\left(2a^3 - 3a^2xc + 6axc^2 - 3xc^3\right)\left(4b^3 - 15b^2yc + 12byc^2 - 3yc^3\right)}{36a^2b^2} \quad \text{(A.74)}$$

Appendix B

SMEARED I-STRINGER CALCULATIONS

A smeared property stiffener ply was added to the laminate design in order to incorporate the I-stringers into the finite element model. The initial I-stringer design is based on matching the effective bending stiffness of the titanium doubler at the wing root joint, and all the stringers are assumed identical. However, the top and bottom flanges are not assumed to be the same width, and the laminate design is allowed to vary. Using the methods developed by Tuttle [380], the effective axial and bending stiffnesses of the skin/I-stringer combination were found.

The areas of the I-stringer cross section are given in equations (B.1 – B.5):

$$\text{Area of the web:} \quad Aw = hw * tweb \tag{B.1}$$

$$\text{Area of the bottom flange:} \quad Abf = tbf * bbf \tag{B.2}$$

$$\text{Area of the top flange:} \quad Atf = ttf * btf \tag{B.3}$$

$$\text{Area of the skin:} \quad Ask = s * tsk \tag{B.4}$$

$$\text{Area of the smeared I-stringer:} \quad As = s * ti \tag{B.5}$$

where hw is the height of the web; tweb, tbf, ttf, tsk, and ti are the thicknesses of the web, bottom flange, top flange, skin, and smeared I-stringer, respectively; and bbf and tbf are the widths of the bottom flange and top flange; and s is the stringer pitch.

The effective axial rigidity of the I-stringer and skin section is given by

$$AEi = AwEw + AbfEbf + AtfEtf + AskEsk \tag{B.6}$$

where Ew, Ebf, Etf, and Esk are the axial stiffnesses of the web, bottom flange, top flange, and skin, respectively.

The effective axial rigidity of the smeared I-stringer and skin section is given by

$$AEs = AsEs + AskEsk \tag{B.7}$$

Equating the effective axial rigidities and solving for Es yields

$$Es = \frac{AEi}{(ti * s)} \tag{B.8}$$

The centroid of the I-stringer and skin is given as

$$zb = \frac{1}{2}\left[\frac{AwEw(hw+2tbf)+tbfAbfEbf+AtfEtf(2tbf+2hw+ttf)}{AEi}\right] + \frac{1}{2}\left[\frac{AskEsk(tsk+2tbf+2hw+2ttf)}{AEi}\right] \tag{B.9}$$

The flexural Young's moduli of the I-stringer bottom flange, top flange, and skin are given as

$$E_{bf}^{fl} = \frac{12}{\left(d_{11}^{bf} tbf^3\right)} \tag{B.10}$$

$$E_{tf}^{fl} = \frac{12}{\left(d_{11}^{tf} ttf^3\right)} \tag{B.11}$$

$$E_{sk}^{fl} = \frac{12}{\left(d_{11}^{sk} tsk^3\right)} \tag{B.12}$$

where d_{11}^{bf}, d_{11}^{tf}, and d_{11}^{sk} are the longitudinal bending stiffnesses of the bottom flange, top flange, and skin, respectively. The moment of inertia of the I-stringer bottom flange, top flange, and skin are

$$I_{bf} = \frac{bbf * tbf^3}{12} \tag{B.13}$$

$$I_{tf} = \frac{btf * ttf^3}{12} \tag{B.14}$$

$$I_{sk} = \frac{s * tsk^3}{12} \tag{B.15}$$

The effective flexural rigidity of the I-stringer and skin section is

$$IEi = \frac{twebEw}{3}\left[(zb-tbf)^3 - (zb-hw-tbf)^3\right] + \left[\left(\frac{zb-tbf}{2}\right)^2 AbfEbf + \left(\frac{zb-tbf-hw-ttf}{2}\right)^2 AtfEtf + I_{bf}E_{bf}^{fl} + I_{tf}E_{tf}^{fl}\right] + \left[\left(\frac{zb-tbf-hw-ttf-tsk}{2}\right)^2 AskEsk + I_{sk}E_{sk}^{fl}\right] \tag{B.16}$$

Similarly, the centroid of the smeared I-stringer and skin section is

$$zbs = \left[\frac{ti^2 Es + 2tskEskti + tsk^2 Esk}{AEs}\right] \tag{B.17}$$

The effective flexural rigidity of the smeared I-stringer and skin section is

$$IEs = \frac{tiEs}{3}\left[zbs^3 - (zbs - ti)^3\right] + \left[\left(\frac{zbs - ti - tsk}{2}\right)^2 AskEsk + I_{sk}E_{sk}^{fl}\right] \tag{B.18}$$

Equating the effective flexural rigidities, substituting equation (A.8) for Es, and gathering terms yields

$$IEs = AAti^3 + BBti^2 + CCti + DD \tag{B.19}$$

where

$$
\begin{aligned}
AA = {} & \frac{\left(Abf^4\,Ebf^4\right)}{\left(3s\left(AbfEbf+AtfEtf+AwEw+Eskstsk\right)^3\right)}+\frac{\left(4Abf^3\,AtfEbf^3\,Etf\right)}{\left(3s\left(AbfEbf+AtfEtf+AwEw+Eskstsk\right)^3\right)} \\
& +\frac{\left(2Abf^2\,Atf^2\,Ebf^2\,Etf^2\right)}{\left(s\left(AbfEbf+AtfEtf+AwEw+Eskstsk\right)^3\right)}+\frac{\left(4AbfAtf^3\,EbfEtf^3\right)}{\left(3s\left(AbfEbf+AtfEtf+AwEw+Eskstsk\right)^3\right)} \\
& +\frac{\left(Atf^4\,Etf^4\right)}{\left(3s\left(AbfEbf+AtfEtf+AwEw+Eskstsk\right)^3\right)}+\frac{\left(4Abf^3\,AwAtfEbf^3\,Ew\right)}{\left(3s\left(AbfEbf+AtfEtf+AwEw+Eskstsk\right)^3\right)} \\
& +\frac{\left(4Abf^2\,AtfAwEbf^2\,EtfEw\right)}{\left(s\left(AbfEbf+AtfEtf+AwEw+Eskstsk\right)^3\right)}+\frac{\left(4AbfAtf^2\,AwEbfEtf^2\,Ew\right)}{\left(s\left(AbfEbf+AtfEtf+AwEw+Eskstsk\right)^3\right)} \\
& +\frac{\left(4Atf^3\,AwEtf^3\,Ew\right)}{\left(3s\left(AbfEbf+AtfEtf+AwEw+Eskstsk\right)^3\right)}+\frac{\left(2Abf^2\,Aw^2\,Ebf^2\,Ew^2\right)}{\left(s\left(AbfEbf+AtfEtf+AwEw+Eskstsk\right)^3\right)} \\
& +\frac{\left(4AbfAtfAw^2\,EbfEtfEw^2\right)}{\left(s\left(AbfEbf+AtfEtf+AwEw+Eskstsk\right)^3\right)}+\frac{\left(2Atf^2\,Aw^2\,Etf^2\,Ew^2\right)}{\left(s\left(AbfEbf+AtfEtf+AwEw+Eskstsk\right)^3\right)} \\
& +\frac{\left(4AbfAw^3\,EbfEw^3\right)}{\left(3s\left(AbfEbf+AtfEtf+AwEw+Eskstsk\right)^3\right)}+\frac{\left(4AtfAw^3\,EtfEw^3\right)}{\left(3s\left(AbfEbf+AtfEtf+AwEw+Eskstsk\right)^3\right)} \\
& +\frac{\left(Aw^4\,Ew^4\right)}{\left(3s\left(AbfEbf+AtfEtf+AwEw+Eskstsk\right)^3\right)}+\frac{\left(2Abf^3\,Ebf^3\,Esktsk\right)}{\left(AbfEbf+AtfEtf+AwEw+Eskstsk\right)^3} \\
& +\frac{\left(6Abf^2\,AtfEbf^2\,EskEtftsk\right)}{\left(AbfEbf+AtfEtf+AwEw+Eskstsk\right)^3}+\frac{\left(6AbfAtf^2\,EbfEskEtf^2tsk\right)}{\left(AbfEbf+AtfEtf+AwEw+Eskstsk\right)^3} \\
& +\frac{\left(2Atf^3\,EskEtf^3tsk\right)}{\left(AbfEbf+AtfEtf+AwEw+Eskstsk\right)^3}+\frac{\left(6Abf^2\,AwEbf^2\,EskEwtsk\right)}{\left(AbfEbf+AtfEtf+AwEw+Eskstsk\right)^3} \\
& +\frac{\left(12AbfAtfAwEbfEskEtfEwtsk\right)}{\left(AbfEbf+AtfEtf+AwEw+Eskstsk\right)^3}+\frac{\left(6Atf^2\,AwEskEtf^2\,Ewtsk\right)}{\left(AbfEbf+AtfEtf+AwEw+Eskstsk\right)^3} \\
& +\frac{\left(6AbfAw^2\,EbfEskEw^2tsk\right)}{\left(AbfEbf+AtfEtf+AwEw+Eskstsk\right)^3}+\frac{\left(6AtfAw^2\,EskEtfEw^2tsk\right)}{\left(AbfEbf+AtfEtf+AwEw+Eskstsk\right)^3} \\
& +\frac{\left(2Aw^3\,EskEw^3tsk\right)}{\left(AbfEbf+AtfEtf+AwEw+Eskstsk\right)^3}+\frac{\left(4Abf^2\,Ebf^2\,Esk^2\,stsk^2\right)}{\left(AbfEbf+AtfEtf+AwEw+Eskstsk\right)^3} \\
& +\frac{\left(8AbfAtfEbfEsk^2\,Etfstsk^2\right)}{\left(AbfEbf+AtfEtf+AwEw+Eskstsk\right)^3}+\frac{\left(4Atf^2\,Etf^2\,Esk^2\,stsk^2\right)}{\left(AbfEbf+AtfEtf+AwEw+Eskstsk\right)^3} \\
& +\frac{\left(8AbfAwEbfEsk^2\,Ewstsk^2\right)}{\left(AbfEbf+AtfEtf+AwEw+Eskstsk\right)^3}+\frac{\left(8AtfAwEtfEsk^2\,Ewstsk^2\right)}{\left(AbfEbf+AtfEtf+AwEw+Eskstsk\right)^3} \\
& +\frac{\left(4Aw^2\,Esk^2\,Ew^2\,stsk^2\right)}{\left(AbfEbf+AtfEtf+AwEw+Eskstsk\right)^3}+\frac{\left(7AbfEbfEsk^3\,s^2tsk^3\right)}{\left(3\left(AbfEbf+AtfEtf+AwEw+Eskstsk\right)^3\right)} \\
& +\frac{\left(7AtfEsk^3\,Etfs^2tsk^3\right)}{\left(3\left(AbfEbf+AtfEtf+AwEw+Eskstsk\right)^3\right)}+\frac{\left(7AwEsk^3\,Ews^2tsk^3\right)}{\left(3\left(AbfEbf+AtfEtf+AwEw+Eskstsk\right)^3\right)}
\end{aligned}
\tag{B.20}
$$

$$BB = \frac{\left(Abf^3 Ebf^3 Esk tsk^2\right)}{\left(AbfEbf + AtfEtf + AwEw + Eskstsk\right)^3} + \frac{\left(3Abf^2 AtfEbf^2 EskEtf tsk^2\right)}{\left(AbfEbf + AtfEtf + AwEw + Eskstsk\right)^3}$$
$$+ \frac{\left(3AbfAtf^2 EbfEskEtf^2 tsk^2\right)}{\left(AbfEbf + AtfEtf + AwEw + Eskstsk\right)^3} + \frac{\left(Atf^3 EskEtf^3 tsk^2\right)}{\left(AbfEbf + AtfEtf + AwEw + Eskstsk\right)^3}$$
$$+ \frac{\left(3Abf^2 AwEbf^2 EskEwtsk^2\right)}{\left(AbfEbf + AtfEtf + AwEw + Eskstsk\right)^3} + \frac{\left(6AbfAtfAwEbfEskEtfEwtsk^2\right)}{\left(AbfEbf + AtfEtf + AwEw + Eskstsk\right)^3}$$
$$+ \frac{\left(3Atf^2 AwEskEtf^2 Ewtsk^2\right)}{\left(AbfEbf + AtfEtf + AwEw + Eskstsk\right)^3} + \frac{\left(6AbfAtfAwEbfEskEtfEwtsk^2\right)}{\left(AbfEbf + AtfEtf + AwEw + Eskstsk\right)^3}$$
$$+ \frac{\left(3Atf^2 AwEskEtf^2 Ewtsk^2\right)}{\left(AbfEbf + AtfEtf + AwEw + Eskstsk\right)^3} + \frac{\left(3AbfAw^2 EbfEskEw^2 tsk^2\right)}{\left(AbfEbf + AtfEtf + AwEw + Eskstsk\right)^3}$$
$$+ \frac{\left(3AtfAw^2 EskEtfEw^2 tsk^2\right)}{\left(AbfEbf + AtfEtf + AwEw + Eskstsk\right)^3} + \frac{\left(Aw^3 EskEw^3 tsk^2\right)}{\left(AbfEbf + AtfEtf + AwEw + Eskstsk\right)^3} \qquad \text{(B.21)}$$
$$+ \frac{\left(4Abf^2 Ebf^2 Esk^2 stsk^3\right)}{\left(AbfEbf + AtfEtf + AwEw + Eskstsk\right)^3} + \frac{\left(8AbfAtfEbfEsk^2 Etfstsk^3\right)}{\left(AbfEbf + AtfEtf + AwEw + Eskstsk\right)^3}$$
$$+ \frac{\left(4Atf^2 Esk^2 Etf^2 stsk^3\right)}{\left(AbfEbf + AtfEtf + AwEw + Eskstsk\right)^3} + \frac{\left(8AbfAwEbfEsk^2 Ewstsk^3\right)}{\left(AbfEbf + AtfEtf + AwEw + Eskstsk\right)^3}$$
$$+ \frac{\left(8AtfAwEsk^2 EtfEwstsk^3\right)}{\left(AbfEbf + AtfEtf + AwEw + Eskstsk\right)^3} + \frac{\left(4Aw^2 Esk^2 Ew^2 stsk^3\right)}{\left(AbfEbf + AtfEtf + AwEw + Eskstsk\right)^3}$$
$$+ \frac{\left(3AbfEbfEsk^3 s^2 tsk^4\right)}{\left(AbfEbf + AtfEtf + AwEw + Eskstsk\right)^3} + \frac{\left(3AtfEsk^3 Etfs^2 tsk^4\right)}{\left(AbfEbf + AtfEtf + AwEw + Eskstsk\right)^3}$$
$$+ \frac{\left(3AwEsk^3 Ews^2 tsk^4\right)}{\left(AbfEbf + AtfEtf + AwEw + Eskstsk\right)^3} + \frac{\left(AskEsk^3 s^2 tsk^2\right)}{\left(AbfEbf + AtfEtf + AwEw + Eskstsk\right)^2}$$

$$CC = \frac{\left(Abf^2 Ebf^2 Esk^2 stsk^4\right)}{\left(AbfEbf + AtfEtf + AwEw + Eskstsk\right)^3} + \frac{\left(2AbfAtfEbfEsk^2 Etfstsk^4\right)}{\left(AbfEbf + AtfEtf + AwEw + Eskstsk\right)^3}$$
$$+ \frac{\left(Atf^2 Esk^2 Etf^2 stsk^4\right)}{\left(AbfEbf + AtfEtf + AwEw + Eskstsk\right)^3} + \frac{\left(2AbfAwEbfEsk^2 Ewstsk^4\right)}{\left(AbfEbf + AtfEtf + AwEw + Eskstsk\right)^3}$$
$$+ \frac{\left(2AtfAwEsk^2 Etfstsk^4\right)}{\left(AbfEbf + AtfEtf + AwEw + Eskstsk\right)^3} + \frac{\left(Aw^2 Esk^2 Ew^2 stsk^4\right)}{\left(AbfEbf + AtfEtf + AwEw + Eskstsk\right)^3}$$
$$+ \frac{\left(AbfEbfEsk^3 s^2 tsk^5\right)}{\left(AbfEbf + AtfEtf + AwEw + Eskstsk\right)^3} + \frac{\left(AtfEsk^3 Etfs^2 tsk^5\right)}{\left(AbfEbf + AtfEtf + AwEw + Eskstsk\right)^3} \qquad \text{(B.22)}$$
$$+ \frac{\left(AwEsk^3 Ews^2 tsk^5\right)}{\left(AbfEbf + AtfEtf + AwEw + Eskstsk\right)^3} - \frac{\left(AbfAskEbfEsk^2 stsk^2\right)}{\left(AbfEbf + AtfEtf + AwEw + Eskstsk\right)^2}$$
$$- \frac{\left(AskAtfEsk^2 Etfstsk^2\right)}{\left(AbfEbf + AtfEtf + AwEw + Eskstsk\right)^2} - \frac{\left(AskAwEsk^2 Ewstsk^2\right)}{\left(AbfEbf + AtfEtf + AwEw + Eskstsk\right)^2}$$
$$+ \frac{\left(AskEsk^3 s^2 tsk^3\right)}{\left(AbfEbf + AtfEtf + AwEw + Eskstsk\right)^2}$$

$$DD = EflskIsk + \frac{\left(Abf^2\,AskEbf^2\,Esktsk^2\right)}{\left(4\left(AbfEbf + AtfEtf + AwEw + Eskstsk\right)^2\right)} + \frac{\left(AbfAskAtfEbfEskEtftsk^2\right)}{\left(4\left(AbfEbf + AtfEtf + AwEw + Eskstsk\right)^2\right)} - \frac{\left(AskAtf^2\,EskEtf^2\,tsk^2\right)}{\left(4\left(AbfEbf + AtfEtf + AwEw + Eskstsk\right)^2\right)} + \frac{\left(AbfAskAwEbfEskEwtsk^2\right)}{\left(2\left(AbfEbf + AtfEtf + AwEw + Eskstsk\right)^2\right)} + \frac{\left(AskAtfAwEskEtfEwtsk^2\right)}{\left(2\left(AbfEbf + AtfEtf + AwEw + Eskstsk\right)^2\right)} + \frac{\left(AskAw^2\,EskEw^2tsk^2\right)}{\left(4\left(AbfEbf + AtfEtf + AwEw + Eskstsk\right)^2\right)} - \frac{\left(AbfAskEbfEsk^2stsk^3\right)}{\left(2\left(AbfEbf + AtfEtf + AwEw + Eskstsk\right)^2\right)} - \frac{\left(AskAtfEsk^2\,Etfstsk^3\right)}{\left(2\left(AbfEbf + AtfEtf + AwEw + Eskstsk\right)^2\right)} - \frac{\left(AskAwEsk^2\,Ewstsk^3\right)}{\left(2\left(AbfEbf + AtfEtf + AwEw + Eskstsk\right)^2\right)} + \frac{\left(AskEsk^3s^2tsk^4\right)}{\left(4\left(AbfEbf + AtfEtf + AwEw + Eskstsk\right)^2\right)} \tag{B.23}$$

Solving equation (A.19) for the smeared I-stringer thickness ti results in three solutions:

$$ti1 = -\frac{BB}{3AA} + \frac{\left[2^{1/3}\left(-BB^2 + 3AACC\right)\right]}{\left[3AA\left(XX + \sqrt{\left(4\left(-BB^2 + 3AACC\right)^3 + XX^2\right)}\right)^{1/3}\right]} - \frac{1}{3*2^{1/3}\,AA}\left[\left(XX + \sqrt{\left(4\left(-BB^2 + 3AACC\right)^3 + XX^2\right)}\right)^{1/3}\right] \tag{B.24a}$$

$$ti2 = -\frac{BB}{3AA} - \frac{\left[\left(1 + i\sqrt{3}\right)\left(-BB^2 + 3AACC\right)\right]}{\left[3*2^{1/3}\,AA\left(XX + \sqrt{\left(4\left(-BB^2 + 3AACC\right)^3 + XX^2\right)}\right)^{1/3}\right]} + \frac{1}{6*2^{1/3}\,AA}\left[\left(\left(1 - i\sqrt{3}\right)XX + \sqrt{\left(4\left(-BB^2 + 3AACC\right)^3 + XX^2\right)}\right)^{1/3}\right] \tag{B.24b}$$

$$ti3 = -\frac{BB}{3AA} - \frac{\left[\left(1 - i\sqrt{3}\right)\left(-BB^2 + 3AACC\right)\right]}{\left[3*2^{1/3}\,AA\left(XX + \sqrt{\left(4\left(-BB^2 + 3AACC\right)^3 + XX^2\right)}\right)^{1/3}\right]} + \frac{1}{6*2^{1/3}\,AA}\left[\left(\left(1 + i\sqrt{3}\right)XX + \sqrt{\left(4\left(-BB^2 + 3AACC\right)^3 + XX^2\right)}\right)^{1/3}\right] \tag{B.24c}$$

where

$$XX = 2BB^3 - 9AABBCC + 27AA^2DD - 27AA^2IEi \tag{B.25}$$

The smeared I-stringer thickness is chosen to be the real value of the solution with a very small imaginary part. The smeared I-stringer stiffness can then be found using equation (A.8). These smeared properties are used in the finite element analysis at each iteration of the design values.

Appendix C

PRELIMINARY WING DESIGN AND ANSYS® RESULTS

Section C.1 contains details of the preliminary wing design, including geometry; airfoil thickness; initial stringer panel property calculations; the applied mass loads; applied fuel pressures; and the emergency landing loads.

The contents of the title page of the University of Washington Subsonic Transport Composite Wing Model (http://depts.washington.edu/amtas/publications/wing/index.html) is shown in Section C.2. In Section C.3 the internal loads from the ANSYS wing model for Panel 18 used as boundary conditions for the FEM analysis in the optimization routine.

C.1 Baseline Wing Design

Table C.1: ANSYS Wing Design Model Keypoint Geometry

Rib	Keypoints	X (m)	Y (m)	Z (m)
1	14	2.43	1.98	-0.649
	17	2.43	1.98	0.472
	16	2.43	6.84	0.378
	15	2.43	6.84	-0.537
2	1	1.63	1.98	-0.649
	2	1.63	1.98	0.472
	3	1.63	6.84	0.378
	4	1.63	6.84	-0.537
3	5	0.80	1.98	-0.649
	6	0.80	1.98	0.472
	7	0.80	6.84	0.378
	8	0.80	6.84	-0.537
4	146	0.00	1.98	-0.649
	147	0.00	1.98	0.472
	148	0.00	6.84	0.378
	13	0.00	6.84	-0.537
5	158	-0.74	2.48	-0.659
	155	-0.74	2.46	0.488
	156	0.00	3.60	0.558
	157	0.00	3.62	-0.683

Table C.1: ANSYS Wing Design Model Keypoint Geometry (continued)

Rib	Keypoints	X (m)	Y (m)	Z (m)
6	154	-1.48	2.97	-0.667
	151	-1.48	2.95	0.504
	152	0.00	5.22	0.506
	153	0.00	5.24	-0.639
7	149	-2.22	3.43	-0.674
	150	-2.22	3.43	0.474
	148	0.00	6.84	0.378
	13	0.00	6.84	-0.537
8	145	-2.80	3.80	-0.663
	142	-2.80	3.80	0.428
	143	-0.64	7.14	0.279
	144	-0.64	7.14	-0.523
9	141	-3.36	4.17	-0.646
	138	-3.36	4.17	0.417
	139	-1.24	7.42	0.272
	140	-1.24	7.42	-0.510
10	137	-3.91	4.53	-0.629
	134	-3.91	4.53	0.406
	135	-1.85	7.71	0.265
	136	-1.85	7.71	-0.497
11	133	-4.47	4.89	-0.612
	130	-4.47	4.89	0.395
	131	-2.46	7.99	0.258
	132	-2.46	7.99	-0.483
12	129	-5.03	5.25	-0.595
	126	-5.03	5.25	0.385
	127	-3.06	8.27	0.251
	128	-3.06	8.27	-0.470
13	125	-5.75	5.72	-0.573
	122	-5.75	5.72	0.370
	123	-3.85	8.64	0.242
	124	-3.85	8.64	-0.453
14	121	-6.48	6.19	-0.551
	118	-6.48	6.19	0.356
	119	-4.64	9.01	0.232
	120	-4.64	9.01	-0.436
15	117	-6.99	6.52	-0.535
	114	-6.99	6.52	0.346
	115	-5.21	9.27	0.226
	116	-5.21	9.27	-0.424

Table C.1: ANSYS Wing Design Model Keypoint Geometry (continued)

Rib	Keypoints	X (m)	Y (m)	Z (m)
16	113	-7.50	6.86	-0.520
	110	-7.50	6.86	0.336
	111	-5.77	9.53	0.219
	112	-5.77	9.53	-0.412
17	109	-8.02	7.19	-0.504
	106	-8.02	7.19	0.326
	107	-6.33	9.80	0.213
	108	-6.33	9.80	-0.400
18	105	-8.54	7.53	-0.488
	102	-8.54	7.53	0.316
	103	-6.89	10.10	0.207
	104	-6.89	10.10	-0.387
19	101	-9.05	7.86	-0.473
	98	-9.05	7.86	0.305
	99	-7.45	10.30	0.200
	100	-7.45	10.30	-0.375
20	97	-9.56	8.20	-0.457
	94	-9.56	8.20	0.295
	95	-8.02	10.60	0.194
	96	-8.02	10.60	-0.363
21	93	-10.10	8.53	-0.441
	90	-10.10	8.53	0.285
	91	-8.58	10.80	0.187
	92	-8.58	10.80	-0.351
22	89	-10.60	8.86	-0.426
	86	-10.60	8.86	0.275
	87	-9.14	11.10	0.181
	88	-9.14	11.10	-0.339
23	85	-11.10	9.20	-0.410
	82	-11.10	9.20	0.265
	83	-9.70	11.40	0.174
	84	-9.70	11.40	-0.327
24	81	-11.60	9.53	-0.394
	78	-11.60	9.53	0.255
	79	-10.30	11.60	0.168
	80	-10.30	11.60	-0.314
25	77	-12.10	9.87	-0.379
	74	-12.10	9.87	0.245
	75	-10.80	11.90	0.161
	76	-10.80	11.90	-0.302

Table C.1: ANSYS Wing Design Model Keypoint Geometry (continued)

Rib	Keypoints	X (m)	Y (m)	Z (m)
26	73	-12.70	10.20	-0.363
	70	-12.70	10.20	0.235
	71	-11.40	12.20	0.155
	72	-11.40	12.20	-0.290
27	69	-13.20	10.50	-0.347
	66	-13.20	10.50	0.224
	67	-11.90	12.40	0.148
	68	-11.90	12.40	-0.278
28	65	-13.70	10.90	-0.332
	62	-13.70	10.90	0.214
	63	-12.50	12.70	0.142
	64	-12.50	12.70	-0.266
29	61	-14.20	11.20	-0.316
	58	-14.20	11.20	0.204
	59	-13.10	12.90	0.135
	60	-13.10	12.90	-0.254
30	57	-14.70	11.50	-0.300
	54	-14.70	11.50	0.194
	55	-13.60	13.20	0.129
	56	-13.60	13.20	-0.241
31	53	-15.20	11.90	-0.285
	50	-15.20	11.90	0.184
	51	-14.20	13.50	0.122
	52	-14.20	13.50	-0.229
32	49	-15.70	12.20	-0.269
	46	-15.70	12.20	0.174
	47	-14.80	13.70	0.116
	48	-14.80	13.70	-0.217
33	45	-16.00	12.40	-0.262
	42	-16.00	12.40	0.169
	43	-15.00	13.80	0.113
	44	-15.00	13.80	-0.211
34	41	-16.20	12.50	-0.254
	38	-16.20	12.50	0.164
	39	-15.30	14.00	0.110
	40	-15.30	14.00	-0.205
35	37	-16.80	12.90	-0.237
	34	-16.80	12.90	0.153
	35	-15.90	14.30	0.103
	36	-15.90	14.30	-0.192

Table C.1: ANSYS Wing Design Model Keypoint Geometry (continued)

Rib	Keypoints	X (m)	Y (m)	Z (m)
36	33	-17.30	13.20	-0.221
	30	-17.30	13.20	0.143
	31	-16.50	14.50	0.096
	32	-16.50	14.50	-0.179
37	29	-17.90	13.60	-0.204
	26	-17.90	13.60	0.132
	27	-17.10	14.80	0.089
	28	-17.10	14.80	-0.166
38	25	-18.40	14.00	-0.187
	22	-18.40	14.00	0.121
	23	-17.70	15.10	0.082
	24	-17.70	15.10	-0.153
39	21	-19.00	14.30	-0.170
	18	-19.00	14.30	0.110
	19	-18.30	15.40	0.075
	20	-18.30	15.40	-0.140
40	10	-19.50	14.70	-0.154
	11	-19.50	14.70	0.099
	12	-18.90	15.70	0.068
	9	-18.90	15.70	-0.127
Tip	166	-18.20	12.80	0.000
	170	-18.20	13.70	0.000
	171	-18.20	14.60	0.000
	180	-18.20	15.40	0.000
	188	-18.20	16.20	0.000

Table C.2: ANSYS Wing Design Model Areas

Upper Skin		Lower Skin		Front Spar		Rear Spar		Ribs		
Panel No.	Area	Panel No.	Area	Panel No.	Area	Panel No.	Area	No.	Area	Thickness T/C Ratio
1	40	1	1	1	118	1	157	1	49	1.532961438
2	41	2	2	2	119	2	158	2	45	1.532961438
3	48	3	193	3	120	3	159	3	46	1.463712413
4	6	4	4	4	121	4	160	4	48	1.392100378
5	7	5	5	5	122	5	161	5	87	
6	43	6	82	6	123	6	162	6	86	
7	42	7	44	7	124	7	163	7	85	1.321783631
8	83	8	8	8	125	8	164	8	81	1.252623699
9	84	9	9	9	126	9	165	9	80	1.184656111
10	88	10	10	10	127	10	166	10	79	1.117846076
11	89	11	11	11	128	11	167	11	78	1.052227645
12	90	12	12	12	129	12	168	12	77	0.99673918
13	91	13	13	13	130	13	169	13	76	0.934128408
14	92	14	14	14	131	14	170	14	75	0.88601358
15	93	15	15	15	132	15	171	15	74	0.854401582
16	94	16	16	16	133	16	172	16	73	0.823259215
17	95	17	17	17	134	17	173	17	72	0.792521583
18	96	18	18	18	135	18	174	18	71	0.764393697
19	97	19	19	19	136	19	175	19	70	0.73238886
20	98	20	20	20	137	20	176	20	69	0.702963463
21	99	21	21	21	138	21	177	21	68	0.674003414
22	100	22	22	22	139	22	178	22	67	0.645452057
23	101	23	23	23	140	23	179	23	66	0.617338562

Table C.2: ANSYS Wing Design Model Areas (continued)

Upper Skin		Lower Skin		Front Spar		Rear Spar		Ribs		
Panel No.	Area	Panel No.	Area	Panel No.	Area	Panel No.	Area	No.	Area	Thickness T/C Ratio
24	102	24	24	24	141	24	180	24	65	0.589688253
25	103	25	25	25	142	25	181	25	64	0.562449116
26	104	26	26	26	143	26	182	26	63	0.535671726
27	105	27	27	27	144	27	183	27	62	0.509306947
28	106	28	28	28	145	28	184	28	61	0.48337941
29	107	29	29	29	146	29	185	29	60	0.457912056
30	108	30	30	30	147	30	186	30	59	0.433589461
31	109	31	31	31	148	31	187	31	58	0.412405266
32	110	32	32	32	149	32	188	32	57	0.391703313
33	111	33	33	33	150	33	189	33	56	0.38184329
34	112	34	34	34	151	34	190	34	55	0.372054454
35	113	35	35	35	152	35	191	35	54	0.350556528
36	114	36	36	36	153	36	192	36	53	0.329460839
37	115	37	37	37	154			37	52	0.308790056
38	116	38	38	38	155			38	51	0.288532561
39	117	39	39	39	156			39	50	0.268678998
								40	47	0.249462918

Table C.3: Wing Design Model Initial Stringer Panel Calculations

Equivalent I-stringer Stiffness Ply									
Composite I-Beam									
bbf (m)	**bbf (in)**	**tbf (m)**	**h (m)**	**h (in)**	**tw (m)**	**btf (m)**	**btf (in)**	**ttf (m)**	**Abf (m^2)**
0.0635	2.5	0.01869	0.1016	4.0	0.01869	0.0635	2.5	0.01869	0.001187
Aw (m^2)	**Atf (m^2)**	**Ibf (m^4)**	**Itf (m^4)**	**Total Height (m)**	**Total Height (in)**	**a11bf**	**a11w**	**a11tf**	**d11bf**
0.001899	0.001187	3.454E-08	3.454E-08	0.1390	5.472	7.225E-10	7.225E-10	7.23E-10	2.507E-5
d11tf	**Ebarxxex /bf (Pa)**	**Ebarxxex /w (Pa)**	**Ebarxxex/tf (Pa)**	**Ebarxxfl /bf (Pa)**	**Ebarxxfl /tf (Pa)**	**zb (m)**	**zb (in)**	**AEbarxx /beam (N)**	**IEbarxx /beam (N-m^2)**
2.507E-5	7.406E10	7.406E10	7.406E10	7.333E10	7.333E10	0.06949	2.736	3.164E8	7.619E5
Composite Panel Stiffness, Bay 5, 12 Stringers									
tsk (m)	**tst (m)**	**wsk (m)**	**wst (m)**	**Ask (m^2)**	**Ast (m^2)**	**a11sk**	**a11st**	**Ebarxxsk (Pa)**	**Ebarxxst (Pa)**
0.01869	0.01869	2.979	0.2286	0.05568	0.004272	7.225E-10	7.225E-10	7.406E10	7.406E10
β	**a11sk-st**	Constant cross section I stringer							
0.5206	3.76E-10								
Composite I-Beam Plate Equivalent									
s (m)	**tI (m)**	**tsk (m)**	**Ebarxxex/I (Pa)**	**Ebarxxex /sk (Pa)**	**a11I**	**AI (m^2)**	**Ask (m^2)**	**Isk (m^4)**	**Ebarxxfl /sk (Pa)**
0.205	0.08633	0.01869	1.789E10	7.406E10	6.475E-10	0.01770	0.003831	1.115E-07	7.333E10
zb (m)	**zb (in)**	**AEbarxx beam (N)**	**EIbarxxbeam (N-m^2)**						
0.06798	2.676	6.003E8	3.907E5						

Table C.4: Wing Design Model Leading and Trailing Edge Applied Mass Loads

Wing Model Point Mass Loads										
Leading Edge Mass Loads			3.75 G Applied Loads				-1.5 G Applied Loads			
Rib	Mass (kg)	Node	3.75 G Force (N)	FZ (N)	MX (N-m)	MY (N-m)	-1.5 G Force (N)	FZ (N)	MX (N-m)	MY (N-m)
5	13.79	1155	-508.08	-295.92	296.29	-204.83	203.23	118.37	-118.52	81.93
		1156		-212.16	251.09	-171.08		84.87	-100.43	68.43
6	14.51	1153	-534.58	-309.52	308.08	-213.11	213.83	123.81	-123.23	85.24
		1154		-225.06	263.22	-179.38		90.03	-105.29	71.75
7	26.94	1152	-992.19	-586.58	571.92	-388.45	396.88	234.63	-228.77	155.38
		1151		-405.61	473.59	-321.66		162.24	-189.43	128.66
8	26.65	3362	-981.75	-598.39	566.50	-384.76	392.70	239.36	-226.60	153.90
		3365		-383.36	451.77	-306.84		153.34	-180.71	122.74
9	26.37	3358	-971.32	-591.25	553.80	-376.14	388.53	236.50	-221.52	150.45
		3361		-380.07	442.91	-300.82		152.03	-177.17	120.33
10	26.09	3354	-960.88	-584.08	541.12	-367.53	384.35	233.63	-216.45	147.01
		3357		-376.80	434.02	-294.78		150.72	-173.61	117.91
11	25.80	3350	-950.44	-576.90	528.48	-358.94	380.18	230.76	-211.39	143.58
		3353		-373.54	425.09	-288.72		149.42	-170.04	115.49
12	25.52	3346	-940.00	-569.70	515.87	-350.38	376.00	227.88	-206.35	140.15
		3349		-370.31	416.14	-282.64		148.12	-166.46	113.06
13	25.20	3342	-928.08	-561.30	500.43	-339.89	371.23	224.52	-200.17	135.96
		3345		-366.79	405.19	-275.20		146.71	-162.08	110.08
14	24.87	3338	-916.16	-552.86	485.05	-329.44	366.46	221.14	-194.02	131.78
		3341		-363.30	394.21	-267.75		145.32	-157.68	107.10

Table C.4: Wing Design Model Leading and Trailing Edge Applied Mass Loads (continued)

Rib	Mass (kg)	Node	3.75 G Force (N)	FZ (N)	MX (N-m)	MY (N-m)	-1.5 G Force (N)	FZ (N)	MX (N-m)	MY (N-m)
15	24.64	3334	-907.68	-546.84	474.15	-322.04	363.07	218.73	-189.66	128.81
		3337		-360.84	386.38	-262.43		144.34	-154.55	104.97
16	24.41	3330	-899.22	-540.81	463.32	-314.68	359.69	216.32	-185.33	125.87
		3333		-358.41	378.57	-257.12		143.37	-151.43	102.85
17	24.18	3326	-890.74	-534.74	452.50	-307.34	356.29	213.90	-181.00	122.93
		3329		-356.00	370.74	-251.81		142.40	-148.30	100.72
18	23.95	3322	-882.25	-528.65	441.74	-300.03	352.90	211.46	-176.70	120.01
		3325		-353.60	362.92	-246.49		141.44	-145.17	98.60
19	23.72	3318	-873.79	-522.56	431.07	-292.78	349.52	209.02	-172.43	117.11
		3321		-351.24	355.13	-241.20		140.50	-142.05	96.48
20	23.49	3314	-865.31	-516.42	420.43	-285.55	346.12	206.57	-168.17	114.22
		3317		-348.89	347.34	-235.91		139.56	-138.94	94.37
21	23.26	3310	-856.85	-510.27	409.88	-278.39	342.74	204.11	-163.95	111.36
		3313		-346.58	339.60	-230.66		138.63	-135.84	92.26
22	23.03	3306	-848.37	-504.37	399.61	-271.41	339.35	201.63	-159.75	108.50
		3309		-344.48	332.06	-225.53		137.71	-132.75	90.16
23	22.80	3302	-839.89	-497.86	388.96	-264.18	335.95	199.14	-155.58	105.67
		3305		-342.03	324.18	-220.18		136.81	-129.67	88.07
24	22.57	3298	-831.43	-491.62	378.65	-257.18	332.57	196.65	-151.46	102.87
		3301		-339.81	316.56	-215.01		135.92	-126.62	86.00
25	22.34	3294	-822.94	-485.33	368.40	-250.21	329.18	194.13	-147.36	100.09
		3297		-337.62	308.97	-209.85		135.05	-123.59	83.94

Table C.4: Wing Design Model Leading and Trailing Edge Applied Mass Loads (continued)

Rib	Mass (kg)	Node	3.75 G Force (N)	FZ (N)	MX (N-m)	MY (N-m)	-1.5 G Force (N)	FZ (N)	MX (N-m)	MY (N-m)
26	22.11	6085	-814.49	-479.01	358.26	-243.33	325.79	191.60	-143.31	97.33
		6088		-335.48	301.46	-204.75		134.19	-120.58	81.90
27	21.88	6081	-806.00	-472.63	348.20	-236.49	322.40	189.05	-139.28	94.60
		6084		-333.37	294.00	-199.68		133.35	-117.60	79.87
28	21.65	6077	-797.52	-466.19	338.23	-229.73	319.01	186.48	-135.29	91.89
		6080		-331.32	286.61	-194.67		132.53	-114.65	77.87
29	21.42	6073	-789.06	-459.72	328.40	-223.05	315.62	183.89	-131.36	89.22
		6076		-329.34	279.33	-189.72		131.74	-111.73	75.89
30	21.19	6069	-780.58	-453.16	318.64	-216.42	312.23	181.27	-127.46	86.57
		6072		-327.41	272.12	-184.82		130.97	-108.85	73.93
31	20.96	6065	-772.12	-446.55	308.81	-210.21	308.85	178.62	-123.52	84.09
		6068		-325.57	264.84	-180.28		130.23	-105.93	72.11
32	20.73	6061	-763.64	-439.84	299.50	-203.42	305.45	175.93	-119.80	81.37
		6064		-323.80	258.02	-175.24		129.52	-103.21	70.10
33	20.62	6057	-759.58	-436.59	294.98	-200.35	303.83	174.64	-117.99	80.14
		6060		-322.99	254.71	-173.00		129.20	-101.88	69.20
34	20.51	6053	-755.50	-433.30	290.47	-197.28	302.20	173.32	-116.19	78.91
		6056		-322.19	251.41	-170.75		128.88	-100.56	68.30
35	20.27	6049	-746.45	-425.92	280.55	-190.55	298.58	170.37	-112.22	76.22
		6052		-320.53	244.18	-165.85		128.21	-97.67	66.34
36	20.02	6045	-737.37	-418.37	270.74	-183.89	294.95	167.35	-108.30	73.55
		6048		-319.00	237.10	-161.03		127.60	-94.84	64.41

Table C.4: Wing Design Model Leading and Trailing Edge Applied Mass Loads (continued)

Rib	Mass (kg)	Node	3.75 G Force (N)	FZ (N)	MX (N-m)	MY (N-m)	-1.5 G Force (N)	FZ (N)	MX (N-m)	MY (N-m)
37	19.77	6041	-728.32	-410.69	261.10	-177.34	291.33	164.27	-104.44	70.94
		6044		-317.63	230.19	-156.34		127.05	-92.08	62.54
38	19.53	6037	-719.27	-402.81	251.60	-170.88	287.71	161.13	-100.64	68.35
		6040		-316.45	223.46	-151.77		126.58	-89.38	60.71
39	19.28	6033	-710.19	-394.71	242.22	-164.51	284.08	157.89	-96.89	65.81
		6036		-315.48	216.90	-147.32		126.19	-86.76	58.93
40	16.43	6031	-605.09	-333.47	201.09	-136.58	242.04	133.39	-80.43	54.63
		6030	6030.00	-271.62	181.71	-123.41		108.65	-72.68	49.37
Trailing Edge Flaps/Spoilers/Ailerons Mass Loads			**3.75 G Applied Loads**				**-1.5 G Applied Loads**			
Rib	**Mass (kg)**	**Node**	**3.75 G Force (N)**	**FZ (N)**	**MX (N-m)**	**MY (N-m)**	**-1.5 G Force (N)**	**FZ (N)**	**MX (N-m)**	**MY (N-m)**
9		3359		-966.26	-1513.60	1001.80		386.50	605.45	-400.70
		3360		-743.25	-1357.70	897.72		297.30	543.09	-359.09
	35.44		-1305.31				522.12			
	10.97		-404.20				161.68			
10		3355		-959.59	-1456.50	964.69		383.84	582.60	-385.87
		3356		-731.55	-1303.80	862.64		292.62	521.50	-345.06
	35.06		-1291.28				516.51			
	10.86		-399.86				159.94			

Table C.4: Wing Design Model Leading and Trailing Edge Applied Mass Loads (continued)

Rib	Mass (kg)	Node	3.75 G Force (N)	FZ (N)	MX (N-m)	MY (N-m)	-1.5 G Force (N)	FZ (N)	MX (N-m)	MY (N-m)
11		3351		-953.02	-1400.10	927.58		381.21	560.04	-371.03
		3352		-719.75	-1250.50	827.61		287.90	500.21	-331.05
	34.68		-1277.25				510.90			
	10.74		-395.52				158.21			
12		3347		-946.51	-1344.30	891.26		378.60	537.72	-356.50
		3348		-707.89	-1197.90	793.41		283.16	479.17	-317.36
	34.30		-1263.23				505.29			
	10.62		-391.17				156.47			
13		3343		-939.81	-1274.90	845.70		375.92	509.96	-338.28
		3344		-693.61	-1132.50	750.44		277.45	453.01	-300.17
	33.86		-1247.21				498.88			
	10.49		-386.21				154.49			
14		3339		-1096.70	-1443.90	957.54		438.69	577.57	-383.02
		3340		-802.68	-1283.10	849.92		321.07	513.25	-339.97
	38.65		-1423.45				569.38			
	12.92		-475.95				190.38			
15		3335		-436.58	-467.84	311.82		174.63	187.14	-124.73
		3336		-300.62	-399.49	266.00		120.25	159.80	-106.40
	17.47		-643.38				257.35			
	2.55		-93.82				37.53			

Table C.4: Wing Design Model Leading and Trailing Edge Applied Mass Loads (continued)

Rib	Mass (kg)	Node	3.75 G Force (N)	FZ (N)	MX (N-m)	MY (N-m)	-1.5 G Force (N)	FZ (N)	MX (N-m)	MY (N-m)
16		3331		-434.63	-448.18	298.88		173.85	179.27	-119.55
		3332		-295.70	-381.43	254.10		118.28	152.57	-101.64
	17.30		-637.38				254.95			
	2.52		-92.94				37.18			
17		3327		-1080.40	-1272.50	845.43		432.16	508.99	-338.17
		3328		-766.28	-1122.80	744.95		306.51	449.10	-297.98
	37.57		-1383.94				553.58			
	12.56		-462.74				185.10			
18		3323		-915.01	-1015.90	675.51		366.01	406.38	-270.21
		3324		-637.75	-890.66	591.39		255.10	356.27	-236.56
	32.19		-1185.62				474.25			
	9.97		-367.14				146.86			
19		3319		-910.51	-969.55	644.94		364.20	387.82	-257.98
		3320		-627.36	-847.85	563.15		250.95	339.14	-225.26
	31.88		-1174.25				469.70			
	9.87		-363.62				145.45			
20		3315		-905.97	-923.51	614.47		362.39	369.40	-245.79
		3316		-616.97	-805.57	535.15		246.79	322.23	-214.06
	31.57		-1162.85				465.14			
	9.78		-360.09				144.04			

Table C.4: Wing Design Model Leading and Trailing Edge Applied Mass Loads (continued)

Rib	Mass (kg)	Node	3.75 G Force (N)	FZ (N)	MX (N-m)	MY (N-m)	-1.5 G Force (N)	FZ (N)	MX (N-m)	MY (N-m)
21		3311		-901.38	-877.99	584.53		360.55	351.19	-233.81
		3312		-606.67	-764.00	507.79		242.67	305.60	-203.12
	31.26		-1151.48				460.59			
	9.68		-356.57				142.63			
22		3307		-896.69	-832.77	554.81		358.68	333.11	-221.92
		3308		-596.43	-722.97	480.80		238.57	289.19	-192.32
	30.95		-1140.08				456.03			
	9.59		-353.04				141.22			
23		3303		-891.87	-787.94	525.51		356.75	315.18	-210.21
		3304		-586.33	-682.59	454.36		234.53	273.04	-181.74
	30.64		-1128.68				451.47			
	9.49		-349.51				139.80			
24		3299		-886.89	-743.78	496.50		354.76	297.51	-198.60
		3300		-576.41	-643.08	428.41		230.57	257.23	-171.36
	30.34		-1117.32				446.93			
	9.39		-345.99				138.40			
25		3295		-881.68	-699.96	467.66		352.67	279.98	-187.06
		3296		-566.70	-604.18	402.78		226.68	241.67	-161.11
	30.03		-1105.92				442.37			
	9.30		-342.46				136.98			

Table C.4: Wing Design Model Leading and Trailing Edge Applied Mass Loads (continued)

Rib	Mass (kg)	Node	3.75 G Force (N)	FZ (N)	MX (N-m)	MY (N-m)	-1.5 G Force (N)	FZ (N)	MX (N-m)	MY (N-m)
26		6086		-876.22	-656.72	439.30		350.49	262.69	-175.72
		6087		-557.27	-566.12	377.80		222.91	226.45	-151.12
	29.72		-1094.55				437.82			
	9.20		-338.94				135.58			
27		6082		-870.43	-613.87	411.20		348.17	245.55	-164.48
		6083		-548.13	-528.70	353.25		219.25	211.48	-141.30
	29.41		-1083.15				433.26			
	9.11		-335.41				134.16			
28		6078		-864.28	-571.60	383.35		345.71	228.64	-153.34
		6079		-539.35	-492.09	329.10		215.74	196.83	-131.64
	29.10		-1071.75				428.70			
	9.01		-331.88				132.75			
29		6074		-857.76	-529.96	356.18		343.10	211.98	-142.47
		6075		-530.98	-456.30	305.78		212.39	182.52	-122.31
	28.79		-1060.38				424.15			
	8.91		-328.36				131.34			
30		6070		-850.82	-488.79	329.36		340.33	195.52	-131.74
		6071		-523.00	-421.19	282.88		209.20	168.48	-113.15
	28.48		-1048.98				419.59			
	8.82		-324.83				129.93			

Table C.4: Wing Design Model Leading and Trailing Edge Applied Mass Loads (continued)

Rib	Mass (kg)	Node	3.75 G Force (N)	FZ (N)	MX (N-m)	MY (N-m)	-1.5 G Force (N)	FZ (N)	MX (N-m)	MY (N-m)
31		6066		-843.48	-448.44	303.05		337.39	179.38	-121.22
		6067		-515.44	-387.00	260.60		206.18	154.80	-104.24
	28.17		-1037.61				415.05			
	8.72		-321.31				128.52			
32		6062		-983.41	-492.76	333.84		393.37	197.10	-133.54
		6063		-603.06	-428.10	288.91		241.22	171.24	-115.56
	32.27		-1188.67				475.47			
	10.80		-397.80				159.12			
33		6058		-332.29	-133.21	91.49		132.92	53.28	-36.59
		6059		-191.98	-111.88	76.53		76.79	44.75	-30.61
	12.07		-444.72				177.89			
	2.16		-79.56				31.82			
34		6054		-330.63	-126.46	87.11		132.25	50.59	-34.84
		6055		-190.73	-106.45	73.01		76.29	42.58	-29.20
	12.01		-442.27				176.91			
	2.15		-79.10				31.64			
35		6050		-326.84	-111.79	77.75		130.74	44.72	-31.10
		6051		-188.07	-94.68	65.53		75.23	37.87	-26.21
	11.86		-436.83				174.73			
	2.12		-78.08				31.23			

Table C.4: Wing Design Model Leading and Trailing Edge Applied Mass Loads (continued)

Rib	Mass (kg)	Node	3.75 G Force (N)	FZ (N)	MX (N-m)	MY (N-m)	-1.5 G Force (N)	FZ (N)	MX (N-m)	MY (N-m)
36		6046		-322.92	-97.61	68.85		129.17	39.05	-27.54
		6047		-185.51	-83.37	58.47		74.20	33.35	-23.39
	11.71		-431.37				172.55			
	2.09		-77.06				30.82			
37		6042		-318.95	-84.15	60.74		127.58	33.66	-24.30
		6043		-183.02	-72.69	52.14		73.21	29.08	-20.86
	11.56		-425.93				170.37			
	2.06		-76.04				30.42			
38		6038		-315.43	-77.54	44.63		126.18	31.02	-17.85
		6039		-180.81	-68.12	39.46		72.32	27.25	-15.78
	11.43		-420.98				168.39			
	2.04		-75.27				30.11			
39		6034		-264.10	-186.91	122.78		105.64	74.76	-49.11
	11.27	6035	-489.04	-224.94	-172.45	113.28	195.62	89.98	68.98	-45.31
	2.01									
40		6032		-224.62	-137.73	90.52		89.85	55.09	-36.21
	9.78	6029	-408.88	-184.26	-124.79	82.01	163.55	73.70	49.92	-32.81
	1.32									

Table C.5: Wing Design Model Tip Applied Mass Loads

Total Tip Mass Loads	3.75 G Applied Loads			-1.5 G Applied Loads		
Nodes	**FZ (N)**	**MX (N-m)**	**MY (N-m)**	**FZ (N)**	**MX (N-m)**	**MY (N-m)**
6030	-459.40	53.53	-418.31	183.76	-21.41	167.33
6031	-525.02	71.67	-434.79	210.01	-28.67	173.91
6029	-258.92	-192.37	-84.28	103.57	76.95	33.71
6032	-299.76	-205.60	-76.46	119.90	82.24	30.59

Table C.6: Wing Design Model Landing Gear Applied Mass Loads

	3.75 G Applied Loads					-1.5 G Applied Loads				
Nodes	**FY (N)**	**FZ (N)**	**MX (N-m)**	**MY (N-m)**	**MZ (N-m)**	**FY (N)**	**FZ (N)**	**MX (N-m)**	**MY (N-m)**	**MZ (N-m)**
431	49.12	-2.00E4	-3.25E4	-8223.80	1.77E4	-19.65	8015.30	1.30E4	3289.50	-7082.00
430	-256.16	-1.73E4	-2.97E4	-6628.20	-1.72E4	102.46	6925.60	1.19E4	2651.30	6898.80
3347	54.11	-2.81E5	-2.06E4	2.77E5	1472.80	-21.65	1.12E5	8228.62	-1.11E5	-589.14
3348	152.93	-1.96E5	-1.67E4	2.23E5	-952.36	-61.17	7.84E4	6666.47	-8.93E4	380.94

Table C.7: Wing Design Model Engine Applied Mass Loads

	3.75 G Applied Loads					
Nodes	**FX (N)**	**FY (N)**	**FZ (N)**	**MX (N-M)**	**MY (N-M)**	**MZ (N-M)**
3339	787.29	9610.60	3.36E4	-2.59E4	3418.04	-127.56
3982	-3006.20	-30815.00	-1115.10	6.47E4	-6520.30	-662.30
3346	2218.90	2.12E4	-2.31E5	2.45E6	-2.50E4	-8.13
	-1.5 G Applied Loads					
Nodes	**FX (N)**	**FY (N)**	**FZ (N)**	**MX (N-m)**	**MY (N-m)**	**MZ (N-m)**
3339	-314.92	-3844.20	-1.34E4	1.04E4	-1367.21	51.03
3982	1202.50	1.23E4	446.04	-2.59E4	2608.10	264.92
3346	-887.57	-8481.80	9.24E4	-9.81E4	1.00E4	3.25

Table C.8: Wing Design Model Applied Fuel Pressures

Volume ID	Volume (m^3)	Fuel Load (N)	Fuel Mass (kg)	Cell Lower Area (m^2)	Fuel Load 3.75 G (N)	Fuel Load -1.5 G (N)	Total Pressure 3.75 G (N/m^2)	Total Pressure -1.5 G (N/m^2)
1	4.479	3.53E+04	3.60E+03	3.88	1.32E+05	-5.30E+04	3.41E+04	-1.37E+04
2	4.674	3.69E+04	3.75E+03	3.88	1.38E+05	-5.53E+04	3.56E+04	-1.42E+04
3	4.441	3.50E+04	3.57E+03	3.88	1.31E+05	-5.25E+04	3.38E+04	-1.35E+04
4	0.716	5.65E+03	5.75E+02	0.60	2.12E+04	-8.47E+03	3.53E+04	-1.41E+04
5	2.180	1.72E+04	1.75E+03	1.80	6.45E+04	-2.58E+04	3.58E+04	-1.43E+04
6	3.446	2.72E+04	2.77E+03	3.00	1.02E+05	-4.08E+04	3.40E+04	-1.36E+04
7	2.987	2.36E+04	2.40E+03	2.83	8.83E+04	-3.53E+04	3.12E+04	-1.25E+04
8	2.645	2.09E+04	2.12E+03	2.61	7.82E+04	-3.13E+04	2.99E+04	-1.20E+04
9	2.517	1.98E+04	2.02E+03	2.55	7.44E+04	-2.98E+04	2.92E+04	-1.17E+04

Table C.8: Wing Design Model Applied Fuel Pressures (continued)

Volume ID	Volume (m^3)	Fuel Load (N)	Fuel Mass (kg)	Cell Lower Area (m^2)	Fuel Load 3.75 G (N)	Fuel Load -1.5 G (N)	Total Pressure 3.75 G (N/m^2)	Total Pressure -1.5 G (N/m^2)
10	2.392	1.32E+04	1.92E+03	2.49	7.07E+04	-2.83E+04	2.84E+04	-1.14E+04
11	2.270	1.25E+04	1.82E+03	2.43	6.71E+04	-2.68E+04	2.77E+04	-1.11E+04
12	2.777	1.53E+04	2.23E+03	3.07	8.21E+04	-3.28E+04	2.68E+04	-1.07E+04
13	2.582	2.04E+04	2.07E+03	2.96	7.63E+04	-3.05E+04	2.58E+04	-1.03E+04
14	1.723	1.36E+04	1.38E+03	2.04	5.09E+04	-2.04E+04	2.49E+04	-9.98E+03
15	1.626	1.28E+04	1.31E+03	1.98	4.81E+04	-1.92E+04	2.42E+04	-9.69E+03
16	1.541	1.22E+04	1.24E+03	1.94	4.56E+04	-1.82E+04	2.35E+04	-9.41E+03
17	1.454	1.15E+04	1.17E+03	1.88	4.30E+04	-1.72E+04	2.28E+04	-9.13E+03
18	1.366	1.08E+04	1.10E+03	1.83	4.04E+04	-1.62E+04	2.21E+04	-8.85E+03
19	1.288	1.02E+04	1.03E+03	1.78	3.81E+04	-1.52E+04	2.14E+04	-8.57E+03
20	1.205	9.50E+03	9.67E+02	1.72	3.56E+04	-1.43E+04	2.07E+04	-8.29E+03
21	1.131	8.92E+03	9.08E+02	1.67	3.34E+04	-1.34E+04	2.00E+04	-8.01E+03
22	1.057	8.33E+03	8.49E+02	1.62	3.13E+04	-1.25E+04	1.93E+04	-7.73E+03
23	0.982	7.74E+03	7.88E+02	1.56	2.90E+04	-1.16E+04	1.86E+04	-7.44E+03
24	0.915	7.22E+03	7.35E+02	1.51	2.71E+04	-1.08E+04	1.79E+04	-7.16E+03
25	0.846	6.67E+03	6.79E+02	1.45	2.50E+04	-1.00E+04	1.72E+04	-6.88E+03
26	0.784	6.18E+03	6.29E+02	1.41	2.32E+04	-9.27E+03	1.65E+04	-6.60E+03
27	0.722	5.69E+03	5.80E+02	1.35	2.14E+04	-8.54E+03	1.58E+04	-6.32E+03
28	0.661	5.21E+03	5.31E+02	1.30	1.95E+04	-7.82E+03	1.51E+04	-6.03E+03
29	0.606	4.78E+03	4.87E+02	1.25	1.79E+04	-7.17E+03	1.44E+04	-5.75E+03
30	0.550	4.34E+03	4.42E+02	1.19	1.63E+04	-6.51E+03	1.37E+04	-5.47E+03
31	0.500	3.94E+03	4.02E+02	1.14	1.48E+04	-5.92E+03	1.30E+04	-5.19E+03

Table C.8: Wing Design Model Applied Fuel Pressures (continued)

Volume ID	Volume (m^3)	Fuel Load (N)	Fuel Mass (kg)	Cell Lower Area (m^2)	Fuel Load 3.75 G (N)	Fuel Load -1.5 G (N)	Total Pressure 3.75 G (N/m^2)	Total Pressure -1.5 G (N/m^2)
32	0.222	1.75E+03	1.78E+02	0.53	6.55E+03	-2.62E+03	1.25E+04	-4.98E+03
33	0.212	1.67E+03	1.70E+02	0.52	6.27E+03	-2.51E+03	1.21E+04	-4.84E+03
34	0.432	3.40E+03	3.47E+02	1.10	1.28E+04	-5.11E+03	1.16E+04	-4.63E+03
35	0.383	3.02E+03	3.07E+02	1.05	1.13E+04	-4.52E+03	1.08E+04	-4.33E+03
36	0.334	2.64E+03	2.68E+02	0.98	9.88E+03	-3.95E+03	1.01E+04	-4.02E+03
37	0.290	2.29E+03	2.33E+02	0.92	8.58E+03	-3.43E+03	9.31E+03	-3.72E+03
38	0.250	1.97E+03	2.01E+02	0.86	7.39E+03	-2.95E+03	8.55E+03	-3.42E+03
39	0.211	1.67E+03	1.70E+02	0.80	6.25E+03	-2.50E+03	7.80E+03	-3.12E+03

Volume ID	Height (m)	KP*	Z Coord. (m)	Common Rib Net Pressure 3.75G (N/m^2)	Common Rib Net Pressure -1.5G (N/m^2)	*Inboard TE line or smallest inboard line height
1	0.915	16	0.378	2724.07	-1089.63	Rib 4 common pressure
2	0.915	3	0.378	905.88	-362.35	
3	0.915	7	0.378	-1082.41	432.96	
4	1.120	147	0.472	1081.31	-432.52	
5	1.147	155	0.488	418.64	-167.46	
6	1.145	152	0.506	-1406.63	562.65	
7	0.915	148	0.378	-1688.31	675.32	
8	0.802	143	0.279	-682.36	272.94	
9	0.781	139	0.272	-393.95	157.58	
10	0.761	135	0.265	-384.80	153.92	

Table C.8: Wing Design Model Applied Fuel Pressures (continued)

Volume ID	Height (m)	KP*	Z Coord. (m)	Common Rib Net Pressure 3.75G (N/m^2)	Common Rib Net Pressure -1.5G (N/m^2)	
11	0.741	131	0.258	-375.72	150.29	
12	0.721	127	0.251	-421.51	168.60	
13	0.695	123	0.242	-462.03	184.81	
14	0.668	119	0.232	-381.18	152.47	
15	0.650	115	0.226	-305.01	122.00	
16	0.631	111	0.219	-298.58	119.43	
17	0.613	107	0.213	-282.39	112.96	
18	0.594	103	0.207	-277.17	110.87	
19	0.575	99	0.200	-268.46	107.38	
20	0.557	95	0.194	-261.45	104.58	
21	0.538	91	0.187	-256.06	102.42	
22	0.519	87	0.181	-241.23	96.49	
23	0.501	83	0.174	-236.01	94.41	
24	0.482	79	0.168	-228.68	91.47	
25	0.463	75	0.161	-214.78	85.91	
26	0.445	71	0.155	-211.83	84.73	
27	0.426	67	0.148	-196.83	78.73	
28	0.407	63	0.142	-194.49	77.80	
29	0.389	59	0.135	-180.24	72.10	
30	0.370	55	0.129	-175.09	70.04	
31	0.352	51	0.122	-163.98	65.59	
32	0.333	47	0.116	-116.25	46.50	
33	0.324	43	0.113	-72.95	29.18	

Table C.8: Wing Design Model Applied Fuel Pressures (continued)

Volume ID	Height (m)	KP*	Z Coord. (m)	Common Rib Net Pressure 3.75G (N/m^2)	Common Rib Net Pressure -1.5G (N/m^2)	
34	0.315	39	0.110	-114.86	45.95	
35	0.295	35	0.103	-147.97	59.19	
36	0.275	31	0.096	-138.00	55.20	
37	0.255	27	0.089	-127.75	51.10	
38	0.235	23	0.082	-118.53	47.41	
39	0.215	19	0.075	-107.97	43.19	

Table C.9: Wing Design Model Emergency Landing Loads

Wing box mass and engine mass only

Position	Link	Mass (kg)	-6G Force (N)	9G Force (N)	3G Force (N)		Emergency Reaction Loads					
TE	1	101.75	6.00E+03	-8.99E+03	-3.00E+03	Node	FX (N)	FY (N)	FZ (N)	MX (N-M)	MY (N-M)	MZ (N-M)
Joint TE	2	203.51	1.20E+04	-1.80E+04	-6.00E+03	3339	-1.62E+04	-1.60E+04	-2.50E+04	1.14E+04	-9.04E+02	-5.82E+03
Mid	3											
Joint LE	4	305.26	1.80E+04	-2.70E+04	-8.99E+03	3982	-3.73E+05	1.28E+04	3.07E+04	-9.25E+04	-2.90E+05	-7.40E+04
LE	5											
Engine CG		4736.51	2.79E+05	-4.19E+05	-1.40E+05	3346	5.12E+04	-4.49E+05	3.10E+05	-1.61E+04	8.39E+04	2.19E+04

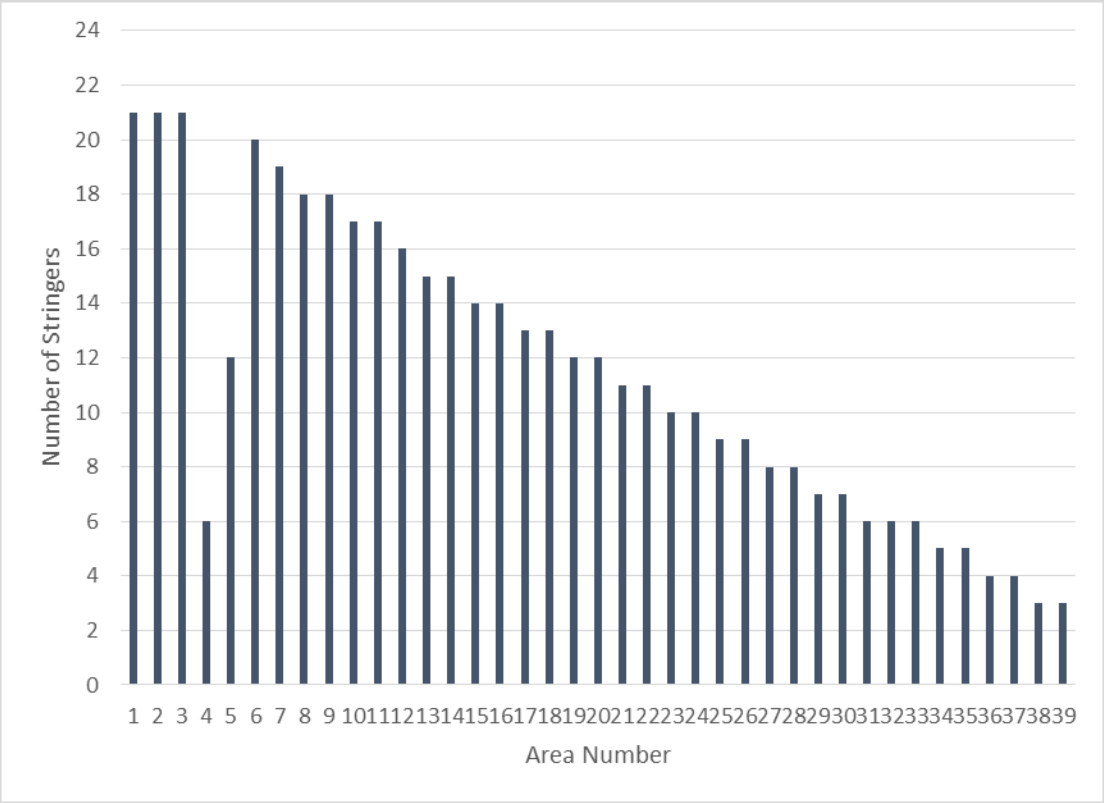

Figure C.1: Number of Stringers per Area of Wing Design Model

C.2 UW Subsonic Transport Composite Wing Model Website

A new benchmark wing model for optimization algorithm comparisons that may include flutter and divergence, aeroelastic tailoring, buckling and post buckling, vibration and natural frequency analyses is proposed. The idea behind this wing model is that the laminate design of the wing root joint is used for the entire wing structural box (upper and lower skin panels, ribs, and front and rear spars). This laminate design is sized to support all the loads that occur at the wing root. The structure is purposely over designed to provide a starting point for subsequent structural optimization. Aerodynamic and structural and fuel masses are included as load conditions.

Reference: Albers, R. G., Tuttle, M. E., and Avery, W. B., "Subsonic Transport Composite Wing Model for Optimization Studies", Proceedings of the 12th AIAA/ISSMO Multidisciplinary Analysis and Optimization Conference, Victoria, British Columbia, Canada, AIAA, Reston, VA, September 10-12, 2008, AIAA-2008-6016.

Files available for download:	Description:
UW Wing Design.xlsx	Excel 2007 spreadsheet
UW Wing Design.xls	Excel 97-2003 spreadsheet
UW Wing Design.SLDPRT	SolidWorks® SP3.1 geometry file
UW Wing Design.IGS	SolidWorks® SP3.1 IGES geometry
UW Wing Model All 3.75G Loads.DB	ANSYS® 11.0 database file
UW Wing Model Load Cases:	ANSYS® 11.0 load case (*.s) files,

UW Wing Model Aero Loads	*.cdb files, and *.iges files (binary)
UW Wing Model 3.75G Mass Loads	(see UW Wing Design Read Me)
UW Wing Model -1.5G Mass Loads	
UW Wing Model 3.75G Fuel Loads	
UW Wing Model -1.5G Fuel Loads	
UW Wing Model Aero & 3.75G Mass Loads	
UW Wing Model Aero & -1.5G Mass Loads	
UW Wing Model Aero & 3.75G Fuel Loads	
UW Wing Model Aero & -1.5G Fuel Loads	
UW Wing Model 3.75G Fuel & Mass Loads	
UW Wing Model -1.5G Fuel & Mass Loads	
UW Wing Model All 3.75G Loads	
UW Wing Model All -1.5G Loads	
UW Wing Model Emergency Landing Loads	
UW Wing Model 3.75 or -1.5G Only	

Questions and comments may be directed to Robert G. Albers, ralbers@u.washington.edu or rgalbers@comcast.net

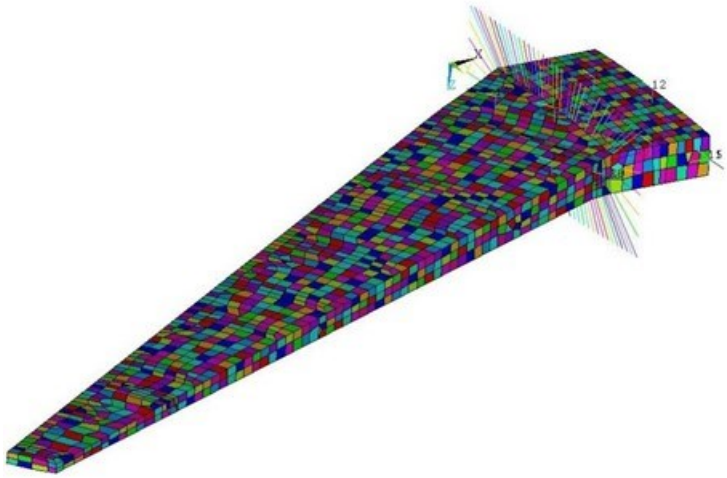

Figure C.2: UW Transonic Transport Wing Model showing ANSYS Mesh

C.3 Panel 18 ANSYS Wing Design Model Internal Loads

Boundary conditions for Panel 18 were determined from ANSYS internal loads applied to the panel, which were rotated and distributed to the nodes in the simplified FEM model. Nodes 1-9 are rib 8 nodes; 10, 20, 30, and 40 are rear spar nodes; 11, 21, and 31 are skin edge nodes; 41-49 are rib 7 nodes; and node 50 is the side-of-body node.

Table C.10: Panel 18 FEM Boundary Conditions for Aerodynamic Loads Only

Node	X (m)	Y (m)	FX	FY	FZ	MX	MY	MZ
1	0.0000	0.0000	6.67E-02	3.18E-03	2.61E-01	-9.29E-03	-2.48E-03	2.82E-03
2	0.1577	0.0000	-6.68E-01	2.68E-01	-4.23E-02	-2.60E-02	-2.49E-02	1.42E-02
3	0.3153	0.0000	4.23E+00	-1.73E+00	1.42E+00	6.32E-01	3.96E-01	-1.47E-01
4	0.4730	0.0000	-2.43E+00	5.63E-02	-1.93E-01	-5.15E-03	-8.57E-02	3.49E-02
5	0.6307	0.0000	-2.68E+01	4.44E+01	-9.47E+00	-5.54E+00	-1.28E+00	4.47E-01
6	0.7884	0.0000	-5.18E+01	-9.91E+00	-8.27E+00	1.19E+00	-1.67E+00	4.02E-01
7	0.9461	0.0000	-3.83E+02	3.13E+02	-1.03E+02	-3.94E+01	-1.56E+01	6.35E+00
8	1.1037	0.0000	7.51E+01	1.02E+02	-7.86E+01	-7.60E+00	2.88E+00	-3.63E-01
9	1.2614	0.0000	1.53E+01	7.87E+00	-8.23E+00	-3.32E-01	6.00E-01	-1.44E-01
10	1.4191	0.0000	-1.21E+02	1.27E+02	-8.58E+01	4.94E+04	-3.54E+04	1.10E+01
11	0.0000	0.1741	-5.45E-01	9.29E-01	-2.41E-01	-1.07E-01	-2.94E-02	9.11E-03
20	1.4191	0.1741	2.26E+02	-2.17E+02	-8.96E+01	8.01E+04	-4.71E+04	-4.80E+00
21	0.0000	0.3482	2.44E-01	3.32E-01	-5.48E-02	-3.86E-02	1.86E-03	3.14E-04
30	1.4191	0.3482	-1.36E+02	-2.67E+00	-1.40E+02	1.88E+04	-2.36E+04	1.53E+01
31	0.0000	0.5223	-7.34E-02	4.36E-01	-5.53E-02	-5.33E-02	-1.07E-02	3.74E-03
40	1.4191	0.5223	2.10E+02	-1.88E+02	-1.20E+02	4.93E+00	-3.60E+00	2.67E+01
41	0.0000	0.6964	2.45E-01	-7.21E-01	7.01E-02	8.90E-02	1.84E-02	-4.49E-03
42	0.1577	0.6964	6.11E-03	2.68E-01	-8.56E-02	-3.11E-02	-3.78E-03	2.58E-03
43	0.3154	0.6964	8.98E-01	-3.04E+00	4.27E-01	3.42E-01	5.87E-02	-1.90E-02
44	0.4730	0.6964	1.13E-01	-3.87E-01	5.49E-02	5.99E-02	7.71E-04	-3.16E-03
45	0.6307	0.6964	-2.58E-02	-5.44E-03	2.26E-01	-8.73E-03	-3.75E-03	-8.50E-03
46	0.7884	0.6964	1.98E-01	4.44E-02	-3.74E-02	5.60E-03	1.53E-03	1.96E-02
47	0.9461	0.6964	-6.21E-02	-2.81E-02	5.56E-01	-2.33E-02	-6.30E-03	-9.65E-03
48	1.1037	0.6964	1.25E+01	7.71E+00	2.31E+00	-9.50E-01	3.72E-01	-9.00E-02
49	1.2614	0.6964	1.39E+00	8.57E-01	2.57E-01	-1.06E-01	4.14E-02	-1.00E-02
50	1.4191	0.6964	-3.88E+01	1.38E+01	7.66E+01	-2.99E+00	1.03E+00	-1.34E+00

Table C.11: Panel 18 FEM Boundary Conditions for 3.75G Mass Loads Only

Node	X (m)	Y (m)	FX	FY	FZ	MX	MY	MZ
1	0.0000	0.0000	2.41E-03	2.47E-04	4.65E-03	9.64E-05	-3.71E-05	0.00E+00
2	0.1577	0.0000	3.11E-03	5.41E-05	-8.14E-04	1.86E-04	-7.17E-05	0.00E+00
3	0.3153	0.0000	-6.74E-03	-4.42E-03	-1.49E-04	3.64E-03	1.06E-03	-1.27E-03
4	0.4730	0.0000	4.64E-03	1.88E-04	-1.94E-03	5.70E-04	-7.46E-05	-7.49E-05
5	0.6307	0.0000	-7.86E-03	2.77E-03	-1.08E-03	2.16E-03	5.22E-04	-8.97E-04
6	0.7884	0.0000	5.44E-03	4.74E-05	-2.22E-03	8.64E-04	-1.63E-04	-1.12E-04
7	0.9461	0.0000	-1.27E-02	4.56E-03	-9.33E-03	2.66E-03	6.25E-04	-8.95E-04
8	1.1037	0.0000	2.42E-02	3.38E-03	-3.57E-04	3.23E-04	8.18E-05	-1.12E-04
9	1.2614	0.0000	3.24E-03	3.50E-04	9.70E-05	0.00E+00	0.00E+00	0.00E+00
10	1.4191	0.0000	-1.12E-02	-2.26E-02	-4.56E-02	1.77E-03	4.33E-04	-2.45E-04
11	0.0000	0.1741	2.63E-03	1.39E-02	-3.03E-03	-1.18E-03	-3.34E-04	1.06E-04
20	1.4191	0.1741	-5.95E-03	1.15E-02	9.81E-03	-4.22E-04	-1.51E-04	-6.79E-04
21	0.0000	0.3482	-5.83E-04	4.81E-04	2.22E-03	2.34E-04	2.26E-04	-3.77E-05
30	1.4191	0.3482	-3.27E-03	8.84E-04	-5.78E-04	-6.63E-05	2.39E-04	0.00E+00
31	0.0000	0.5223	-7.93E-04	-9.29E-03	6.26E-03	9.27E-04	5.96E-04	-1.30E-04
40	1.4191	0.5223	-1.07E-02	4.37E-03	5.17E-03	-2.20E-04	8.46E-05	0.00E+00
41	0.0000	0.6964	5.00E-03	4.22E-03	1.17E-02	-1.68E-03	-6.23E-04	4.00E-04
42	0.1577	0.6964	5.41E-04	8.68E-04	3.06E-03	-6.04E-04	-2.05E-04	1.82E-04
43	0.3154	0.6964	5.21E-03	4.50E-03	1.21E-02	-1.65E-03	-6.08E-04	4.31E-04
44	0.4730	0.6964	-1.19E-02	-2.75E-03	7.37E-04	-6.31E-04	9.22E-05	5.17E-05
45	0.6307	0.6964	1.52E-02	3.81E-03	1.06E-02	-4.59E-04	-8.35E-05	6.34E-04
46	0.7884	0.6964	-1.53E-02	-4.19E-03	7.08E-04	-5.07E-05	-1.30E-05	7.93E-05
47	0.9461	0.6964	2.17E-02	6.12E-03	9.18E-03	1.47E-04	5.37E-04	0.00E+00
48	1.1037	0.6964	1.80E-03	-6.46E-03	9.63E-03	-5.27E-04	-1.39E-04	-2.58E-05
49	1.2614	0.6964	2.00E-04	-7.18E-04	1.07E-03	-5.85E-05	-1.54E-05	-2.86E-06
50	1.4191	0.6964	1.96E-02	-3.00E-03	3.90E-03	-1.33E-04	2.86E-04	0.00E+00

Table C.12: Panel 18 FEM Boundary Conditions for -1.5G Mass Loads Only

Node	X (m)	Y (m)	FX	FY	FZ	MX	MY	MZ
1	0.0000	0.0000	-2.56E-03	-1.39E-04	-1.78E-02	6.82E-04	1.82E-04	-9.76E-05
2	0.1577	0.0000	8.02E-04	-1.08E-03	-8.00E-05	7.58E-05	2.02E-05	-1.08E-05
3	0.3153	0.0000	4.13E-03	1.11E-02	9.74E-03	-6.30E-03	-1.98E-03	7.21E-04
4	0.4730	0.0000	1.57E-03	-4.98E-04	2.85E-03	-3.74E-04	-1.15E-04	4.24E-05
5	0.6307	0.0000	-1.53E-03	7.11E-03	4.69E-03	-3.24E-03	-1.01E-03	4.37E-04
6	0.7884	0.0000	2.07E-03	-2.71E-04	2.26E-03	-2.07E-04	-5.97E-05	4.12E-05
7	0.9461	0.0000	3.58E-03	9.25E-03	4.54E-03	-3.09E-03	-9.77E-04	5.20E-04
8	1.1037	0.0000	-3.04E-03	-1.22E-03	6.06E-03	-5.68E-04	-1.46E-04	6.52E-05
9	1.2614	0.0000	-4.32E-04	-2.99E-04	6.90E-04	-2.23E-05	-2.81E-06	0.00E+00
10	1.4191	0.0000	4.46E-03	1.20E-02	1.27E-02	-1.51E-03	-4.45E-04	1.25E-04
11	0.0000	0.1741	-2.89E-03	-2.44E-02	6.06E-03	1.77E-03	5.89E-04	-1.78E-04
20	1.4191	0.1741	-3.13E-03	-9.69E-03	5.93E-04	5.63E-04	2.07E-04	-1.25E-04
21	0.0000	0.3482	3.85E-05	-2.07E-03	2.66E-04	2.73E-04	9.20E-05	-2.68E-05
30	1.4191	0.3482	6.66E-03	-1.03E-02	-1.38E-03	8.20E-04	4.58E-04	5.03E-05
31	0.0000	0.5223	1.13E-03	-6.36E-03	6.31E-05	4.11E-04	1.26E-04	-3.56E-05
40	1.4191	0.5223	8.77E-03	-1.16E-02	-2.36E-03	6.61E-04	4.18E-04	1.44E-04
41	0.0000	0.6964	5.32E-04	8.78E-03	1.56E-04	-8.63E-04	-2.58E-04	1.75E-04
42	0.1577	0.6964	8.49E-04	-1.52E-03	6.00E-04	-1.46E-04	-9.36E-06	1.95E-05
43	0.3154	0.6964	-4.98E-04	8.31E-03	-6.27E-04	-6.31E-04	-1.54E-04	1.23E-04
44	0.4730	0.6964	-5.82E-04	9.19E-04	2.14E-04	-1.82E-04	2.05E-05	1.54E-05
45	0.6307	0.6964	-9.49E-04	-1.02E-04	-3.45E-04	1.63E-05	-6.27E-06	0.00E+00
46	0.7884	0.6964	1.39E-03	3.62E-04	1.04E-04	1.42E-05	-5.45E-06	0.00E+00
47	0.9461	0.6964	-2.79E-03	-7.32E-04	-3.79E-04	-2.97E-05	1.14E-05	0.00E+00
48	1.1037	0.6964	2.09E-03	-5.76E-03	-5.02E-03	8.92E-06	-3.43E-06	0.00E+00
49	1.2614	0.6964	2.32E-04	-6.40E-04	-5.58E-04	9.91E-07	-3.81E-07	0.00E+00
50	1.4191	0.6964	-1.48E-02	-3.14E-03	-3.43E-03	2.92E-04	5.08E-05	-8.08E-04

Table C.13: Panel 18 FEM Boundary Conditions for 3.75G Fuel Loads Only

Node	X (m)	Y (m)	FX	FY	FZ	MX	MY	MZ
1	0.0000	0.0000	-4.02E-01	-7.26E-02	-1.31E+00	5.06E-02	1.34E-02	-1.72E-02
2	0.1577	0.0000	9.05E-02	-1.14E-01	-3.07E-02	8.51E-03	4.13E-03	1.74E-03
3	0.3153	0.0000	3.82E-01	1.20E+00	4.22E-01	-6.30E-01	-1.89E-01	5.96E-02
4	0.4730	0.0000	1.07E-01	-1.27E-02	1.54E-01	-3.55E-02	-9.23E-03	8.94E-03
5	0.6307	0.0000	-3.05E-01	7.05E-01	1.70E-01	-3.22E-01	-9.79E-02	3.19E-02
6	0.7884	0.0000	2.02E-01	-6.60E-03	1.15E-01	-1.43E-02	1.04E-03	1.02E-02
7	0.9461	0.0000	-1.14E-01	1.02E+00	1.05E-01	-2.98E-01	-9.28E-02	2.85E-02
8	1.1037	0.0000	-1.98E-01	-6.39E-02	3.76E-01	-2.86E-02	-8.92E-04	7.72E-03
9	1.2614	0.0000	-2.25E-02	-2.42E-02	4.56E-02	1.14E-03	1.37E-03	5.32E-04
10	1.4191	0.0000	-4.41E-01	1.49E+00	1.49E+00	-1.44E-01	-2.37E-02	-1.83E-02
11	0.0000	0.1741	-9.15E-01	-2.85E+00	6.62E-01	1.76E-01	5.44E-02	-1.71E-02
20	1.4191	0.1741	-1.06E-01	-1.54E+00	3.41E-01	5.28E-02	2.08E-02	-5.40E-04
21	0.0000	0.3482	-7.45E-03	-1.71E-01	9.05E-03	2.68E-02	8.56E-03	-2.70E-03
30	1.4191	0.3482	1.42E-01	-1.08E+00	2.43E-01	6.97E-02	3.06E-02	1.64E-02
31	0.0000	0.5223	7.09E-01	-2.38E+00	3.52E-01	1.65E-01	4.62E-02	-1.35E-02
40	1.4191	0.5223	9.01E-01	-1.77E+00	-5.12E-03	7.32E-02	3.42E-02	1.97E-02
41	0.0000	0.6964	4.12E-01	1.56E+00	-2.80E-01	-2.48E-01	-6.63E-02	4.50E-02
42	0.1577	0.6964	1.88E-01	-1.93E-01	2.28E-01	-5.27E-02	-1.78E-02	1.61E-03
43	0.3154	0.6964	5.07E-01	1.22E+00	-4.25E-01	-1.95E-01	-5.52E-02	3.10E-02
44	0.4730	0.6964	2.55E-01	1.51E-01	-3.34E-01	-1.44E-02	-3.13E-03	7.94E-03
45	0.6307	0.6964	-4.88E-01	-5.45E-02	-3.92E-01	1.92E-02	5.53E-03	-2.31E-02
46	0.7884	0.6964	5.43E-01	1.04E-01	-2.03E-01	6.62E-03	2.28E-03	2.94E-02
47	0.9461	0.6964	-9.56E-01	-2.15E-01	-6.02E-01	2.51E-02	6.28E-03	-5.02E-02
48	1.1037	0.6964	3.16E-01	-1.34E+00	-1.02E+00	-4.58E-02	-1.07E-02	6.65E-03
49	1.2614	0.6964	3.51E-02	-1.49E-01	-1.13E-01	-5.09E-03	-1.18E-03	7.39E-04
50	1.4191	0.6964	-2.66E+00	-5.69E-01	-6.67E-01	4.30E-02	1.62E-02	-1.19E-01

Table C.14: Panel 18 FEM Boundary Conditions for -1.5G Fuel Loads Only

Node	X (m)	Y (m)	FX	FY	FZ	MX	MY	MZ
1	0.0000	0.0000	1.19E+00	3.31E-01	2.86E+00	-1.10E-01	-2.94E-02	5.28E-02
2	0.1577	0.0000	2.63E-02	-6.29E-02	2.92E-01	-2.12E-02	-1.83E-03	-3.94E-03
3	0.3153	0.0000	-5.00E-01	-2.26E-01	-2.30E+00	6.51E-01	1.96E-01	-4.53E-02
4	0.4730	0.0000	-2.55E-01	-1.34E-01	-1.44E-01	3.49E-02	1.62E-02	-1.81E-02
5	0.6307	0.0000	-8.33E-02	-4.07E-01	-9.85E-01	2.92E-01	9.30E-02	-2.48E-02
6	0.7884	0.0000	-4.10E-01	-1.32E-02	-7.35E-02	1.51E-02	1.09E-02	-2.24E-02
7	0.9461	0.0000	2.12E-01	-7.53E-01	-5.79E-01	2.35E-01	7.64E-02	-7.19E-03
8	1.1037	0.0000	-6.49E-01	7.62E-03	-2.57E-01	3.14E-02	2.65E-03	-3.46E-02
9	1.2614	0.0000	-8.52E-02	1.28E-02	-2.30E-02	2.11E-04	-8.64E-04	-4.25E-03
10	1.4191	0.0000	4.44E-03	-3.03E-01	-7.98E-01	8.77E-02	3.08E-02	2.50E-03
11	0.0000	0.1741	8.89E-01	2.00E+00	-3.63E-01	-1.49E-01	-4.45E-02	1.39E-02
20	1.4191	0.1741	5.55E-01	9.50E-01	2.99E-01	-6.20E-02	-4.62E-03	2.32E-03
21	0.0000	0.3482	9.50E-02	2.34E-01	-7.45E-02	-2.13E-02	-1.61E-03	9.03E-04
30	1.4191	0.3482	-8.40E-01	9.91E-01	5.00E-01	-3.53E-02	-9.86E-03	-8.34E-02
31	0.0000	0.5223	-1.94E-01	1.09E+00	6.61E-02	-8.75E-02	-2.79E-02	7.87E-03
40	1.4191	0.5223	-6.98E-01	1.43E+00	1.79E-01	-6.65E-02	-1.79E-02	-1.07E-01
41	0.0000	0.6964	-8.60E-01	-1.18E+00	-1.22E+00	1.67E-01	5.72E-02	-7.22E-02
42	0.1577	0.6964	4.23E-02	1.34E-01	-1.12E-01	2.03E-02	-4.26E-03	2.06E-02
43	0.3154	0.6964	-1.30E+00	-1.22E+00	-9.83E-01	1.09E-01	6.13E-02	-5.85E-02
44	0.4730	0.6964	1.96E+00	2.94E-01	-1.43E+00	7.86E-02	2.56E-02	1.83E-01
45	0.6307	0.6964	-1.28E+00	-3.48E-01	-1.62E+00	6.83E-02	1.89E-02	-1.04E-01
46	0.7884	0.6964	1.13E+00	1.80E-01	-1.60E+00	8.28E-02	2.26E-02	8.97E-02
47	0.9461	0.6964	-1.57E+00	-4.64E-01	-1.36E+00	5.52E-02	1.53E-02	-1.32E-01
48	1.1037	0.6964	1.76E-01	9.89E-01	9.07E-01	3.41E-02	1.30E-02	7.86E-03
49	1.2614	0.6964	1.96E-02	1.10E-01	1.01E-01	3.79E-03	1.44E-03	8.74E-04
50	1.4191	0.6964	4.73E-01	8.34E-01	-5.84E-01	-9.89E-02	-7.48E-03	5.29E-02

Table C.15: Panel 18 FEM Boundary Conditions for 3.75G Mass and Aerodynamic Loads

Node	X (m)	Y (m)	FX	FY	FZ	MX	MY	MZ
1	0.0000	0.0000	1.19E-02	9.39E-04	4.21E-02	-1.57E-03	-4.20E-04	4.35E-04
2	0.1577	0.0000	6.28E-03	3.56E-04	-4.49E-03	2.59E-03	7.55E-04	-3.45E-04
3	0.3153	0.0000	-3.24E-02	1.36E-01	-8.53E-02	3.58E-04	-2.70E-03	3.93E-04
4	0.4730	0.0000	-2.35E-02	-3.92E-02	-2.96E-02	1.14E-02	7.52E-04	-3.19E-04
5	0.6307	0.0000	-3.25E+00	4.62E+00	-1.17E+00	-5.69E-01	-1.45E-01	4.90E-02
6	0.7884	0.0000	-4.00E+00	-1.23E+00	-6.57E-01	1.72E-01	-1.24E-01	2.48E-02
7	0.9461	0.0000	-3.28E+01	2.92E+01	-1.02E+01	-3.62E+00	-1.34E+00	5.57E-01
8	1.1037	0.0000	6.59E+00	6.65E+00	-5.77E+00	-4.34E-01	2.65E-01	-6.16E-02
9	1.2614	0.0000	1.33E+00	3.73E-01	-5.63E-01	2.78E-03	5.39E-02	-1.64E-02
10	1.4191	0.0000	-3.88E+00	6.01E+00	-1.44E+01	4.94E+04	-3.54E+04	1.40E+00
11	0.0000	0.1741	-3.36E-02	5.42E-02	-7.90E-03	-5.13E-03	-2.14E-03	6.24E-04
20	1.4191	0.1741	8.39E+00	-1.14E+01	1.90E+00	8.01E+04	-4.71E+04	-1.45E+00
21	0.0000	0.3482	-1.52E-02	-3.37E-03	-7.08E-04	3.66E-04	-2.82E-04	6.24E-05
30	1.4191	0.3482	1.33E+01	-1.64E+01	-2.39E+01	1.88E+04	-2.36E+04	3.95E+00
31	0.0000	0.5223	-5.90E-03	1.28E-02	-2.32E-03	-1.35E-03	-4.89E-04	1.59E-04
40	1.4191	0.5223	4.18E+01	-3.54E+01	-2.29E+01	6.66E-01	-5.55E-01	5.20E+00
41	0.0000	0.6964	-2.00E-03	-9.80E-03	3.28E-03	2.93E-03	7.06E-04	-2.26E-04
42	0.1577	0.6964	5.12E-03	-3.75E-03	-2.66E-04	-7.04E-05	3.26E-04	-2.51E-05
43	0.3154	0.6964	-1.35E-03	-5.67E-02	9.23E-03	9.06E-03	1.65E-03	-4.70E-04
44	0.4730	0.6964	-8.91E-03	-9.34E-03	3.85E-03	1.14E-03	2.02E-04	-5.88E-05
45	0.6307	0.6964	1.41E-02	4.06E-03	2.29E-03	2.06E-04	-7.91E-05	0.00E+00
46	0.7884	0.6964	-1.59E-02	-4.52E-03	2.70E-03	-9.69E-05	3.73E-05	0.00E+00
47	0.9461	0.6964	1.73E-02	5.74E-03	-4.87E-04	1.48E-04	-5.70E-05	0.00E+00
48	1.1037	0.6964	4.54E-01	2.56E-01	5.27E-02	-3.03E-02	1.41E-02	-4.22E-03
49	1.2614	0.6964	5.05E-02	2.85E-02	5.86E-03	-3.37E-03	1.57E-03	-4.68E-04
50	1.4191	0.6964	-7.42E+00	5.53E+00	6.52E+00	-1.99E-01	1.28E-01	-8.01E-01

Table C.16: Panel 18 FEM Boundary Conditions for -1.5G Mass and Aerodynamic Loads

Node	X (m)	Y (m)	FX	FY	FZ	MX	MY	MZ
1	0.0000	0.0000	5.85E-02	5.41E-03	2.09E-01	-7.52E-03	-2.00E-03	2.73E-03
2	0.1577	0.0000	-6.57E-01	3.27E-01	-3.62E-02	-3.69E-02	-2.80E-02	1.85E-02
3	0.3153	0.0000	4.45E+00	-2.16E+00	1.63E+00	6.86E-01	4.23E-01	-1.66E-01
4	0.4730	0.0000	-2.63E+00	1.40E-01	-1.27E-01	-2.49E-02	-9.82E-02	4.24E-02
5	0.6307	0.0000	-2.90E+01	4.90E+01	-1.01E+01	-6.14E+00	-1.42E+00	5.00E-01
6	0.7884	0.0000	-5.82E+01	-1.02E+01	-9.33E+00	1.27E+00	-1.88E+00	4.35E-01
7	0.9461	0.0000	-4.11E+02	3.40E+02	-1.11E+02	-4.26E+01	-1.68E+01	6.86E+00
8	1.1037	0.0000	8.25E+01	1.09E+02	-8.36E+01	-8.05E+00	3.17E+00	-4.33E-01
9	1.2614	0.0000	1.66E+01	8.27E+00	-8.74E+00	-3.36E-01	6.54E-01	-1.61E-01
10	1.4191	0.0000	-1.38E+02	1.44E+02	-8.05E+01	4.94E+04	-3.54E+04	1.06E+01
11	0.0000	0.1741	-6.70E-01	1.00E+00	-2.70E-01	-1.18E-01	-3.39E-02	1.04E-02
20	1.4191	0.1741	2.34E+02	-2.33E+02	-9.84E+01	8.01E+04	-4.71E+04	-5.54E+00
21	0.0000	0.3482	2.90E-01	4.04E-01	-5.78E-02	-4.62E-02	2.18E-03	4.58E-04
30	1.4191	0.3482	-1.82E+02	3.71E+01	-9.15E+01	1.88E+04	-2.36E+04	1.20E+01
31	0.0000	0.5223	1.78E-02	3.01E-01	-1.92E-02	-3.85E-02	-5.29E-03	2.20E-03
40	1.4191	0.5223	1.63E+02	-1.53E+02	-9.67E+01	4.31E+00	-2.97E+00	2.17E+01
41	0.0000	0.6964	2.92E-01	-6.71E-01	7.22E-02	7.52E-02	1.52E-02	-2.84E-03
42	0.1577	0.6964	-3.85E-02	2.66E-01	-7.75E-02	-3.34E-02	-5.95E-03	2.93E-03
43	0.3154	0.6964	1.07E+00	-3.04E+00	4.53E-01	3.24E-01	5.58E-02	-1.69E-02
44	0.4730	0.6964	1.26E-01	-3.90E-01	7.77E-02	4.03E-02	6.91E-03	-2.75E-03
45	0.6307	0.6964	3.57E-02	9.77E-04	2.69E-01	-1.19E-02	-3.16E-03	-3.44E-03
46	0.7884	0.6964	7.51E-02	1.19E-02	1.92E-02	2.05E-03	6.13E-04	8.43E-03
47	0.9461	0.6964	-9.23E-02	-3.89E-02	4.98E-01	-2.04E-02	-5.44E-03	-1.01E-02
48	1.1037	0.6964	1.09E+01	7.75E+00	2.57E+00	-9.43E-01	3.21E-01	-7.22E-02
49	1.2614	0.6964	1.21E+00	8.61E-01	2.86E-01	-1.05E-01	3.57E-02	-8.02E-03
50	1.4191	0.6964	-3.59E+01	1.27E+01	6.79E+01	-2.78E+00	8.21E-01	-1.10E+00

Table C.17: Panel 18 FEM Boundary Conditions for 3.75G Fuel and Aerodynamic Loads

Node	X (m)	Y (m)	FX	FY	FZ	MX	MY	MZ
1	0.0000	0.0000	3.03E-01	1.98E-02	7.50E-01	-2.77E-02	-7.36E-03	1.10E-02
2	0.1577	0.0000	-6.58E-01	4.30E-01	-1.63E-01	1.26E-02	-1.65E-02	1.47E-03
3	0.3153	0.0000	2.55E+00	-1.26E+00	3.90E-01	1.19E+00	5.29E-01	-1.51E-01
4	0.4730	0.0000	-1.85E+00	-1.21E-01	-7.55E-01	1.54E-01	-1.72E-02	-4.43E-03
5	0.6307	0.0000	-2.09E+01	3.23E+01	-9.25E+00	-3.24E+00	-6.73E-01	2.38E-01
6	0.7884	0.0000	-3.21E+01	-1.02E+01	-5.35E+00	1.41E+00	-9.75E-01	2.53E-01
7	0.9461	0.0000	-3.04E+02	2.39E+02	-8.45E+01	-2.88E+01	-1.16E+01	4.66E+00
8	1.1037	0.0000	6.07E+01	7.03E+01	-5.91E+01	-5.11E+00	2.24E+00	-2.52E-01
9	1.2614	0.0000	1.23E+01	5.03E+00	-6.08E+00	-1.85E-01	4.61E-01	-1.04E-01
10	1.4191	0.0000	-9.33E+01	9.59E+01	-8.40E+01	4.94E+04	-3.54E+04	8.84E+00
11	0.0000	0.1741	-6.94E-01	2.15E+00	-5.36E-01	-2.23E-01	-6.32E-02	2.03E-02
20	1.4191	0.1741	1.89E+02	-1.56E+02	-6.92E+01	8.01E+04	-4.71E+04	-1.70E+00
21	0.0000	0.3482	1.44E-01	1.54E-01	-3.08E-02	-1.13E-02	3.31E-03	-6.40E-05
30	1.4191	0.3482	2.10E+01	-1.40E+02	-3.19E+02	1.88E+04	-2.36E+04	2.65E+01
31	0.0000	0.5223	-1.26E+00	3.81E+00	-9.70E-01	-3.04E-01	-9.04E-02	2.68E-02
40	1.4191	0.5223	3.51E+02	-2.76E+02	-1.71E+02	6.02E+00	-4.66E+00	3.87E+01
41	0.0000	0.6964	-5.55E-01	-1.35E+00	4.34E-01	5.11E-01	1.48E-01	-6.73E-02
42	0.1577	0.6964	1.91E-01	5.66E-02	-3.58E-01	4.66E-02	2.92E-02	-9.66E-03
43	0.3154	0.6964	-1.82E+00	-2.16E+00	2.95E-01	8.23E-01	2.28E-01	-9.58E-02
44	0.4730	0.6964	-1.66E-01	-2.21E-01	5.72E-01	8.66E-02	2.33E-02	1.45E-03
45	0.6307	0.6964	9.46E-02	7.27E-02	1.24E+00	-6.31E-02	-1.76E-02	-5.96E-03
46	0.7884	0.6964	1.25E-02	-2.18E-02	3.27E-01	3.55E-03	6.98E-04	1.49E-02
47	0.9461	0.6964	2.69E-01	1.51E-01	1.93E+00	-9.13E-02	-2.49E-02	3.29E-03
48	1.1037	0.6964	1.98E+01	1.24E+00	-8.04E-02	2.43E-01	6.39E-01	-1.54E-01
49	1.2614	0.6964	2.19E+00	1.38E-01	-8.94E-03	2.70E-02	7.10E-02	-1.71E-02
50	1.4191	0.6964	-3.07E+01	6.42E+00	9.89E+01	-3.25E+00	1.96E+00	-1.16E+00

Table C.18: Panel 18 FEM Boundary Conditions for -1.5G Fuel and Aerodynamic Loads

Node	X (m)	Y (m)	FX	FY	FZ	MX	MY	MZ
1	0.0000	0.0000	-3.31E-02	-1.62E-03	-3.07E-01	1.22E-02	3.30E-03	-1.64E-03
2	0.1577	0.0000	-7.50E-01	4.20E-01	-3.51E-02	-6.01E-02	-3.66E-02	2.35E-02
3	0.3153	0.0000	4.89E+00	-2.78E+00	2.47E+00	6.13E-01	4.14E-01	-1.68E-01
4	0.4730	0.0000	-2.88E+00	3.59E-01	8.10E-02	-9.25E-02	-1.23E-01	5.37E-02
5	0.6307	0.0000	-3.28E+01	5.42E+01	-1.05E+01	-7.01E+00	-1.67E+00	6.06E-01
6	0.7884	0.0000	-6.64E+01	-9.82E+00	-1.08E+01	1.23E+00	-2.17E+00	4.72E-01
7	0.9461	0.0000	-4.52E+02	3.75E+02	-1.21E+02	-4.71E+01	-1.86E+01	7.68E+00
8	1.1037	0.0000	9.06E+01	1.20E+02	-9.10E+01	-8.97E+00	3.56E+00	-5.59E-01
9	1.2614	0.0000	1.83E+01	9.05E+00	-9.50E+00	-3.81E-01	7.32E-01	-1.89E-01
10	1.4191	0.0000	-1.46E+02	1.52E+02	-8.59E+01	4.94E+04	-3.54E+04	1.20E+01
11	0.0000	0.1741	-2.61E-01	7.47E-01	-2.40E-01	-8.10E-02	-2.35E-02	7.15E-03
20	1.4191	0.1741	2.50E+02	-2.57E+02	-1.05E+02	8.01E+04	-4.71E+04	-7.15E+00
21	0.0000	0.3482	2.00E-01	7.03E-01	-9.76E-02	-8.10E-02	-5.86E-03	3.12E-03
30	1.4191	0.3482	-2.30E+02	7.69E+01	-4.82E+01	1.88E+04	-2.36E+04	9.92E+00
31	0.0000	0.5223	-2.46E-02	4.14E-01	-2.16E-02	-5.34E-02	-9.40E-03	3.41E-03
40	1.4191	0.5223	1.36E+02	-1.35E+02	-7.80E+01	4.12E+00	-2.36E+00	1.94E+01
41	0.0000	0.6964	3.87E-01	-8.55E-01	5.34E-02	9.66E-02	2.22E-02	-6.33E-03
42	0.1577	0.6964	-1.42E-01	3.31E-01	-1.05E-01	-4.31E-02	-9.36E-03	2.03E-03
43	0.3154	0.6964	1.36E+00	-3.47E+00	4.99E-01	3.58E-01	6.58E-02	-2.02E-02
44	0.4730	0.6964	2.24E-01	-4.32E-01	1.17E-01	4.32E-02	7.99E-03	2.74E-03
45	0.6307	0.6964	1.94E-01	2.31E-02	2.88E-01	-1.22E-02	-3.05E-03	1.10E-02
46	0.7884	0.6964	-3.25E-01	-1.01E-01	1.67E-01	-6.32E-03	-1.44E-03	-2.88E-02
47	0.9461	0.6964	-6.94E-02	-2.91E-02	3.27E-01	-1.37E-02	-3.47E-03	-5.18E-03
48	1.1037	0.6964	8.30E+00	8.05E+00	3.24E+00	-9.00E-01	2.57E-01	-5.43E-02
49	1.2614	0.6964	9.23E-01	8.95E-01	3.61E-01	-9.99E-02	2.85E-02	-6.04E-03
50	1.4191	0.6964	-3.69E+01	1.45E+01	5.97E+01	-2.76E+00	5.51E-01	-1.18E+00

Table C.19: Panel 18 FEM Boundary Conditions for 3.75G Mass and Fuel Loads

Node	X (m)	Y (m)	FX	FY	FZ	MX	MY	MZ
1	0.0000	0.0000	2.24E-02	8.02E-03	3.12E-01	-1.20E-02	-3.22E-03	1.29E-03
2	0.1577	0.0000	-8.51E-03	-1.57E-02	3.03E-02	6.06E-03	2.43E-03	-1.38E-03
3	0.3153	0.0000	-2.58E-02	1.39E-01	-4.14E-01	-3.73E-02	-6.93E-03	4.71E-03
4	0.4730	0.0000	-3.41E-02	-9.25E-03	-2.62E-02	5.57E-03	2.41E-03	-1.80E-03
5	0.6307	0.0000	-9.73E-02	6.29E-02	-1.98E-01	-2.01E-02	-4.00E-03	2.45E-03
6	0.7884	0.0000	-4.11E-03	1.18E-02	-3.23E-02	7.01E-03	3.66E-03	-2.00E-03
7	0.9461	0.0000	-7.82E-02	1.42E-01	-1.36E-01	-2.50E-02	-5.88E-03	3.14E-03
8	1.1037	0.0000	-1.96E-01	-3.70E-02	3.75E-02	4.33E-03	1.75E-03	-3.38E-03
9	1.2614	0.0000	-2.33E-02	-6.83E-03	6.80E-03	9.51E-04	3.19E-04	-4.76E-04
10	1.4191	0.0000	-2.63E-01	5.18E-01	4.56E-01	-2.46E-02	4.58E-03	-9.32E-03
11	0.0000	0.1741	-5.72E-02	-3.36E-01	9.44E-02	8.00E-03	9.56E-04	-4.61E-04
20	1.4191	0.1741	1.80E-01	-3.67E-01	1.68E-01	5.97E-03	3.94E-03	2.96E-03
21	0.0000	0.3482	1.25E-02	-4.55E-02	1.84E-03	7.29E-03	2.16E-03	-6.75E-04
30	1.4191	0.3482	-4.92E-02	-6.51E-02	1.48E-01	4.83E-03	5.73E-03	-9.12E-03
31	0.0000	0.5223	2.47E-01	-4.81E-01	1.04E-01	2.94E-02	6.77E-03	-2.03E-03
40	1.4191	0.5223	2.26E-01	-3.03E-01	6.33E-02	9.53E-03	4.87E-03	-1.03E-02
41	0.0000	0.6964	-1.35E-01	2.50E-01	-2.84E-01	-3.40E-02	-6.30E-03	-2.68E-04
42	0.1577	0.6964	2.78E-02	-1.40E-02	3.27E-02	-6.86E-03	-2.19E-03	1.92E-03
43	0.3154	0.6964	-1.46E-01	1.81E-01	-3.05E-01	-2.53E-02	-4.34E-03	-3.96E-03
44	0.4730	0.6964	5.40E-01	1.37E-01	-2.36E-01	4.88E-03	1.95E-03	3.78E-02
45	0.6307	0.6964	-6.02E-01	-1.39E-01	-3.21E-01	1.43E-02	3.74E-03	-3.71E-02
46	0.7884	0.6964	6.60E-01	1.48E-01	-2.42E-01	1.06E-02	2.99E-03	4.07E-02
47	0.9461	0.6964	-8.46E-01	-2.30E-01	-4.49E-01	1.90E-02	4.70E-03	-4.97E-02
48	1.1037	0.6964	9.60E-02	-9.02E-02	-1.88E-01	-2.60E-03	4.84E-04	2.83E-03
49	1.2614	0.6964	1.07E-02	-1.00E-02	-2.09E-02	-2.88E-04	5.38E-05	3.14E-04
50	1.4191	0.6964	-9.74E-01	1.04E-01	-2.63E-01	2.97E-03	-1.44E-03	-2.18E-02

Table C.20: Panel 18 FEM Boundary Conditions for -1.5G Mass and Fuel Loads

Node	X (m)	Y (m)	FX	FY	FZ	MX	MY	MZ
1	0.0000	0.0000	-1.56E-01	-2.93E-02	-4.83E-01	1.85E-02	4.95E-03	-6.92E-03
2	0.1577	0.0000	2.22E-02	-2.64E-02	-5.36E-03	1.83E-03	4.35E-04	2.77E-04
3	0.3153	0.0000	1.60E-01	3.16E-01	2.77E-01	-1.63E-01	-5.18E-02	1.91E-02
4	0.4730	0.0000	5.24E-02	-7.73E-04	7.06E-02	-1.04E-02	-3.24E-03	2.44E-03
5	0.6307	0.0000	-1.53E-02	1.87E-01	1.35E-01	-8.01E-02	-2.56E-02	1.04E-02
6	0.7884	0.0000	5.35E-02	-7.12E-03	6.19E-02	-5.99E-03	-1.62E-03	2.37E-03
7	0.9461	0.0000	7.30E-02	2.34E-01	1.17E-01	-7.29E-02	-2.37E-02	1.09E-02
8	1.1037	0.0000	-2.19E-02	-1.99E-02	1.25E-01	-1.27E-02	-2.27E-03	1.41E-04
9	1.2614	0.0000	-3.77E-03	-6.21E-03	1.38E-02	-4.41E-04	8.98E-05	-1.50E-04
10	1.4191	0.0000	1.01E-01	2.08E-01	2.38E-01	-3.24E-02	-9.89E-03	3.11E-03
11	0.0000	0.1741	-1.31E-01	-6.23E-01	1.51E-01	4.60E-02	1.51E-02	-4.57E-03
20	1.4191	0.1741	-1.09E-01	-1.99E-01	1.85E-02	1.25E-02	4.36E-03	-3.02E-03
21	0.0000	0.3482	1.26E-03	-6.83E-02	1.11E-02	7.82E-03	2.34E-03	-7.09E-04
30	1.4191	0.3482	9.46E-02	-2.01E-01	-1.07E-02	1.34E-02	5.64E-03	4.83E-03
31	0.0000	0.5223	3.73E-02	-2.92E-01	2.15E-02	2.35E-02	7.46E-03	-2.10E-03
40	1.4191	0.5223	1.03E-01	-2.35E-01	-1.79E-02	1.21E-02	5.23E-03	5.50E-03
41	0.0000	0.6964	7.03E-02	2.95E-01	6.72E-02	-4.18E-02	-1.34E-02	8.15E-03
42	0.1577	0.6964	3.74E-02	-3.29E-02	4.07E-02	-5.66E-03	-8.12E-04	9.12E-04
43	0.3154	0.6964	3.71E-02	2.60E-01	4.35E-02	-3.17E-02	-9.46E-03	5.97E-03
44	0.4730	0.6964	-6.18E-02	1.74E-02	1.11E-02	-4.38E-03	-1.29E-03	-5.30E-03
45	0.6307	0.6964	3.87E-02	1.15E-02	4.54E-02	-1.67E-03	-4.59E-04	3.43E-03
46	0.7884	0.6964	-2.45E-02	-5.31E-03	1.03E-02	-4.82E-04	-1.39E-04	-2.53E-03
47	0.9461	0.6964	7.76E-03	3.51E-03	4.57E-02	-1.83E-03	-5.32E-04	2.38E-03
48	1.1037	0.6964	4.84E-02	-1.86E-01	-7.69E-02	-5.46E-03	-1.45E-03	6.07E-04
49	1.2614	0.6964	5.38E-03	-2.07E-02	-8.54E-03	-6.07E-04	-1.61E-04	6.74E-05
50	1.4191	0.6964	-2.45E-01	-1.30E-01	-7.00E-02	5.57E-03	2.36E-03	-1.48E-02

Table C.21: Panel 18 FEM Boundary Conditions for All 3.75G Loads

Node	X (m)	Y (m)	FX	FY	FZ	MX	MY	MZ
1	0.0000	0.0000	3.69E-01	8.80E-02	3.16E+00	-1.21E-01	-3.23E-02	1.89E-02
2	0.1577	0.0000	-6.58E-03	-3.63E-02	1.56E-01	1.80E-02	1.09E-02	-5.46E-03
3	0.3153	0.0000	-6.71E-01	-7.54E-01	-2.99E+00	2.65E-01	1.04E-01	-3.98E-02
4	0.4730	0.0000	-8.82E-02	-2.90E-01	-5.01E-01	7.98E-02	1.85E-02	-7.70E-03
5	0.6307	0.0000	-7.40E+00	1.01E+01	-4.49E+00	-1.12E+00	-2.64E-01	7.96E-02
6	0.7884	0.0000	-8.87E+00	-3.44E+00	-1.72E+00	4.64E-01	-2.51E-01	5.52E-02
7	0.9461	0.0000	-7.94E+01	6.50E+01	-2.56E+01	-8.37E+00	-3.21E+00	1.26E+00
8	1.1037	0.0000	1.20E+01	2.69E+01	-1.85E+01	-1.69E+00	5.82E-01	-1.26E-02
9	1.2614	0.0000	2.73E+00	2.34E+00	-1.91E+00	-7.95E-02	1.23E-01	-2.12E-02
10	1.4191	0.0000	-1.67E+01	1.60E+01	-3.76E+01	6.12E+04	-2.36E+04	3.61E+00
11	0.0000	0.1741	1.12E-02	4.31E-01	-1.29E-01	-6.88E-02	-3.51E-02	9.51E-03
20	1.4191	0.1741	4.90E+01	-5.70E+01	-4.00E-02	9.19E+04	-3.53E+04	-1.59E+00
21	0.0000	0.3482	-2.93E-02	-2.12E-01	6.05E-02	2.50E-02	1.53E-04	-7.08E-04
30	1.4191	0.3482	5.17E+01	-7.21E+01	-1.09E+02	3.06E+04	-1.18E+04	1.23E+01
31	0.0000	0.5223	9.00E-01	-5.99E-01	1.03E-01	-3.52E-02	-2.96E-02	7.99E-03
40	1.4191	0.5223	1.38E+02	-1.10E+02	-6.87E+01	2.11E+00	-1.56E+00	1.60E+01
41	0.0000	0.6964	-1.20E+00	5.28E-01	-2.30E+00	1.77E-01	8.04E-02	-2.91E-02
42	0.1577	0.6964	-6.41E-02	-2.19E-01	-7.01E-02	2.98E-02	1.16E-02	-1.42E-02
43	0.3154	0.6964	-1.38E+00	2.35E-01	-2.61E+00	2.91E-01	1.10E-01	-5.04E-02
44	0.4730	0.6964	1.87E+00	4.80E-01	-1.02E+00	6.46E-02	2.26E-02	1.26E-01
45	0.6307	0.6964	-2.72E+00	-6.06E-01	-4.53E+00	1.81E-01	4.80E-02	-1.59E-01
46	0.7884	0.6964	3.16E+00	7.77E-01	-1.10E+00	4.40E-02	1.28E-02	2.08E-01
47	0.9461	0.6964	-2.62E+00	-7.05E-01	-3.61E+00	1.43E-01	3.69E-02	-1.38E-01
48	1.1037	0.6964	3.94E+00	2.15E+00	-1.95E+00	3.90E-02	1.53E-01	-4.23E-02
49	1.2614	0.6964	4.38E-01	2.39E-01	-2.17E-01	4.33E-03	1.70E-02	-4.70E-03
50	1.4191	0.6964	-2.22E+01	1.09E+01	2.03E+01	-6.45E-01	4.02E-01	-1.76E+00

Table C.22: Panel 18 FEM Boundary Conditions for All -1.5G Loads

Node	X (m)	Y (m)	FX	FY	FZ	MX	MY	MZ
1	0.0000	0.0000	3.47E-03	2.17E-04	3.05E-02	-1.14E-03	-3.06E-04	5.28E-05
2	0.1577	0.0000	-6.13E-05	-2.28E-03	1.62E-03	-8.92E-05	6.13E-05	-4.71E-05
3	0.3153	0.0000	-1.33E-03	-3.99E-03	-2.26E-02	1.09E-02	3.28E-03	-3.62E-04
4	0.4730	0.0000	-1.41E-03	-3.00E-03	-2.75E-03	9.10E-04	3.84E-04	-1.41E-04
5	0.6307	0.0000	4.04E-03	-9.94E-03	-1.05E-02	4.98E-03	1.64E-03	-2.69E-04
6	0.7884	0.0000	-5.05E-03	8.00E-04	-2.82E-03	3.72E-04	2.14E-04	-1.51E-04
7	0.9461	0.0000	6.07E-03	-1.56E-02	-7.79E-03	4.13E-03	1.39E-03	-1.56E-04
8	1.1037	0.0000	-9.23E-03	1.21E-03	-5.35E-03	4.85E-04	-1.56E-05	-2.67E-04
9	1.2614	0.0000	-1.26E-03	3.99E-04	-5.50E-04	-4.32E-06	-2.37E-05	-3.12E-05
10	1.4191	0.0000	-3.93E-03	-3.78E-03	-1.34E-02	1.49E-03	6.92E-04	-2.93E-05
11	0.0000	0.1741	2.22E-02	3.62E-02	-5.96E-03	-2.64E-03	-7.64E-04	2.40E-04
20	1.4191	0.1741	1.51E-02	1.65E-02	7.34E-03	-1.17E-03	-1.86E-05	7.15E-06
21	0.0000	0.3482	2.32E-03	4.48E-03	-1.74E-03	-3.42E-04	2.36E-05	3.50E-06
30	1.4191	0.3482	-9.64E-03	1.40E-02	8.06E-03	-7.23E-04	-2.67E-04	-6.09E-04
31	0.0000	0.5223	4.30E-03	1.46E-02	3.06E-03	-1.59E-03	-5.24E-04	1.47E-04
40	1.4191	0.5223	-1.65E-03	2.04E-02	1.25E-03	-1.55E-03	-5.50E-04	-6.69E-04
41	0.0000	0.6964	3.31E-03	-1.69E-02	-1.02E-02	2.36E-03	8.64E-04	3.21E-04
42	0.1577	0.6964	-5.51E-03	2.09E-03	-3.35E-03	3.54E-04	-1.60E-04	-4.57E-04
43	0.3154	0.6964	-1.09E-02	-2.38E-02	-8.50E-03	1.47E-03	1.15E-03	1.49E-04
44	0.4730	0.6964	-9.04E-03	-5.03E-03	5.56E-03	-2.73E-04	4.52E-05	-6.55E-04
45	0.6307	0.6964	1.48E-04	7.67E-04	-1.08E-02	4.44E-04	1.31E-04	4.83E-05
46	0.7884	0.6964	3.45E-03	9.90E-04	-4.62E-03	1.86E-04	6.61E-05	3.22E-04
47	0.9461	0.6964	-6.42E-03	-1.79E-03	-9.62E-03	3.62E-04	1.04E-04	-5.82E-04
48	1.1037	0.6964	6.03E-04	2.09E-02	1.82E-02	6.74E-04	2.40E-04	6.33E-05
49	1.2614	0.6964	6.70E-05	2.32E-03	2.03E-03	7.49E-05	2.67E-05	7.03E-06
50	1.4191	0.6964	-7.62E-05	3.05E-02	-9.33E-03	-2.28E-03	-2.88E-04	4.52E-04

Table C.23: Panel 18 FEM Boundary Conditions for Emergency Landing Loads

Node	X (m)	Y (m)	FX	FY	FZ	MX	MY	MZ
1	0.0000	0.0000	-1.54E-01	-2.27E-02	-4.26E-01	1.64E-02	4.38E-03	-6.39E-03
2	0.1577	0.0000	1.24E-01	-6.17E-02	9.01E-03	8.61E-03	3.12E-03	1.81E-03
3	0.3153	0.0000	1.86E-01	4.38E-01	2.06E-01	-1.00E-01	-3.23E-02	1.46E-02
4	0.4730	0.0000	1.05E-01	-1.34E-05	6.80E-02	-2.69E-03	-3.39E-04	4.22E-03
5	0.6307	0.0000	1.04E-01	1.11E-01	1.25E-01	-3.49E-02	-1.06E-02	9.43E-03
6	0.7884	0.0000	9.78E-02	-5.54E-03	5.80E-02	-1.49E-04	2.21E-03	4.54E-03
7	0.9461	0.0000	4.45E-01	-6.88E-02	1.80E-01	-2.22E-02	-7.90E-03	1.11E-02
8	1.1037	0.0000	-6.36E-02	-5.24E-02	2.19E-01	-1.48E-02	-5.45E-03	-3.13E-04
9	1.2614	0.0000	-1.47E-02	-5.51E-03	2.47E-02	-1.49E-03	-5.51E-04	-2.05E-04
10	1.4191	0.0000	2.41E-01	9.92E-02	1.37E-01	-1.31E-02	-5.70E-03	6.72E-03
11	0.0000	0.1741	-5.94E-01	-3.54E-01	1.20E-01	3.63E-02	1.15E-02	-3.54E-03
20	1.4191	0.1741	-1.68E-01	1.93E-01	2.17E-03	-7.30E-03	1.66E-03	-4.22E-03
21	0.0000	0.3482	1.76E-01	-2.10E-01	3.08E-02	2.32E-02	7.56E-03	-2.24E-03
30	1.4191	0.3482	6.39E-02	-3.45E-02	1.92E-02	8.05E-03	3.06E-03	-8.56E-03
31	0.0000	0.5223	4.06E-01	-6.30E-01	7.02E-02	5.34E-02	1.83E-02	-5.06E-03
40	1.4191	0.5223	3.39E-02	-6.92E-02	2.73E-02	1.15E-02	2.71E-03	-8.18E-03
41	0.0000	0.6964	-1.13E-01	4.63E-01	1.84E-01	-9.70E-02	-3.21E-02	1.37E-02
42	0.1577	0.6964	2.72E-02	-2.24E-02	8.50E-02	-1.38E-02	-3.77E-03	2.45E-03
43	0.3154	0.6964	-8.10E-02	3.12E-01	1.30E-01	-6.84E-02	-2.29E-02	9.92E-03
44	0.4730	0.6964	-8.62E-03	4.02E-02	3.06E-02	-9.32E-03	-3.01E-03	1.91E-03
45	0.6307	0.6964	-3.27E-02	-9.08E-03	8.17E-03	-5.52E-04	-8.74E-05	-2.52E-03
46	0.7884	0.6964	1.38E-02	3.12E-03	4.09E-02	-1.88E-03	-4.57E-04	2.16E-03
47	0.9461	0.6964	9.82E-02	1.54E-02	5.15E-02	-2.46E-03	-7.07E-04	6.28E-03
48	1.1037	0.6964	2.48E-02	-6.13E-02	3.28E-02	-9.22E-03	-3.52E-03	8.72E-04
49	1.2614	0.6964	2.76E-03	-6.82E-03	3.65E-03	-1.02E-03	-3.92E-04	9.69E-05
50	1.4191	0.6964	-1.60E-01	3.05E-02	-1.14E-02	-6.40E-03	-2.60E-03	-1.35E-03

Table C.24: Panel 18 FEM Applied Aerodynamic Loads

Element	Area (m^2)	Applied Surface Pressure (Pa)	
19	0.027452	358183.1	
20	0.027452	358183.1	
28	0.027452	358183.1	
29	0.027452	358183.1	
8	0.027452	268123.4	
9	0.027452	268123.4	
17	0.027452	268123.4	
18	0.027452	268123.4	
Node	**X (m)**	**Y (m)**	**Applied Moments My (N-m)**
10	1.419076	0.0000	-23567.2
20	1.419076	0.1741	-23567.2
30	1.419076	0.3482	-23567.2

Appendix D

GLOBAL STOCHASTIC OPTIMIZATION ALGORITHM TEST FUNCTION RESULTS

D.1 Initial Global Stochastic Optimization Algorithms Results

A test problem was chosen to investigate the performance of IHR with an objective function with multiple local minima and far away from a spherically symmetric function [229]. It is given as:

Objective function:

$$f(\mathbf{x}) = -\left[A\prod_{k=1}^{n} sin(x_k) + \prod_{k=1}^{n} sin(5x_k) \right] \tag{D.1}$$

where A is a constant.

Minimize f(x)
Such that: $0 \le x_k \le \pi$, k = 1,…, n.

The trigonometric objective function above was chosen by Zabinsky et al. for several reasons. It has a known minimum point at $\left(\frac{\pi}{2},\frac{\pi}{2},...,\frac{\pi}{2}\right)$; it has multiple local minima; and is easily generalized to n dimensions. Also, the influence of the depth of the local minima can be explored by manipulating the constant A; as A becomes large the function becomes spherically symmetric. In addition, the number of local minima is given by

$$\sum_{i=0}^{\lfloor n/2 \rfloor} \left(\frac{n!}{(n-2i)!(2i)!} * 3^{n-2i} * 2^{2i} \right) \tag{D.2}$$

where n/2 is rounded down to the nearest integer [30]. For the runs made, there are 13 local minima when n is two, and 4,882,813 local minima when n is ten. This helps explain why the large dimension problem needs many iterations to find the global minimum.

D.1.1 Improving Hit-and-Run (IHR) Results

As discussed in Section 2.2.1, Improving Hit-and-Run is a sequential random global optimization algorithm. As an example, the objective function above was run four times with different parameters (see Table D.1). The constant A was 5.0 for all runs. There were 30 starts

for each run. In the code, N is the number of design variables (dimension) and maxiter is the maximum number of iterations allowed. Some of the key results are shown below in Table D.2.

It can be seen that the complexity of the problem increases greatly for larger dimensions. However, IHR found the global minimum within 2% for even large dimensions, such as N equal to ten, with a minimum amount of calculation time. More discussion of IHR's performance on this and other test problems can be found in Graesser [30] and Zabinsky [228].

Table D.1: Optimization Test Problem Results with IHR

Run	Dimension (n)	Number of Iterations (i)
1	2	100
2	2	1000
3	10	100
4	10	1000

Table D.2: Test Problem Results Using IHR

Run	Number of Starts Within 2% of Theoretical Value (6)	Average Number of Improving Points	Number of Starts in Local Minima (< 80% of Theoretical Value)
1	12	7	0
2	30	12	0
3	0	12	16
4	1 (6 within 3%)	41	8

D.1.2 Multi-Particle Simulated Annealing (MPSA) Results

As discussed briefly in Section 2.2.2, the MPSA algorithm is an earlier version of the IPA that does not include a cooling schedule that interacts and depends on particles' history. Here the stopping criteria was either 100 or 1,000 iterations when the objective function was within 0.01 of the previous value (see Table D.3). Both design problems had n*10 particles, i.e., runs 1 and 2 had 20 particles and runs 3 and 4 had 100 particles. Runs 1 and 2 had n*2 starts; runs 3 and 4 had 30 starts, similar to the IHR example above. Some of the key results are shown below in Table D.4.

For the constraints placed on the MPSA algorithm for runs 3 and 4 it can be seen that the results are not as good as that seen with IHR. In Molvalioglu et al. [34] many more iterations of a problem this size result in good convergence to the global minimum. Note that these problems have no feasibility constraints. In the wing panel optimization, however, there are many constraints and many more design variables. It will be shown that the MPSA algorithm is able to handle this type of large, composite variable design problem.

Table D.3: Optimization Test Problem Results with MPSA

Run	Dimension (n)	Number of Iterations (stop)
1	2	100
2	2	1000
3	10	100
4	10	1000

Table D.4: Test Problem Results Using MPSA

Run	Number of Particles Within 2% of Theoretical Value (6)	Average Number of Improving Points	Number of Particles in Local Minima (< 80% of Theoretical Value)
1	10	4	0
2	15	7	0
3	0	2	98
4	1 (within 4%)	22	95

D.2 Test Function Improving Hit-and-Run (IHR) Results

The Improving Hit-and-Run code used for the test problem evaluation was obtained from Charonchai Khompatraporn (Charlie) [461]. The name of the code is uwihr_anova.c. Table D.5 shows the results of the test function experiments on the IHR algorithm.

Table D.5: IHR Example Run Output and Results

Run 1 (n = 2, i = 100)					
Start	**-F(x)**	**X1**	**X2**	**% Within Theoretical Value**	**Number of Improving Points**
1	5.80956	1.64947	1.48647	3.17	3
2	5.87806	1.53575	1.65494	2.03	7
3	5.98558	1.55883	1.59945	0.24	7
4	5.71963	1.60352	1.43513	4.67	5
5	5.89876	1.48842	1.57769	1.69	6
6	5.65901	1.65306	1.70418	5.68	7
7	5.66058	1.55412	1.72361	5.66	6
8	5.72191	1.70257	1.52537	4.63	4
9	5.89794	1.52184	1.50321	1.70	14
10	**5.99802**	**1.57675**	**1.56097**	**0.03**	**10**
11	5.99571	1.56889	1.55399	0.07	7
12	5.77934	1.49123	1.66665	3.68	7
13	5.92666	1.50824	1.60317	1.22	9
14	5.72109	1.70918	1.58049	4.65	5
15	5.86948	1.63579	1.63975	2.18	12

Table D.5: IHR Example Run Output and Results (continued)

Start	-F(x)	X1	X2	% Within Theoretical Value	Number of Improving Points
16	5.48208	1.47216	1.74157	8.63	1
17	5.82849	1.67864	1.56417	2.86	3
18	5.97342	1.61005	1.58624	0.44	12
19	5.90795	1.51762	1.51211	1.53	7
20	5.9889	1.58366	1.5948	0.18	8
21	5.91251	1.63973	1.53644	1.46	5
22	5.81552	1.60732	1.67731	3.07	10
23	5.47503	1.44887	1.72963	8.75	4
24	5.97066	1.58686	1.61212	0.49	3
25	5.8501	1.65452	1.51311	2.50	12
26	5.57221	1.51145	1.73582	7.13	3
27	5.71193	1.44455	1.50406	4.80	2
28	5.87525	1.49712	1.62676	2.08	8
29	5.74544	1.66148	1.67006	4.24	11
30	5.91368	1.55955	1.49535	1.44	8

Run 2 (n = 2, i = 1000)					
Start	**-F(x)**	**X1**	**X2**	**% Within Theoretical Value**	**Number of Improving Points**
1	5.99905	1.57872	1.5717	0.02	8
2	5.99995	1.57225	1.57195	0.00	17
3	5.99965	1.57496	1.57332	0.01	10
4	5.99502	1.55617	1.55991	0.08	9
5	5.99933	1.56413	1.57144	0.01	12
6	5.99916	1.57206	1.57817	0.01	10
7	5.99981	1.57369	1.56865	0.00	11
8	5.99244	1.57741	1.54933	0.13	13
9	5.99984	1.56749	1.57093	0.00	9
10	5.99863	1.57346	1.57999	0.02	12
11	**5.99996**	**1.56937**	**1.57**	**0.00**	**13**
12	5.99903	1.56846	1.57851	0.02	15
13	5.99906	1.5633	1.56827	0.02	15
14	5.99966	1.56861	1.57502	0.01	20
15	5.9968	1.5782	1.55819	0.05	11
16	5.99974	1.57494	1.57066	0.00	16
17	5.9993	1.56409	1.56951	0.01	19
18	5.99487	1.55599	1.55969	0.09	14
19	5.99754	1.55837	1.56769	0.04	10
20	5.99853	1.5783	1.57728	0.02	11
21	5.99994	1.5691	1.57184	0.00	9

Table D.5: IHR Example Run Output and Results (continued)

Start	-F(x)	X1	X2	% Within Theoretical Value	Number of Improving Points
22	5.99532	1.56953	1.55317	0.08	4
23	5.99684	1.58424	1.56533	0.05	10
24	5.99969	1.57475	1.56854	0.01	21
25	5.99897	1.57907	1.57038	0.02	3
26	5.99881	1.57871	1.56671	0.02	12
27	5.99949	1.56926	1.56518	0.01	4
28	5.99706	1.55707	1.56806	0.05	11
29	5.99906	1.57759	1.56674	0.02	16
30	5.99977	1.5744	1.56926	0.00	14

Table D.5: IHR Example Run Output and Results (continued)

Run 3 (n = 10, i = 100)													
Start	**-F(x)**	**X1**	**X2**	**X3**	**X4**	**X5**	**X6**	**X7**	**X8**	**X9**	**X10**	**% Within Theoretical Value**	**No. of Improving Points**
1	3.12741	1.37419	2.19297	1.50034	1.90583	1.51121	1.55553	1.83006	1.12248	1.4763	1.29802	47.88	12
2	0.26216	3.57269	1.60563	2.19635	2.11352	2.23755	0.96494	3.27742	3.44785	0.79862	2.96394	95.63	3
3	2.51796	1.7472	1.35203	1.6785	1.59574	1.76138	2.20057	1.73835	1.49901	2.27754	1.13254	58.03	16
4	2.83755	1.29677	1.36204	1.28266	1.91186	0.85201	1.30687	1.68415	1.64732	1.93636	1.69626	52.71	21
5	0.17978	1.59069	2.34235	1.02601	1.17587	2.69346	1.0209	3.6978	3.42991	1.43373	1.77514	97.00	4
6	3.14701	1.25961	1.64564	1.02237	1.51729	1.21586	1.4737	1.78722	1.06632	1.37355	1.46593	47.55	24
7	0.04306	3.95291	3.90845	0.06266	2.32689	3.59447	0.42304	3.01034	2.75992	2.89266	2.88425	99.28	3
8	3.75649	1.70828	1.46086	1.32551	1.92797	1.49902	1.60444	1.34337	1.69079	1.64668	2.08537	37.39	16
9	4.09449	1.54602	1.50132	1.72546	1.16664	1.87574	1.431	1.65053	1.71245	1.54106	1.81345	31.76	19
10	0.05947	2.76475	3.29527	0.2907	2.63801	1.56572	2.23899	3.19323	0.26547	2.71825	1.08838	99.01	7
11	0.52203	0.20063	2.20773	2.86394	2.83176	2.76718	0.20203	2.17163	2.90028	1.04527	0.88995	91.30	10
12	2.73659	1.21159	1.29336	1.34059	1.77907	1.44397	1.85225	1.98849	1.87756	1.52561	2.26383	54.39	22
13	0.01478	2.29206	3.3256	1.22596	2.96574	2.99383	2.19118	2.80182	3.48234	0.95646	3.08765	99.75	5
14	3.88914	1.60531	1.10178	1.16764	1.64643	1.43689	1.80384	1.41124	1.5461	1.44872	1.66256	35.18	16
15	0.679	2.94547	2.8861	1.52568	0.36784	0.90106	2.13183	2.81148	2.83914	0.29679	2.8008	88.68	20
16	0.28238	0.97685	2.7921	2.99348	1.4819	1.47209	0.18244	2.26926	0.24293	2.84185	2.96244	95.29	8
17	0.19025	2.753	3.05198	1.62389	1.61284	2.39289	0.40568	2.82845	0.35585	2.82406	2.18939	96.83	14
18	0.03244	3.07959	0.8853	2.67271	2.42114	1.3853	2.86775	3.39561	2.84796	2.02565	2.78531	99.46	4
19	2.14775	2.29584	1.37142	1.86357	1.56359	1.92734	0.97527	1.20598	1.90035	1.19183	1.2867	64.20	14
20	2.46096	2.02035	1.87896	1.33153	1.53447	0.94626	1.31165	1.95103	1.27236	1.06446	1.32754	58.98	11
21	0.61848	1.6299	2.22103	0.27852	2.78932	2.20766	0.37166	2.78225	2.09563	0.92094	0.43638	89.69	10
22	0.52967	2.8872	1.57506	2.27566	2.89284	2.04042	0.9512	1.60507	0.95865	0.33986	1.68419	91.17	5
23	3.82016	1.94115	1.82841	1.5268	1.47312	1.60078	1.81885	1.86605	1.32984	1.59057	1.24404	36.33	13
24	0.8755	2.13909	1.5719	1.04423	2.32723	2.07511	2.1724	1.80154	0.9437	2.45647	1.03619	85.41	27
25	0.18847	2.22455	3.51722	1.59929	0.48203	2.79129	3.31877	2.96494	2.6389	3.99904	3.51814	96.86	5
26	**4.18419**	**1.68392**	**1.71628**	**1.47295**	**1.26149**	**1.84184**	**1.59301**	**1.4826**	**1.49438**	**1.36545**	**1.85938**	**30.26**	**22**
27	4.16689	1.55417	1.42883	1.75087	1.36248	1.63796	1.35927	1.56448	1.95441	1.3959	1.74012	30.55	13
28	3.06049	1.78576	2.01082	1.2314	1.62667	1.54781	1.34271	1.60778	1.32938	2.13324	1.1668	48.99	7
29	0.0239	1.7355	2.80273	2.80345	0.15664	2.30674	0.81766	0.89707	0.36083	2.86099	3.15718	99.60	3
30	0.76367	1.23966	1.15427	0.74316	2.54031	1.59353	2.10537	1.20189	1.75205	1.49985	0.62623	87.27	15

Table D.5: IHR Example Run Output and Results (continued)

Run 4 (n = 10, i = 1000)													
Start	**-F(x)**	**X1**	**X2**	**X3**	**X4**	**X5**	**X6**	**X7**	**X8**	**X9**	**X10**	**% Within Theoretical Value**	**No. of Improving Points**
1	5.54622	1.49371	1.47563	1.5737	1.54231	1.61978	1.56914	1.69562	1.54091	1.58511	1.57462	7.56	41
2	5.67412	1.68825	1.64333	1.58467	1.58165	1.60231	1.58717	1.52598	1.54156	1.57623	1.55436	5.43	42
3	0.98691	2.82886	2.79988	0.31939	0.31898	1.57404	2.81693	2.81939	0.31862	2.82328	0.3197	83.55	36
4	5.71305	1.65426	1.57852	1.59871	1.55931	1.51611	1.59843	1.56957	1.49718	1.59081	1.512	4.78	51
5	5.33247	1.49122	1.63404	1.43984	1.56745	1.49487	1.50523	1.55904	1.5236	1.44919	1.52335	11.13	68
6	0.53791	0.35957	0.92295	2.87629	2.19657	2.86954	2.21821	3.26867	2.83715	1.57378	2.80274	91.03	21
7	0.98559	2.82129	0.94654	2.81965	0.32914	2.83139	2.19203	2.2	0.94888	0.31775	0.34383	83.57	28
8	**5.91015**	**1.53411**	**1.57731**	**1.5792**	**1.59329**	**1.56921**	**1.58936**	**1.54513**	**1.58927**	**1.62261**	**1.58324**	**1.50**	**46**
9	5.67442	1.58086	1.61114	1.48815	1.5471	1.52405	1.57083	1.6039	1.52002	1.58906	1.47712	5.43	48
10	5.8775	1.58873	1.60369	1.54311	1.60839	1.59208	1.53254	1.53177	1.57564	1.54038	1.59382	2.04	48
11	5.79251	1.57924	1.54288	1.57449	1.53223	1.65319	1.58457	1.58199	1.62292	1.55734	1.52218	3.46	38
12	0.57096	3.29346	2.83853	0.87955	0.30105	0.88965	0.24092	0.94856	2.81476	0.28233	1.53892	90.48	18
13	4.88074	1.68083	1.64608	1.61189	1.45187	1.57151	1.52071	1.82498	1.6202	1.55233	1.66787	18.65	48
14	0.99714	2.83134	2.82771	2.19223	2.19472	0.3115	2.82511	2.82018	2.82751	2.19112	2.18597	83.38	31
15	5.63186	1.57759	1.61149	1.53528	1.46894	1.59527	1.65776	1.52355	1.62876	1.59427	1.56948	6.14	60
16	5.87811	1.57984	1.58437	1.5895	1.53044	1.55854	1.57292	1.6395	1.56353	1.55869	1.53793	2.03	53
17	5.63785	1.62248	1.54059	1.62179	1.6035	1.57658	1.50094	1.52227	1.66447	1.51308	1.59676	6.04	57
18	5.82913	1.58917	1.55832	1.53263	1.63829	1.58972	1.52764	1.59693	1.53234	1.58248	1.60238	2.85	41
19	5.49382	1.60958	1.60131	1.58362	1.69626	1.51004	1.5614	1.66435	1.49729	1.51275	1.55075	8.44	50
20	5.49812	1.51718	1.52771	1.50248	1.55901	1.57123	1.63295	1.71114	1.60305	1.63373	1.60553	8.36	47
21	0.98473	0.32259	1.58403	2.21245	2.82403	2.22811	0.32077	0.32631	0.30242	0.94933	2.20795	83.59	39
22	5.5422	1.58067	1.57455	1.57559	1.60231	1.57016	1.70329	1.66958	1.54139	1.51204	1.61905	7.63	41
23	5.84782	1.56705	1.56049	1.57505	1.61556	1.56285	1.5206	1.59346	1.56986	1.62181	1.62365	2.54	41
24	5.6743	1.63132	1.51786	1.55685	1.54217	1.6554	1.54803	1.65486	1.54438	1.56964	1.53571	5.43	50
25	5.69478	1.52919	1.60993	1.6084	1.51439	1.60305	1.64074	1.49269	1.57238	1.62043	1.55684	5.09	54
26	0.29954	2.85712	2.23405	1.50095	2.76845	2.82721	2.87551	2.84322	2.80997	3.21419	1.56544	95.01	19
27	0.50309	0.29746	0.33121	2.12413	3.27292	0.92725	0.94062	2.79355	2.8514	2.82039	2.9104	91.62	11
28	5.81638	1.58904	1.60305	1.62472	1.57622	1.59808	1.60196	1.56727	1.59482	1.54392	1.64565	3.06	45
29	5.77346	1.56902	1.6063	1.58747	1.60437	1.49887	1.57866	1.5584	1.50293	1.6303	1.57218	3.78	38
30	5.86703	1.56443	1.55052	1.59824	1.53354	1.52261	1.57925	1.56302	1.62203	1.53347	1.55744	2.22	30

D.3 Test Function Multiple Particle Simulated Annealing (MPSA) Results

Table D.6 shows the results of the test function experiments using the MPSA algorithm.

Table D.6: MPSA Example Run Output and Results

Run 1 (n = 2, stop = 100)					
Particle	**-F(x)**	**X1**	**X2**	**% Within Theoretical Value**	**Number of Improving Points**
1	5.08332	1.31551	1.65728	15.28	3
2	5.95258	1.56533	1.62692	0.79	6
3	5.95511	1.52953	1.53445	0.75	4
4	5.66383	1.58322	1.72317	5.60	2
5	5.90117	1.49741	1.53431	1.65	4
6	5.73833	1.44353	1.61599	4.36	3
7	5.8742	1.55671	1.66204	2.10	6
8	5.21144	1.73051	1.3699	13.14	4
9	5.95019	1.52414	1.53642	0.83	4
10	5.82299	1.68676	1.46337	2.95	2
11	5.65655	1.68676	1.46337	5.72	3
12	5.81644	1.62145	1.67143	3.06	3
13	5.85719	1.63201	1.49271	2.38	3
14	5.90299	1.51034	1.62524	1.62	1
15	5.97719	1.57161	1.53176	0.38	2
16	**5.99972**	**1.57709**	**1.63612**	**0.00**	**5**
17	5.93590	1.57709	1.63612	1.07	5
18	5.55260	1.63388	1.40240	7.46	4
19	5.99585	1.56612	1.58385	0.07	4
20	5.98627	1.56612	1.54347	0.23	2

Run 2 (n = 2, stop = 1000)					
Particle	**-F(x)**	**X1**	**X2**	**% Within Theoretical Value**	**Number of Improving Points**
1	5.96969	1.59947	1.53598	0.51	5
2	5.95517	1.59685	1.52245	0.75	8
3	5.94312	1.51865	1.60426	0.95	10
4	5.92061	1.64342	1.56238	1.32	7
5	**5.99946**	**1.57579**	**1.57416**	**0.01**	**9**
6	5.90920	1.62205	1.51115	1.51	12
7	5.99828	1.58126	1.56846	0.03	0
8	5.99282	1.55743	1.55345	0.12	0

Table D.6: MPSA Example Run Output and Results (continued)

Particle	-F(x)	X1	X2	% Within Theoretical Value	Number of Improving Points
9	5.88187	1.57169	1.66016	1.97	10
10	5.99604	1.55790	1.58067	0.07	6
11	5.85702	1.52836	1.66022	2.38	7
12	5.80259	1.60641	1.45981	3.29	4
13	5.96000	1.56302	1.62198	0.67	6
14	5.99807	1.58184	1.57341	0.03	0
15	5.85250	1.63505	1.49298	2.46	8
16	5.73854	1.44241	1.61209	4.36	11
17	5.98364	1.59204	1.54543	0.27	9
18	4.33790	1.02132	4.07100	27.70	6
19	5.92797	1.57817	1.64001	1.20	10
20	5.98718	1.57827	1.59909	0.21	10

Table D.6: MPSA Example Run Output and Results (continued)

Run 3 (n = 10, stop = 100)													
Particle	**-F(x)**	**X1**	**X2**	**X3**	**X4**	**X5**	**X6**	**X7**	**X8**	**X9**	**X10**	**% Within Theoretical Value**	**No. of Improving Points**
1	0.02420	2.63061	1.11783	0.46373	3.99947	1.22918	2.30845	3.92635	3.27090	3.48026	0.92759	99.60	0
2	0.00022	3.29707	1.90170	0.01613	2.17629	2.38439	0.07457	1.15889	2.70155	3.86834	0.78135	100.00	0
3	-0.0149	1.20913	1.90733	3.03929	4.13216	0.58909	3.92926	3.42935	1.94406	2.10514	0.44414	100.25	0
4	-0.0001	2.41275	1.63710	0.00067	0.28978	2.08717	3.61988	2.27019	3.49871	2.81591	3.79253	100.00	0
5	0.00973	3.62899	3.65314	1.27506	2.16167	0.76844	1.54107	1.73055	0.36803	0.08201	0.71702	99.84	0
6	0.20243	1.91109	2.91115	1.99566	1.94808	1.35348	2.36171	1.08249	2.38100	1.75823	2.57213	96.63	1
7	0.00018	2.69594	2.63975	1.15783	1.24978	1.10967	4.09405	0.10851	0.92249	0.30293	3.18799	100.00	0
8	-0.0035	1.93751	2.94132	3.79302	2.74919	3.92414	3.19689	1.71429	2.12351	1.52838	2.08971	100.06	0
9	4.10259	1.77966	1.53715	1.85849	1.41017	1.61988	1.56039	1.22085	1.33605	1.70430	1.76767	31.62	11
10	0.00442	3.93691	0.43567	3.48549	2.95869	3.37198	1.86003	3.10968	2.38834	2.75194	3.52981	99.93	0
11	-0.0164	0.16028	0.88441	1.79799	2.60781	4.07727	3.90105	0.49090	1.76972	3.34809	2.46009	100.27	0
12	0.04599	2.35307	1.82368	1.27445	2.74408	2.32308	1.66704	3.33846	1.08411	3.62618	0.65447	99.23	0
13	0.10047	0.50731	2.63407	2.49663	2.06287	1.41210	0.92710	2.70313	1.21377	3.80882	4.10683	98.33	5
14	0.10926	3.37810	0.59742	1.38579	1.09193	2.66083	1.80452	0.73597	1.55439	1.24767	3.86594	98.18	0
15	-0.0003	2.99115	3.24807	0.10535	0.94796	0.58808	0.65020	4.11184	1.16593	1.01863	3.69901	100.00	0
16	-0.0342	3.97138	2.81833	0.83752	1.77490	2.46092	2.70460	0.61616	4.07242	3.65018	0.78083	100.57	0
17	-0.0646	0.61887	1.97488	2.21324	1.59170	3.57480	0.86557	2.67542	0.41454	1.10251	0.62460	101.08	0
18	-0.0747	2.22247	1.23725	3.33490	2.17853	3.96325	4.12025	2.62834	1.67962	3.50464	4.01315	101.25	0
19	0.00558	0.11789	1.18805	3.67571	1.56453	1.36243	0.33429	2.62120	3.59701	0.74784	2.45094	99.91	4
20	-0.0028	3.39306	0.13503	1.56344	0.47085	0.87942	0.59857	0.49341	1.88099	3.61658	3.62015	100.05	11
21	0.00830	1.46868	1.54586	4.11883	0.99548	3.90024	4.07214	3.17733	2.28254	3.44618	3.76800	99.86	0
22	0.03261	1.00411	2.80218	1.49158	0.10657	3.39367	2.41347	0.79114	2.38946	0.14259	1.12467	99.46	0
23	-0.0116	1.91520	2.20276	0.53858	3.20321	3.48445	1.92700	4.09882	0.98871	1.92228	0.47659	100.19	0
24	0.00583	1.63784	3.91765	1.15733	3.16620	1.76976	3.97287	0.69973	1.53954	3.48741	2.99231	99.90	0
25	0.01748	0.47119	3.94892	0.24454	1.69735	1.83500	0.91559	0.21035	3.82928	1.16642	2.30616	99.71	0
26	-0.0143	3.68752	3.77378	1.41115	1.66551	0.71330	0.44726	2.85983	2.95709	3.90663	1.90497	100.24	8
27	-0.1221	0.44743	1.70000	0.61106	1.19215	0.55528	0.38455	1.15243	0.82932	1.46878	4.05471	102.03	0
28	0.01185	3.47863	1.75154	0.20176	4.11636	2.00280	2.76753	2.90728	2.34351	2.49636	0.53309	99.80	0
29	0.06899	2.24508	2.08358	4.04542	0.41805	2.17223	3.49558	2.27294	1.30039	2.12348	2.07035	98.85	0
30	0.01448	3.82083	2.39740	1.33022	0.18132	1.93730	0.41966	1.45476	0.35885	0.36974	3.85411	99.76	0
31	-0.0360	1.32741	0.79430	0.94075	2.80893	1.68094	3.61344	1.35084	2.40826	3.73798	3.41902	100.60	1
32	-0.0911	1.18060	4.09982	3.95577	1.49261	2.18471	4.06225	1.25547	3.05548	4.05922	4.03725	101.52	0
33	0.00001	0.13197	0.61186	0.57136	1.59703	3.04180	3.64102	2.47970	0.17558	1.77299	3.11349	100.00	8

Table D.6: MPSA Example Run Output and Results (continued)

Particle	-F(x)	X1	X2	X3	X4	X5	X6	X7	X8	X9	X10	% Within Theoretical Value	No. of Improving Points
34	0.25246	4.11761	1.13908	0.99786	3.47547	1.66104	2.25713	3.70686	1.52574	3.89789	1.33945	95.79	0
35	-0.0037	3.70649	4.09945	1.14919	2.67897	1.11332	0.02403	2.75826	1.75430	2.78653	2.95515	100.06	1
36	0.01201	2.59091	3.66208	0.07843	2.63686	3.37716	2.07682	4.02119	2.17295	1.67110	1.73559	99.80	14
37	-0.0007	1.47265	1.56774	2.22259	3.75991	0.01585	2.15060	2.00631	3.29310	2.38830	3.24869	100.01	0
38	0.03261	2.92989	1.92152	3.48998	3.64375	3.35556	2.38500	1.41532	3.45057	2.79089	1.47667	99.46	20
39	-0.1516	1.29955	3.37244	1.91150	1.78418	0.69953	0.66129	0.48866	1.09439	1.83485	1.21578	102.53	1
40	0.00072	2.88704	2.80092	1.09910	0.19250	3.14851	1.13733	0.70986	0.25495	3.35259	2.47273	99.99	0
41	-0.0419	2.31044	2.77774	2.41165	2.99509	0.90815	2.89631	3.94459	3.18992	2.82998	0.86352	100.70	0
42	-0.0014	2.90392	3.18442	2.58751	1.42824	3.08618	3.10471	1.01030	3.39441	3.30108	3.33515	100.02	0
43	-0.0008	1.02248	2.39004	2.63466	3.12473	0.44793	2.25854	0.32685	1.18773	3.00239	0.67630	100.01	0
44	-0.0058	0.82546	3.96454	2.95811	2.51758	1.87206	3.53335	4.02515	3.31091	2.64224	4.13047	100.10	0
45	-0.0018	3.23901	1.85108	0.56920	2.42924	1.96287	4.10581	2.17691	2.77320	3.25794	0.13579	100.03	0
46	0.59749	1.87679	1.61684	1.93368	0.92074	2.65388	0.83230	0.93532	0.64988	1.57783	1.58404	90.04	3
47	-0.0264	1.97917	3.86647	3.74548	4.13272	3.02184	1.09876	1.17198	1.98315	2.61552	2.73899	100.44	0
48	-0.0272	2.78063	3.45529	1.68690	2.94737	1.74814	1.07027	1.36355	2.32894	1.57608	3.10543	100.45	0
49	-0.0000	0.76537	0.00648	1.86245	0.70976	2.43893	3.16655	0.38766	2.95389	1.94035	2.48487	100.00	0
50	0.00642	2.40747	3.40290	1.73238	1.94886	2.41980	0.95555	2.97921	1.58176	3.08354	0.97331	99.89	0
51	0.00286	0.10072	0.15758	0.64351	2.80727	0.63434	1.71164	1.09855	0.47643	0.94985	1.89265	99.95	0
52	0.00188	2.95674	0.67448	0.97563	2.89874	1.92948	1.75324	0.45914	3.10072	4.05619	3.24663	99.97	6
53	0.00160	0.08989	0.73550	0.19409	0.26934	1.73155	1.91644	0.45246	1.34852	3.40776	0.71326	99.97	1
54	-0.0058	2.63585	3.08487	2.77119	1.69182	0.07934	0.09749	1.96071	0.19544	3.51909	2.09362	100.10	0
55	-0.0027	0.54973	0.40236	0.09818	0.33340	0.10479	2.00592	3.36200	3.17588	3.41382	0.70855	100.04	1
56	0.11857	1.99027	1.21689	4.06777	1.32294	1.13453	0.87853	0.87906	3.35036	0.55364	0.66182	98.02	0
57	0.03419	4.11607	2.47259	1.77100	1.70050	0.80369	0.95704	3.43688	2.84702	3.80749	3.68170	99.43	5
58	0.00011	3.12853	0.23519	2.62855	4.13040	3.68157	2.68726	0.00522	4.12174	1.06425	1.36575	100.00	0
59	0.09469	1.19220	1.05843	2.69257	1.82955	1.87744	1.80709	3.33671	2.33846	1.40811	3.59495	98.42	0
60	0.00001	1.81961	1.86769	3.03573	1.42199	3.60717	2.28454	1.13317	4.06971	0.03953	3.12647	100.00	0
61	0.04656	3.84015	2.66474	1.67043	3.46970	1.39725	1.93881	3.93579	0.78849	0.96480	3.50732	99.22	0
62	0.00009	3.55464	0.13764	1.89205	1.58637	0.85734	0.00167	2.08597	3.94957	2.97291	1.73416	100.00	0
63	3.78567	1.59441	1.19144	1.32134	1.66889	1.67429	1.17339	1.88795	1.75313	1.70760	1.66132	36.91	9
64	-0.0147	0.64958	3.56144	3.32182	1.95836	0.56766	2.61318	1.00871	3.96273	2.78805	1.54239	100.24	8
65	0.00009	1.85369	3.09080	3.74563	0.08927	1.41577	2.00421	1.03761	2.56812	3.16435	2.01873	100.00	9
67	-0.0001	3.85833	1.24404	3.12837	2.98354	0.81236	0.25204	0.24055	2.44967	1.25040	0.48472	100.00	2
68	0.10490	1.54828	3.44445	2.21718	1.19826	0.83593	4.00657	2.77261	2.10885	0.60420	1.88697	98.25	7

Table D.6: MPSA Example Run Output and Results (continued)

Particle	-F(x)	X1	X2	X3	X4	X5	X6	X7	X8	X9	X10	% Within Theoretical Value	No. of Improving Points
69	0.00052	0.17647	0.36945	2.51418	0.30608	2.97975	0.64417	2.91625	1.82038	3.66275	4.13112	99.99	10
70	-0.0000	0.14126	2.48927	2.22278	3.13395	2.92285	1.52057	2.47884	3.89446	3.85003	0.03700	100.00	0
71	0.02013	3.29186	2.60799	1.30311	1.44178	3.41121	0.80011	3.00290	1.04626	0.99070	3.39954	99.66	3
72	0.03426	2.75383	1.55544	3.26434	4.01537	0.78043	3.03995	1.51117	3.64895	2.40063	0.46310	99.43	6
73	0.04757	3.81245	2.31769	3.32950	1.63800	2.86913	1.07303	1.32042	1.11553	1.50438	0.83419	99.21	5
74	0.00736	2.57120	0.82584	3.33641	1.71782	1.34496	0.93604	3.32130	1.31273	0.55315	2.99330	99.88	0
75	0.00284	1.38963	2.50748	0.21435	4.10327	2.66351	1.68430	1.34904	3.11494	4.03921	0.63861	99.95	0
76	0.01408	4.08271	1.29822	2.61501	3.60471	2.73204	0.08514	0.16340	2.29392	1.07563	1.06539	99.77	0
77	-0.0022	3.08145	2.84047	1.08278	2.95520	4.05716	3.94351	2.87039	1.92167	1.27473	3.64714	100.04	0
78	0.01744	1.84111	1.12101	2.13179	3.55793	1.83330	2.58061	0.60229	3.56296	1.32947	0.10064	99.71	3
79	-0.0781	0.32274	0.69974	3.70008	1.26767	0.98527	1.85961	3.72979	1.97738	3.54620	1.23145	101.30	14
80	0.00404	2.71711	1.89786	1.01517	0.18934	0.91355	3.88898	2.34045	2.86971	4.09824	0.92495	99.93	0
81	-0.0076	2.00358	0.86617	3.53136	2.84540	3.18577	1.58659	2.12928	0.34203	3.19778	3.71183	100.13	0
82	-0.0019	3.01185	2.03372	1.16292	3.93747	0.20071	3.09685	2.77581	1.96784	3.18684	0.83025	100.03	0
83	-0.0081	2.15331	3.96105	3.07793	0.81119	2.69422	3.61966	0.80603	3.59893	1.39048	1.88616	100.14	1
84	0.00419	2.18719	2.17214	2.25573	0.75336	2.24576	2.07917	0.25613	0.61490	3.16852	3.34141	99.93	0
85	**4.02146**	**1.55085**	**1.20271**	**1.32085**	**1.71968**	**1.48081**	**1.49693**	**1.43315**	**1.98109**	**1.45905**	**1.59331**	**32.98**	**10**
86	0.01384	1.93271	3.01370	2.92869	4.11811	2.09902	1.57112	2.64822	2.36098	2.71019	1.11371	99.77	0
87	0.00463	1.52808	3.35922	1.69519	2.00988	0.05162	2.81191	2.07552	0.51988	3.88811	3.18113	99.92	0
88	-0.0116	3.49760	1.53281	3.98459	2.11597	3.73677	2.78760	3.04795	2.55804	0.25253	0.23313	100.19	0
89	0.00982	4.07811	2.55181	0.66137	3.05188	2.31679	0.53989	2.24505	1.58327	1.42976	3.33370	99.84	0
90	0.00022	2.56432	1.98927	0.20675	2.54433	2.28703	2.40209	3.18094	3.27396	1.73759	1.69478	100.00	0
91	-0.0218	3.09886	1.42024	3.94174	1.03647	2.54731	2.60722	4.09306	1.52674	3.86991	1.76674	100.36	3
92	-0.0011	1.28916	3.04164	0.39716	0.07184	1.26622	1.13959	0.40628	1.63006	1.31403	3.42526	100.02	0
93	0.02470	0.67427	2.77426	0.28028	0.39206	1.92777	1.98260	2.50645	3.98495	2.15840	3.87003	99.59	1
94	-0.0000	0.32929	4.08626	0.11930	3.18481	3.83046	0.58940	0.01983	3.74774	0.56648	3.74906	100.00	10
95	0.11858	2.31860	0.47540	1.71652	2.90990	0.51253	1.53498	2.11850	3.32819	1.62509	2.26768	98.02	8
96	-0.0029	3.05322	4.11883	2.67702	3.89454	1.42251	1.47744	0.67924	0.02826	2.85365	1.45496	100.05	0
97	-0.1815	1.68809	1.68190	0.95062	2.91245	3.98950	1.05054	0.51201	2.37690	1.90182	1.93348	103.02	0
98	0.06440	2.60157	1.56689	1.97155	3.34724	3.67887	1.35670	0.83003	4.03648	2.24242	3.51183	98.93	3
99	0.01120	2.49929	3.29087	1.33615	0.49560	1.36064	1.54133	0.49828	0.40275	2.33089	3.46930	99.81	0
100	-0.0032	0.50752	3.41797	2.14121	1.39572	3.65612	3.43910	3.23578	3.54850	1.26449	1.21552	100.05	1

Table D.6: MPSA Example Run Output and Results (continued)

Run 4 (n = 10, stop = 1000)													
Particle	**-F(x)**	**X1**	**X2**	**X3**	**X4**	**X5**	**X6**	**X7**	**X8**	**X9**	**X10**	**% Within Theoretical Value**	**No. of Improving Points**
1	-0.0003	1.89780	3.18799	0.96894	2.76653	2.62402	4.01534	1.82320	2.98840	1.45023	3.52488	100.00	32
2	0.01219	2.47137	2.49875	1.62279	3.52900	3.02611	1.03045	3.61212	3.44762	4.08260	1.63249	99.80	12
3	0.15601	2.98030	1.56521	1.64337	1.66980	2.13042	3.48809	0.26603	1.98431	1.09549	0.38021	97.40	14
4	-0.0003	0.02498	0.48621	2.53760	2.54352	0.25833	1.68109	3.57182	4.05554	3.05714	1.48738	100.00	8
5	0.01473	3.89074	1.71547	0.61722	0.64754	3.24390	1.79246	2.68530	3.98798	0.72968	3.74900	99.75	18
6	0.11883	3.47199	2.38994	3.54655	3.70749	0.99964	1.59649	2.23821	2.36372	3.60050	1.64212	98.02	21
7	-0.0000	2.60401	3.74883	0.35526	2.94677	0.05149	0.91655	0.19262	1.86740	2.35576	3.98136	100.00	0
8	0.01355	1.64163	0.44414	2.09441	3.73673	4.10221	1.88103	0.79752	3.47254	3.59422	0.17616	99.77	21
9	0.00074	2.82112	2.84406	3.52904	3.80091	1.25048	0.41448	0.12678	2.96635	4.11995	1.67955	99.99	21
10	0.02063	0.78328	4.13466	0.19659	1.87177	2.34007	2.19133	2.00110	1.15631	3.01469	3.89563	99.66	0
11	-0.0011	1.19596	1.98932	0.08945	2.91677	2.80818	0.78968	3.55165	3.19084	1.97086	3.20019	100.02	67
12	0.03058	0.91917	0.98066	1.98246	0.52113	2.37691	2.40617	3.64031	0.71392	3.96118	0.29002	99.49	0
13	-0.0002	1.59525	3.84601	2.40003	2.50233	2.40162	2.39762	0.02388	1.60680	3.12531	1.73818	100.00	28
14	-0.0474	1.43231	2.20407	3.42057	2.66293	1.97475	3.86911	3.79935	1.37664	2.70406	0.67166	100.79	0
15	0.01276	0.58532	3.70051	3.65331	3.58158	3.68231	2.45412	0.52306	1.12391	0.33592	1.13711	99.79	72
16	-0.0059	2.69704	2.35597	0.38069	3.13450	2.04369	4.01162	2.86179	1.66094	0.26067	2.40024	100.10	18
17	0.00863	0.29466	2.43578	4.06187	2.25065	0.42477	0.02380	2.38600	0.99143	3.68925	2.09440	99.86	3
18	0.04979	1.45813	3.81347	3.83110	3.62766	1.63531	1.91235	2.67997	3.66246	0.27230	1.56633	99.17	23
19	0.00280	0.67811	1.44225	3.48171	2.04396	2.13671	1.37170	3.17722	0.43783	3.08228	3.48022	99.95	52
20	-0.0271	4.02304	2.39210	2.86298	3.36239	0.30275	3.27821	3.20092	3.24680	2.82449	2.64529	100.45	94
21	-0.0071	3.75629	0.48068	0.16304	3.64531	3.38767	2.16066	1.83722	2.22819	2.61046	1.94248	100.12	24
22	0.07082	1.72104	2.26687	4.07921	1.29188	3.46246	0.50054	3.70806	4.10176	3.77669	3.79896	98.82	20
23	0.00988	3.70724	4.04663	2.32827	4.04949	0.09462	3.86078	1.34404	1.82541	2.93959	2.78247	99.84	45
24	0.14477	0.91303	2.75084	1.05736	0.97755	3.63714	4.05337	0.80643	1.84409	0.47554	0.85955	97.59	34
25	-0.0007	1.20617	3.18780	0.25373	4.03039	0.44819	3.77927	1.16092	0.88642	3.25580	3.81362	100.01	59
26	0.00377	4.06280	2.72442	1.41170	3.80000	2.06796	3.10513	2.72236	0.63025	2.59616	1.31469	99.94	56
27	0.09144	0.54083	1.46790	0.55962	3.50911	1.86093	1.41912	2.37912	1.83741	3.86816	2.68160	98.48	0
28	0.00312	0.16001	1.14501	3.24793	4.04379	1.57514	3.59699	0.63593	0.10816	4.08983	2.86959	99.95	50
29	-0.0026	3.07377	0.77275	1.79289	1.11985	4.07961	0.57435	3.45909	0.27479	3.78172	2.29665	100.04	1
30	-0.0148	2.46565	3.05812	2.70665	2.04471	2.78793	0.90731	1.73658	2.25867	3.61787	0.54317	100.25	16
31	0.00001	2.99202	1.49764	0.62834	0.97144	1.38801	0.40392	2.69157	2.30334	3.14025	0.09809	100.00	23
32	0.00049	3.65330	3.12697	4.09996	1.45776	1.49775	1.70165	0.05935	0.46558	3.65683	0.03575	99.99	14
33	0.04682	1.41897	1.11795	0.40115	3.59163	2.72215	1.10616	1.56224	0.96511	3.76809	0.37475	99.22	22

Table D.6: MPSA Example Run Output and Results (continued)

Particle	-F(x)	X1	X2	X3	X4	X5	X6	X7	X8	X9	X10	% Within Theoretical Value	No. of Improving Points
34	1.74997	1.88419	1.03360	1.09896	0.67155	1.46625	1.63154	1.28969	1.91863	1.38615	2.07269	70.83	25
35	-0.0095	2.99965	3.32583	0.72394	1.07303	0.16571	3.16502	3.35250	0.99764	1.06710	0.42278	100.16	32
36	-0.0124	1.69423	4.02455	3.61787	3.86076	1.05899	0.11143	2.76907	1.80929	1.49428	3.56920	100.21	51
37	0.00226	1.87588	2.51139	0.86888	2.08651	0.03120	0.13685	1.93217	1.99487	2.71591	0.94056	99.96	33
38	-0.0061	3.94349	2.74180	1.37201	3.19494	2.90300	0.73590	3.19341	2.98005	2.82534	1.73147	100.10	0
39	-0.0010	1.73165	3.00791	1.71828	2.21963	0.62216	2.59955	3.98212	1.85363	2.31169	3.12910	100.02	13
40	-0.0000	0.03641	3.78463	0.87782	3.16825	0.84817	3.02213	3.84337	0.46751	2.57638	1.19342	100.00	19
41	-0.0255	3.11457	3.54225	0.23500	0.27047	1.32844	0.39160	0.42902	2.78217	2.78428	0.21889	100.42	53
42	0.00000	0.45163	3.04839	2.00739	3.86897	2.46196	1.29656	0.15267	0.00425	0.16302	0.61146	100.00	18
43	-0.0012	0.92807	2.08330	1.96930	3.03416	1.44822	0.99389	3.14953	0.06268	2.36135	2.26178	100.00	42
44	0.00001	3.68659	2.49122	3.39250	3.15653	0.07123	3.02996	0.58541	0.22089	0.54138	2.56968	100.16	25
45	-0.0094	1.24513	2.13809	4.02680	1.79085	3.46416	3.04207	2.49493	2.77786	3.97516	0.66084	100.16	29
46	-0.0093	0.22603	1.18619	0.90582	1.13769	0.53639	3.94164	2.01549	3.19274	1.66184	3.80957	100.01	0
47	-0.0004	0.03599	0.47860	1.63898	3.95726	1.39688	1.86622	3.46456	3.74800	3.20041	3.80281	99.53	0
48	0.02843	1.59668	1.05448	1.49343	0.05566	1.37116	1.51297	3.64954	1.99627	3.35258	0.49317	100.04	2
49	-0.0022	2.66174	3.30146	2.80284	0.91838	1.19151	2.53294	3.80540	3.74554	1.62700	3.00715	100.00	51
50	-0.0002	3.20220	3.16395	2.04301	2.24665	0.63019	0.41421	0.34745	1.63417	1.89301	3.81712	100.28	81
51	-0.0171	2.90084	2.95953	3.53396	2.65815	3.67054	3.25917	1.69854	0.08816	1.48156	1.78976	100.09	0
52	-0.0055	1.73164	1.90191	2.80852	2.60824	3.36337	0.61419	2.86723	1.25990	2.69498	2.61457	99.98	1
53	0.00125	0.32378	0.99093	2.52131	3.19549	2.73685	3.65415	2.85574	2.74415	2.46635	0.33439	99.45	43
54	0.03305	4.04874	3.21259	0.77384	3.93684	1.73745	2.26862	3.55644	3.32588	3.24530	2.92134	4.81	44
55	5.71126	1.64097	1.56989	1.53414	1.50618	1.53547	1.49025	1.56916	1.54658	1.60080	1.60934	100.03	63
56	-0.0015	2.29498	0.70968	2.68997	0.60869	3.79009	0.02006	1.79975	0.77173	1.99851	2.79437	100.00	52
57	-0.0002	1.33966	3.75690	3.27038	3.10161	2.88207	3.19184	3.09429	2.09744	2.82630	3.51391	100.02	0
58	-0.0010	2.21784	0.22271	0.80101	0.49992	3.16572	0.05458	3.57410	2.09547	3.72267	0.71684	99.96	70
59	0.00240	1.93564	0.79924	2.49498	1.36867	0.16259	1.50048	3.40680	3.61002	3.20327	3.89941	100.00	17
60	0.00005	2.51256	3.09763	0.11858	4.06358	3.44529	3.47730	0.34510	2.97053	1.13213	0.06018	101.62	14
61	-0.0972	3.76361	2.22677	1.70584	0.72532	2.04976	2.19749	2.04075	0.62218	0.90524	2.92224	100.24	22
62	-0.0144	2.51537	2.51642	4.11763	1.39127	2.37150	0.76810	2.36752	1.50435	3.05061	0.34156	99.92	18
63	0.00467	2.59653	0.60087	2.78883	3.10470	3.63130	3.43094	0.23592	0.18663	0.96457	0.90929	100.03	0
64	-0.0017	3.29474	2.71456	0.59545	2.47806	0.70351	3.19544	1.85150	1.76819	1.87044	3.64981	99.13	0
65	0.05202	1.18111	1.49675	1.19836	0.53978	0.27602	3.83215	0.63815	1.88759	3.60434	2.57464	99.81	7
67	0.01160	1.45042	0.67043	2.24078	0.12368	3.81358	3.66237	1.69020	2.47109	2.79309	0.65366	100.00	0
68	-0.0001	3.22220	2.16832	0.81623	3.35779	3.16013	0.27468	1.47098	0.53012	1.27600	1.88561	100.00	20

Table D.6: MPSA Example Run Output and Results (continued)

Particle	-F(x)	X1	X2	X3	X4	X5	X6	X7	X8	X9	X10	% Within Theoretical Value	No. of Improving Points
69	-0.0002	1.32348	4.10736	2.92778	0.03829	3.63181	1.86838	3.15737	3.50637	1.58767	2.70914	101.45	28
70	-0.0870	1.58540	1.00118	0.83618	2.66412	1.85694	1.42488	2.28101	4.00466	2.96918	0.50443	100.28	26
71	-0.0171	1.74258	4.00641	2.39734	3.09261	2.00031	3.74088	3.74856	0.56171	2.07208	1.65549	100.68	0
72	-0.0405	2.72629	1.30006	0.90128	0.72881	2.33348	1.74707	2.69870	3.41038	3.41127	3.93702	101.16	1
73	-0.0694	0.57602	1.94923	0.52067	0.34952	1.15943	1.45883	3.87321	2.54273	2.37615	0.75012	100.04	15
74	**5.77982**	**1.56315**	**1.59394**	**1.66140**	**1.57856**	**1.54435**	**1.61278**	**1.54116**	**1.51563**	**1.55128**	**1.56790**	**3.67**	**19**
75	-0.0041	0.07034	1.83969	0.32670	3.46809	3.88287	2.18791	2.93186	1.36203	3.63992	0.07450	100.07	30
76	0.01219	0.97770	0.27371	2.80703	0.65742	1.01254	3.06234	1.40860	3.93705	1.45790	2.27407	99.80	0
77	-0.0032	0.98031	3.25524	3.92134	1.28083	1.56519	3.96593	1.04489	1.25719	0.01678	1.67369	100.05	0
78	-0.0181	2.75542	0.16938	0.51355	1.13869	3.71193	1.64605	0.28484	1.91703	1.90044	1.25363	100.30	24
79	-0.0016	3.53934	1.28861	3.48069	2.46750	0.63222	3.53859	0.10625	3.50148	3.61249	1.34633	100.03	0
80	0.00003	2.49027	2.61257	2.02972	0.93216	2.96104	3.03826	0.13521	4.03724	3.13765	1.93252	100.00	2
81	0.00144	0.92051	1.55382	3.65773	3.18210	3.90065	0.85593	0.31769	0.38313	0.00598	2.92794	99.98	4
82	0.01172	2.21696	1.55099	1.04950	1.09462	3.99463	2.94607	3.57174	2.76996	1.85864	2.35513	99.80	13
83	0.00000	3.76362	0.98845	2.37195	0.57147	2.36455	0.01224	3.43715	0.04749	3.19891	1.41675	100.00	0
84	-0.0436	2.78340	1.36906	1.56279	0.89494	0.43285	3.58713	0.36564	0.72131	1.62401	0.61272	100.73	0
85	0.00030	2.50753	2.46897	3.48901	3.03589	1.70780	0.41534	1.09706	2.78880	0.15784	2.69887	100.00	21
86	-0.0046	1.59158	2.03031	3.53718	3.21875	3.28651	3.74780	2.29279	1.29132	3.46303	1.69046	100.08	21
87	-0.0814	3.28721	1.74061	1.70527	0.86330	3.52481	4.00550	2.28144	0.79889	1.26249	1.38904	101.36	47
88	0.04027	3.60128	1.30431	1.42899	2.97016	4.12958	3.96123	3.55220	2.33324	2.38211	0.22266	99.33	35
89	0.02097	2.60754	3.98721	2.71064	0.25394	1.17818	0.82256	0.23675	2.20897	3.79248	2.03441	99.65	0
90	0.00921	0.46484	1.29456	2.81090	0.67993	1.52164	0.40810	2.90642	2.53547	1.74863	0.48001	99.85	0
91	-0.0075	0.39500	4.10974	2.45854	2.20623	2.40266	0.95744	2.00477	3.28914	3.38416	1.23067	100.12	28
92	0.03518	2.51711	3.66750	1.00767	1.34250	3.61023	0.56494	2.39454	2.89140	1.30063	2.30228	99.41	21
93	0.15543	1.13116	2.08631	0.37188	0.82811	1.50948	3.87110	3.67485	2.63722	2.20123	2.01575	97.41	10
94	5.23769	1.63930	1.53965	1.51691	1.74695	1.58687	1.60754	1.57744	1.60581	1.49144	1.70290	12.71	19
95	5.60069	1.56161	1.63797	1.59216	1.56837	1.55774	1.51994	1.46892	1.50536	1.50177	1.62756	6.66	28
96	0.00028	1.84593	0.00558	3.41409	2.33740	2.77327	1.77981	2.78422	3.00323	0.70230	2.04969	100.00	58
97	0.03920	1.62441	2.29282	3.95815	0.10222	2.17454	1.89311	1.10764	1.92276	1.50623	3.35019	99.35	20
98	-0.0002	3.90425	3.38484	1.09211	0.44463	0.81250	0.60945	1.02186	3.14292	1.58743	2.67080	100.00	1
99	-0.0150	2.85569	4.11093	0.59255	2.97624	1.55186	2.98583	0.50760	2.44887	2.73219	2.83054	100.25	19
100	-0.1252	1.00782	2.27512	1.68454	1.87389	3.51514	3.89139	1.43092	0.85823	2.84371	4.13739	102.09	0